The University of New South Wales

Water Research Laboratory

A STUDY OF NEAR WELL GROUNDWATER FLOW AND THE IMPLICATIONS IN WELL DESIGN

by

R.J. Cox

Report No. 148

March 1977.

BIBLIOGRAPHIC DATA SHEET	1. REPORT No. 148	2. I.S.B.N. 0/85824/225/7

3. TITLE AND SUBTITLE

A STUDY OF NEAR WELL GROUND WATER FLOW AND THE IMPLICATIONS IN WELL DESIGN

4. REPORT DATE

MARCH 1977

5. AUTHOR(S)

R.J. COX

6. SPONSORING ORGANIZATION

WATER RESEARCH LABORATORY

7. SUPPLEMENTARY NOTES

8. ABSTRACT

This report presents the results of an investigation of groundwater flow to wells in which the finite element method was used to examine a wide range of practical well flow problems that have not been previously investigated in sufficient detail. The results of the numerical solutions so obtained provide practising groundwater hydrologists with more complete information which may be used in the selection of an optimal well design. Since the flow within the near well zone exerts a disproportionately large effect on the performance of a well, considerable emphasis is placed upon investigating factors which may significantly alter the flow behaviour close to the well. The effects of non-linear flow, aquifer inhomogeneity, well geometry and boundary conditions are examined in detail. Verification of the finite element solutions by comparison with known analytical solutions and experimental results from an electrolytic tank analogue and a large scale sand-box model is described. For the various well-aquifer systems investigated, the well performance results are presented in design tables and figures. Extensive use of general dimensionless groupings of the design variables simplifies the presentation of results. The application of the results in the optimisation of well design is discussed.

9. DISTRIBUTION STATEMENT

Enquiries re. purchase of report should be directed to the Officer-in-Charge, Water Research Laboratory, University of New South Wales, King Street, Manly Vale, N.S.W. 2093.

10. KEY WORDS	Groundwater; water wells; finite elements; design	
11. CLASSIFICATION	12. NUMBER OF PAGES Approx 350	13. PRICE $10.00.

Acknowledgements

The author would like to thank Mr. C.R.Dudgeon for his active encouragement and guidance during his supervision of this thesis. Thanks are also given to Mr. K.K.Watson and Mr. D.N.Foster for supervision undertaken at various stages of the work.

Financial support provided by the Commonwealth Scientific and Industrial Research Organisation and the Australian Water Resources Council is gratefully acknowledged.

The interest and help received from all members of the Water Research Laboratory staff are much appreciated. Mrs.P.Decent and Mrs.P.Auld deserve special thanks for their painstaking effort in typing the manuscript and drafting the figures.

Abstract

This thesis reports the results of an investigation of groundwater flow to wells in which the finite element method was used to examine a wide range of practical well flow problems that have not been previously investigated in sufficient detail.

The results of the numerical solutions so obtained provide practising groundwater hydrologists with more complete information which may be used in the selection of an optimal well design.

Since the flow within the near well zone exerts a disproportionately large effect on the performance of a well, considerable emphasis is placed upon investigating factors which may significantly alter the flow behaviour close to the well. The effects of non-linear flow, aquifer inhomogeneity, well geometry and boundary conditions are examined in detail.

Verification of the finite element solutions by comparison with known analytical solutions and experimental results from an electrolytic tank analogue and a large scale sand-box model is described.

For the various well-aquifer systems investigated, the well performance results are presented in design tables and figures. Extensive use of general dimensionless groupings of the design variables simplifies the presentation of results. The application of the results in the optimisation of well design is discussed.

Table of Contents

Table of Contents (cont'd.)

Table of Contents (cont'd.)

Table of Contents (cont'd.)

List of Figures

List of Figures (cont'd.)

List of Figures (cont'd.)

List of Figures (cont'd.)

List of Figures (cont'd.)

List of Figures (cont'd.)

List of Figures (cont'd.)

List of Tables

List of Tables (cont'd.)

List of Main Symbols

All symbols are defined within the text. For convenience, the more commonly occurring symbols are defined in the list below. Definitions of symbols and subscripts which are not listed will be found in the text, immediately following the use of the symbol or subscript concerned. Symbols used in appendices are defined within the text of the appendices.

a - coefficient in exponential non-linear flow relationship $I=aV^n$

a, b - coefficient in Forchheimer non-linear flow equation $I = aV + bV^2$: may be subscripted to refer to a zone of aquifer inhomogeneity: see definitive figures.

d - characteristic length dimension of porous media.

$\vec{e}_i$ - unit vectors along cartesian coordinate axes.

f - friction factor

f - general function

g - acceleration due to gravity

h - hydraulic head above base of aquifer

h_c - average thickness of capillary fringe layer

h_f - free surface height (head) at well in unconfined aquifer

h_o - saturated thickness of unconfined aquifer

h_o - hydraulic head at radius of influence

h_w - water level (head) within the well

$\bar{h}$ - prescribed hydraulic head

$h_o(x_i)=h(x_i, t=0)$ - initial head distribution

$\left|\frac{\partial h}{\partial l}\right|, I$ - absolute hydraulic gradient

i, j - subscripts referring to components along coordinate axes

j - superscript referring to iteration number for boundary condition of prescribed well discharge

k - superscript referring to iteration number for non-linear flow solution procedure

k - subscript referring to iteration number for free surface location procedure

List of Main Symbols (cont'd.)

l - position along the well screen

l_b - depth above base of unconfined aquifer to open bottom end of a large diameter well

l_s - length of well screen

m - number of nodes in a finite element

m - thickness of a confined aquifer: may be subscripted to refer to the thickness of a layer of aquifer inhomogeneity: see definitive figures

n - exponent of exponential non-linear flow relationship $I = aV^n$

n - number of experimental points derived in permeameter testing

n - total number of nodes in the discretization of the entire flow region.

n - number of layers in multilayered aquifer

n - subscript referring to time step number

n_i - components of unit outward normal vector

p - number of network nodes situated on the well screen

q - flux per unit area

$\bar{q}$ - prescribed flux per unit area

q^* - uniform flux distribution value

r - radial distance from the centre of well: may be subscripted to refer to a zone of aquifer inhomogeneity: see definitive figures

r_o - radius of influence

r_w - radius of well

Δr - length of line segment in one dimensional discretization

Δr - radial spacing of nodes in two dimensional discretization

s - drawdown in aquifer ($=h_o - h$)

s_w - drawdown in the well ($=h_o - h_w$)

List of Main Symbols (cont'd.)

t - time

Δt - time step increment

$1/u$ - dimensionless time variable ($=\frac{4Tt}{r^2S}$)

v_i - components of velocity vector

x_i - cartesian coordinates

z - vertical coordinate

ΔA - surface area of control volume

B - boundary of entire flow region

B^1 - boundary portion where flux or flow rate is prescribed

B^2 - boundary portion where hydraulic head is prescribed

B^c - impervious boundary portion

B^f - free surface boundary portion

B^s - seepage face boundary portion

C - coefficient of non-linear effective hydraulic conductivity ($= 1/(a+b|\mathbf{V}|)$)

$[D]^e, [D]$ - element and gross matrices

E - number of elements per line segment in one-dimensional isoparametric ring element discretization

E^e, E^t - functional over individual finite element and entire flow region R

$\{F\}^e, \{F\}$ - element and gross column matrices

$[\bar{G}]^e, [\bar{G}]$ - element and gross matrices for Darcy flow

$[G]^e, [G]$ - element and gross matrices for non-linear flow

H - prescribed elevation of water level in the well: only referred to in unsteady solution procedure

I - hydraulic gradient

I, J - subscripts referring to either nodes belonging to an element or the entire flow region

List of Main Symbols (cont'd.)

$[J]$ - Jacobian matrix

K - hydraulic conductivity: may be subscripted to refer to a zone of aquifer inhomogeneity: see definitive figures

$[K]$ - hydraulic conductivity matrix

M, N - number of vertical and radial "tubes" in two-dimensional finite element discretization

$[N]$ - element shape function matrix

Q - well discharge

Q_a - discharge contributed by the aquifer

Q_w - discharge derived from well storage

$\bar{Q}$ - prescribed well discharge

Q_D - Dupuit equation steady well discharge for unconfined aquifer

Q_T - Thiem equation steady well discharge for confined aquifer

$\mathbb{R}_e = Vd/\nu$ - Reynolds Number

R - entire flow region

R^e - finite element flow region

S - storage coefficient

S_s - specific storage coefficient

$[S]$ - element slope matrix

T - transmissivity

V - flow velocity

ΔV - arbitrary control volume

$W(u)$ - dimensionless drawdown variable ($= 4\pi T(h_o - h)/Q$)

α - over-relaxation factor

α, β - subscripts in matrix partition form: see equation (4.47): referring to nodes on and off the well screen

List of Main Symbols (cont'd.)

ϵ - head variation near the well ($= h(r,m) - h(r_w,m)$)

ϵ - free surface variation near the well ($= h(r,$ free surface$)-h_f$)

ϵ_f - prescribed free surface tolerance for convergence of iterative solution for free surface boundary condition

ϵ_H - prescribed head tolerance for convergence of iteration solution for non-linear flow

ϵ_Q - prescribed discharge tolerance for convergence of iterative solution for prescribed well discharge boundary condition

$\lambda(t)$ - well storage coefficient ($= - 2\pi r_w^2 / \Delta t$)

ν - kinematic viscosity of fluid

(ξ,η) - isoparametric coordinates

ρ - density of water

$\sigma\%$ - percentage deviation of Forchheimer expression as fitted to experimental data: see equation (2.6)

ϕ - general function

ω - over-relaxation factor

1. Introduction

Analytical solutions to problems involving groundwater flow to a well are available only for relatively simple boundary conditions. Most of these solutions assume that Darcy's law is valid throughout the flow domain and have been obtained only after making many simplifying assumptions about the flow behaviour near the well. An abundance of published information on such classical solutions is available. Methods of applying the solutions in the evaluation of aquifer properties from the results of field pumping tests are well known to groundwater hydrologists the world over. Many texts give an adequate resumé of analytical solutions and methods of application (Hantush (1964), Walton (1970), Hazel (1973)).

The rapid development of high speed digital computers has led to widespread use of numerical techniques for solving many previously intractible problems in various fields of the physical sciences, including groundwater and seepage flow. A wide range of groundwater well flow problems have been solved by numerical methods (Zienkiewicz and Cheung (1965), Taylor and Brown (1967), Javandel and Witherspoon (1968), Taylor and Luthin (1969), Neuman and Witherspoon (1971), Brutsaert et al (1971), France et al (1971)). Although these solutions extend the range of well aquifer systems that can be analysed, the flow is still assumed to obey Darcy's law and simplifying assumptions are again made about the flow in the vicinity of the well.

In many practical well-flow problems, velocities high enough to invalidate Darcy's law may occur near the well. A non linear

velocity-hydraulic gradient relationship is then required to describe the flow. The governing field equations incorporating non-linear flow behaviour are virtually insoluble by analytical techniques for boundary conditions encountered in practice. Analytical, sand-box model and electrical analog solutions for steady state non-linear flow in idealised well-aquifer flow problems have been reported by Engelund (1953), Grcic (1961) and Baturic-Rubcic (1966) respectively. Trollope et al (1970) analysed steady state one dimensional axisymmetric non-linear flow using the field equation and the finite element technique outlined by Volker (1969). Huyakorn (1974) solved a number of non-linear flow problems using a two-regime concept in which the Forchheimer (1901) equation is used to describe the non-linear flow in a zone around the well and the Darcy equation is used beyond this zone. This approach has the disadvantage that a limiting velocity or Reynolds number must be specified to separate the two regimes. It is shown in this thesis that the use of a single Forchheimer equation provides simpler and sufficiently accurate solutions. Fewer parameters are required and thus the task of presenting well design data is made easier.

The method of finite elements is used extensively within this thesis for deriving numerical solutions to a wide range of common practical well flow problems that have not been previously investigated in sufficient detail. The versatility of the finite element method is demonstrated by the relative ease with which problems involving non-linear flow, complex well geometries and boundary conditions, and aquifer inhomogeneities are solved. The results of the numerical solutions so obtained provide the basis for the fulfilment of the major aim of this thesis, which is to provide practising groundwater hydrol-

ogists with more complete information which may be used in the selection of an optimal well design.

Since the flow within the near well zone exerts a disproportionately large effect on the performance of a well, considerable emphasis is placed upon investigating various factors which may significantly alter the flow behaviour close to the well. The effects of non-linear flow, aquifer inhomogeneity and well geometry are examined in detail.

When comparing the performance of individual wells for purposes of design optimisation, it is necessary in most cases only to consider the steady state behaviour since pumping periods are usually long enough to allow the relatively rapid changes of water level in the well during early pumping times to be neglected. The work detailed in this thesis thus concentrates on steady state conditions. To illustrate the complexity of unsteady (transient) flow in early times and close to the well (previous solutions grossly oversimplify the early time and near well flow behaviour) several examples of unsteady confined aquifer well flow are considered in Chapter 6.

Information which comes from the finite element solution of an individual problem includes the well drawdown-discharge relationship and the distribution of head and velocity throughout the aquifer. For purposes of well design, the importance of the drawdown-discharge relationship is uppermost and is thus emphasised. It is this relationship which is required by the designer when making an economic comparison of alternative well designs. Head and velocity distributions are of secondary importance in well design. A knowledge of the head distribution is required when interpreting field data to determine aquifer

coefficients. The selection and placement of observation wells to obtain maximum benefits from planned field testing also depends upon an understanding of possible head distributions within the aquifer. Velocities at the well screen or intake section are important in regard to particle movement, head loss through the screen and corrosion/encrustation problems (Peterson (1955), Prakash (1962), Smith (1963), Blair (1970)).

It should be noted that screen losses and flow losses within the well casing are ignored in this thesis. Such effects will be small if screen entrance velocities are kept within normally accepted levels.

In this introduction, only general references to the literature have been provided. Specifically relevant publications are referred to in the appropriate places throughout the remainder of the thesis. In addition to literature referenced within the text, further publications that are considered worthy of mention in relation to groundwater well flow are included in the list of references.

2. The Velocity-Hydraulic Gradient Relationship

2.1 General

In 1856 Darcy investigated the flow of water in vertical homogeneous sand filters. Based on his results, he concluded that the flow of fluid through porous media could be described by a linear relationship between discharge velocity (V) and hydraulic gradient (I). Simply,

$$V = KI \tag{2.1}$$

where K is termed the hydraulic conductivity. Most of Darcy's tests were confined to relatively low velocities but he recognised that there was an upper limit to the validity of his law.

Many problems in groundwater flow have been solved on the assumption of Darcy's law which adequately describes the flow situation provided flow rates are not large.

Many attempts have been made to derive Darcy's law, or, more generally the equations of motion in porous media, from the basic principles underlying the theory of hydrodynamics. In most cases theoretical justification of Darcy's law has been made through the use of conceptual models. Detailed reviews of these theories are given by Scheidegger (1960) and Irmay (1964). However, none of the theoretical derivations gives any means of calculating limits of validity of Darcy's law although they do offer explanations for the breakdown of the linear motion equation. Derivations based on the Navier-Stokes equations imply an upper limit when the inertial terms become significant, while those based on analogy with flow in tubes suggest a breakdown of the law when turbulence commences.

Many experimental investigations have been carried out to determine the upper limit of validity of Darcy's law. A number of these have been associated with attempts to define a general equation for the non-linear relationship at high flow rates.

The existence of a lower limit of validity to Darcy's law and a so called pre-linear regime has been recognised by some investigators. For well flow problems the effects of a possible pre-linear regime may be neglected and no further mention will be made of it.

A schematic classification of the flow behaviour through porous media in terms of the I-V relationship is given in Figure 2.1. Such a classification is supported by the work of Tek (1957), Hubbert (1956), Ward (1964) and Wright (1968).

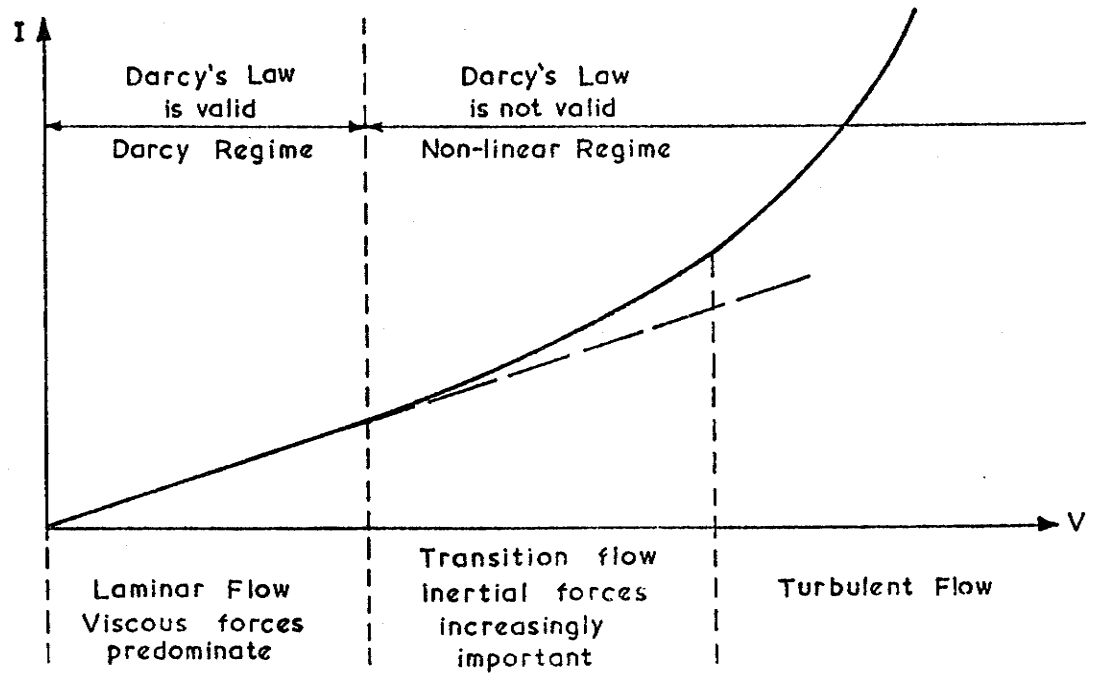

FIGURE 2.1: FLOW CLASSIFICATION

The flow is composed of two separate regimes:

(a) Darcy Regime.

For this regime the flow is laminar, viscous forces predominate and the linear relationship described by Darcy's law applies.

(b) Non-linear Regime.

Beyond a certain point, deviation from Darcy's law continually increases as inertial effects become more pronounced. Turbulent flow will eventually develop at higher flow rates.

2.2 The Range of Validity of Darcy's Law

By analogy to pipe flow, it has become customary to employ the Reynolds number ($\mathbb{R}_e$) as a criterion to distinguish between the Darcy and the non-linear flow regimes. For flow through porous media, the Reynolds number is given by

$$\mathbb{R}_e = Vd/\nu \qquad (2.2)$$

where V is the macroscopic discharge velocity, ν is the kinematic viscosity of the fluid and d is some length dimension characteristic of the porous matrix.

Bakhmeteff and Feodoroff (1937), Rose and Rizk (1949), Cohen de Lara (1955), Yalin and Franke (1961), Karadi and Nagy (1961), Anandakrishnan and Varadarajulu (1963), Ward (1964) and Wright (1968) are some of the investigators who have expressed results in terms of Reynolds numbers. However, due to the difficulty of determining a suitable characteristic length for the particles or pores of the medium, together with the fact that other factors such as particle shape and grading and porosity affect the upper limit of validity, a wide range of limiting Reynolds numbers has been reported.

Scheidegger (1960) quotes a range of limiting $\mathbb{R}_e$ based on mean grain diameter of 0.1 to 75. It appears doubtful whether one Reynolds number can ever characterise the upper limit except for geometrically similar packings of the same type of material.

Schneebeli (1955), Dudgeon (1966), Wright (1968) and others have observed that the onset of turbulence occurs at $\mathbb{R}_e$ values at least one order of magnitude higher than the $\mathbb{R}_e$ at which a significant deviation from Darcy's law becomes apparent.

2.3 Non-linear Regime Relationships

A large number of proposed non-linear motion equations, resulting from various theoretical and/or experimental investigations are reviewed by Scheidegger (1960) and Kirkham (1967). Three types of expression are commonly used.

(a) Forchheimer (1901) suggested a simple polynominal expression for the non-linear relationship between I and V at high flow rates. For one dimensional flow this may simply be written as

$$I = aV + bV^2 \qquad (2.3)$$

where a and b are constants. Forchheimer subsequently added a third term to obtain improved correlations with experimental data. However, equation (2.3) is generally referred to as Forchheimer's equation. The Forchheimer equation has been derived theoretically using a microscopic approach by Irmay (1958), Watson (1963), Sunada (1965) and Stark and Volker (1967). It has been used by Ergun (1952), Schneebeli (1955), Ward (1964), Irmay (1964) and others to fit experimental data.

Stark and Volker (1967) using idealised porous media obtained results that supported the Forchheimer equation. However, a single Forchheimer relation did not hold accurately over a wide range of flows. Rather, the results indicated the existence of several non-linear ranges, each of which could be described by a Forchheimer expression to within an accuracy of one or two per cent.

(b) Various exponential equations of the form

$$I = aV^n \tag{2.4}$$

have been used to fit experimental data. White (1935), Escande (1953), Wilkins (1955), Parkin (1963) and Curtis (1965) are some of the experimenters who have used the exponential form. These investigators have quoted a wide variation of the value of the exponent n. Cohen de Lara (1955) realised that both a and n would not be constant in the transition from laminar to turbulent flow.

This variation in a and n has been recognised by investigators who have carried out tests over a sufficiently wide range of velocities. From experimental results on sands and gravels, both Anandakrishnan and Varadarajulu (1963) and Dudgeon (1964) proposed the existence of several post linear flow regimes each of which could be described by an exponential non-linear relation.

(c) Equations of the form

$$I = \frac{f V^2}{2 gd} \tag{2.5}$$

similar to the Darcy equation used for pipe flow have been proposed to generalise the more basic I-V relationship. The friction factor, f, is usually related to a Reynolds number.

The existence of a wide range of friction factor - Reynolds

number relationships as determined by experiment (Lindquist (1933), Bakhmeteff and Feodoroff (1937), Yalin and Franke (1961), Anderson (1963), Ward (1964), Wright (1968)), clearly indicates the inability of this form to yield one general relationship for high flow rates through all types of porous media. In the absence of a general relationship no advantage can be gained from using the f-IR_e forms over the more basically derived I-V forms since groundwater flow computations are performed in terms of I and V.

2.4 Selection of Appropriate I-V Relationship

The choice of a velocity-hydraulic gradient relationship to describe the flow behaviour has been made on the basis of how well the relationship has been found to fit experimental results and the ease with which it can be applied to the solution of problems involving flow near wells.

A Forchheimer equation with single values of a and b has been chosen since it can be made to fit experimental data sufficiently accurately over the range of velocities encountered in flow towards wells. This equation also presents fewer difficulties in solving well flow problems.

The use of the exponential type of non-linear equation was ruled out since it is not possible to use a single exponential relationship (one set of a and n) to describe flow behaviour which encompasses both Darcy and non-linear regimes. The incorporation of variable coefficient a and exponent n over the flow would present little difficulty in the numerical solution techniques to be described in later

chapters. However, the use of any relationship involving more than single valued equation coefficients means the introduction of at least one additional dimensionless parameter to the already large number of such parameters required to fully describe a particular well flow problem.

The application of a single Forchheimer non-linear expression to cover a wide range of flows will not give as accurate a description of the flow behaviour as several post-linear regime relationships. However, it will be shown that a single Forchheimer relationship will fit experimental data with much less error than the errors introduced in determining aquifer permeabilities by available techniques.

2.5 Fitting Forchheimer Equation to Experimental Data

Sunada (1965) was able to fit a single Forchheimer equation to experimental results from various sources with the percentage deviation not exceeding experimental error. The range of flow rates in the majority of analysed results was not large.

Dudgeon (1964) presented detailed and consistent experimental investigations over a wide range of flow velocities for a range of materials in which non-linear and Darcy regimes were noted. There is little scatter in Dudgeon's results for values of VI greater than 10^{-4} feet per minute. Below this value the methods employed in overcoming the difficulties in measuring low flow rates and small head losses could cause bias of the results.

The experimental results ($VI > 10^{-4}$ feet per minute) for several granular materials studied by Dudgeon have been analysed. The mat-

erials were four river gravels ranging from a coarse sand to a 3/4 inch gravel and three crushed dolerites ranging from 3/16 to 3/4 inch. The particle size distributions of the seven materials are given in Figures 2.2 and 2.3.

Initially a Forchheimer relationship based on the equations proposed by Sunada (1965) was fitted to the experimental points. The statistically based equations described by Sunada give more emphasis to the smaller values of velocity in an attempt to improve on the fit given by the method of least squares. However, the resultant fit was still poor for the coarser materials at low velocities.

An algebraic evaluation of the constants for a single Forchheimer equation through two carefully chosen experimental points (V, I) from the range of results for the material in question was found to give a better overall fit. A log-log plot of I/V versus V for the experimental results and fitted Forchheimer relationships is shown in Figure 2.4. On this graph the Darcy regimes plot as horizontal lines and are easily recognised.

As a measure of the degree of fit, the percentage deviation ($\sigma'\%$) as defined by

$$\sigma'\% = \left\{ \sum_{i=1}^{n} \frac{\left(\frac{I_i - a V_i - b V_i^2}{I_i} \right)^2}{n} \right\}^{\frac{1}{2}} \times 100 \qquad (2.6)$$

was used.

The Forchheimer expression coefficients (a and b) used for the fitted curves of Figure 2.4 and the resulting percentage deviations are summarised in Table 2.1. For comparative purposes Table 2.1 also presents the a, b coefficients and $\sigma'\%$ that would be obtained by

Table 2.1: Non-linear Forchheimer Coefficients and Percentage Deviations when applied to Experimental Data.

Material	Investigator	Fit based on Algebraic fit to two points			Fit based on Sunada (1965) equations		
		a min/ft.	b min^2/ft^2	σ %	a min/ft	b min^2/ft^2	σ %
River Sand	Dudgeon	3.5	2.5×10^{-1}	4.2%	3.5	2.1×10^{-1}	3.8%
-$\frac{1}{4}$ R. Gravel	"	3.5×10^{-1}	6.2×10^{-2}	2.3%	3.5×10^{-1}	6.2×10^{-2}	2.3%
3/8 R. Gravel	"	9.0×10^{-2}	6.0×10^{-2}	4.1%	10^{-1}	5.7×10^{-2}	6.1%
3/4 R. Gravel	"	8.5×10^{-3}	8.0×10^{-3}	8.6%	1.3×10^{-2}	6.9×10^{-3}	25%
3/16 Blue Dolerite	"	6.5×10^{-2}	2.8×10^{-2}	2.3%	6.9×10^{-2}	2.7×10^{-2}	3.2%
3/8 Blue Dolerite	"	3.3×10^{-2}	1.8×10^{-2}	6.4%	3.8×10^{-2}	1.6×10^{-2}	10.3%
3/4 Blue Dolerite	"	7.0×10^{-3}	6.5×10^{-3}	8.1%	9.6×10^{-3}	6.0×10^{-3}	19%
Fine Sand	Anandakrishnan and Varadarajulu	4.83	6.19	-	*4.90	5.6	9%
Medium "		12.7	8.00	-			
Coarse "		8.64	6.97	-	*9.15	6.4	9%

*These values taken from Sunada (1965) as fitted to data obtained by estimation of published graphs by Anandakrishnan and Varadarajulu.

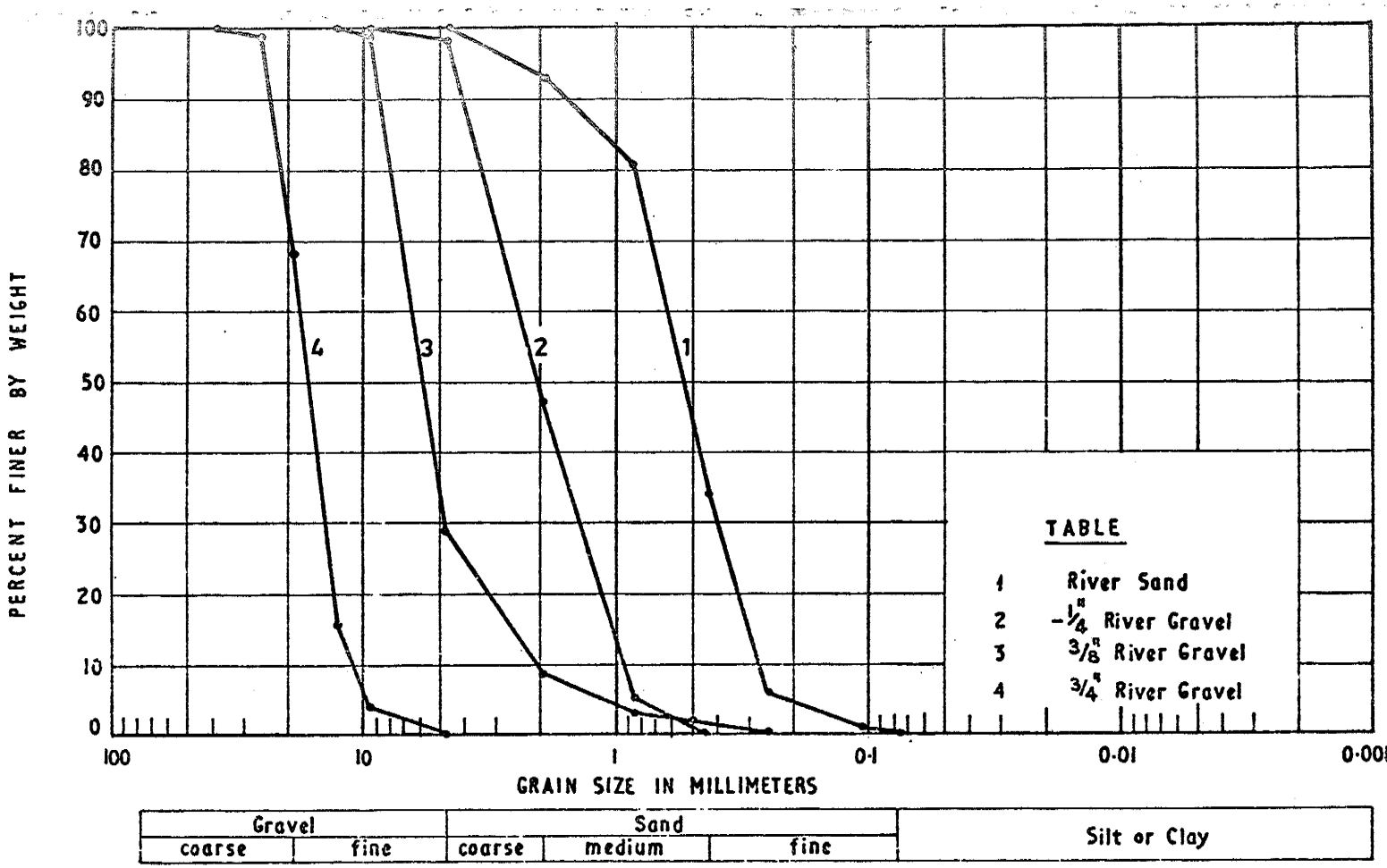

FIGURE 2·2: SIEVE ANALYSES OF RIVER GRAVELS (DUDGEON(1964))

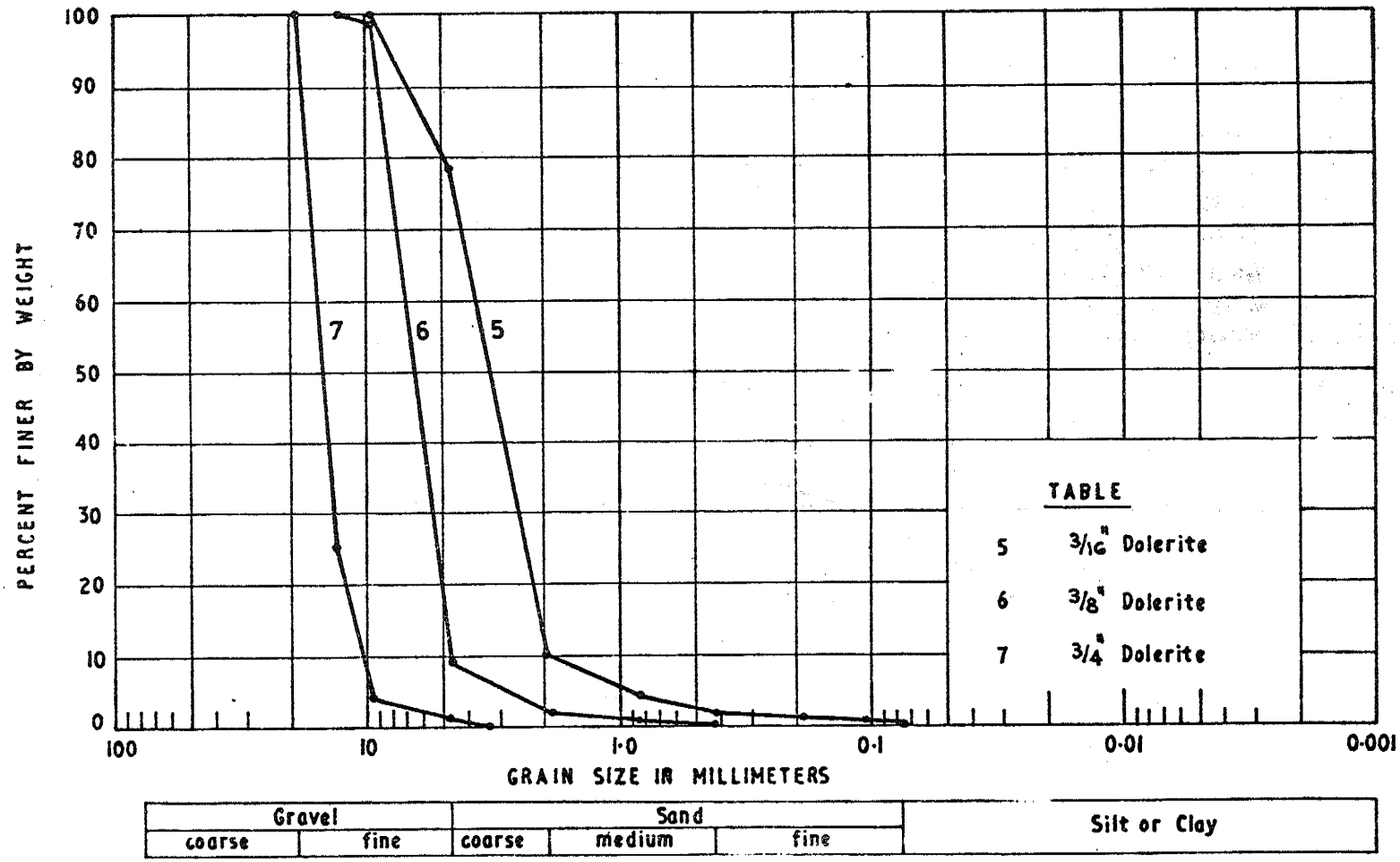

FIGURE 2·3: SIEVE ANALYSES OF CRUSHED DOLERITES (DUDGEON (1964))

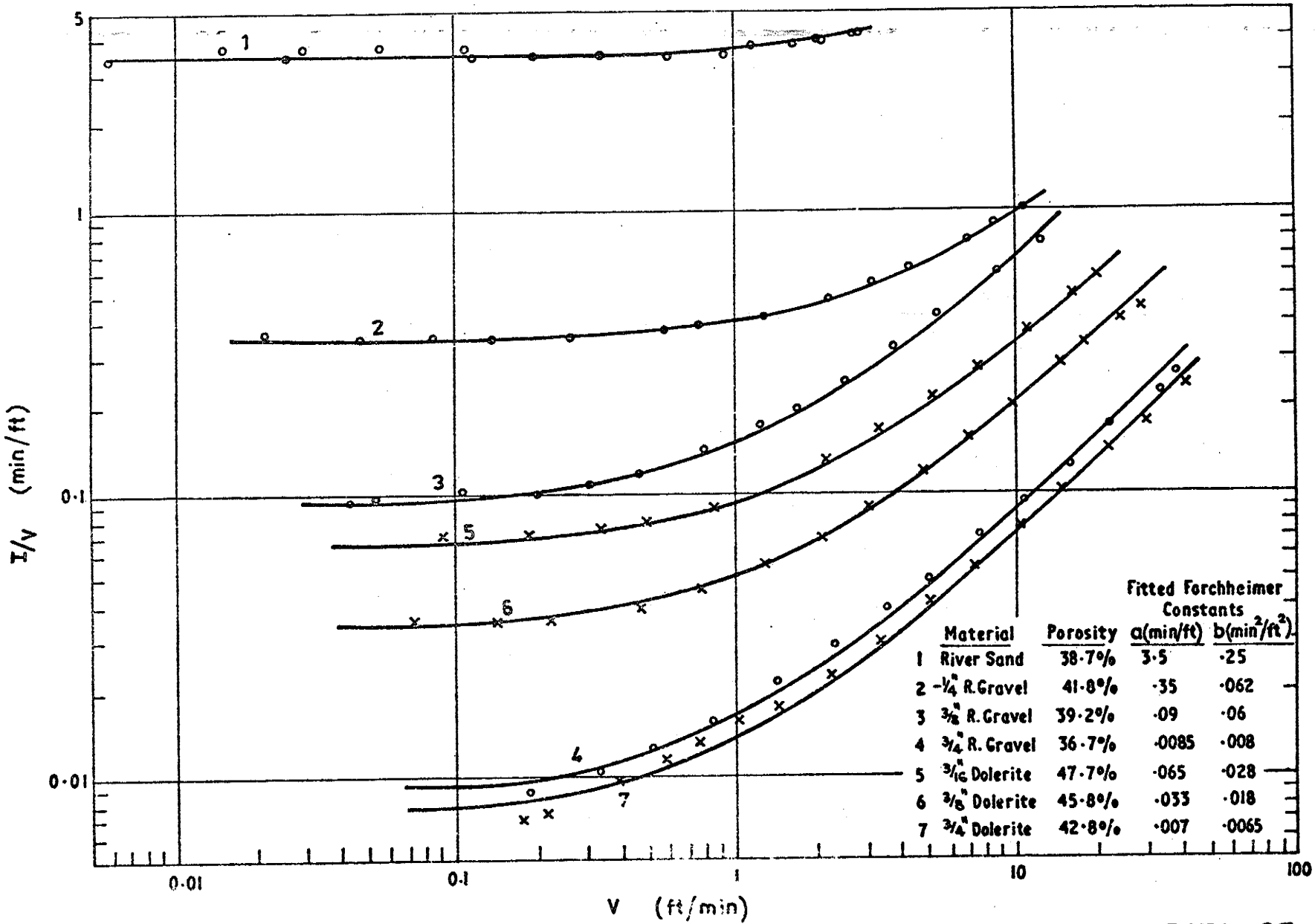

FIGURE 2·4: FORCHHEIMER RELATIONSHIPS FITTED TO EXPERIMENTAL DATA OF DUDGEON (1964)

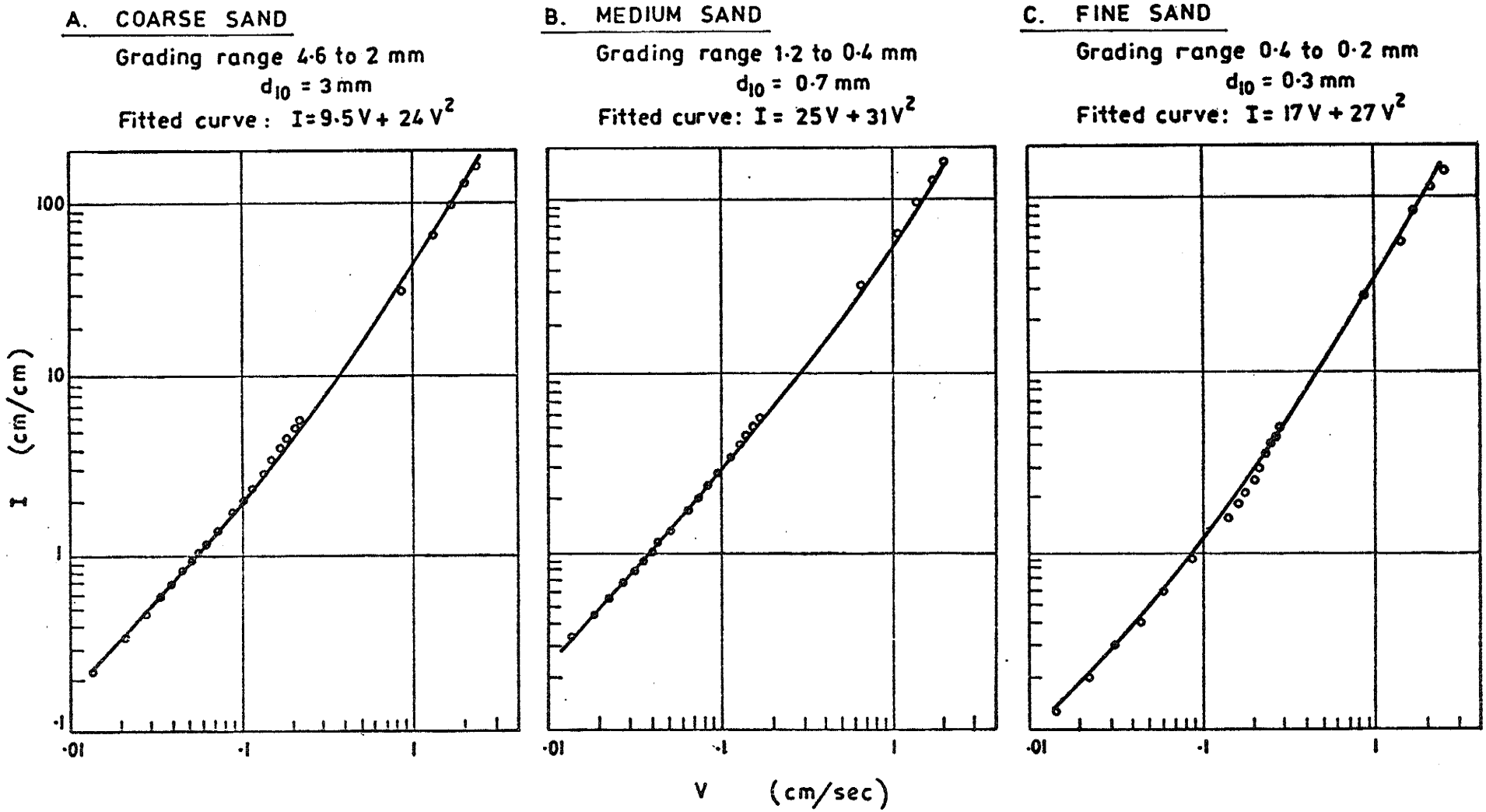

FIGURE 2·5: FORCHHEIMER RELATIONSHIPS FITTED TO EXPERIMENTAL DATA OF ANANDAKRISHNAN AND VARADARAJULU (1963)

using the equations proposed by Sunada (1965). As can be seen the relatively simple algebraic fit is better for all materials tested than the more complex statistical method described by Sunada. The ease and speed with which the algebraic fit was obtained with percentage deviation not exceeding 9% in any instance should be emphasised. More complex statistical methods will at best give as good a fit for considerably more effort and thus their continued use does not seem justified.

Using the algebraic fit described above, Forchheimer expressions were derived to fit the results of Anandakrishnan and Varadarajulu (1963), see Figure 2.5 and Table 2.1. Since these results were available only as plotted points on printed graphs no error estimates were made.

As can be seen in Table 2.1 and Figures 2.4 and 2.5, a single Forchheimer equation can be used to fit closely experimental results for a range of flows involving both Darcy and non-linear regimes.

2.6 Estimation of Aquifer Characteristics

Estimates of the hydraulic characteristics of aquifer materials are commonly made in two ways.

(i) Samples of the aquifer are taken and the I-V relationship determined by laboratory tests in a permeameter. Several investigators have demonstrated the sensitivity of the hydraulic constants to the porosity of the material (Givan (1934), Engelund (1953), Cohen de Lara (1955), Dudgeon (1964)). Generally the hydraulic conductivity is approximately proportional to the porosity to the fourth or fifth power and thus small changes in porosity can cause large variations in the pre-

dicted flow behaviour. Due to the difficulty in obtaining undisturbed samples of unconsolidated materials it appears unlikely that the porosity and packing of the grain matrix of the laboratory tested sample will bear any resemblance to the original state of the material in the aquifer. Predictions of aquifer material characteristics by this method could be in error by one hundred per cent or more.

(ii) In situ field tests for aquifer characteristics are commonly used in groundwater investigations and are recommended practice. The field test data are applied to a mathematical model of the aquifer field system to determine the numerical values of the material constants. The mathematical model used is a simplification of the real system and thus the resulting values of coefficients will only be as good as the model allows. Any form of field testing generally becomes an expensive undertaking. Even so, planning, control and supervision of the test are too often inadequate with the resultant data being of dubious quality.

In light of the difficulties involved in determining hydraulic constants for in situ materials the errors introduced by using a single Forchheimer expression for cases involving non-linear flow are relatively insignificant. The use of multiple regime relationships in practical field system problems merely complicates an already complex situation.

3. Governing Field Equations for Well Flow Problems

3.1 Differential Equations of Motion

In many groundwater problems the behaviour of the flow through the aquifer medium can be adequately described by Darcy's law. However, where steep hydraulic gradients occur in some aquifers Darcy's law will be invalidated. In such cases a Forchheimer non-linear equation (equation 2.3) can be used to describe the velocity-hydraulic gradient relationship over the entire range of flow.

Tensor notation is now used to describe the three dimensional differential equations of motion based on both the Darcy and Forchheimer relationships.

3.3.1 Equation based on Darcy's Law

A right hand system of cartesian co-ordinate axes (x_1, x_2, x_3) with axis x_3 vertically upwards and datum plane $x_1 - x_2$ is adopted.

$\vec{e}_1$, $\vec{e}_2$, $\vec{e}_3$ are the three unit vectors along the x_1, x_2 and x_3 axes respectively;

$h(x_i, t)$ is the hydraulic head at point $P(x_1, x_2, x_3)$ at time t.

The velocity vector $\vec{V}$ and the hydraulic gradient vector $\vec{\nabla h}$ can be expressed as

$$\vec{V} = v_i \vec{e}_i \tag{3.1}$$

$$\vec{\nabla h} = \frac{\partial h}{\partial x_i} \vec{e}_i \tag{3.2}$$

where the repeated subscripts denote summation over the full range, from 1 to 3.

For three dimensional flow through anisotropic aquifers,

$$\vec{V} = - \vec{\vec{K}} \vec{\nabla h} \tag{3.3}$$

where $\vec{\vec{K}}$ is the hydraulic conductivity tensor; a second order symmetric tensor which may be expressed as

$$\vec{\vec{K}} = K_{ij} \vec{e_i} \vec{e_j} \tag{3.4}$$

in which K_{ij} are the components of $\vec{\vec{K}}$.

Equation (3.3) may be more simply written as

$$v_i = - K_{ij} \frac{\partial h}{\partial x_j} \tag{3.5}$$

For an isotropic aquifer $\vec{\vec{K}}$ has only one independent component which is the commonly used hydraulic conductivity K.

In general K_{ij} and K are functions of coordinates, unless the aquifer is homogeneous.

3.1.2 Equation based on Forchheimer Relationship

For three dimensional non-linear flow through anisotropic media, equation 2.3 can be written in the following vector differential form

$$\vec{\nabla h} = - \left(\vec{\vec{a}} + \vec{\vec{b}} |V| \right) \vec{V} \tag{3.6}$$

where $\vec{\vec{a}}$ and $\vec{\vec{b}}$ denote the two hydraulic resistance tensors, the components of which are a_{ij} and b_{ij} respectively. $|V|$ is the magnitude of the velocity vector $\vec{V}$ and is given by $|V| = (v_i v_i)^{\frac{1}{2}}$ (3.7)

In tensor subscript form equation (3.6) becomes

$$\frac{\partial h}{\partial x_i} = - \left(a_{ij} + b_{ij} |V| \right) v_j \tag{3.8}$$

The components of the non-linear effective hydraulic conductivity tensor, C_{ij} are now defined by

$$C_{ij} = 1/(a_{ij} + b_{ij} |V|) \tag{3.9}$$

For isotropic aquifers, equation (3.8) becomes

$$\frac{\partial h}{\partial x_i} = - (a + b |V|) v_i \tag{3.10}$$

and equation (3.9) reduces to

$$C = 1/\ (a+b\ |V|\ ) \qquad (3.11)$$

where C may be termed "the coefficient of non-linear effective hydraulic conductivity".

3.2 The Equation of Continuity

3.2.1 General

Jacob was probably the first to consider flow in compressible and elastic aquifers. His theory was finalised in an article on groundwater flow (Jacob 1950), and his expression for the storage coefficient was not questioned for many years.

De Wiest (1966) criticised Jacob's derivation of the equation of continuity on the basis that "in one side of the equation the net inward mass flux was calculated for a volume element without deformation while in the other side of the equation, to compute the rate of change of the mass inside the volume element, the element itself was deformed".

In a more rigorous analysis De Wiest arrived at the same final expression for the equation of continuity as Jacob, although, in the process he redefined the specific storage.

Cooper (1966) subsequently proceeded to rederive the flow equation for both fixed and deforming co-ordinates, showing that Jacob's expressions for specific storage are correct if the vertical z co-ordinate is considered to be a deforming co-ordinate.

More complex derivations of the equations governing flow in porous media have been made. These have been reviewed and combined into a detailed and coherent formulation by Bear (1972).

However, Bear, like the majority of other workers, when applying the equations to groundwater hydrology, returns to a form of equation identical to that originally proposed by Jacob (1950).

The contention over the precise definition of the storage coefficient in terms of the elastic properties of the medium and the fluid seems trivial when in practical use the coefficient must be determined by actual field experiments (such as pumping tests).

The approach taken in the following derivation is as rigorous as necessary for practical application to well flow problems.

3.2.2 Derivation of Continuity Equation

Consider an arbitrary control volume $\Delta\forall$ of the aquifer situated in the flow field. The surface area of the closed boundary of $\Delta\forall$ will be ΔA. The law of conservation of mass requires that the net rate of mass of fluid entering the closed boundary of $\Delta\forall$ must be balanced by the rate of accumulation of fluid mass within $\Delta\forall$.

The net rate of mass of water entering ΔA is

$$-\int_{\Delta A} n_i \rho v_i \, dA$$

where n_i are the components of the unit outward normal vector of the differential area dA, v_i are the components of the velocity vector, and ρ is the density of water.

Although the water is compressible, variations in density will be neglected and the water will be assumed to be a homogeneous fluid of constant density.

The rate of mass of water accumulation within $\Delta\forall$ is

$$\int_{\Delta\forall} \frac{\partial M}{\partial t} \frac{dV}{\Delta\forall}$$

Since mass is conserved

$$-\int_{\Delta A} n_i \rho v_i \, dA = \int_{\Delta\forall} \frac{\partial M}{\partial t} \frac{dV}{\Delta\forall} \tag{3.12}$$

The surface integral may be transformed into a volume integral by the divergence theorem and the terms rearranged to give

$$\int_{\Delta\forall} \left[\rho \frac{\partial v_i}{\partial x_i} + \frac{\partial M}{\partial t} \frac{}{\Delta\forall} \right] d\forall = 0 \tag{3.13}$$

Since the choice of $\Delta\forall$ has been made arbitrarily, the integrand in equation (3.13) must vanish. That is,

$$-\frac{\partial v_i}{\partial x_i} = \frac{\partial M}{\partial t} \frac{}{\rho \Delta\forall} \tag{3.14}$$

Following Jacob's (1950) theory for a compressible aquifer medium, it may be shown that the rate of mass of water accumulated and the rate of change of hydraulic head are related by

$$\frac{\partial M}{\partial t} \frac{}{\rho \Delta\forall} = S_s \frac{\partial h}{\partial t} \tag{3.15}$$

where S_s, termed the specific storage of the aquifer is defined as the volume of water released from storage in the aquifer per unit (bulk) volume of aquifer and per unit decline of head. In an inhomogeneous aquifer S_s may vary in space but it will be assumed constant in time.

Combining equations (3.14) and (3.15) yields the required continuity equation

$$-\frac{\partial v_i}{\partial x_i} = S_s \frac{\partial h}{\partial t} \tag{3.16}$$

3.3 The Governing Field Equations

The differential equation of motion describing water flow through a particular porous medium has been shown in Chapter 2 to

fall into one of two classes which may be simply referred to as Darcy and non-linear flow.

3.3.1 Field Equation for Darcy Flow

The Darcy differential equation of motion and the continuity equation can be combined to give the second order linear field equation describing transient three dimensional Darcy flow in anisotropic and inhomogeneous aquifer media.

Combining equations (3.5) and (3.16) leads to the required result,

$$\frac{\partial}{\partial x_i}\left(K_{ij}\,\frac{\partial h}{\partial x_j}\right) = S_s\,\frac{\partial h}{\partial t} \tag{3.17}$$

For isotropic and homogeneous aquifers, equation (3.17) reduces to

$$\frac{\partial}{\partial x_i}\left(K\,\frac{\partial h}{\partial x_i}\right) = S_s\,\frac{\partial h}{\partial t} \tag{3.18}$$

where the coefficient K is a constant.

Rearranging equation (3.18) results in

$$\frac{\partial^2 h}{\partial x_i\,\partial x_i} = \frac{S_s}{K}\,\frac{\partial h}{\partial t} \tag{3.19}$$

3.3.2 Field Equation for Non-linear Flow

The Forchheimer differential equation of motion when combined with the continuity equation leads to the field equation for non-linear three dimensional transient flow through anisotropic and inhomogeneous aquifer media.

Rearranging equation (3.8) leads to

$$v_j = -\left(a_{ij} + b_{ij}\,|V|\right)^{-1}\,\frac{\partial h}{\partial x_i} \tag{3.20}$$

Combining equation (3.20) and (3.16) results in the field equation

$$\frac{\partial}{\partial x_j}\left[\left(a_{ij} + b_{ij}\,|V|\right)^{-1}\,\frac{\partial h}{\partial x_i}\right] = S_s\,\frac{\partial h}{\partial t} \tag{3.21}$$

Solution of the non-linear anisotropic equation (3.21) is beyond the scope of the present study. Assuming the aquifer to be isotropic leads to a simplified non-linear field equation involving only h as a dependent variable.

For isotropic aquifers, equation (3.8) reduces to

$$\frac{\partial h}{\partial x_i} = -\left(a + b|V|\right) v_i \qquad (3.22)$$

Contracting subscript i gives

$$\frac{\partial h}{\partial x_i}\frac{\partial h}{\partial x_i} = \left(a + b|V|\right)^2 v_i v_i \qquad (3.23)$$

The absolute hydraulic gradient is now defined as

$$\left|\frac{\partial h}{\partial \ell}\right| = \left(\frac{\partial h}{\partial x_i}\frac{\partial h}{\partial x_i}\right)^{1/2} \qquad (3.24)$$

Equation (3.24) can be rearranged to give

$$\frac{\partial h}{\partial x_i}\frac{\partial h}{\partial x_i} = \left|\frac{\partial h}{\partial \ell}\right|^2 \qquad (3.25)$$

Now

$$v_i v_i = |V|^2 \qquad (3.26)$$

Substituting equation (3.25) and (3.26) into equation (3.23) gives

$$\left|\frac{\partial h}{\partial \ell}\right|^2 = \left(a + b|V|\right)^2 |V|^2 \qquad (3.27)$$

Solving for $|V|$ gives

$$|V| = \frac{-a}{2b} + \sqrt{\left(\frac{a}{2b}\right)^2 + \left|\frac{\partial h}{\partial \ell}\right|\Big/ b} \qquad (3.28)$$

From equation (3.27)

$$|V|\Big/\left|\frac{\partial h}{\partial \ell}\right| = 1\Big/\left(a + b|V|\right) \qquad (3.29)$$

Combining equations (3.22), (3.28) and (3.29) leads to

$$v_i = \left(-\frac{\partial h}{\partial x_i}\right)\left[\frac{-a}{2b} + \sqrt{\left(\frac{a}{2b}\right)^2 + \left|\frac{\partial h}{\partial \ell}\right|\Big/ b}\right]\Big/\left|\frac{\partial h}{\partial \ell}\right| \qquad (3.30)$$

Equation (3.30) may now be substituted into the continuity equation to give the required field equation

$$\frac{\partial}{\partial x_i}\left[\left(\frac{-a}{2b} + \sqrt{\left(\frac{a}{2b}\right)^2 + \left|\frac{\partial h}{\partial \ell}\right|\Big/ b}\right)\left(\frac{\partial h}{\partial x_i}\right)\Big/\left|\frac{\partial h}{\partial \ell}\right|\right] = S_s \frac{\partial h}{\partial t} \qquad (3.31)$$

Equation (3.31) can be written as

$$\frac{\partial}{\partial x_i}\left(C\,\frac{\partial h}{\partial x_i}\right) = S_s\,\frac{\partial h}{\partial t} \qquad (3.32a)$$

where

$$C = \left(\frac{-a}{2b} + \sqrt{\left(\frac{a}{2b}\right)^2 + \left|\frac{\partial h}{\partial \ell}\right|/b}\right)\Bigg/\left|\frac{\partial h}{\partial \ell}\right|$$

Rationalizing the square root term in the expression for C results in

$$C = 1\Bigg/\left[\frac{a}{2} + \sqrt{\frac{a^2}{4} + b\left|\frac{\partial h}{\partial \ell}\right|}\;\right] \qquad (3.32b)$$

C has previously been termed "the coefficient of non-linear effective hydraulic conductivity". (Section 3.1.2 and equation (3.11)

3.4 Initial and Boundary Conditions

A unique solution to either of the general field equations (3.17) or (3.31) can only be obtained when the initial and boundary conditions of the flow domain are specified.

Certain types of initial and boundary conditions which are relevant to well flow problems are now considered:

3.4.1 Initial Condition

Generally for transient well flow problems, the initial distribution of hydraulic head throughout the aquifer region is assumed to be a presdribed function of co-ordinates.

The initial condition may be expressed as

$$h(x_i, 0) = h_o(x_i) \qquad (3.33)$$

within the closed region of the flow

$h_o(x_i)$ is the initial head distribution function.

3.4.2 Pervious Boundary Condition

Flux interchange between the flow system and its surroundings is said to take place across pervious boundaries of the system. Two

different conditions are likely to occur on pervious boundaries.

(a) Prescribed Flux or Flow Rate

"The prescribed flux" boundary condition arises when the flux distribution on the boundary is known at any instant of time. "The prescribed flow rate" boundary condition occurs when only the total flow rate across the boundary is known as a function of time. These two conditions may be expressed mathematically as follows:

B^1 is the portion of a pervious boundary where the flux distribution or total flow rate is prescribed. If $\bar{q}$ denotes the prescribed inflow flux per unit area, then "the prescribed flux" condition is

$$v_i n_i = \bar{q} \quad \text{on} \quad B^1 \tag{3.34}$$

where v_i and n_i are the components of the velocity vector $\vec{V}$ and the outward normal vector of the boundary surface respectively.

If $\bar{Q}(t)$ denotes the prescribed flow rate at time t, "The prescribed flow rate" condition is

$$Q(t) = \bar{Q}(t) \quad \text{across} \quad B^1 \tag{3.35}$$

(b) Prescribed Head Condition

"The prescribed head" boundary condition arises when the distribution of hydraulic head on a pervious boundary is known at any instant of time. It can be written as

$$h = \bar{h} \text{ on } B^2 \tag{3.36}$$

where $\bar{h}$ denotes the prescribed head function and B^2 denotes the portion of the boundary on which the head is prescribed.

3.4.3 Impervious Boundary Condition

Across impervious boundaries, the velocities normal to the boundary surfaces are zero. The boundary is thus a streamline or

stream surface of the flow.

The boundary condition is given by

$$v_i n_i = 0 \text{ on } B^c \tag{3.37}$$

where B^c denotes the impervious boundary portion.

3.4.4 Free Surface

A free surface will be defined as a stream surface along which the pressure is atmospheric, that is, a phreatic surface. Under steady state conditions, neglecting the effects of the capillary zone, two conditions are satisfied on the free surface.

The first condition is similar to that for an impervious boundary in that no flow takes place across the free surface, viz.

$$v_i n_i = 0 \text{ on } B^f \tag{3.38}$$

The second condition states that the head must equal the elevation of the free surface. Thus

$$h(x_i) = z(x_1, x_2) \text{ on } B^f \tag{3.39}$$

where $z(x_1, x_2)$ is the height of the free surface above the datum plane at point (x_1, x_2).

B^f denotes the free surface boundary portion.

As the position of the free surface is not known a priori, it is located by an iteration process based upon equation (3.39) during the solution of unconfined flow problems.

3.4.5 Seepage Face

In solving unconfined well flow problems, the presence of a vertical seepage face at the well may be considered. The seepage face is located along any exposed length of screen at the well, below the water table and above the water level within the well. The boundary condition is

similar to that for the free surface and can be written as

$$h(x_i) = x_3 \quad \text{on } B^S \tag{3.40}$$

where B^S denotes the seepage face boundary.

4. Solution of Equations for Well Flow Problems

4.1 Introduction

Solutions of the governing field equations for well flow problems can be made by techniques of analytical mathematics only in simplified cases. More complex problems can be solved by numerical techniques involving the use of digital computers. The numerical methods of finite differences and finite elements have been applied to various groundwater problems. The relative merits of these two methods are dependent upon the particular problem being solved and the computer to be used.

The finite element method has advantages over the method of finite differences in dealing with the complex boundary conditions and possible anisotropy and inhomogeneity of aquifer media which commonly occur in practical well flow problems. A further advantage of the finite element method is the ease with which the mesh may be refined in critical regions of the flow such as those that occur in the vicinity of a pumping well.

The finite element analysis of flow towards a pumped well is developed in this chapter. Both Darcy flow and possible non-linear flow as described by the Forchheimer expression are treated.

Anisotropy of the aquifer medium is only considered for the Darcy flow case. The analysis of non-linear flow behaviour in anisotropic aquifers involves complex non-linear velocity - hydraulic gradient relationships, the theoretical basis and experimental verification of which have not been adequately established. Further research is needed in developing an understanding of the behaviour of the coefficients of the Forchheimer relationship for flow in aniso-

tropic media.

Homogeneity within an individual finite element is assumed in the analysis. However, there is no restriction on abrupt property changes from one element to the next. Thus, by suitable selection of the finite element mesh, any overall aquifer inhomogeneity may be treated.

The procedures for analysis of both steady state and transient flow in confined aquifer systems are developed. For unconfined aquifer systems, only steady state solutions are presented.

4.2 General Statement of the Method of Finite Elements

The finite element method based on the principle of minimum potential energy has proved to be highly efficient for the solution of boundary value problems. Basic finite element theory has been well documented by Zienkiewicz (1971). Only essential features of the procedure will be recapitulated.

In Chapter 3, the equations needed to describe a range of well flow problems involving possible non-linear flow behaviour were presented. The solution to a particular problem reduces to finding the function h which satisfies the differential field equation and initial boundary conditions.

An alternative approach is possible through the use of variational calculus (Fox, (1950), Wienstock(1952)). A variational, extremum principle valid over the entire flow region is postulated and the problem solution is transformed into finding the distribution of the function h which minimises the "functional", E, subject to the same constraints of the flow system. The functional is defined by a suitable integration of the unknown quantities over the region.

The two approaches are mathematically equivalent, an exact solution of one being the solution of the other.

The method of finite differences attempts a direct approximate solution of the field equations and initial and boundary conditions.

An approximate solution for the variational presentation of the problem can be obtained by the finite element method. The continuous region of the flow system is subdivided into a finite number of closed subregions termed "finite elements". The finite elements are assumed to be interconnected at a discrete number of nodal points situated on their boundaries. A chosen function uniquely defines the hydraulic head distribution within an element in terms of its nodal parameters. Each element contributes to the functional over the entire flow region. The minimisation process is accomplished by evaluating the individual elemental contributions, adding all such contributions, differentiating the resulting functional with respect to the nodal parameters and equating the differentials to zero. This procedure results in a system of simultaneous algebraic equations which may be solved by direct elimination and/or iterative techniques.

4.3 Variational Formulation of Well Flow Equations

Variational forms of the previously derived field equations for both Darcy and non-linear flow may be obtained by considering an equivalent variational problem and employing the Euler equation from the calculus of variations (Wienstock, (1952)).

As previously stated, (x_1, x_2, x_3) represents a right hand system of Cartesian co-ordinate axes.

Let $h(x_i, t)$ be an admissible function with second order space

and first order time derivatives which are continuous everywhere in the flow region.

If at a particular instant in time the time derivatives of h and all other parameters are treated as prescribed functions of the space co-ordinates then the general functional to be minimised over the space region R at that instant in time may be expressed as

$$E^t = \int_R f\left(x_i, h, \frac{\partial h}{\partial x_i}, \frac{\partial h}{\partial t}\right) dR \qquad (4.1)$$

The well-known Euler theorem states that if the functional (E^t) is to be minimised, then the necessary and sufficient condition for this minimum to be reached is that the function h should satisfy the following equation

$$\frac{\partial f}{\partial h} - \frac{\partial}{\partial x_i}\left[\frac{\partial f}{\partial\left(\frac{\partial h}{\partial x_i}\right)}\right] = 0 \qquad (4.2)$$

The previously derived field equations(Chapter 3) belong to one of the classes of partial differential equations represented by equation (4.2). By comparing the field equations with equation (4.2) the expressions for function f may be found and hence the functionals.

The field equation for Darcy flow through anisotropic aquifer media may be written as

$$\frac{-\partial}{\partial x_i}\left(K_{ij}\frac{\partial h}{\partial x_j}\right) + S_s\left(\frac{\partial h}{\partial t}\right) = 0 \qquad (4.3)$$

Comparing equations (4.2) and (4.3) yields

$$f = \frac{1}{2} K_{ij}\frac{\partial h}{\partial x_j}\frac{\partial h}{\partial x_i} + S_s h \frac{\partial h}{\partial t} \qquad (4.4)$$

Hence the functional describing Darcy flow behaviour at an instant in time is given by

$$E^t = \int_R \left[\frac{1}{2} K_{ij} \frac{\partial h}{\partial x_j} \frac{\partial h}{\partial x_i} + S_s h \frac{\partial h}{\partial t} \right] dR \qquad (4.5)$$

The field equation describing non-linear flow through isotropic aquifers (equation 3.31) may be rewritten as

$$-\frac{\partial}{\partial x_i}\left[\left(\frac{-a}{2b} + \sqrt{\left(\frac{a}{2b}\right)^2 + \left|\frac{\partial h}{\partial \ell}\right|/b}\right)\left(\frac{\partial h}{\partial x_i}\right)\Big/\left|\frac{\partial h}{\partial \ell}\right|\right] + S_s \frac{\partial h}{\partial t} = 0 \qquad (4.6)$$

Comparing equations (4.6) and (4.2) yields

$$f = \frac{-a}{2b}\left|\frac{\partial h}{\partial \ell}\right| + \frac{2b}{3}\left[\left(\frac{a}{2b}\right)^2 + \left|\frac{\partial h}{\partial \ell}\right|/b\right]^{3/2} + S_s h \frac{\partial h}{\partial t} \qquad (4.7)$$

Hence the functional describing non-linear flow behaviour at an instant in time is given by

$$E^t = \int_R \left[\frac{-a}{2b}\left|\frac{\partial h}{\partial \ell}\right| + \frac{2b}{3}\left\{\left(\frac{a}{2b}\right)^2 + \left|\frac{\partial h}{\partial \ell}\right|/b\right\}^{3/2} + S_s h \frac{\partial h}{\partial t}\right] dR \qquad (4.8)$$

The variational problem reduces to finding an admissible function h that minimises the relevant functional over the region whilst satisfying the boundary conditions.

The impervious boundary condition along B^c is automatically satisfied by function h minimising the functional. The admissible function h may be chosen to automatically satisfy the prescribed head and seepage face conditions on the B^2 and B^s portions of the entire flow boundary. The boundary condition requirement along portion B^1 where the flux is prescribed may be satisfied by the addition of the term $\int_{B^1} h\,\bar{q}\,dB$ to the functional. $\bar{q}$ need not necessarily be constant, but, in general may be a prescribed function of time. In the finite element formulation of well flow problems to follow, boundary conditions along B^c, B^2, B^s and B^1 are all satisfied in the above manner.

The prescribed flow rate and free surface boundary conditions are specifically treated in sections 4.5.6 and 4.6 respectively.

4.4 Subscript Notation

The following subscript notation is adopted in developing the general three dimensional finite element formulation:

Both capital and small letter subscripts are used. The capital letter subscript refers to a particular node belonging to either an element or the entire flow region. The range of the subscript is from one to the number of nodes on the element boundary, if reference is made to the element, or from one to the total number of nodes, if reference is made to the entire flow region. The small letter subscript refers to a particular component along the coordinate axis. Its range is from one to three for the three-dimensional space region.

Repeated subscripts are interpreted as summation over the full range unless otherwise indicated.

4.5 Finite Element Analysis of Well Flow in Confined Aquifers

4.5.1 General

Consider the general problem of three dimensional transient flow towards a pumped well penetrating a confined aquifer.

Consider a particular instant in time.

Let the flow region be divided into a network of interconnected finite elements; the total number of nodes in the discretisation of the

entire flow region be n, and the number of nodes situated on an individual element boundary be m.

The head distribution within each element may be approximated by

$$h(x_i, t) = N_I(x_i)\, h_I(t) \tag{4.9}$$

where $N_I(x_i)$ are piecewisely defined functions of coordinates (x_1, x_2, x_3) within the element, $h_I(t)$ are the nodal values of h at the particular time t and the repeated subscript I denotes summation over the full range from 1 to m.

In the selection of shape functions (N_I), care should be taken to avoid any discontinuity of h arising between adjacent elements.

All elements are assembled through the specification of the reduced compatibility condition, which requires that the function h be the same at coincident nodes of adjacent elements.

If E^e is the contribution of a typical element "e" to the function E^t then

$$E^t = \sum_e E^e \tag{4.10}$$

the summation being taken over all the elements.

The minimisation process is best achieved by evaluating individual element contributions and adding all such contributions and equating to zero. Thus

$$\frac{\partial E^t}{\partial h_I} = \sum_e \frac{\partial E^e}{\partial h_I} = 0 \tag{4.11}$$

for I = 1, n

Only elements adjacent to node I will contribute to $\frac{\partial E^t}{\partial h_I}$.

This results in a banded matrix which has certain advantages as regards necessary computer storage and solution time.

4.5.2 Element Matrix Formulation

The evaluation of elemental contributions will now be considered for both Darcy and non-linear flow behaviour.

Equation (4.9) may be more simply written as

$$h = N_I h_I \tag{4.12}$$

It follows that

$$\frac{\partial h}{\partial x_i} = \frac{\partial N_I}{\partial x_i} h_I \tag{4.13}$$

Contracting subscript i gives

$$\frac{\partial h}{\partial x_i} \frac{\partial h}{\partial x_i} = \frac{\partial N_I}{\partial x_i} h_I \frac{\partial N_J}{\partial x_i} h_J \tag{4.14}$$

Now

$$\left| \frac{\partial h}{\partial \ell} \right|^2 = \frac{\partial h}{\partial x_i} \frac{\partial h}{\partial x_i} \tag{4.15}$$

Differentiating equation (4.15) with respect to h_I gives

$$\frac{\partial}{\partial h_I}\left(\left| \frac{\partial h}{\partial \ell} \right| \right) = \left[\frac{\partial h}{\partial x_i} \frac{\partial}{\partial h_I}\left(\frac{\partial h}{\partial x_i} \right) \right] \Bigg/ \left| \frac{\partial h}{\partial \ell} \right| \tag{4.16}$$

Also, from equation (4.13)

$$\frac{\partial}{\partial h_I}\left(\frac{\partial h}{\partial x_i} \right) = \frac{\partial N_I}{\partial x_i} \tag{4.17}$$

Substituting equations (4.13) and (4.17) into equation (4.16) results in

$$\frac{\partial}{\partial h_I}\left(\left| \frac{\partial h}{\partial \ell} \right| \right) = \left[\frac{\partial N_J}{\partial x_i} h_J \frac{\partial N_I}{\partial x_i} \right] \Bigg/ \left| \frac{\partial h}{\partial \ell} \right| \tag{4.18}$$

Since N_I are time invariant functions, it follows that

$$h \frac{\partial}{\partial h_I}\left(\frac{\partial h}{\partial t} \right) = N_J h_J \frac{\partial N_I}{\partial t} = 0 \tag{4.19}$$

and

$$\frac{\partial h}{\partial t} \frac{\partial h}{\partial h_I} = \frac{\partial h_J}{\partial t} N_J N_I \tag{4.20}$$

(a) Darcy flow - elemental contributions

The individual element function may be expressed as

$$E^e = \int_{R^e} \left[\frac{1}{2} K_{ij} \frac{\partial h}{\partial x_j} \frac{\partial h}{\partial x_i} + S_s h \frac{\partial h}{\partial t} \right] dR + \int_{B^{1e}} h \bar{q} \, dB \qquad (4.21)$$

where the second integral only applies if the element has an external boundary coincident with the prescribed flux boundary portion of the overall flow region.

Differentiating equation (4.21) with respect to h_I gives

$$\frac{\partial E^e}{\partial h_I} = \int_{R^e} \left[K_{ij} \frac{\partial h}{\partial x_j} \frac{\partial}{\partial h_I} \left(\frac{\partial h}{\partial x_i} \right) + S_s h \frac{\partial}{\partial h_I} \left(\frac{\partial h}{\partial t} \right) + S_s \frac{\partial h}{\partial t} \frac{\partial h}{\partial h_I} \right] dR + \int_{B^{1e}} \bar{q} \frac{\partial h}{\partial h_I} \, dB \qquad (4.22)$$

Substituting equations (4.17), (4.19) and (4.20) into equation (4.22) gives,

$$\frac{\partial E^e}{\partial h_I} = \int_{R^e} \left[K_{ij} \frac{\partial N_J}{\partial x_j} h_J \frac{\partial N_I}{\partial x_i} + S_s \frac{\partial h_J}{\partial t} N_J N_I \right] dR + \int_{B^{1e}} \bar{q} N_I \, dB \qquad (4.23)$$

In matrix notation equation (4.23) may be written as

$$\left\{ \frac{\partial E}{\partial h} \right\}^e = [\bar{G}]^e \{h\}^e + [D]^e \left\{ \frac{\partial h}{\partial t} \right\}^e + \{F\}^e \qquad (4.24)$$

where

$$\left\{ \frac{\partial E}{\partial h} \right\}^e = \begin{bmatrix} \frac{\partial E^e}{\partial h_1} \\ \vdots \\ \frac{\partial E^e}{\partial h_m} \end{bmatrix}, \quad \{h\}^e = \begin{bmatrix} h_1 \\ \vdots \\ h_m \end{bmatrix}, \text{ and } \left\{ \frac{\partial h}{\partial t} \right\}^e = \begin{bmatrix} \frac{\partial h_1}{\partial t} \\ \vdots \\ \frac{\partial h_m}{\partial t} \end{bmatrix}$$

The element matrices $[\bar{G}]^e$, $[D]^e$ and $\{F\}^e$ are defined by

$$[\bar{G}]^e = \int_{R^e} [S]^T [K] [S] \, dR \qquad (4.25a)$$

$$[D]^e = \int_{R^e} S_s [N]^T [N] \, dR \qquad (4.25b)$$

$$\{F\}^e = \int_{B^{1e}} \bar{q} [N]^T \, dB \qquad (4.25c)$$

It should be noted that the small letter s is not a "small letter subscript" as defined by section 4.4. S_S merely denotes the specific storage of the aquifer and should not be confused with the matrix $[S]$.

$[S]^T$ is the transpose of matrix $[S]$ and is given by

$$[S]^T = \begin{bmatrix} \partial N_1/\partial x_1 & \cdots & \partial N_m/\partial x_1 \\ \partial N_1/\partial x_2 & \cdots & \partial N_m/\partial x_2 \\ \partial N_1/\partial x_3 & \cdots & \partial N_m/\partial x_3 \end{bmatrix}^T \qquad (4.26)$$

$[K]$ is the hydraulic conductivity matrix,

$$[K] = \begin{bmatrix} K_{11} & K_{12} & K_{13} \\ K_{21} & K_{22} & K_{23} \\ K_{31} & K_{32} & K_{33} \end{bmatrix} \qquad (4.27)$$

$[N]$ is the shape function matrix,

$$[N] = [N_1 \text{----------} N_m] \qquad (4.28)$$

(b) Non-linear flow-element matrices

The individual element functional may be written as

$$E^e = \int_{R^e} \left[\frac{-a}{2b} \left| \frac{\partial h}{\partial \ell} \right| + \frac{2b}{3} \left\{ \left(\frac{a}{2b} \right)^2 + \left| \frac{\partial h}{\partial \ell} \right| / b \right\}^{3/2} + S_s h \frac{\partial h}{\partial t} \right] dR + \int_{B^{1e}} h \bar{q} \, dB \qquad (4.29)$$

where the second integral only applies to elements whose boundaries fall upon the B^1 boundary of the entire flow region.

Differentiating equation (4.26) with respect to h_I gives

$$\frac{\partial E^e}{\partial h_I} = \int_{R^e} \left[\frac{-a}{2b} \frac{\partial}{\partial h_I} \left(\left| \frac{\partial h}{\partial \ell} \right| \right) + \left\{ \left(\frac{a}{2b} \right)^2 + \left| \frac{\partial h}{\partial \ell} \right| / b \right\}^{1/2} \frac{\partial}{\partial h_I} \left(\left| \frac{\partial h}{\partial \ell} \right| \right) + S_s h \frac{\partial}{\partial h_I} \left(\frac{\partial h}{\partial t} \right) + S_s \frac{\partial h}{\partial t} \frac{\partial h}{\partial h_I} \right] dR \qquad (4.30)$$

$$+ \int_{B^{1e}} \bar{q} \frac{\partial h}{\partial h_I} \, dB$$

Substituting equations (4.18), (4.19) and (4.20) into equation (4.30) gives

$$\frac{\partial E^e}{\partial h_I} = {}_{R^e}\int \left[\frac{-a}{2b} + \left\{ \left(\frac{a}{2b}\right)^2 + \left|\frac{\partial h}{\partial \ell}\right| / b \right\}^{1/2} \right] \Big/ \left|\frac{\partial h}{\partial \ell}\right| \frac{\partial N_J}{\partial x_i} \frac{\partial N_I}{\partial x_i} h_J \, dR$$

$$+ {}_{R^e}\int S_s \frac{\partial h_J}{\partial t} N_J N_I \, dR \quad + {}_{B^{1e}}\int \bar{q} N_I \, dB \tag{4.31}$$

In matrix notation equation (4.31) may be written as

$$\left\{\frac{\partial E}{\partial h}\right\}^e = [G]^e \{h\}^e + [D]^e \left\{\frac{\partial h}{\partial t}\right\}^e + \{F\}^e \tag{4.32}$$

where all terms other than $[G]^e$ have been previously defined for the Darcy flow case.

The matrix $[G]^e$ is defined by

$$[G]^e = {}_{R^e}\int C \, [S]^T [S] \, dR \tag{4.33}$$

where C, the coefficient of non-linear effective hydraulic conductivity has been previously defined in equation (3.32). An alternative way of writing C is

$$C = 1 \Big/ \left[\frac{a}{2} + \sqrt{\frac{a^2}{4} + b \left|\frac{\partial h}{\partial \ell}\right|} \right] \tag{4.34}$$

where the term $\left|\frac{\partial h}{\partial \ell}\right|$ may be evaluated by the following expression

$$\left|\frac{\partial h}{\partial \ell}\right| = \left(\frac{\partial N_I}{\partial x_i} \frac{\partial N_J}{\partial x_i} h_I h_J \right)^{1/2} \tag{4.35}$$

4.5.3 Gross Matrix Formulation

Once again consider a particular instant in time.

The minimisation procedure requires the assembly of all the differentials of E^t from individual finite elements and the equating of the resulting expression to zero.

The resulting equations for the whole flow system for both Darcy and non-linear flow are respectively:

$$[\bar{G}] \{h\} + [D] \left\{\frac{\partial h}{\partial t}\right\} + \{F\} = 0 \tag{4.36}$$

and

$$[G] \{h\} + [D] \left\{\frac{\partial h}{\partial t}\right\} + \{F\} = 0 \tag{4.37}$$

where the gross matrices are obtained by summation of element matrices over all elements.

$$[\overline{G_{IJ}}] = \sum_e [\overline{G_{IJ}}]^e \qquad (4.38a)$$

$$[G_{IJ}] = \sum_e [G_{IJ}]^e \qquad (4.38b)$$

$$[D_{IJ}] = \sum_e [D_{IJ}]^e \qquad (4.38c)$$

$$\{F_I\} = \sum_e \{F_I\}^e \qquad (4.38d)$$

and

$$\{h\} = \begin{bmatrix} h_1 \\ \vdots \\ h_n \end{bmatrix} \qquad \left\{\frac{\partial h}{\partial t}\right\} = \begin{bmatrix} \frac{\partial h_1}{\partial t} \\ \vdots \\ \frac{\partial h_n}{\partial t} \end{bmatrix}$$

4.5.4 Transient flow - Solution Procedures

The time domain may be divided into a finite number of incremental time steps. A step-by-step solution routine based on mid-difference procedures is presented.

Let it be assumed that in the time interval Δt, the nodal values of $\{h\}$ vary linearly with time as shown in Figure 4.1.

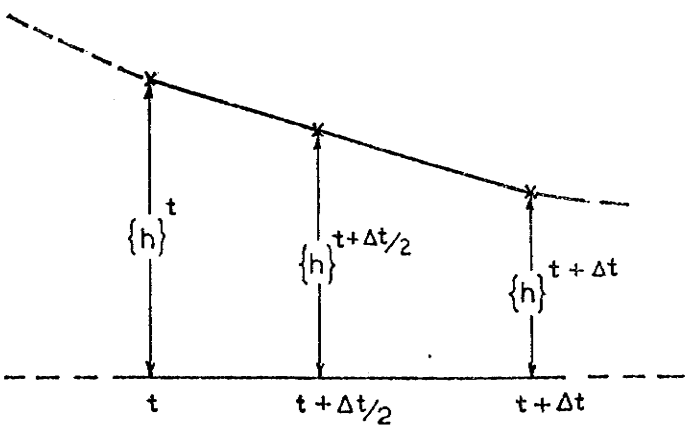

FIGURE 4.1: VARIATION OF NODAL VALUES OVER Δt

Then at the mid-point of t and t + Δ t,

$$\{h\}^{t+\Delta t/2} = \frac{1}{2}\left(\{h\}^{t} + \{h\}^{t+\Delta t}\right) \qquad (4.39a)$$

Matrices $\{F\}$ and $[G]$ may both be functions of time, and the following assumptions based on linear variation over the time step Δt will also be made,

$$\{F\}^{t+\Delta t/2} = \frac{1}{2}\left(\{F\}^{t} + \{F\}^{t+\Delta t}\right) \qquad (4.39b)$$

$$[G]^{t+\Delta t/2} = \frac{1}{2}\left([G]^{t} + [G]^{t+\Delta t}\right) \qquad (4.39c)$$

At the mid point of the time interval (t, t+ Δ t) for non-linear flow, equation 4.37) may be expressed as

$$[G]^{t+\Delta t/2}\{h\}^{t+\Delta t/2} + [D]\left(\frac{\{h\}^{t+\Delta t} - \{h\}^{t}}{\Delta t}\right) + \{F\}^{t+\Delta t/2} = 0 \qquad (4.40)$$

Rearranging equation (4.39a),

$$\{h\}^{t+\Delta t} = 2\{h\}^{t+\Delta t/2} - \{h\}^{t} \qquad (4.41)$$

Substituting equation (4.41) into equation (4.40), results in

$$\left(\frac{\Delta t}{2}[G]^{t+\Delta t/2} + [D]\right)\{h\}^{t+\Delta t/2} + \frac{\Delta t}{2}\{F\}^{t+\Delta t/2} = [D]\{h\}^{t} \qquad (4.42)$$

Equations (4.41) and (4.42) provide suitable recurrence relations for solution of the initial value problem. The solution starts at initial time, t = 0, and proceeds in a step-wise manner. At the beginning of the first time step, the nodal head values $\{h\}^{t=0}$ are specified by the initial conditions.

These values are substituted for $\{h\}^{t}$ in equation (4.42) and used to solve for $\{h\}^{t+\Delta t/2}$ which may be substituted in equation (4.41) to evaluate $\{h\}^{t+\Delta t}$, the head values at the end of the time step. The

currently obtained head values at the end of a time step may then be used as the initial head values $\{h\}^t$ for the following time step.

For Darcy flow, $[G]^{t+\Delta t/2}$ in equation (4.42) is replaced by $[\bar{G}]$ which is invariant in time,

$$\left(\frac{\Delta t}{2}[\bar{G}]+[D]\right)\{h\}^{t+\Delta t/2} + \frac{\Delta t}{2}\{F\}^{t+\Delta t/2} = [D]\{h\}^t \qquad (4.43)$$

For steady state flow problems, equation (4.42) reduces to

$$[G]\{h\} + \{F\} = 0 \qquad (4.44)$$

subject to the prevailing boundary conditions.

4.5.5 Iterative Solution of Non-linear Algebraic Equations

The set of simultaneous equations resulting from flow based on Darcy's law are linear (equation 4.43) and may be solved by direct Gaussian elimination.

For non-linear flow, the analysis results in a system of non-linear equations as described by equation (4.42).

The coefficients of matrix $[G]^{t+\Delta t/2}$ are dependent upon the unknown values of head $\{h\}^{t+\Delta t/2}$ and as such they are not known a priori, but must be evaluated by an iterative solution approach which will now be outlined.

To accelerate convergence of the iterative procedure, an over-relaxation scheme is employed. It is convenient to drop the $t + \Delta t/2$ superscript and replace it by another superscript k which denotes an iteration number.

An initial solution $\{h\}^{k=0}$ is found assuming Darcy flow and solving equation (4.43) wherein the evaluation of matrix $[\bar{G}]$ is made by assuming the hydraulic conductivity $K = 1/a$. The values of

$\{h\}^{k=0}$ thus obtained are used to evaluate matrix $[G]^{k=0}$ and the resulting equation (4.42) may be solved for more accurate values of $\{h\}^{k+1}$ by direct Gaussian elimination.

Before starting the next iteration, the following over-relaxation formula is used to modify $\{h\}^{k+1}$,

$$\{h\}^{k+1} = \{h\}^{k} + \alpha\left(\{h\}^{k+1} - \{h\}^{k}\right) \qquad (4.45)$$

where α is the over-relaxation factor, having a value between 1 and 2. It was found that a value of α between 1.5 and 1.9 gave fast convergence with only 4 or 5 iterations being required to achieve satisfactory results. In general, the optimum value of α tends to increase with the total number of equations solved.

The modified values of $\{h\}^{k+1}$ which become $\{h\}^{k}$ for the next iteration are used to re-evaluate $[G]^{k}$ and equation (4.42) can again be solved for more accurate values of $\{h\}^{k+1}$.

This process is repeated until the change in successive solutions is within defined acceptable limits. The iteration scheme is said to have converged when the following criterion is satisfied,

$$\Delta h_{max} = \max \left| h^{k+1} - h^{k} \right| \leqslant \mathcal{E}_H \qquad (4.46)$$

where Δh_{max} denotes the maximum absolute difference in nodal head values between successive iterations and $\mathcal{E}_H$ is the prescribed head tolerance.

The accuracy of finite element solutions improved as the prescribed head tolerance was reduced. However, negligible improvement in solution accuracy was achieved by choosing values of $\mathcal{E}_H$ less than $1/200^{th}$ of the well drawdown.

4.5.6 Well Boundary Conditions for Transient Flow

In solving problems of transient flow to a pumped well, two types of well boundary condition are possible.

If the well is pumped in such a way that the water level in the well remains constant, a constant prescribed head condition will result. In establishing such a condition, the fluid level in the well is suddenly lowered and maintained at a certain elevation throughout the pumping operation. This condition occurs frequently in the oil industry but only rarely in water well applications.

A pumping operation that is more practical, easier to control, and thus widely used in field testing of groundwater aquifers is the case where the total rate of discharge from the well is kept constant throughout the pumping period. Under such circumstances the condition of constant prescribed flow rate must be satisfied at the well boundary. In the procedure described in this section the well discharge need not necessarily be constant, but may vary with time.

(i) Constant Prescribed Head Condition

The treatment of a constant prescribed head condition at the well boundary has been described for Darcy flow by Javandel and Witherspoon (1968). A similar procedure will now be presented for non-linear flow.

Consider the typical pumped well shown in Figure 4.2.

The total number of nodes in the flow region is 'n'. Only nodes which fall on the portion of the well boundary that is screened will have head values that are constant with time and equal to the water level above the datum plane, H. Let the number of nodes situated on

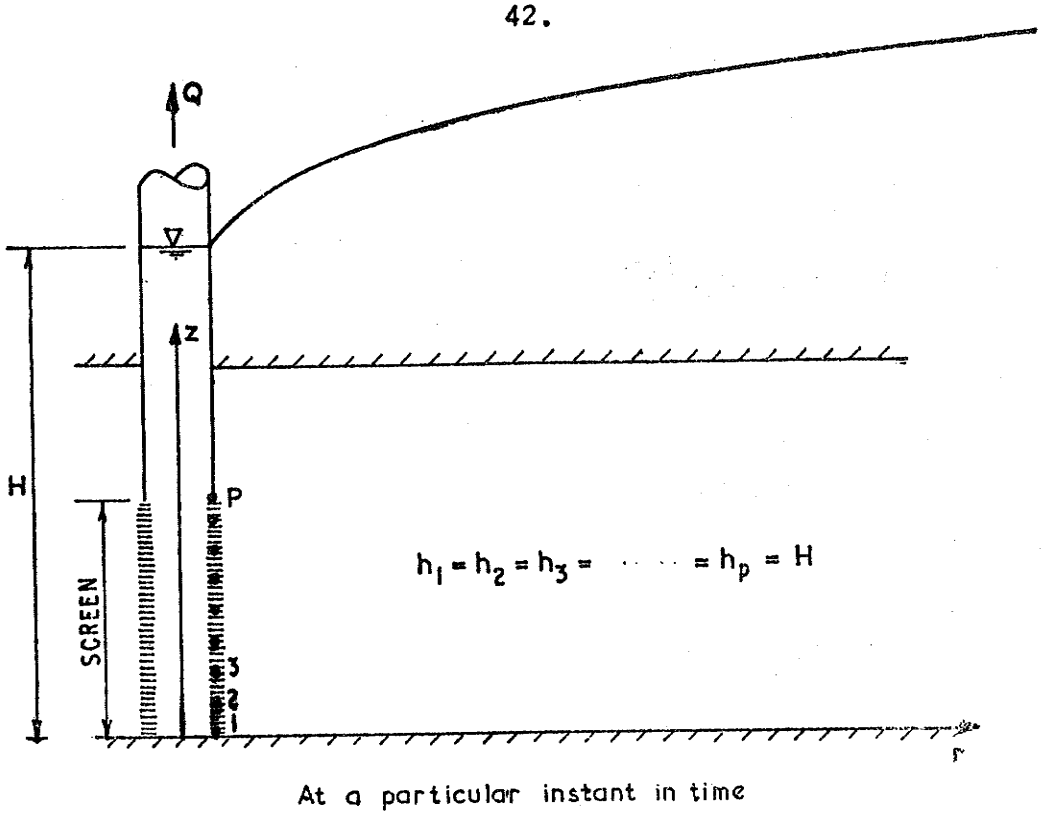

FIGURE 4.2: TYPICAL PUMPED WELL BOUNDARY CONDITIONS

the well screen be 'p'.

By dropping the $t + \frac{\Delta t}{2}$ superscript, equation (4.42) may be written in the following matrix partition form

$$\left(\frac{\Delta t}{2}\begin{bmatrix} G_{\alpha\alpha}\ (p\times p) & G_{\alpha\beta}\ (p\times(n-p)) \\ G_{\beta\alpha}\ ((n-p)\times p) & G_{\beta\beta}\ ((n-p)\times(n-p)) \end{bmatrix} + \begin{bmatrix} D_{\alpha\alpha}\ (p\times p) & D_{\alpha\beta}\ (p\times(n-p)) \\ D_{\beta\alpha}\ ((n-p)\times p) & D_{\beta\beta}\ ((n-p)\times(n-p)) \end{bmatrix}\right)\begin{Bmatrix} h_\alpha\ (p\times 1) \\ h_\beta\ ((n-p)\times 1) \end{Bmatrix}$$

$$+\frac{\Delta t}{2}\begin{Bmatrix} F_\alpha\ (p\times 1) \\ F_\beta\ ((n-p)\times 1) \end{Bmatrix} = \begin{bmatrix} D_{\alpha\alpha}\ (p\times p) & D_{\alpha\beta}\ (p\times(n-p)) \\ D_{\beta\alpha}\ ((n-p)\times p) & D_{\beta\beta}\ ((n-p)\times(n-p)) \end{bmatrix}\begin{Bmatrix} h_\alpha\ (p\times 1) \\ h_\beta\ ((n-p)\times 1) \end{Bmatrix}^t \qquad (4.47)$$

The prescribed head condition requires

$$\{h_\alpha\} = \{h_\alpha\}^{t+\Delta t/2} = \{h_\alpha\}^{t} = H \qquad (4.48)$$

Now equation (4.47) may be simplified to:

$$\left(\frac{\Delta t}{2}[G_{\beta\beta}]+[D_{\beta\beta}]\right)\{h_\beta\}+\frac{\Delta t}{2}[G_{\beta\alpha}]\{h_\alpha\}+\frac{\Delta t}{2}\{F_\beta\}=[D_{\beta\beta}]\{h_\beta\}^{t} \qquad (4.49a)$$

and

$$\left(\frac{\Delta t}{2}[G_{\alpha\beta}]+[D_{\alpha\beta}]\right)\{h_\beta\}+\frac{\Delta t}{2}[G_{\alpha\alpha}]\{h_\alpha\}+\frac{\Delta t}{2}\{F_\alpha\}=[D_{\alpha\beta}]\{h_\beta\}^{t} \qquad (4.49b)$$

Equation (4.49a) represents a set of (n-p) non-linear algebraic equations which may be solved by the iterative procedure described in Section 4.5.5. If required, the values of the flux at the nodal points along the well screen can be calculated by substituting the final solution values of $\{h_\beta\}$ into equation (4.49b) and solving for $\{F_\alpha\}$.

The total discharge from the aquifer into the well is then given by

$$Q = \sum_{\alpha=1}^{P} F_\alpha \qquad (4.50)$$

(ii) Prescribed Flow Rate Condition

Available solutions for the controlled discharge pumping operation require that the total rate of discharge be maintained at a constant value over the period of pumping. For these conditions, Javandel and Witherspoon (1968) have presented detailed procedures applicable to numerical solutions for Darcy flow. They treated both the simple case where the total discharge is uniformly distributed along the well screen, and the more general case of non-uniform flux distribution.

A more general procedure applicable to non-linear flow will be presented which merely requires that the variation in time of the total rate of discharge be known over the pumping period. The flux distribution along the well boundary is rarely uniform and the prescribed flow

rate condition for non-uniform flux will be treated by an iterative process for each time step.

Previous solutions have assumed that the discharge pumped is met fully by the aquifer. For short times after the start of pumping, this can be quite misleading. The pump will draw mainly from the water standing within the well during the initial stages of pumping. As time increases, the proportion of the total flow discharge contributed by water standing within the well decreases whilst the discharge supplied by the aquifer increases. The effects of well storage will be included in the analysis.

Again consider the typical well shown in Figure 4.2. When the flow rate is prescribed, the water level in the well will not be constant but must vary with time.

The head values of nodes along the well screen at time $t+\Delta t/2$ may be written as

$$h_1^{t+\Delta t/2} = h_2^{t+\Delta t/2} = \text{-------} = h_p^{t+\Delta t/2} = H^{t+\Delta t/2} \qquad (4.51)$$

where $H^{t+\Delta t/2}$ is the unknown height of the water level in the well at time $t + \Delta t/2$.

For a particular time step, let t_{n+1} and t_n denote the current and preceding times respectively, and let the mid-time be denoted by $t_{n+\frac{1}{2}}$ where

$$t_{n+\frac{1}{2}} = \frac{1}{2}\left(t_{n+1} + t_n\right) \qquad (4.52)$$

The total discharge is assumed to vary linearly within each time step. The mid-time value of the prescribed discharge $\bar{Q}\ (t_{n+\frac{1}{2}})$ can be written in terms of the current and preceding values as

$$\bar{Q}\left(t_{n+\frac{1}{2}}\right) = \frac{1}{2}\left(\bar{Q}(t_{n+1}) + \bar{Q}(t_n)\right) \qquad (4.53)$$

The level of water in the well, $H(t_{n+\frac{1}{2}})$, required to satisfy the total flow rate $\bar{Q}(t_{n+\frac{1}{2}})$ may be found by the following iterative scheme.

For the first iteration, j = 1, an initial estimate of the value of $H(t_{n+\frac{1}{2}})$ is made from

$$H^1(t_{n+\frac{1}{2}}) = \left[H(t_n) - H(t_{n-1})\right]\left[\log\left(t_{n+\frac{1}{2}}/t_n\right)\right] \Big/ \left[\log\left(t_n/t_{n-1}\right)\right] + H(t_n) \quad (4.54)$$

for $n \gg 2$.

The initial estimate for the first two time steps is made from

$$H^1(t_{n+\frac{1}{2}}) = H(t_n) + \Delta H \quad (4.55)$$

for n = 0, 1

where the value of ΔH is selected from experience.

The discharge contributed by water standing within the well is assumed constant over the time step. If $Q_w{}^j(t_{n+\frac{1}{2}})$ denotes the discharge derived from well storage during the time step, then

$$Q_w^j(t_{n+\frac{1}{2}}) = \lambda(t)\left[H^j(t_{n+\frac{1}{2}}) - H(t_n)\right] \quad (4.56a)$$

where $\lambda(t)$ is a constant for the time step given by

$$\lambda(t) = -2\pi r_w^2 \Big/ \left(t_{n+1} - t_n\right) \quad (4.56b)$$

and r_w is the well radius.

The trial value of $H^j(t_{n+\frac{1}{2}})$ is used in solving equations (4.49a) and (4.49b) for the unknown nodal heads throughout the region and the flux values at the well respectively. The discharge contributed by the aquifer $Q_a{}^j(t_{n+\frac{1}{2}})$ is then obtained by summation of the nodal flux values along the well screen (see equation 4.50).

The total discharge $Q^j(t_{n+\frac{1}{2}})$ given by

$$Q^j(t_{n+\frac{1}{2}}) = Q_w^j(t_{n+\frac{1}{2}}) + Q_a^j(t_{n+\frac{1}{2}}) \quad (4.57)$$

may be compared with the prescribed discharge $\bar{Q}(t_{n+\frac{1}{2}})$.

$$\text{If } \left| \left\{ Q^{j}(t_{n+\frac{1}{2}}) - \bar{Q}(t_{n+\frac{1}{2}}) \right\} \Big/ \bar{Q}(t_{n+\frac{1}{2}}) \right| > \varepsilon_Q \tag{4.58}$$

where ε_Q is the prescribed tolerance for the discharge ratio, a new trial head value is calculated from

$$H^{2}(t_{n+\frac{1}{2}}) = H(t_n) + \left\{ H^{1}(t_{n+\frac{1}{2}}) - H(t_n) \right\} \bar{Q}(t_{n+\frac{1}{2}}) \Big/ Q^{1}(t_{n+\frac{1}{2}}) \tag{4.59}$$

Solution for the unknown nodal head and flux values is then repeated and the aquifer discharge recalculated, added to the new well storage discharge and the total discharge retested for convergence in equation (4.58).

If convergence is still not obtained, the following formula is applied

$$H^{j+1} = H^{j} + \left(\bar{Q} - Q^{j} \right) \Big/ \left[\lambda(t) + \left(Q_a^{j} - Q_a^{j-1} \right) \Big/ \left(H^{j} - H^{j-1} \right) \right]_{\text{for } j \geq 3} \tag{4.60}$$

where the $(t_{n+\frac{1}{2}})$notation has been dropped from all terms in which it occurs.

The process is repeated until a value of water level in the well $H^{j}\,(t_{n+1})$ is found for which the prescribed total rate of flow $\bar{Q}\,(t_{n+1})$ is satisfied.

The above iteration procedure was found to give quite satisfactory results when a discharge ratio tolerance ε_Q of 5 per cent was chosen. For earlier times the convergence criterion was satisfied after a few iterations. For later times, convergence often resulted after only one iteration.

The effects of well storage may be excluded from the analysis merely by equating $\lambda(t)$ to zero.

The same general approach may be adopted in treating the sim-

pler case of Darcy flow. The nodal flux values at the well used to evaluate the aquifer discharge are more simply found by solving the sets of linear equations formed when $[G]$ is replaced by $[\bar{G}]$ in equations (4.49a) and (4.49b). For the Darcy flow case convergence to the prescribed discharge is guaranteed within three iterations for all time steps irrespective of the choice of $\mathcal{E}_Q$ (assuming that the chosen tolerance is not so small that computer roundoff errors affect the results).

4.5.7 Elimination Scheme - Solution of a System of Linear Equations

For Darcy flow the resulting set of simultaneous equations are linear (equation 4.43). Consideration of non-linear flow behaviour leads to a system of non-linear algebraic equations which can be reduced to a set of linear equations by the iterative technique described in Section 4.5.5.

A banded Gaussian elimination scheme is used to solve for the unknown nodal head values in the resultant linear system of equations. The scheme takes into account the banded character and symmetry of the gross matrices $[G]$ or $[\bar{G}]$ and $[D]$. The process of elimination is achieved by reducing the system of equations to an equivalent triangular form through a series of arithmetic operations on the equation coefficients. Then starting from the last equation, the last unknown is solved and the remaining unknowns are found by back substitution in the preceding equations.

Due to symmetry of matrices $[G]$ or $[\bar{G}]$ and $[D]$, it is only necessary to operate on the terms in their upper triangles. By numbering the nodes of the entire flow region consecutively from bottom to top of the aquifer along vertical lines of the discretisation mesh, the

abovementioned symmetric gross matrices are also arranged in a compact banded form. The half-band width of each matrix is computed as the length between the diagonal term and the last non-zero term in each row. The $[G]$ or $[\bar{G}]$ and $[D]$ matrices are converted into gross vectors by stringing together the half-bands of all successive rows. This conversion greatly reduces the storage requirements of the gross matrices. Furthermore, the solution time is reduced due to the smaller number of arithmetic operations required.

4.6 Finite Element Analysis of Steady State Well Flow in Unconfined Aquifers

In this section, the finite element formulation for general three-dimensional steady state flow to a well in an unconfined aquifer is presented. The task is greatly simplified since much of the formulation previously presented in Section 4.5 dealing with confined aquifer flows is equally applicable to the unconfined aquifer problems. In fact, further specific attention is only required to provide a method of locating the a priori unknown free surface and so satisfy the free surface, B^f, boundary conditions discussed in Section 3.4.4. The effects of a capillary fringe above the free surface are neglected.

The iteration scheme by which the finite element solution of the problem is formulated may be described as follows:-

Step (1): An initial trial free surface is assumed.

Step (2): The bounded flow region so defined is divided into a network of finite elements. Individual element matrices are generated and assembled to obtain the gross matrix equations for the

flow behaviour within the region. The procedures employed are similar to those described for confined aquifers in Sections 4.5.1, 4.5.2 and 4.5.3. Since only steady flow is being considered, terms involving the time dimension are ignored. The resulting equations for Darcy and non-linear flow are respectively

$$[\bar{G}]\{h\} + \{F\} = 0 \qquad (4.61)$$

$$[G]\{h\} + \{F\} = 0 \qquad (4.62)$$

where all matrix terms have been previously defined. The head values throughout the entire trial flow region are found by solving equations (4.61) or (4.62) by the methods outlined in Sections 4.5.5 and 4.5.7. Treatment of the boundary conditions along portions B^c, B^2 and B^s has been described in Section 4.3.

Step (3): The trial free surface position is checked to ensure that

$$|h - z| \leqslant \epsilon_f \quad \text{on} \quad B^f \qquad (4.63)$$

where ϵ_f is the prescribed tolerance of the free surface height. If condition (4.63) is not satisfied everywhere upon the free surface, then a new trial free surface is generated according to

$$z_{k+1} = z_k + w[h_k - z_k] \qquad (4.64)$$

where subscript k denotes the k-th iteration and w is an over-relaxation factor.

Solution for the flow region defined by the new trial free surface proceeds from Step 2.

Step (4): The cycle is continued until the condition of equation (4.63) is satisfied. At this stage the head distribution throughout the aquifer satisfies all boundary conditions including those specifically

given in equations (3.38) and (3.39) for the conditions along the free surface boundary portion B^f. Once the nodal head values throughout the finalised flow region have been found the discharge flux values at the well and hence total well discharge may be evaluated.

It was found that values of ω between 1.0 and 1.4 gave fast convergence, only 3 or 4 iterations being required to achieve satisfactory results. Difficulties arose with higher values of ω due to over-adjustment of the free surface.

Solution accuracy improved as the prescribed value of ϵ_f was reduced. High accuracy solutions were achieved with values $0.005h_o < \epsilon_f < 0.001\ h_o$. h_o is the undisturbed original height of the water table above the aquifer base.

4.7 Finite Elements for Axisymmetric Well Flow Problems

In previous sections the finite element formulation has been presented as a general procedure applicable to three-dimensional well flow problems. The flow to a well in many practical instances may be described as being axisymmetric. For such cases, the element matrix formulation may be simplified by employing the cylindrical co-ordinate system (r, z). The entire flow region may be subdivided into a finite number of ring elements concentric about the vertical axis of the well. The elements are readily generated by revolving plane elemental sections about the z axis. A typical triangular ring element is shown in Figure 4.3.

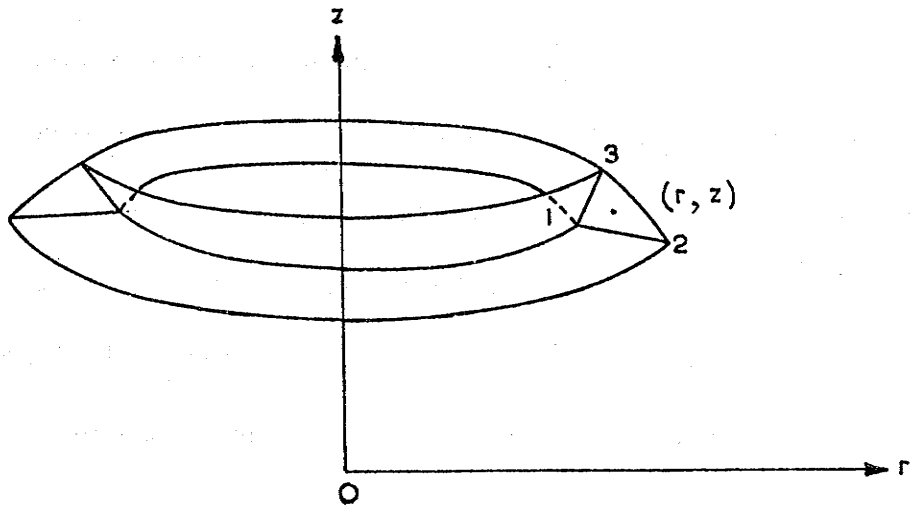

FIGURE 4·3: A TRIANGULAR RING ELEMENT

The evaluation of element matrices for the ring elements formed by revolving the various plane figures shown in Figure 4.4 is presented in Appendix 1.

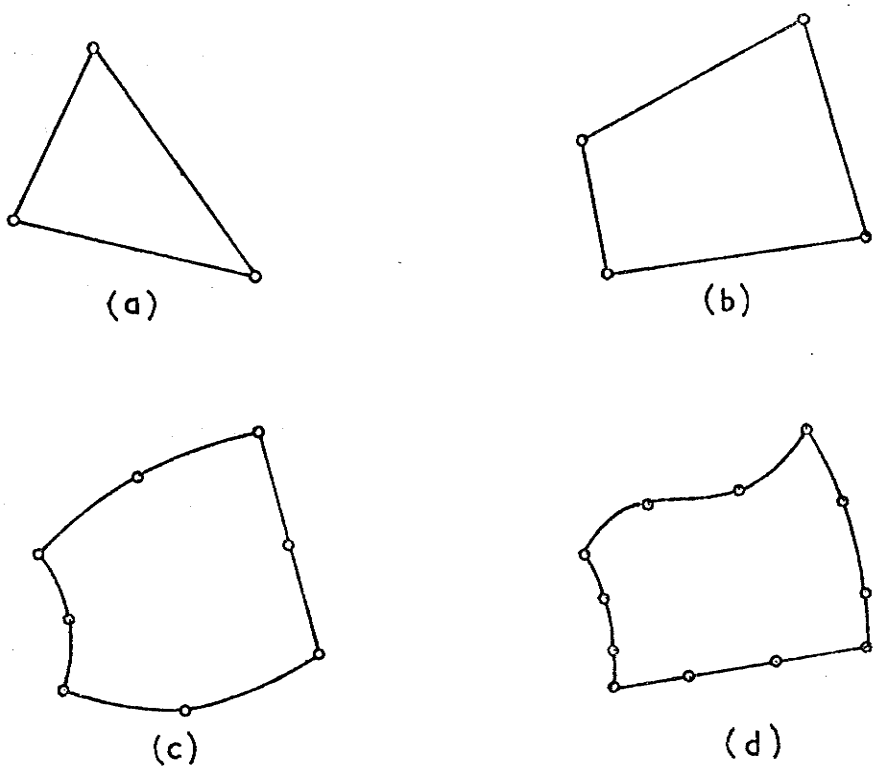

FIGURE 4·4: FINITE ELEMENT PLANE SECTIONS

The simple linear triangular element has been used extensively in the solution of various field problems reported in the literature. The increasingly higher order elements shown in Figures 4.4(b), (c) and (d) belong to the family of curved isoparametric quadrilaterals described by Ergatoudis et al (1968).

Trials were undertaken to establish the most suitable elements for use in the axisymmetric well flow problems to be investigated by the author. The results are discussed below.

(i) Accuracy

In well flow problems, the network nodal spacing at the well, Δr_1, was found to be the controlling factor in determining the accuracy of a particular finite element solution. For coarse nodal networks, considerable improvement in solution accuracy resulted from using higher order elements. However, for fine nodal networks in which Δr_1 was equal to or less than the well diameter, very little improvement in accuracy was achieved by employing higher order elements.

(ii) Equation solution time

In the banded Gaussian elimination scheme described in Section 4.5.7 for the solution of the resulting set of simultaneous equations, the solution time is approximately proportional to nb^2 where n is the total number of equations (network nodes) and b is the band width within the equivalent triangular form of the assembled gross matrix (Zienkiewicz (1971)). For reasonably accurate finite element solutions, the overall effect of using higher order elements was to increase the equation solution time, no doubt due to the larger band widths encountered. For equal nodal spacing at the well ($\Delta r_1 \leqslant$ well

diameter) the solution of equations was found to take approximately twice as long when using parabolic or cubic quadrilateral elements as when using linear quadrilateral or triangular elements.

(iii) Element matrix generation

A factor militating against the use of higher order elements is the disproportionate increase in computer time required in deriving the elemental matrices. The evaluation of triangular element matrices is relatively direct and requires little computer time. In contrast, exact integration of the expressions for the matrices of general distorted quadrilateral elements is not feasible and numerical integration must be used. The procedures for numerical evaluation of the elemental matrices by use of the Gaussian quadrature formula have been described by Zienkiewicz (1971). The formulation of a quadrilateral element matrix by application of the 9-point Gaussian quadrature formula was found to take about 5 times longer than the generation of a triangular element matrix. For the special case where the quadrilateral element becomes a rectangular element, the need for numerical Gaussian integration was eliminated (see Appendix 1.3). The time for generation of a rectangular element matrix was found to be only slightly more than that for a linear triangular element matrix.

(iv) Data preparation

Since a wide range of well flow problems was to be examined, it was decided quite early that automatic mesh generation subroutines should be included in the finite element computer programs to be developed. Automatic generation of finite element networks nullifies

one of the major advantages so commonly afforded by the use of higher order elements, viz. the considerable reduction in data preparation.

(v) Network refinement

Refinement of the finite element mesh in regions known to be critical is easily accomplished by using simple triangular elements, whereas certain difficulties may be encountered with quadrilateral elements due to the introduction of floating nodes (Barry (1974)).

In almost every aspect pertaining to programming efficiency, the simple linear triangular and rectangular ring elements were superior to the higher order elements for the axisymmetric well flow problems under investigation. The rectangular element was marginally superior to the triangular element in regard to solution accuracy and ease of automatic mesh generation but was marginally inferior in regard to equation solution and matrix formulation times. In the numerical solution of well flow problems to follow, finite element networks incorporating only linear rectangular and triangular ring elements are used to discretize the flow domain. For confined aquifer problems, the bulk of the mesh is composed of rectangular ring elements and triangular ring elements are only used in areas where the mesh gradation changes (see Figure 5.6). For unconfined aquifers, triangular ring elements are used exclusively (see Figure 5.27).

In general, analytical solutions can be found for problems of one-dimensional radial flow towards a well. Although the necessity for numerical solutions of such problems does not exist, one-dimensional finite element solutions may be usefully compared with the exact an-

alytical expressions as a check upon the more general three-dimensional finite element formulation. The evaluation of matrices for one-dimensional isoparametric ring elements is presented in Appendix 1.4.

5. Solutions to Typical Steady Well Flow Problems

5.1 General

A number of computer programs were developed by applying the theory and finite element formulation presented in the preceding chapters. These programs, coded in FORTRAN IV language were used to solve a wide range of steady state well flow problems which were previously insoluble by analytical techniques. The solutions presented in this chapter incorporate Darcy and non-linear behaviour for flow to wells in confined and unconfined aquifers subject to a variety of different conditions.

The grouping of the relevant system variables into dimensionless parameters has been used extensively in simplifying the presentation of results.

Many of the results of this chapter form the basis for the detailed discussion given in Chapter 8 regarding the hydraulic aspects of well design.

The finite element computer programs were verified by comparison with either known analytical solutions, analogous electrolytic tank results, or experimental results from a large scale sandbox type model.

Guide lines for the selection of a finite element network to solve a particular problem within certain limits of accuracy are given.

In all cases the aquifer material is assumed to be isotropic unless specifically stated otherwise. For reasons previously declared, non-linear anisotropic behaviour has not been considered in this

thesis. Anisotropic Darcy flow problems may be treated by the commonly employed techniques of co-ordinate transformation to an equivalent isotropic problem.

5.2 Fully Screened Well in an Homogeneous Confined Aquifer

5.2.1 General

Consider the steady state behaviour of a well fully screened through the entire thickness of a confined aquifer being pumped at a discharge Q as shown in Figure 5.1. The flow will be radial one-dimensional everywhere.

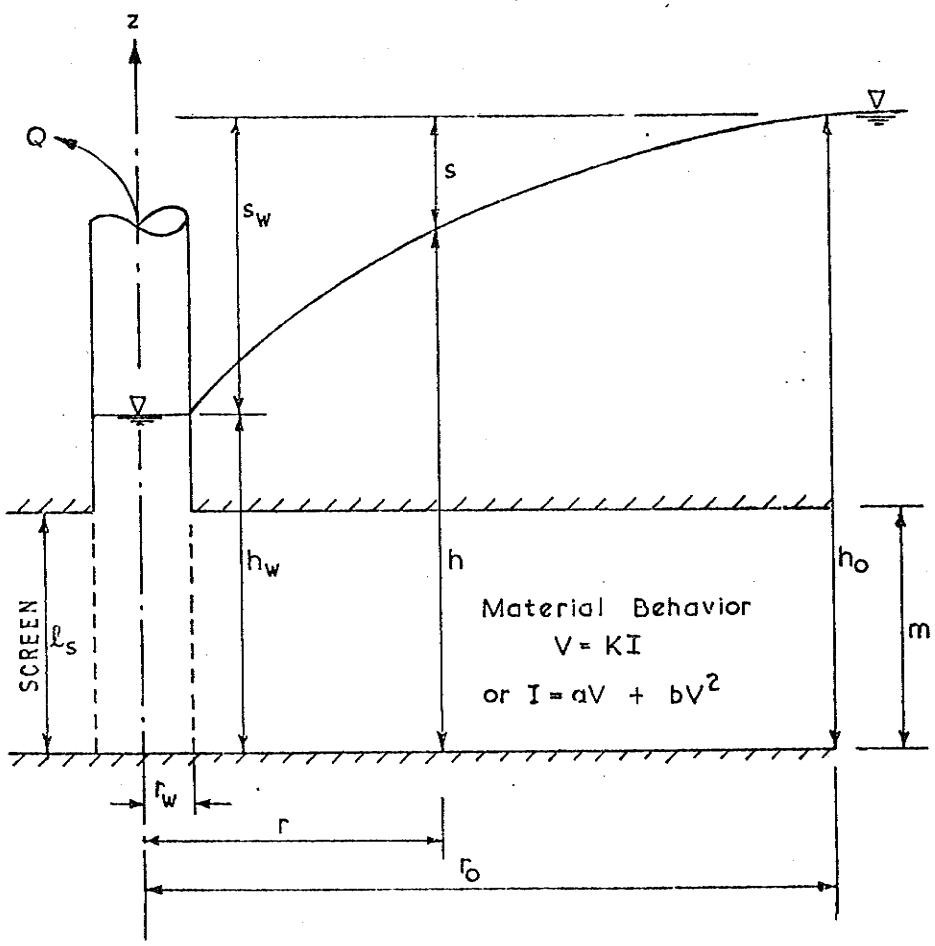

FIGURE 5·1: FULLY SCREENED WELL IN A CONFINED AQUIFER

If the flow through the aquifer material obeys Darcy's law then the established Thiem equation accurately describes the behaviour of the system,

$$Q = 2\pi K m (h_o - h) \Big/ \ln(r_o/r) \qquad (5.1)$$

where K is the hydraulic conductivity defined by Darcy's law,

$$V = -K \frac{dh}{dr} \qquad (5.2)$$

Engelund ((1953), p.49-53)first presented an analytical expression for the well discharge-drawdown relationship for a system in which both Darcy and non-linear flow (as described by the Forchheimer equation) could occur.

In Chapter 2 a Forchheimer relationship was shown to be a good representation of the non-linear material flow behaviour which occurs when the upper limits of validity of Darcy's law are exceeded. A single Forchheimer non-linear expression was shown to accurately predict the flow behaviour over a wide range of velocities including those low enough to be normally described by Darcy's law.

In a manner similar to that presented by Engelund, it can be shown that the radial distribution of drawdown for wholly non-linear Forchheimer flow is given by,

$$s = h_o - h = \frac{aQ}{2\pi m} \ln(r_o/r) + b\left(\frac{Q}{2\pi m}\right)^2 \left(\frac{1}{r} - \frac{1}{r_o}\right) \qquad (5.3)$$

where a, b are the Forchheimer equation coefficients relating velocity and hydraulic gradient,

$$-\frac{dh}{dr} = aV + bV^2 \qquad (5.4)$$

5.2.2 Dimensionless Parameters for Non-Linear Flow

Equation (5.3) may be rearranged to yield

$$\frac{2\pi m s}{aQ} = \ln(\tau_0/\tau) + \frac{bQ}{a2\pi m \tau_0}\left(\frac{\tau_0}{\tau} - 1\right) \qquad (5.5)$$

In equation (5.5) the radial distribution of drawdown is fully described by the use of three dimensionless terms, i.e.

$$\phi\left\{\frac{2\pi m s}{aQ}, \frac{\tau}{\tau_0}, \frac{bQ}{a2\pi m \tau_0}\right\} = 0 \qquad (5.6)$$

where ϕ indicates the existence of a function.

From equation (5.5) the well drawdown-discharge relationship may be written as

$$\frac{2\pi m s_w}{aQ} = \frac{2\pi m}{aQ}(h_0 - h_w) = \ln(\tau_0/\tau_w) + \frac{bQ}{a2\pi m \tau_0}\left(\frac{\tau_0}{\tau_w} - 1\right) \qquad (5.7)$$

Applying the rules of dimensional analysis for combining terms, it can be shown that the following alternative sets of dimensionless terms may be used to describe the well discharge-drawdown relationship for one-dimensional non-linear flow.

$$\phi\left\{\frac{2\pi m s_w}{aQ}, \frac{\tau_0}{\tau_w}, \frac{bQ}{a2\pi m \tau_0}\right\} = 0 \qquad (5.8a)$$

$$\phi\left\{\frac{2\pi m s_w}{aQ}, \frac{\tau_0}{\tau_w}, \frac{bQ}{a2\pi m \tau_w}\right\} = 0 \qquad (5.8b)$$

$$\phi\left\{\frac{2\pi m s_w}{aQ}, \frac{\tau_0}{\tau_w}, \frac{b s_w}{a^2 \tau_w}\right\} = 0 \qquad (5.8c)$$

It is important to note that the non-linear material characteristics (a and b) are not isolated in a dimensionless term excluding all other variables. Rather, the measure of degree of non-linearity is in terms of $\frac{bs_w}{a^2\tau_w}$ or $\frac{bQ}{a2\pi m \tau_w}$. The importance of these terms is emphasised in Chapter 8.

A very useful dimensionless term may be found to replace

$\frac{2\pi m s_w}{aQ}$ in the following manner

$$\frac{2\pi m s_w}{aQ} = \frac{2\pi m s_w}{a \ln(r_o/r_w)} \times \frac{\ln(r_o/r_w)}{Q} = \frac{Q_T}{Q} \ln(r_o/r_w) \quad (5.9)$$

where Q_T would be the discharge from the well if fully screened and the flow behaviour was fully described by Darcy's law. Q_T will be given by the Thiem equation,

$$Q_T = 2\pi K m s_w / \ln(r_o/r_w) \quad (5.10a)$$

with $K = 1/a$ (5.10b)

(Note: At low flow velocities the bV^2 term of the Forchheimer equation (equation 5.4) becomes negligible and the Forchheimer equation becomes Darcy's law with $K = 1/a$).

Combining equations (5.8c), (5.9), (5.10a) and (5.10b) gives

$$\phi\left\{ \frac{Q}{Q_T}, \frac{r_o}{r_w}, \frac{b s_w}{a^2 r_w} \right\} = 0 \quad (5.11)$$

Equation (5.11) represents a most useful grouping of dimensionless terms. Q/Q_T is a measure of the deviation from Darcy flow behaviour for a specified geometry (r_o/r_w) due to a specified degree of non-linearity as measured by the term $\frac{b s_w}{a^2 r_w}$

For one dimensional non-linear flow, the variation of Q/Q_T with $bs_w/a^2 r_w$ for different specific values of r_o/r_w is presented in Figure 5.2. The evaluation of the curves is based on direct solution of equation (5.7) in the form of equation (5.8a) and the subsequent combination and conversion of the dimensionless terms to the more appropriate set used in Figure 5.2 and described by equation (5.11).

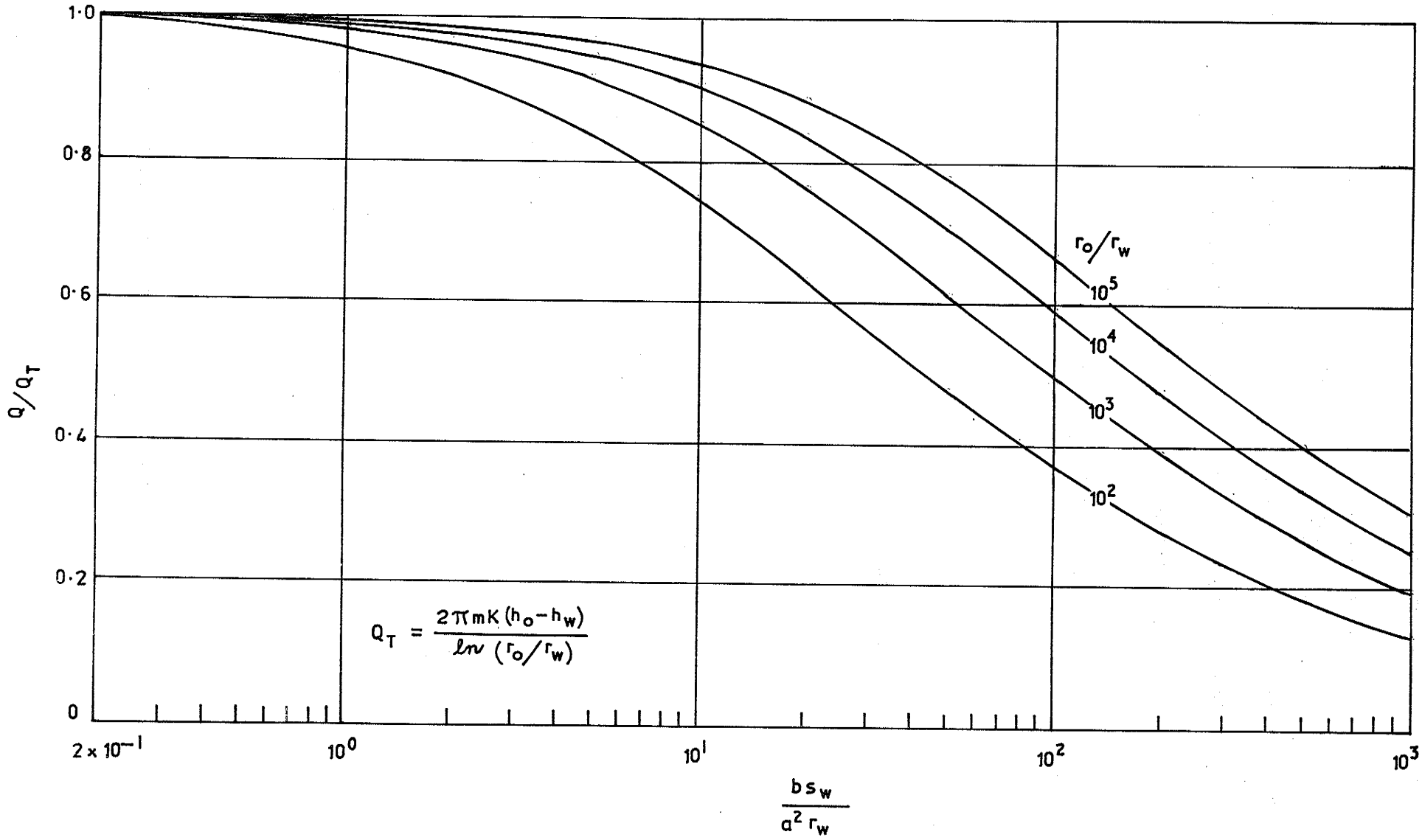

FIGURE 5·2: EFFECT OF NON-LINEAR FLOW ON WELL DRAWDOWN-DISCHARGE RELATIONSHIP FULLY SCREENED CONFINED AQUIFER

5.2.3 Non-linear Flow. Finite Element Solution

To verify the finite element analysis of the flow problem, four steady flow cases as described below were solved using a finite element program incorporating three noded one-dimensional isoparametric ring elements.

Problem Data for Steady Non-linear Flow to a Fully Screened Well in a Confined Aquifer.				
Well radius, r_w = 1 Radius of Influence, r_o = 100 Aquifer Thickness, m = 10				
Problem No.	Material Non-linear Flow Constants a	b	Well Discharge Q	$\frac{bQ}{a2\pi m r_o}$
1	1	0	62.83	0 (Darcy)
2	1	1	62.83	0.01
3	1	5	62.83	0.05
4	1	10	62.83	0.10

A finite element network similar to Figure 5.3 consisting of 6 elements and 13 nodes was used to solve the four problems. The analytical solutions based on equation (5.5) for the same four problems were evaluated.

Figure 5.4 shows the comparison of the finite element and the analytical solutions for the dimensionless radial distribution of drawdown. It can be seen that excellent agreement between the two solutions was achieved.

5.2.4 One Dimensional Finite Element Network Selection

A general one-dimensional finite element network is shown in Figure 5.3. As shown, the one-dimensional flow region is divided

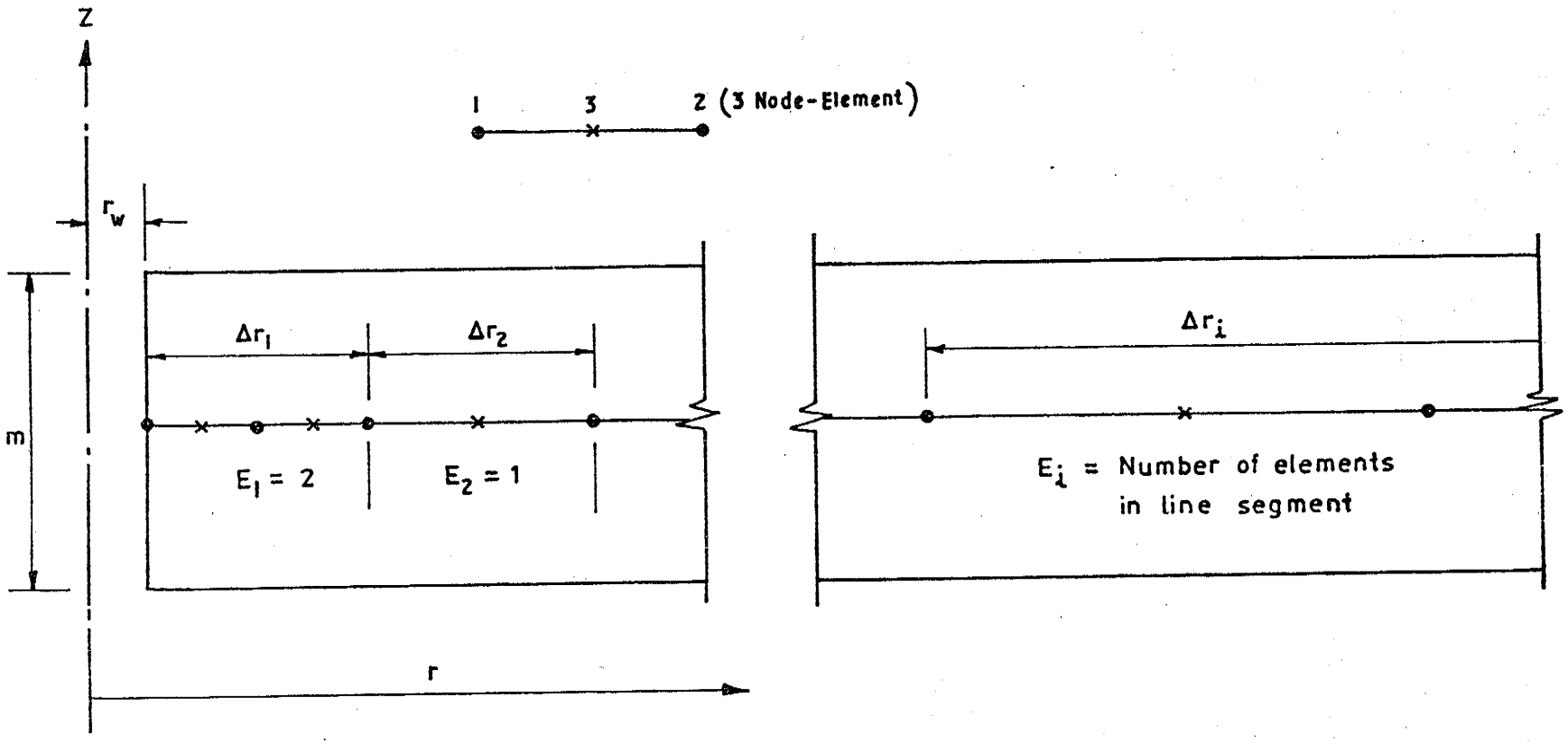

Number of Elements $= \sum E_i$

Number of Nodes $= 2\left(\sum E_i\right) + 1$

FIGURE 5·3: ONE-DIMENSIONAL FINITE ELEMENT NETWORK FOR A FULLY SCREENED WELL IN A CONFINED AQUIFER.

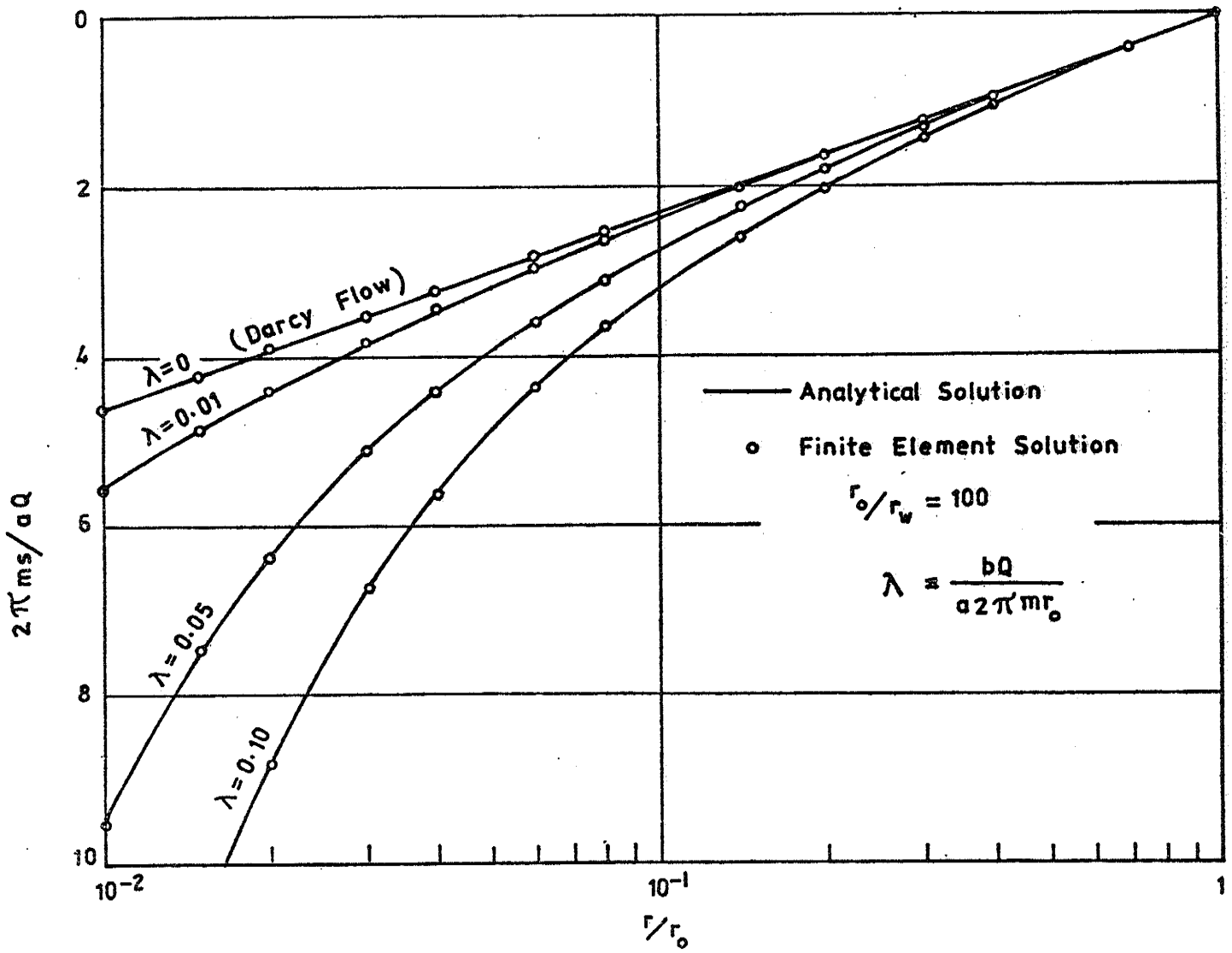

FIGURE 5·4: DIMENSIONLESS RADIAL DISTRIBUTION OF DRAWDOWN FOR STEADY ONE DIMENSIONAL NON-LINEAR FLOW.

into a number of line segments, each of which is further subdivided into a number of 3 noded isoparametric elements. The length of each line segment is Δr_i and the number of elements per line segment is E_i. Based on program accuracy tests, several guidelines for selection of a network to give an accurate solution may be given:

(i) The length of elements near the well should be at the most equal to the well diameter and preferably equal to the well radius or smaller.

(ii) The selection of the length of and the number of elements per line segment should be such that the radial positioning of the network nodes is approximately evenly spread logarithmically.

5.3 Partially Screened Well in an Homogeneous Confined Aquifer

5.3.1 General

Consider the steady state behaviour of a well which screens only a portion of the thickness of a confined aquifer and which is being pumped at a discharge Q (see Figure 5.5).

Near the well the flow will be two-dimensional axisymmetric. As distance from the well increases the effect of partial screening upon the flow diminishes until the flow becomes essentially radial one-dimensional.

Although the screened portion is shown in Figure 5.5 in the lower section of the aquifer, it should be recognised that solutions obtained for such a case are equally applicable to screening the upper section of the aquifer.

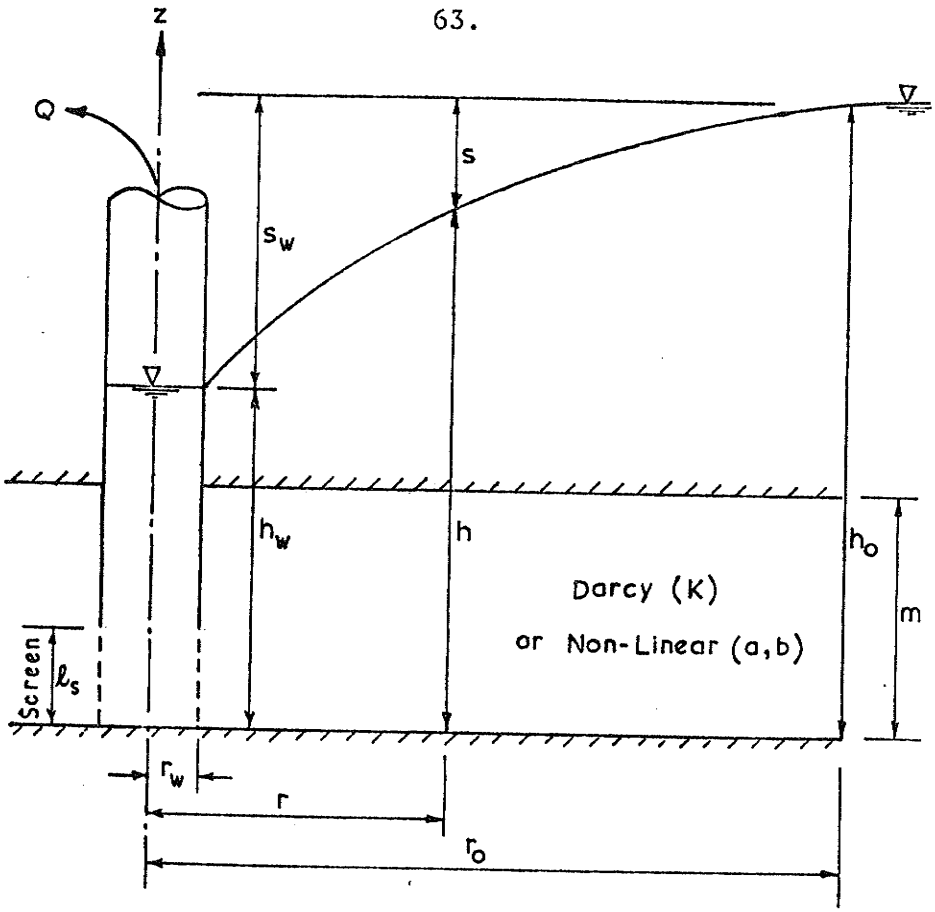

FIGURE 5·5: PARTIALLY SCREENED WELL IN A CONFINED AQUIFER

Approximate analytical solutions for problems involving steady Darcy flow of partially screened confined aquifers have been presented by various workers, the most notable being Kozeny (1933), Muskat (1937) and Polubarinova - Kochina (1951). Most approximate theories are based on the assumption of a specified distribution of flux over the screen length, usually uniform. This can be quite erroneous as will be demonstrated later.

Only Kirkham (1959) presented an exact theory satisfying proper boundary conditions (specifically constant head at the well). However, for practical problems his solution is quite laborious to apply and converges slowly.

No analytical solution exists for the problem of steady state, non-linear flow towards a partially screened well in a confined

aquifer. Because of the difficulty of handling the non-linear flow equation it is unlikely that a solution will be developed in the near future.

5.3.2 Dimensionless Parameters

The techniques of dimensional analysis were applied to the problem variables to obtain the relevant groupings of non-dimensional terms necessary for a thorough description of the two-dimensional axisymmetric flow behaviour within a partially screened aquifer system.

Darcy Flow

In cases involving the distribution of drawdown for two-dimensional flow an appropriate presentation is in terms of contours of drawdown. For Darcy flow dimensional analysis yields the following expression for the drawdown distribution

$$\phi\left\{ \frac{s}{s_w}, \frac{r}{r_w}, \frac{z}{m}, \frac{m}{r_w}, \frac{r_o}{m}, \frac{l_s}{m} \right\} = 0 \qquad (5.12)$$

The dimensionless well drawdown-discharge relationship has the form

$$\phi\left\{ \frac{Q}{Q_T}, \frac{m}{r_w}, \frac{r_o}{m}, \frac{l_s}{m} \right\} = 0 \qquad (5.13)$$

where $Q_T = \frac{2\pi K m s_w}{\ln(r_o/r_w)}$ is the flow that would occur if the aquifer were fully screened. Q/Q_T is only dependent on the relative geometry of the problem in question.

Non-Linear Flow

In the dimensionless presentation for non-linear behaviour

it was proposed that a single term be used to describe the non-linear flow effects. As for the one-dimensional non-linear flow case (Section 5.2.2) the proposed term is $bs_w/a^2 r_w$. This term is a com-

bination of the two separate terms b/a^2 and s_w/r_w which are indicated by a dimensional analysis of the problem variables. The validity of combining and replacing the individual dimensionless terms b/a^2 and s_w/r_w by the single term $bs_w/a^2\tau_w$ was demonstrated by a series of tests using the finite element model. As in equations (5.8b) and (5.8c) an alternative to $bs_w/a^2\tau_w$ would be $\frac{bQ}{a2\pi m\tau_w}$

A complete description of the drawdown distribution and discharge-drawdown relationship for non-linear flow may now be given by sets of non-dimensional terms as follows:

$$\phi\left\{\frac{s}{s_w}, \frac{T}{\tau_w}, \frac{z}{m}, \frac{m}{\tau_w}, \frac{\tau_o}{m}, \frac{\ell_s}{m}, \frac{bs_w}{a^2\tau_w} \text{ or } \frac{bQ}{a2\pi m\tau_w}\right\} = 0 \qquad (5.14)$$

$$\phi\left\{\frac{Q}{Q_T}, \frac{m}{\tau_w}, \frac{\tau_o}{m}, \frac{\ell_s}{m}, \frac{bs_w}{a^2\tau_w} \text{ or } \frac{bQ}{a2\pi m\tau_w}\right\} = 0 \qquad (5.15)$$

where once again $Q_T = 2\pi Km s_w / \ln(\tau_o/\tau_w)$ for $K = 1/a$

5.3.3 Finite Element Model Verification

Darcy Flow

The two-dimensional axisymmetric finite element program incorporating both rectangular and triangular ring elements for solving Darcy flow problems was verified in the following manner.

A network of elements in which the radial spacing of nodes was the same as that employed in the one-dimensional program verification (Section 5.2.3) was found to give an identical solution to the dimensionless distribution of drawdown for Darcy flow $\left(bQ/a2\pi m\tau_o = 0\right)$ for the fully screened well problem previously solved and plotted in Figure 5.4. Thus the two dimensional program's ability to handle the simplified one-dimensional radial flow was demonstrated.

To verify the program's ability to predict two-dimensional Darcy flow behaviour, the partial screening problems described in Table 5.1 were solved; in all six cases the finite element solutions compared favourably with the analagous results derived from experiments using an electrolytic tank apparatus which is fully described in Appendix 2.

Table 5.1: Problem Data for Darcy Flow to Partially Screened Wells in a Confined Aquifer

Flow Case No.	m/r_w	r_o/m	l_s/m
1	10	2	0.75
2	10	2	0.50
3	10	2	0.25
4	20/3	3	0.75
5	20/3	3	0.50
6	20/3	3	0.25

The network used in the finite element solution of flow cases 1 to 3 is shown in Figure 5.6. As shown in Figure 5.7 the finite element solution for the dimensionless distribution of drawdown for flow case 2 is identical to the electrolytic tank model results except in the top region of the aquifer close to the well. In this region, accurate positioning of head contours is difficult in both the finite element and electrolytic tank solutions since the flow velocities and hydraulic gradients are very small and the position of the drawdown contour may vary considerably without affecting the overall flow system.

Non.-Linear Flow

The finite element model for Darcy flow was modified to solve two dimensional flow problems involving non-linear flow as described by the Forchheimer relationship. The verification of this modified finite element analysis by comparison with experimental results is presented in Chapter 7.

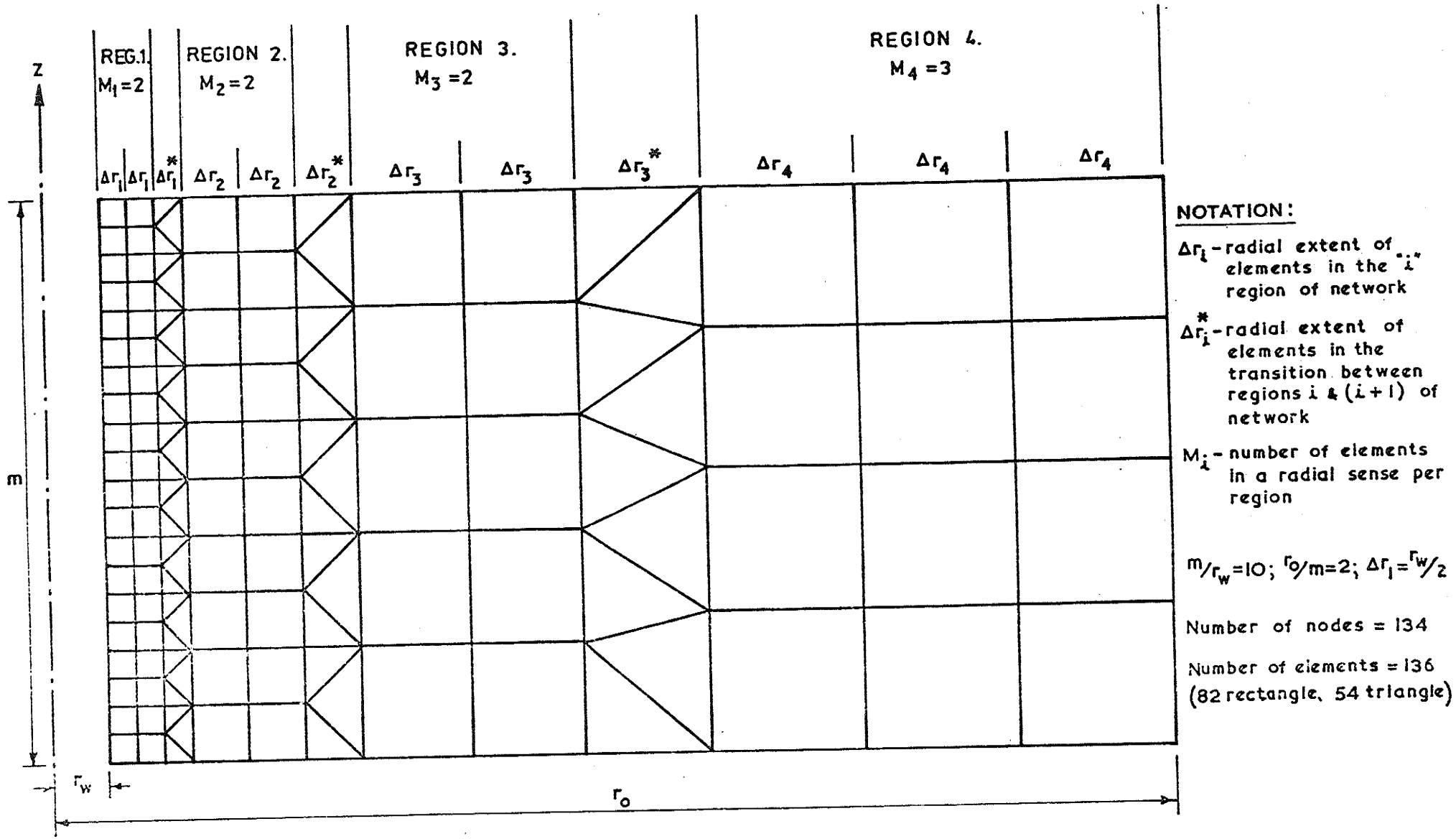

FIGURE 5.6: TYPICAL FINITE ELEMENT NETWORK - CONFINED AQUIFER

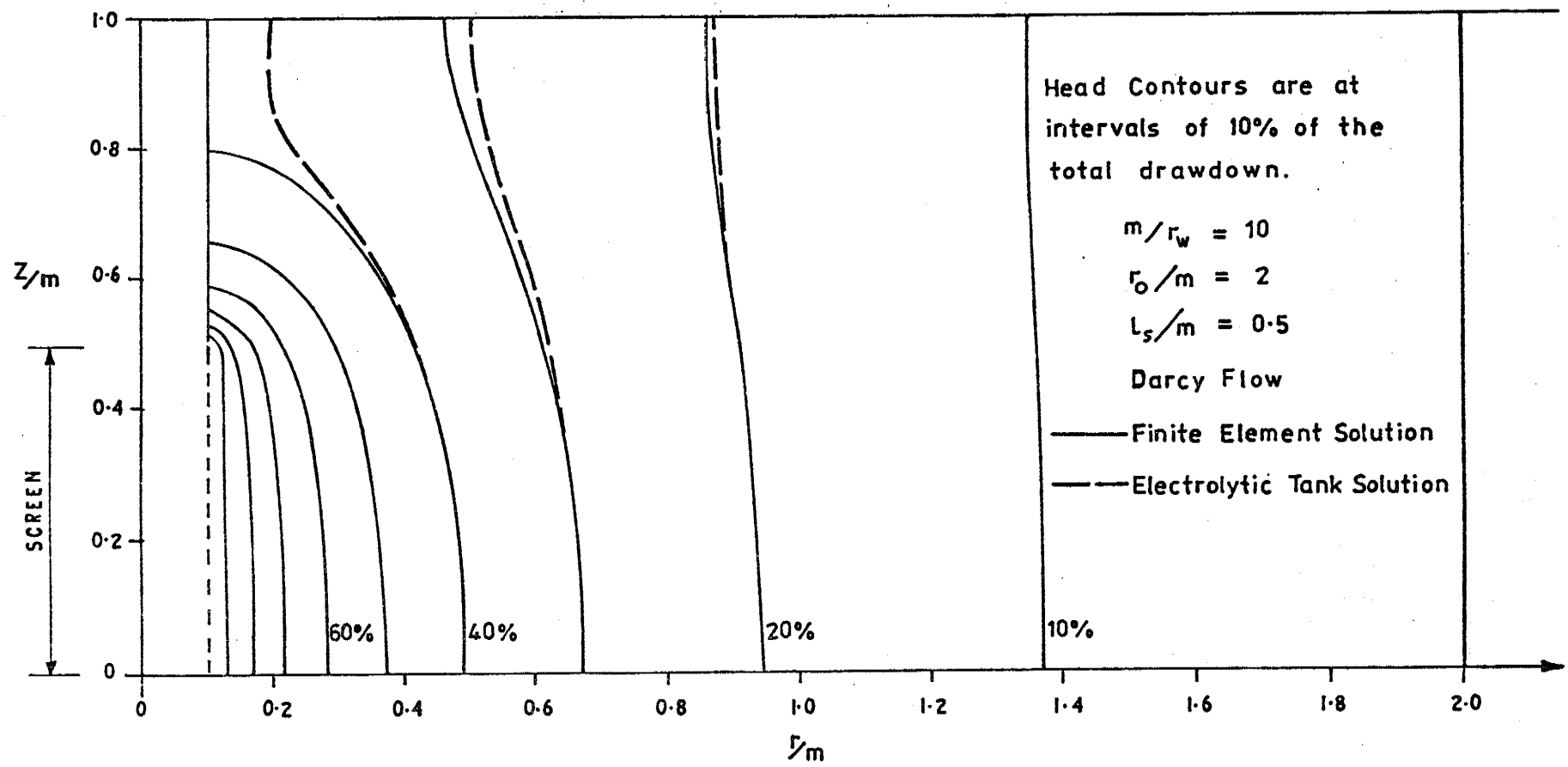

FIGURE 5·7: PARTIALLY SCREENED WELL IN A CONFINED AQUIFER.

COMPARISON OF FINITE ELEMENT & ELECTROLYTIC TANK HEAD DISTRIBUTIONS - DARCY FLOW.

5.3.4 Finite Element Network Selection - Confined Aquifer

Program trials have indicated the following guidelines regarding the selection of appropriate two-dimensional axisymmetric networks for confined aquifer problems. The notation is that given in Figure 5.6.

(i) Elements in the vicinity of the well should be kept as "square" as possible. As the radial distance of an element from the well increases the element may become more rectangularly elongated up to a limit where the radial to vertical side ratio does not exceed five.

(ii) The spacing of the nodes in the region closest to the well (Δr_1) exerts the major influence upon the accuracy of a solution. The accuracy achieved by a particular nodal spacing (Δr_1) is dependent upon the geometry of the problem being solved. Specific values for the accuracy of various network refinements (as gauged by the nodal spacing at the well, Δr_1) for a range of problems will be presented later.

(iii) For regions close to the well, negligible improvement in accuracy is achieved by increasing the number of elements in the radial sense above three. Generally this may be stated as,

$$M_i = 2 \text{ or } 3 \text{ for } i < 4 \qquad (5.16)$$

(iv) The radial positioning of nodes in the network should be approximately logarithmically spaced.

5.3.5 Darcy Flow Solutions

Bearing in mind the network selection guidelines of section 5.3.4, the verified two-dimensional Darcy flow finite element program was used to solve a wide range of partially screened confined aquifer problems.

The finite element solution model used over-estimates both the discharge derived from an aquifer for a specified well drawdown and the drawdown at any point within the flow region. As the finite element network is refined the solution becomes more accurate thus reducing the over-estimate in well discharge and point drawdown. An accurate solution for each problem was obtained by progressive refinement of the finite element network until no significant change in solution accuracy occurred with further refinement.

The percentage over-estimates of discharge for various network refinements (as gauged by the nodal spacing at the well, Δr_1) for a range of partially screened confined aquifer systems are given in Table 5.2. Table 5.2 clearly indicates the network refinement required to solve a particular problem within specified limits of accuracy.

The accuracy of the drawdown at a particular location close to the well for a given network and problem closely follows Table 5.2. The over-estimate of drawdown steadily decreases from the values indicated in Table 5.2 as radial distance from the well increases.

The finite element program results indicating the relative effects of partially screened wells upon the Darcy flow performance of various confined aquifer systems are presented in Table 5.3 and Figure 5.8.

The drawdown distribution for the Darcy flow problem ($m/r_w = 10$, $r_o/m = 10$, $l_s/m = 0.4$) is shown in Figure 5.9.

Typical distributions of the drawdown along both top and base of an aquifer screened in the lower portion are given in Figure 5.10.

In all cases investigated the hydraulic head distribution was characterized by the following significant features:-

Table 5.2: Finite element errors in overestimation of well discharge-Darcy flow to a partially screened well in a confined aquifer.

Tabulated values of percentage overestimate in discharge to the nearest ½%		r_o/m = 10				
m/r_w	Network nodal spacing at well (Δr_1)	Fully Screened	l_s/m			
		1	0.8	0.6	0.4	0.2
10	$2r_w$	2.5	6.0	8.5	13.5	24.5
	r_w	0.5	1.5	3.0	6.0	9.0
	$r_w/2$	0.0	0.5	1.0	2.5	4.0
	$r_w/4$	0.0	0.0	0.0	1.0	1.5
	$r_w/8$	0.0	0.0	0.0	0.5	1.0
20	$4r_w$	5.5	10,5	15.0	21.5	37.5
	$2r_w$	2.0	4.5	6.5	9.0	16.5
	r_w	0.5	1.5	2.5	3.5	6.5
	$r_w/2$	0.0	0.5	1.0	1.5	3.0
	$r_w/4$	0.0	0.0	0.0	0.5	1.0
40	$4r_w$	3.5	6.0	8.5	12.5	20.0
	$2r_w$	1.0	1.5	2.0	4.0	7.0
	r_w	0.0	0.0	0.0	0.5	1.0
	$r_w/2$	0.0	0.0	0.0	0.5	1.0
80	$8r_w$	7.5	12.0	16. 0	21.5	35.5
	$4r_w$	2.5	4.5	6.0	8.5	15.0
	$2r_w$	0.5	1.0	2.0	3.0	5.0
	r_w	0.0	0.0	0.0	0.5	1.0

Table 5.3: Reduction in Performance of a Well in a Confined Aquifer due to Partial Screening - Darcy Flow.

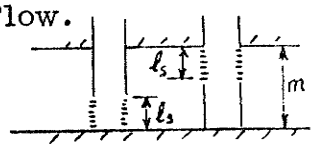

Tabulated Values of Q/Q_T

$Q_T = 2\pi Kms_w/\ln(r_o/r_w)$

r_o/m	m/r_w	l_s/m				
		0.2	0.4	0.6	0.8	1
10	10	.545	.734	.868	.966	1.0
10	20	.483	.687	.836	.945	1.0
10	40	.448	.653	.817	.938	1.0
10	80	.396	.613	.785	.920	1.0

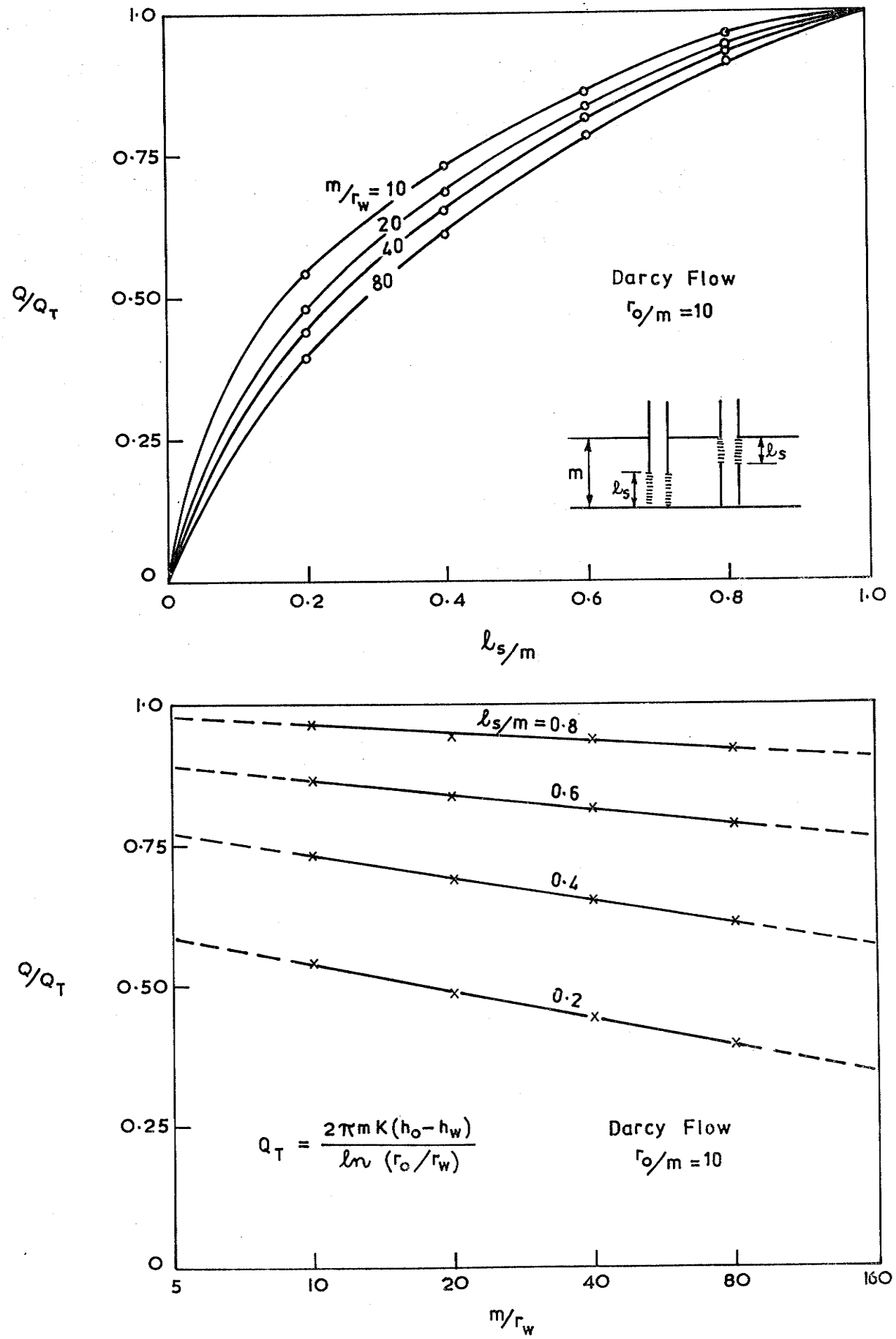

FIGURE 5·8: PARTIALLY SCREENED WELL IN A CONFINED AQUIFER. REDUCTION IN PERFORMANCE OF WELL FOR DARCY FLOW.

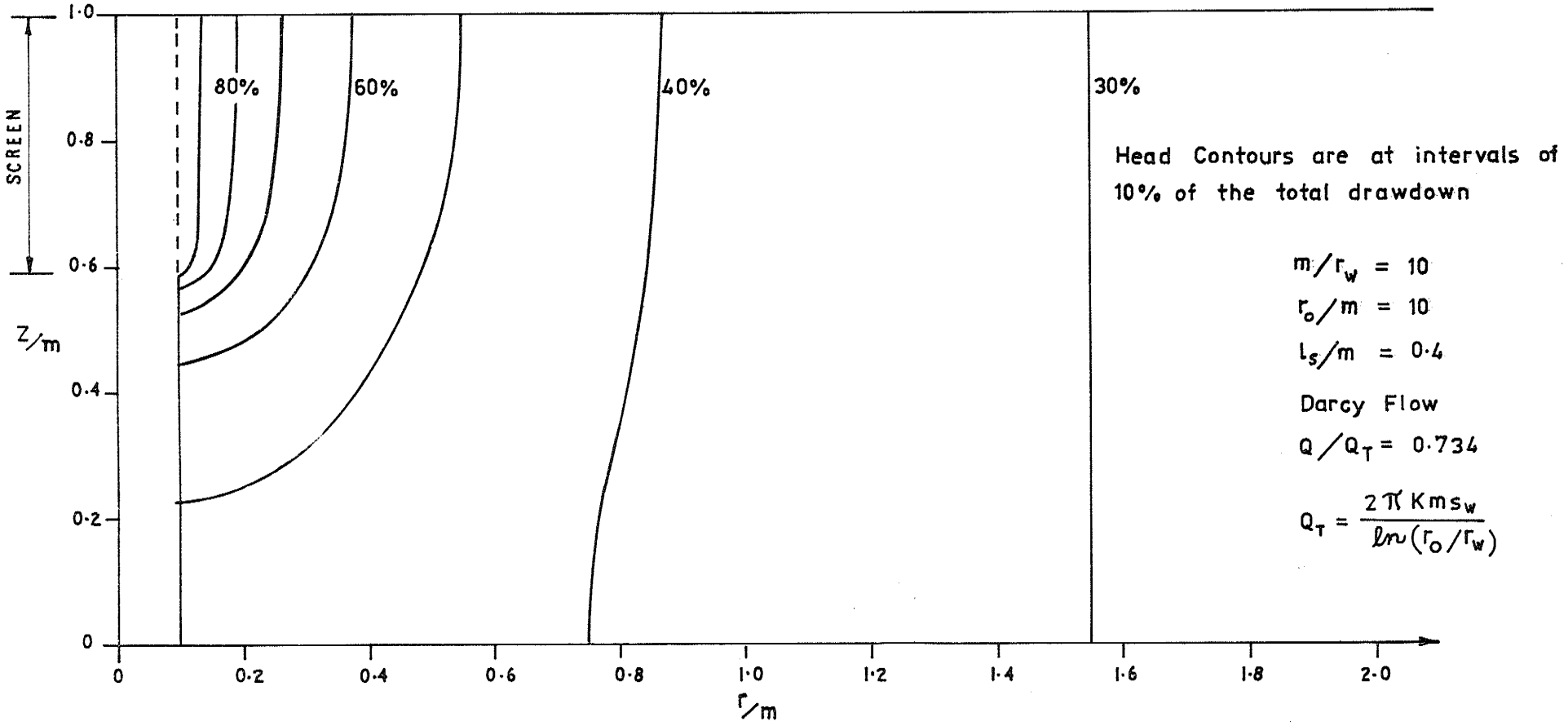

FIGURE 5·9: PARTIALLY SCREENED WELL IN A CONFINED AQUIFER.
TYPICAL HEAD DISTRIBUTION FOR DARCY FLOW

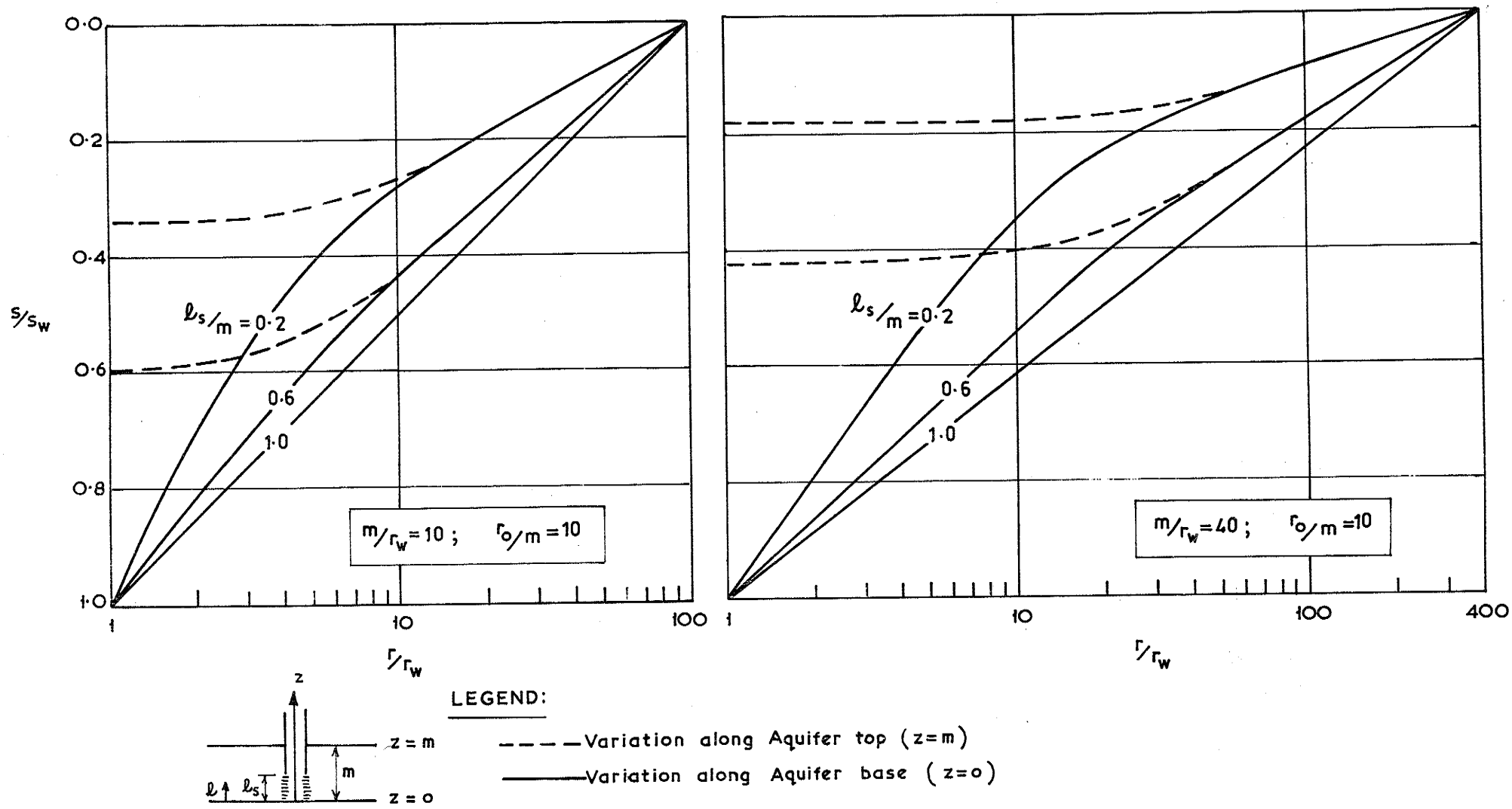

FIGURE 5·10: PARTIALLY SCREENED WELL IN A CONFINED AQUIFER
TYPICAL DRAWDOWN DISTRIBUTIONS ALONG AQUIFER BASE
AND TOP FOR DARCY FLOW.

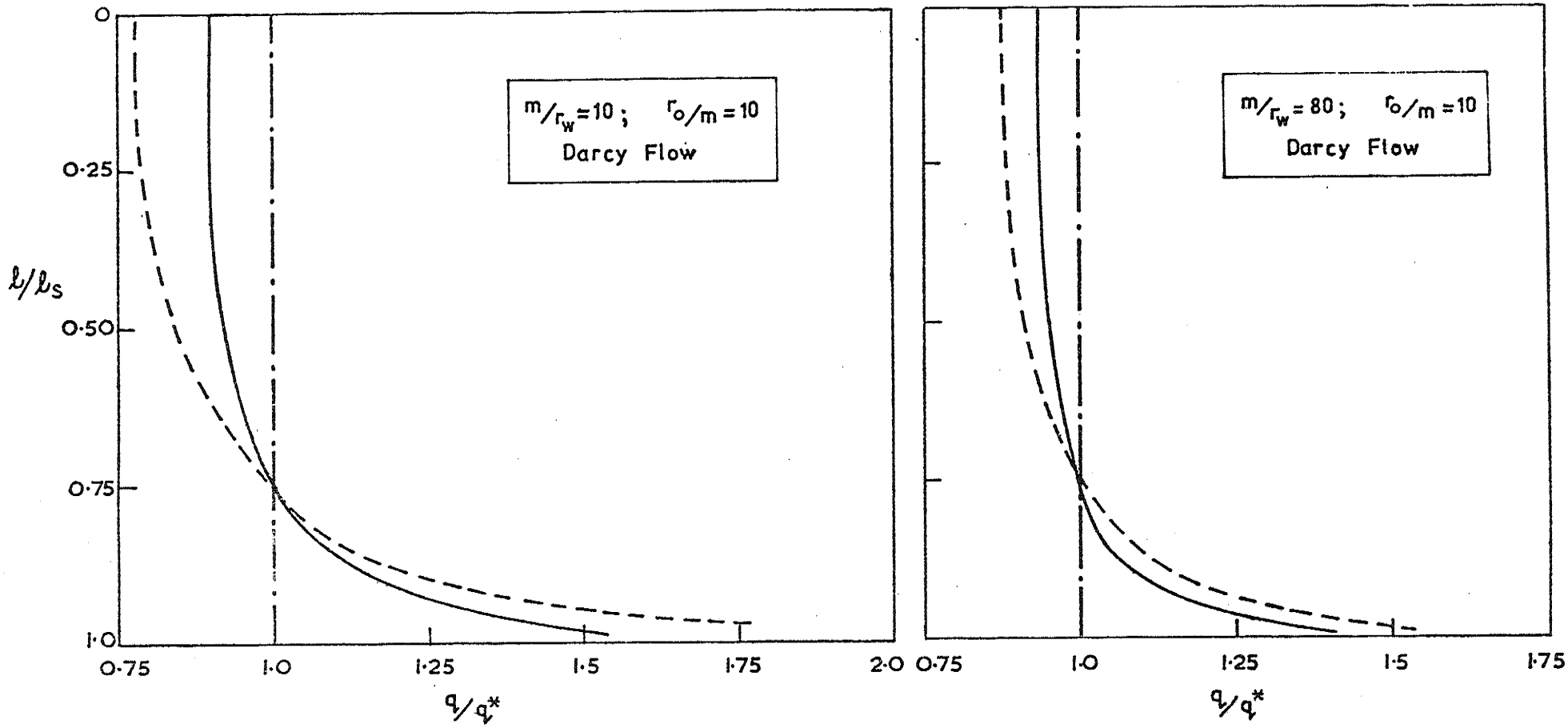

FIGURE 5-11: PARTIALLY SCREENED WELL IN A CONFINED AQUIFER
TYPICAL DISCHARGE FLUX DISTRIBUTIONS ALONG SCREEN
FOR DARCY FLOW

(i) Two dimensional flow effects arising from the partial screening were negligible beyond a radial distance from the well of twice the aquifer thickness. The Thiem equation (5.1) accurately described the flow for $r \geqslant 2m$.

(ii) The flow was radially one-dimensional for $z < l_s/2$.

(iii) Within the flow region ($r < l_s$, $z < l_s/2$) the expression

$$h-h_w = \left(\frac{Q \ln(r/r_w)}{2\pi K l_s}\right)\left[1+\left\{\left(1-\frac{l_s}{m}\right)\Big/ \ln\left(m/r_w\right)\right\}\right] \qquad (5.17)$$

accurately predicted $h-h_w$ with an error not exceeding 3%.

(iv) Near the well, the variation in head along the top of the aquifer, ($z=m$) was small as the following equations demonstrate

$$h(r,\ z=m) - h(r_w,\ z=m) = \epsilon \qquad (5.18a)$$

ϵ was negligible for $r < 0.2\ (m-l_s)$ (5.18b)

$\epsilon < (h_o-h_w)/200$ for $r<0.4\ (m-l_s)$ (5.18c)

The distribution of discharge flux along the screen is presented in Figure 5.11 for several typical flow cases. In all problems solved the flux q equalled the uniform flux distribution value $q^* = Q/l_s$ at the position $l/l_s = 0.75$ along the screen. For the most severe case examined ($m/r_w = 10$, $r_o/m = 10$, $l_s/m = 0.2$), the flux at the screen extremity $l/l_s = 1$ was of the order of twice the uniform flux q^*. In general the distribution of flux along the screen became more uniform with (i) increase in l_s/m. In the limit, for the fully screened condition, $l_s/m = 1$, the distribution is uniform,

(ii) increase in m/r_w.

The flux distributions for $r_o/m = 10$ as shown in Figure 5.11 are equally applicable for any larger radius of influence.

5.3.6 Non-linear Flow Solutions

A wide range of problems involving non-linear flow in partially screened confined aquifers was examined using the two-dimensional finite element program.

In applying the finite element model the boundary condition at the well was satisfied by fixing the water level and thus the drawdown s_w in the well. The inflow flux distribution and thus the total well discharge were not known a priori and could only be evaluated after the solution for the distribution of head within the aquifer had been found. Under such circumstances the $\frac{bs_w}{a^2 r_w}$ term in equations (5.14) and (5.15) proved to be a far more practical measure of non-linear effects than the $\frac{bQ}{a\, 2\pi\, m\, r_w}$ term, the value of which is found only after the basic problem has been solved.

The results of the finite element investigation of the effects of non-linear flow upon the performance of partially screened wells in confined aquifer systems are fully presented in Table 5.4 whilst the results for the typical case ($m/r_w = 40$, $r_o/m = 10$) are shown in Fig. 5.12.

The evaluation of the Q/Q_T values in Table 5.4 was accomplished in the following manner. To reduce computer time, networks with nodal spacings at the well of $r_w/2$, r_w, r_w, $2r_w$ were used for problems having m/r_w ratios of 10, 20, 40, 80 respectively. If the flow were fully Darcy the errors involved for various partial screening ratios (ls/m) would be given by Table 5.2. Let these percentage over-estimates be denoted by ϵ_1. The range of ϵ_1 can be seen to vary from zero to a

Table 5.4: Effect of non-linear flow on well drawdown-discharge relationship - Partially screened confined aquifer.

Tabulated values of Q/Q_T. $Q_T = \frac{2\pi K m s_w}{\ln(r_o/r_w)}$ and $K = 1/a$

m/r_w	r_o/m	bs_w/a^2r_w	l_s/m				
			0.2	0.4	0.6	0.8	1.0
10	10	Darcy	.55	.74	.87	.97	1
		.25	.53	.72	.86	.95	.99
		.5	.51	.70	.84	.94	.98
		1	.48	.67	.82	.92	.96
		2	.44	.63	.78	.88	.92
		4	.38	.57	.71	.81	.86
		8	.32	.49	.62	.73	.77
		12.5	.28	.43	.56	.66	.71
		25	.22	.35	.46	.54	.59
		50	.17	.27	.36	.44	.47
		100	.13	.20	.28	.34	.37
		200	.09	.15	.21	.25	.28
		400	.07	.11	.15	.19	.21
		800	.05	.08	.11	.14	.15
20	10	Darcy	.48	.69	.84	.95	1
		.25	.47	.67	.82	.93	.99
		.5	.46	.66	.81	.92	.98
		1	.44	.64	.79	.90	.96
		2	.41	.61	.76	.88	.94
		4	.36	.56	.71	.83	.89
		8	.31	.49	.63	.75	.81
		12.5	.27	.44	.57	.69	.75
		25	.22	.36	.48	.58	.64
		50	.17	.28	.38	.47	.52
		100	.12	.21	.29	.36	.41
		200	.09	.16	.22	.28	.31
		400	.07	.12	.16	.21	.23
		800	.05	.09	.12	.15	.17
40	10	Darcy	.45	.65	.82	.94	1
		.25	.44	.64	.81	.93	.99
		.5	.43	.64	.80	.93	.99
		1	.42	.62	.79	.91	.97
		2	.39	.59	.76	.89	.95
		4	.36	.55	.72	.84	.91
		8	.31	.49	.65	.77	.84
		12.5	.28	.45	.60	.72	.78
		25	.22	.37	.50	.62	.68
		50	.17	.29	.41	.50	.56
		100	.13	.23	.32	.40	.45
		200	.10	.17	.24	.30	.34
		400	.07	.13	.18	.23	.26
		800	.05	.09	.13	.17	.19

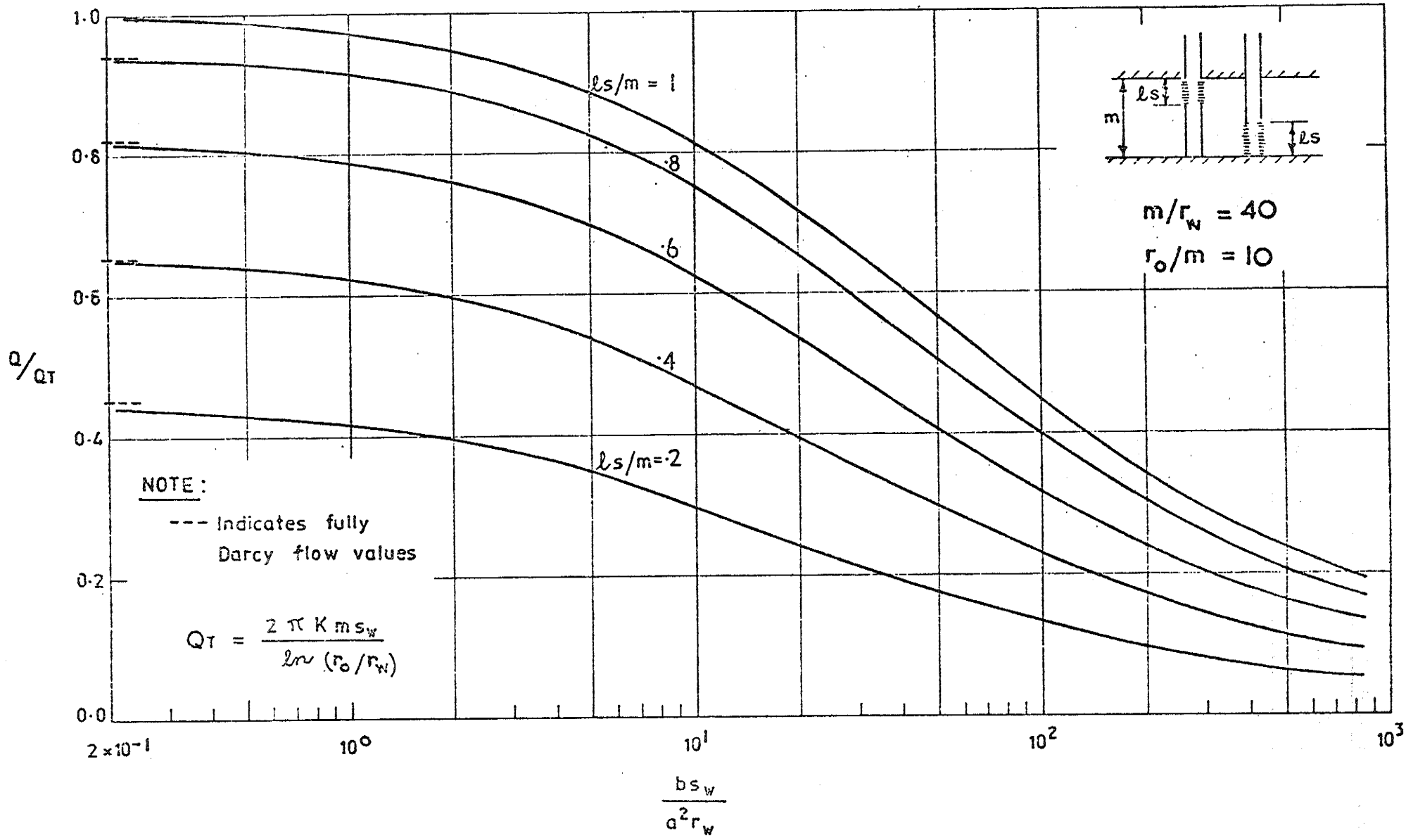

FIGURE 5·12: PARTIALLY SCREENED WELL IN A CONFINED AQUIFER
TYPICAL REDUCTION IN WELL PERFORMANCE FOR
NON LINEAR FLOW

Table 5.4 (cont'd.)

m/r_w	r_o/m	bs_w/a^2r_w	l_s/m				
			0.2	0.4	0.6	0.8	1.0
80	10	Darcy	.40	.61	.79	.92	1
		.25	.39	.60	.77	.91	.99
		.5	.38	.60	.77	.90	.99
		1	.37	.59	.76	.89	.98
		2	.35	.57	.73	.87	.96
		6.25	.30	.50	.66	.80	.89
		12.5	.26	.44	.59	.72	.81
		25	.21	.37	.50	.63	.71
		50	.17	.30	.41	.52	.60
		100	.13	.23	.32	.41	.48
		200	.09	.17	.25	.32	.37
		400	.07	.13	.19	.24	.28
		800	.05	.09	.14	.18	.21

maximum of $6\frac{1}{2}\%$ for the networks used.

With increasing non-linearity a particular finite element solution based on a certain network becomes less accurate since the network has to cope with steeper gradients. A measure of the further over-estimate in discharge due to a specified degree of non-linearity bs_w/a^2r_w for given r_o/m, m/r_w and chosen network was evaluated by comparing the finite element discharge solution for the fully screened case ($l_s/m = 1$) with the equivalent analytical discharge value found by solving equation (5.7). Let this percentage over-estimate error be denoted by ϵ_2. Typical values of ϵ_2 as found are given in Table 5.5.

If the finite element solution discharge is denoted by Q_{prog} then the corrected value of discharge Q used in evaluating Q/Q_T in Table 5.4 was calculated using the expression

$$Q = Q_{prog} \Big/ \left[\left(1 + \frac{\epsilon_1}{100}\right)\left(1 + \frac{\epsilon_2}{100}\right)\right] \qquad (5.19)$$

In several cases, including the more severe problems solved, network refinement was carried out until accurate solutions were attained. The resultant values of Q/Q_T agreed completely with those found by applying the above correction procedures to coarser network solutions. The values of Q/Q_T listed in Table 5.4 may be considered reliable to the second decimal place.

In all cases solved partial screening effects were negligible for $r > 2m$ and beyond this distance from the well the flow was fully radial. The effects of non-linear flow behaviour were negligible at $r = r_o = 10m$ even for the extreme case of $\frac{bs_w}{a^2r_w} = 800$. The flow could be described by the Thiem equation (5.1) for Darcy flow ($K = 1/a$) for $r > 10m$.

Table 5.5: Values of Percentage Over-estimate in Discharge for Certain Networks - Fully Screened Wells and Non-linear flow.

r_o/m	m/r_w	Network Nodal Spacing at well	Degree of Non-linearity $bs_w/a^2 r_w$		
			1	25	800
10	10	$r_w/2$	0.5	1.0	1.0
10	20	r_w	0.5	1.5	2.5
10	40	r_w	0.5	1.0	1.5
10	80	$2r_w$	0.5	3.0	6.5

The typical drawdown distribution shown in Figure 5.13 for the case (r_o/m = 10, m/r_w = 10, ls/m = 0.4, bs_w/a^2r_w = 100) may be compared with the Darcy solution for the same geometry (Figure 5.9) With increasing non-linearity drawdown contours move closer to the well and the distance between contours near the well is reduced.

The distributions of drawdown along the base and top of the aquifer are shown in Figure 5.14 for some typical cases of non-linear flow. As for the Darcy flow case, the drawdown distribution along the base of the aquifer was an accurate description for the drawdown along any horizontal line within a depth of 50% of the screen length from the base of the aquifer. Thus the flow within this zone was effectively radial.

The effects of non-linearity on the flux distribution along the screen are demonstrated in Figure 5.15. The flux distribution is seen to become more uniform with increase in non-linearity as measured by bs_w/a^2r_w. As for the Darcy flow cases considered in Section 5.3.5 the flux q equals the uniform distribution flux, $q^*=Q/l_s$, at the position l/l_s = 0.75 along the screen. The effects on flux distribution of varying l_s/m and m/r_w were found to be the

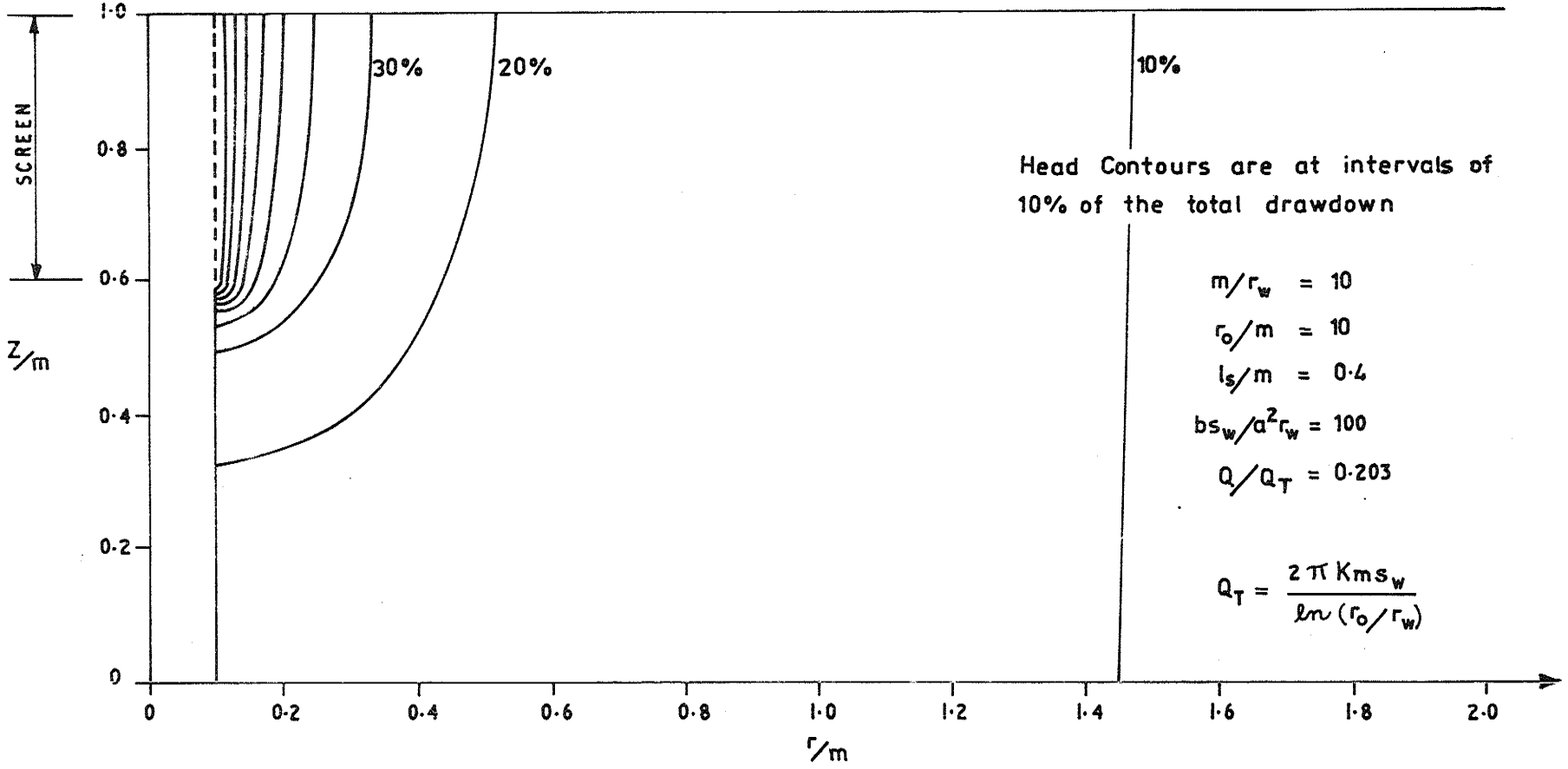

FIGURE 5·13: PARTIALLY SCREENED WELL IN A CONFINED AQUIFER.
TYPICAL HEAD DISTRIBUTION FOR NON-LINEAR FLOW.

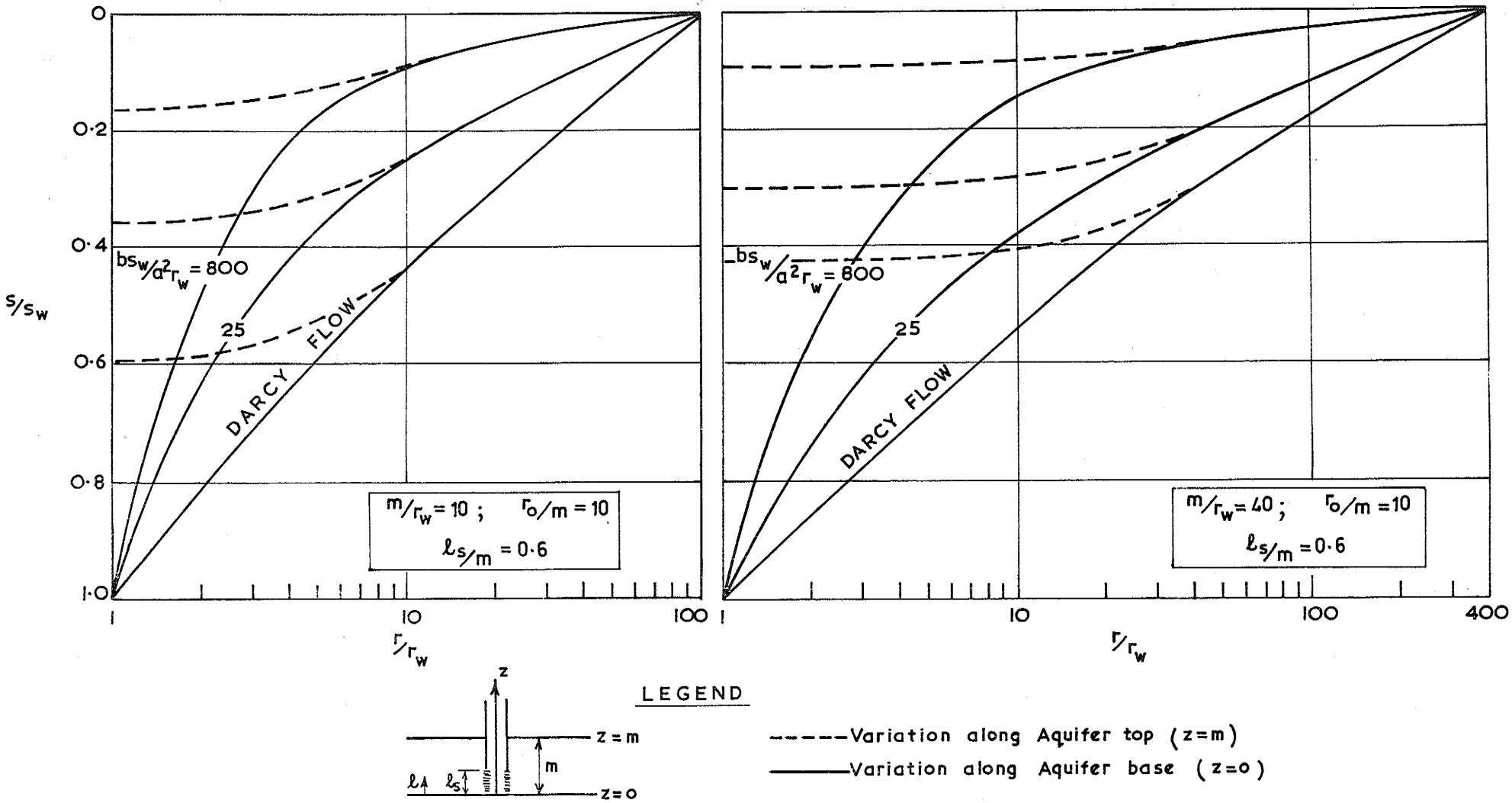

FIGURE 5·14: PARTIALLY SCREENED WELL IN A CONFINED AQUIFER

TYPICAL DRAWDOWN DISTRIBUTIONS ALONG AQUIFER BASE AND TOP FOR NON-LINEAR FLOW

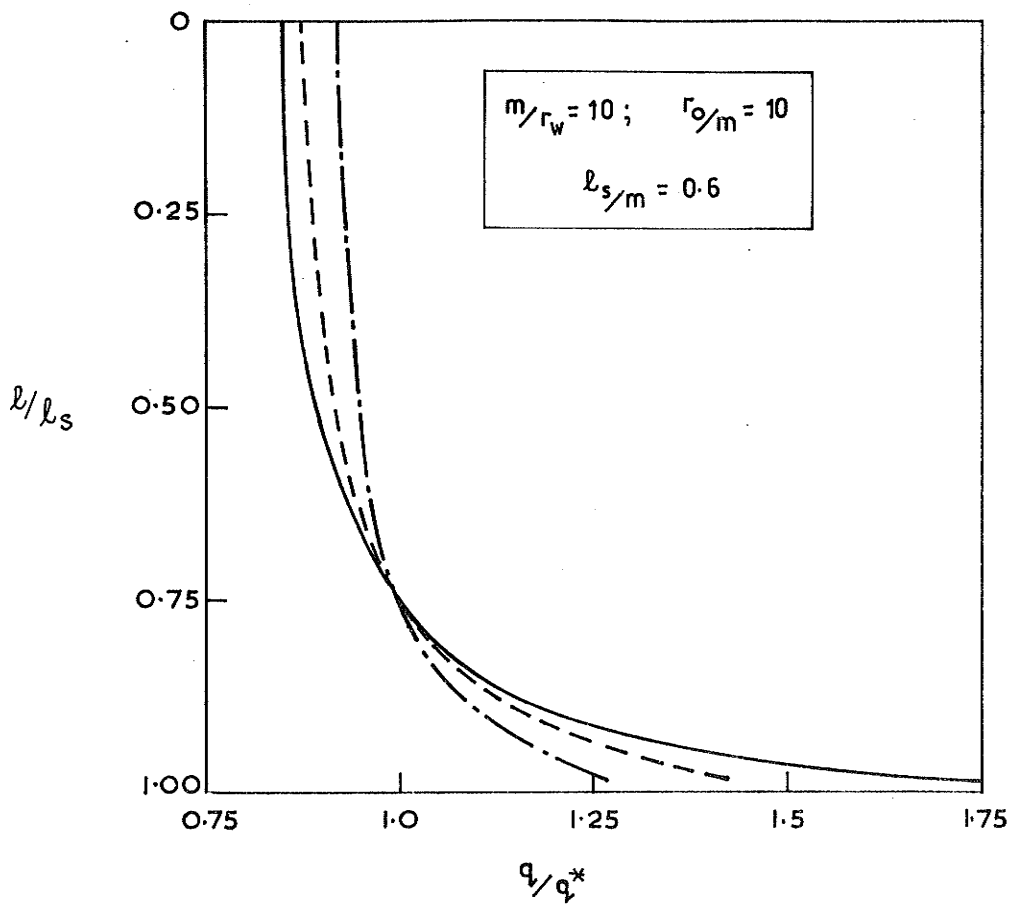

FIGURE 5·15: PARTIALLY SCREENED WELL IN A CONFINED AQUIFER.
TYPICAL DISCHARGE FLUX DISTRIBUTIONS ALONG SCREEN FOR NON-LINEAR FLOW.

same as previously recorded for Darcy flow (Section 5.3.5).

The results of this section describing non-linear flow to partially screened wells in confined aquifers incorporate as special cases the earlier work described in Sections 5.2 and 5.3.5. The fully screened well case ($l_s/m=1$) was analytically solved for both Darcy and non-linear flow in Section 5.2. Darcy flow ($\frac{bs_w}{a^2 r_w} = 0$) to a partially screened well was solved in Section 5.3.5.

5.4 Multi-Layered Confined Aquifer Systems

Consider the problem of a well screened through a portion of a confined aquifer which is made up of 'n' different material layers as shown in Figure 5.16. Each individual material layer is assumed to be both homogeneous and isotropic.

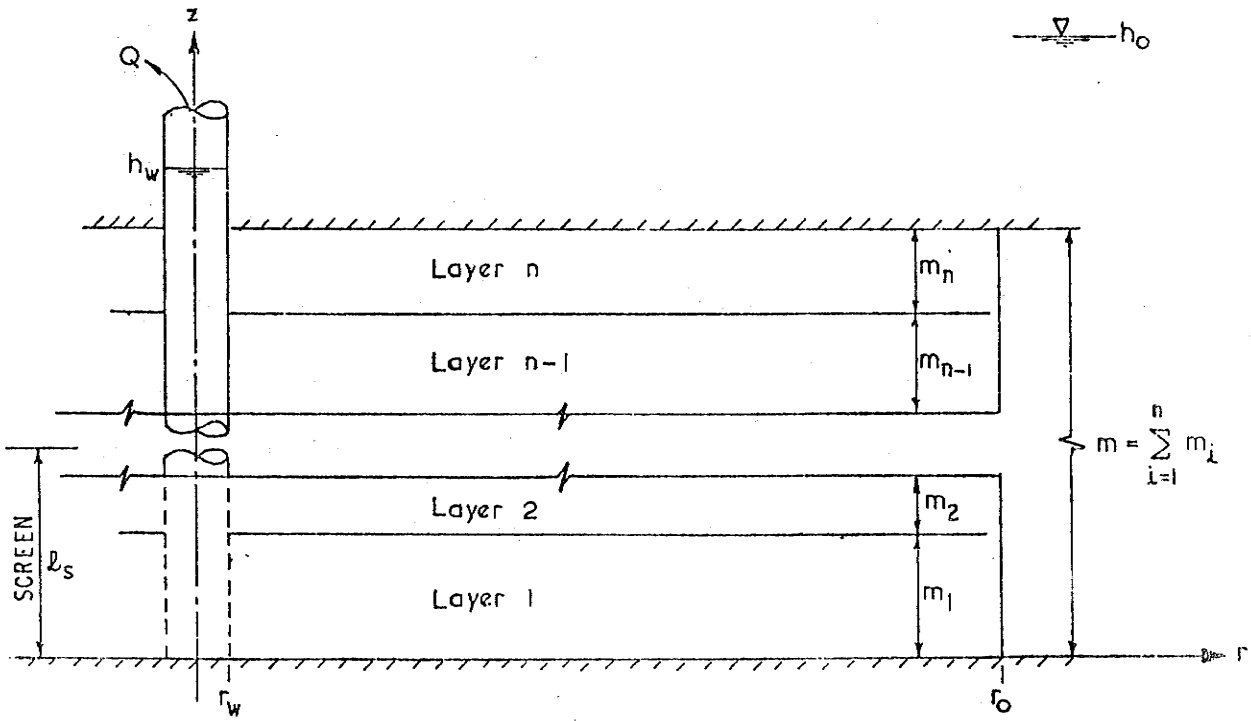

FIGURE 5·16: WELL IN A MULTI-LAYERED CONFINED AQUIFER

5.4.1 Darcy Flow - Fully Screened

For the simplified case where all material layers are screened and the flow within all layers obeys Darcy's law, the flow will be everywhere radial under steady state pumping conditions. In such circumstances the flow within each layer may be described by the Thiem equation (equation (5.1)) and the total well discharge evaluated as the summation of the discharges from the individual layers;

$$Q_{total} = \sum_{i=1}^{n} Q_i \qquad (5.20a)$$

$$Q_{total} = \frac{2\pi(h_o - h_w)}{\ln(r_o/r_w)} \sum_{i=1}^{n} K_i m_i \qquad (5.20b)$$

where K_i is the hydraulic conductivity of the "i" th layer.

5.4.2 Non-linear Flow - Fully Screened

If the flow behaviour within any of the aquifer layers is non-linear, the flow will not be everywhere radial even for the fully screened condition under consideration. Near the well, where non-linear effects are more pronounced vertical flux exchange between layers exhibiting different degrees of non-linear behaviour may occur.

An investigation of fully screened two-layered aquifer systems involving non-linear flow in the upper layer was made using a finite element model. The element network was selected so that individual element boundaries coincided with boundaries of aquifer inhomogeneity. The appropriate material properties were then applied to individual elements depending upon their position within the aquifer system.

Typical drawdown distributions from the computer results are given in Figure 5.17. Vertical flow from the upper non-linear layer

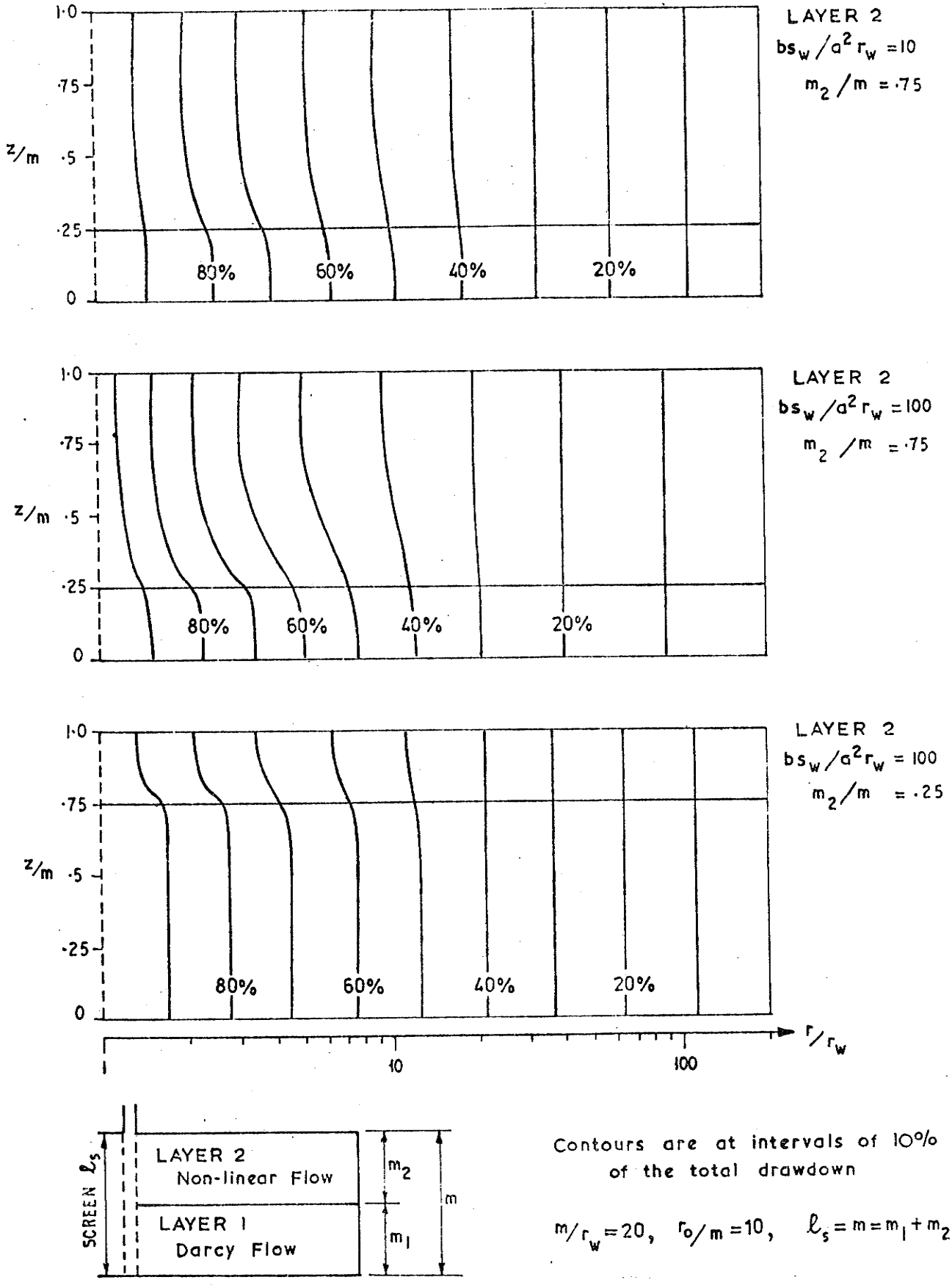

FIGURE 5·17: FULLY SCREENED TWO-LAYER CONFINED AQUIFER.

TYPICAL HEAD DISTRIBUTIONS FOR NON-LINEAR FLOW.

to the lower Darcy flow layer is clearly indicated by the curvature of the drawdown contours as the well is approached. The deviation from radial flow increases with both the thickness and the degree of non-linearity (bs_w/a^2r_w) of the upper layer.

An approximate value for the total well discharge may be found by summing the individual layer discharge contributions as calculated by assuming the flow to be everywhere radial, i.e.

$$Q^*_{total} = \sum_{i=1}^{n} Q_i^* \qquad (5.21a)$$

where for Darcy flow layers

$$Q_i^* = 2\pi K_i m_i (h_o - h_w) \Big/ \ln(r_o/r_w) \qquad (5.21b)$$

and for non-linear flow layers Q_i^* is found from,

$$h_o - h_w = \frac{a_i Q_i^*}{2\pi m_i} \ln(r_o/r_w) + b_i \left(\frac{Q_i^*}{2\pi m_i}\right)^2 \left(\frac{1}{r_w} - \frac{1}{r_o}\right) \qquad (5.21c)$$

The asterisk superscript is used in equation (5.21) to denote an approximation based on the assumption of radial flow.

The computer results indicated that the discharge contributions from the non-linear and Darcy flow layers are respectively less than and more than the discharge values calculated from equations (5.21c) and (5.21b).

The approximate solution (Q^*_{total}) given by equations (5.21) was shown to underestimate the total well discharge (Q_{total}).

If ϵ^* denotes the percentage underestimate, then

$$\epsilon^* = 100\,(Q_{total} - Q^*_{total})/Q_{total} \qquad (5.22)$$

Values of ϵ^* for a typical two layered mixed flow aquifer system are given in Table 5.6.

Table 5.6: Percentage Underestimates for Total Well Discharge Based on Radial Flow Assumption. Typical Values.

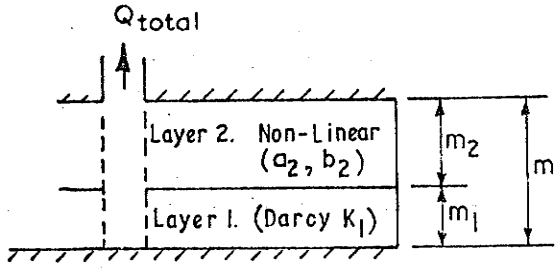

Fully screened $l_s = m$

$m/r_w = 20, r_o/m = 10$

$a_2 = 1/K_1$

m_2/m	(bs_w/a^2r_w) Value for Layer 2		
	1	10	100
.25	0	1%	3.5%
.50	0	1.5%	7%
.75	0	1.5%	7.5%

Computer results for a wide range of two-layered conditions ($10 < m/r_w < 100$, $r_o/m \gg 10$, $.2 < m_2/m < .8$) indicated that the value of ϵ^* would be negligible, less than 2% and less than 10% respectively for values of the upper layer non-linear parameter (bs_w/a^2r_w) less than 1, 10 and 100.

In the limiting cases where $m_2/m = 0$ or 1 the problem reduces to a single layer aquifer system involving fully radial Darcy or non-linear flow respectively. The flow behaviour within such systems is fully described by equations (5.1) and (5.3).

5.4.3 Darcy Flow in an Aquifer-Aquitard System

In multi-layered confined aquifer systems it is general practice to screen only the more permeable layers. The finite element program was used to investigate the Darcy flow behaviour of an aquifer-aquitard system as shown in Figure 5.18. The well is screened from the base to the top of the main aquifer and the entire system is

confined by impermeable strata.

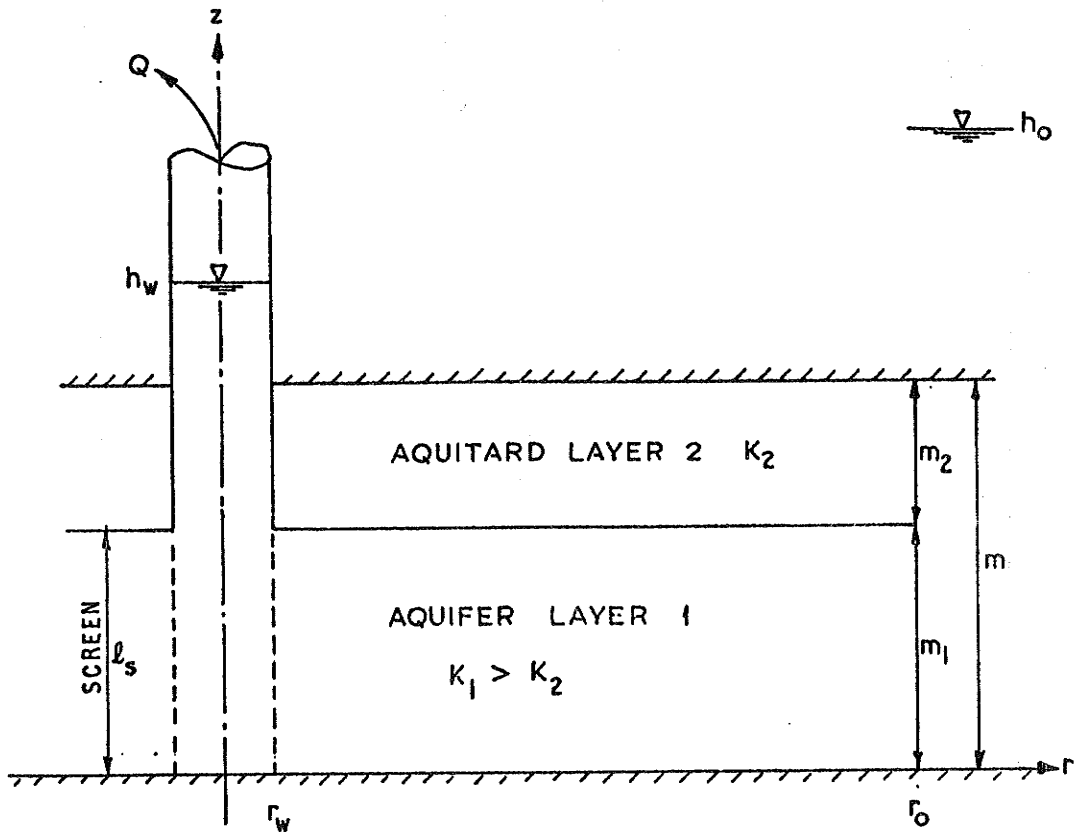

FIGURE 5·18: WELL IN A CONFINED AQUIFER - AQUITARD SYSTEM

Typical drawdown distributions from the computer results are given in Figure 5.19.

Typical well performance results are given in Table 5.7 in the form of Q/Q_1 where Q_1 is the discharge calculated by applying the Thiem equation to the fully screened aquifer layer,

i.e. $$Q_1 = 2\pi K_1 m_1 s_w / \ln(r_o/r_w)$$

The case $K_2/K_1 = 1$ has been previously treated in Section 5.3.5 when partially screened homogeneous aquifer problems were investigated.

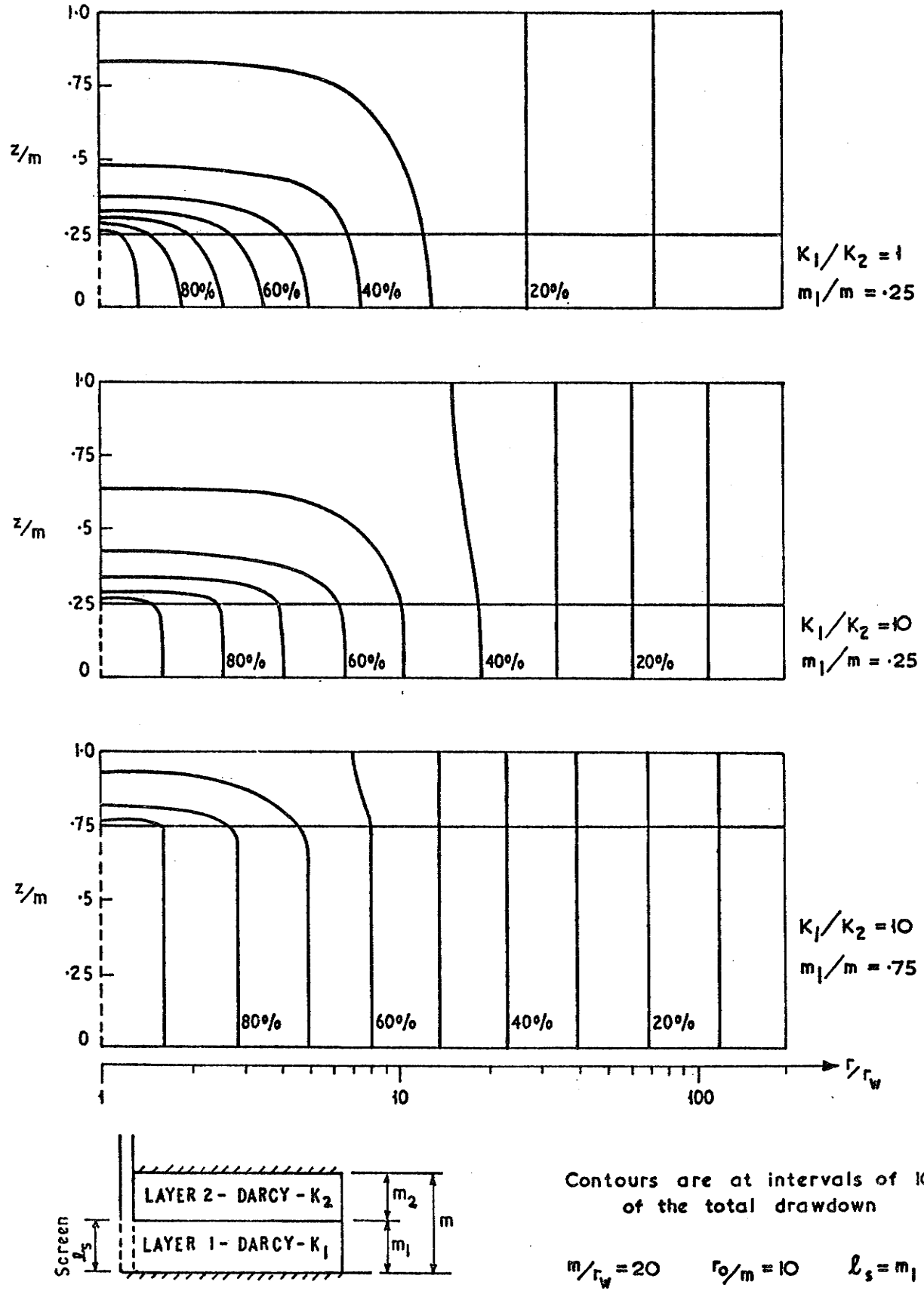

FIGURE 5·19: CONFINED AQUIFER - AQUITARD SYSTEM.
TYPICAL HEAD DISTRIBUTIONS FOR DARCY FLOW.

Table 5.7: Well Performance in an Aquifer-Aquitard System.
Darcy Flow - Aquifer Fully Screened.

Tabulated Values of Q/Q_1: $Q_1 = 2\pi K_1 m_1 s_w / \ln (r_o/r_w)$

$m/r_w = 20$ $r_o/m = 10$

$m_1/m = l_s/m$	K_2/K_1			
	1	.1	.01	.001
.75	1.23	1.03	1.00	1.00
.50	1.54	1.06	1.00	1.00
.25	2.20	1.16	1.00	1.00

The results indicate that with increase in K_1/K_2 and $m_1/m = l_s/m$:

(i) the flow within the aquifer layer approaches the logarithmic radial distribution described by the classical Thiem equation, and,

(ii) the aquitard contribution to well discharge becomes small.

From a wide range of computed results ($10 < m/r_w < 100$, $r_o/m = 10$, $.2 < m_1/m < .8$), it was found that for values of $\frac{m_1 K_1}{m K_2} > 10$ flow through the aquitard may be ignored and the problem effectively treated as the simplified case of a homogeneous fully screened single layer aquifer of thickness m_1 and hydraulic conductivity K_1.

5.5 Radial Inhomogeneity about a Well in a Confined Aquifer

5.5.1 General

Field evidence has shown that well performance can be greatly affected by permeability variations which occur in a zone immediately surrounding the well. Near well aquifer inhomogeneity may occur naturally or may result from the drilling and completion of the well.

All drilling methods impair the ability of an aquifer to deliver water to a completed well. Formation damage caused by the invasion of foreign fluids and/or solids into the exposed aquifer is well recognised as the main cause of reduced permeability around a well. In an experimental study of the effects of drilling muds on unconsolidated aquifer materials, Dudgeon and Cox (1975) showed that both the radial extent and the severity of formation damage of the invaded zone may be high. Within the invaded zone the damaged material was found to be uniformly homogeneous.

Well development and stimulation techniques are used in attempts to remove drilling damage and/or to increase the permeability of the material around the well. Under favourable conditions, continued development of the well may lead to a zone of improved permeability in the vicinity of the well.

A gravel pack is frequently used to act as a restraining filter to prevent aquifer material from entering the screen or slotted casing. If the gravel pack is selected and placed correctly, it will behave as a zone of improved permeability.

Consider the general case of a well in a confined aquifer where permeability variation occurs in a zone surrounding the well as

shown in Figure 5.20. Both the original confined aquifer and the affected zone of radial extent r_a, are assumed to be homogeneous and isotropic.

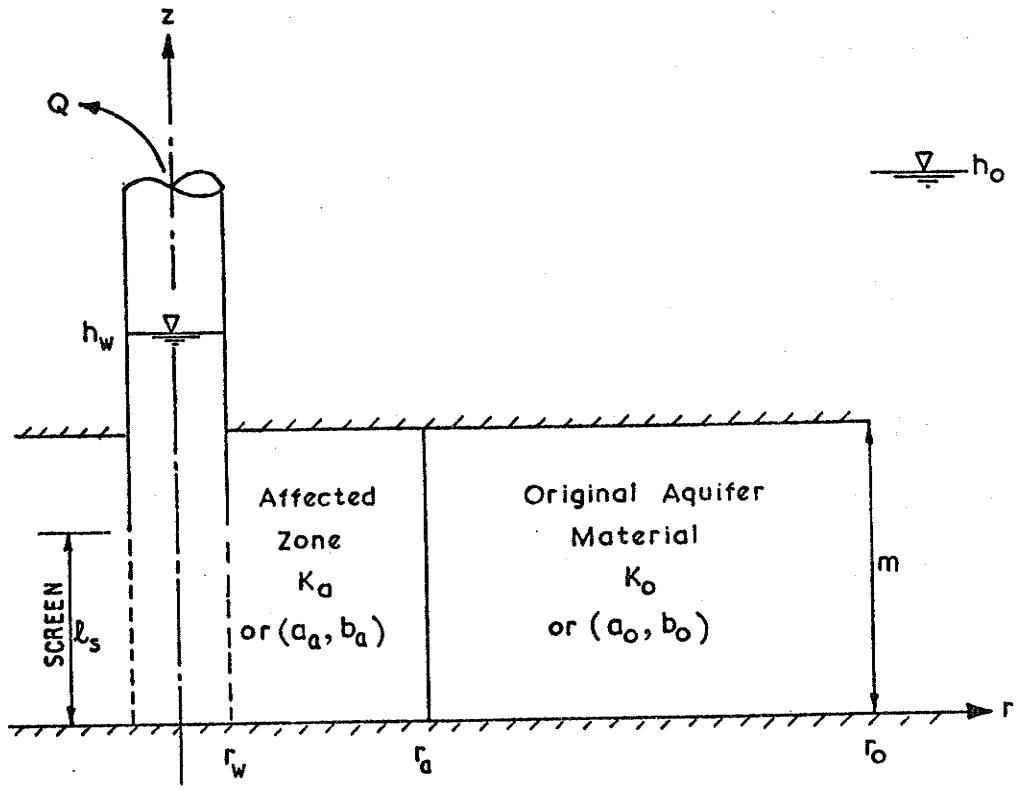

FIGURE 5·20: RADIAL INHOMOGENEITY ABOUT A WELL IN A CONFINED AQUIFER

5.5.2 Fully Screened Well

If the full depth of the aquifer is screened, the flow will be radial and analytical solutions may be derived for the effects of radial permeability variations upon the performance of the well, whether the flow behaviour be Darcy or non-linear.

A complete description of the flow behaviour in the system is given by the following equations.

For the affected zone: $r_w \leqslant r \leqslant r_a$

Darcy Flow $$h-h_w = Q \ln(r/r_w) \Big/ 2\pi m K_a \qquad (5.23a)$$

Non-linear flow $$h-h_w = \frac{a_a Q}{2\pi m} \ln(r/r_w) + b_a \left(\frac{Q}{2\pi m}\right)^2 \left(\frac{1}{r_w} - \frac{1}{r}\right) \qquad (5.23b)$$

For the unaffected original aquifer: $r_a \ll r \ll r_o$

Darcy flow $$h_o-h = Q \ln(r_o/r) \Big/ 2\pi m K_o \qquad (5.23c)$$

Non-linear flow $$h_o-h = \frac{a_o Q}{2\pi m} \ln(r_o/r) + b_o \left(\frac{Q}{2\pi m}\right)^2 \left(\frac{1}{r} - \frac{1}{r_o}\right) \qquad (5.23d)$$

The subscripts 'o' and 'a' are used as pertaining to the original aquifer and affected zone materials respectively.

The effect of permeability variation upon well performance may be simply stated in terms of the ratio of the productivity of the two zone system (Q) to the productivity from the original unaffected aquifer system (Q_o) for the same well drawdown.

For Darcy flow within both the affected zone and the original aquifer it can be readily shown that

$$Q/Q_o = \ln(r_o/r_w) \Big/ \left[\ln(r_o/r_w) + \ln(r_a/r_w)\left(\frac{K_o}{K_a} - 1\right)\right] \qquad (5.24)$$

where $$Q_o = 2\pi K_o m (h_o - h_w) \Big/ \ln(r_o/r_w)$$

Figure 5.2.1 illustrates the effect of permeability variation and the radius of the affected zone upon the performance of a well in a typical fully screened aquifer where the flow obeys Darcy's law throughout. It can be seen that the discharge ratio may be substantially reduced by serious permeability reduction (small values of K_a/K_o) which needs only be restricted to a narrow zone (small r_a/r_w). Slight permeability reduction in a zone of greater extent may also cause a significant decline in well performance. The improvement in well performance, due to a zone of increased permeability of specific radial extent (r_a/r_w), is seen to approach an upper limit at

large values of K_a/K_o. At large values of K_a/K_o equation (5.24) reduces to

$$Q/Q_o = \ln(r_o/r_w) \Big/ \ln(r_o/r_a) \qquad (5.25)$$

and the upper limit for improvement in well performance is seen to correspond to an effective increase in well radius to the radius of the affected zone of increased permeability.

5.5.3 Partially Screened Well

Two-dimensional axisymmetric finite element programs were used to investigate the effects of permeability variation on the performance of partially screened wells. Analytical solutions do not exist for such cases. The general problem is shown in Figure 5.20.

The change in well performance due to permeability variation in the vicinity of the partially screened well was measured by the ratio of the two-zone discharge (Q) to the discharge from the original unaffected aquifer system (Q_o) for the same screening and well drawdown. Values of Q_o for partial screening of the original homogeneous aquifer may be found from Tables 5.3 or 5.4 for Darcy or nonlinear flow behaviour respectively.

Typical results from the computer investigation are given in Table 5.8 and Figure 5.22 for problems in which the flow obeys Darcy's law throughout the system. Well performance values shown in Table 5.8 and Figure 5.22 for the simplified fully screened case ($l_s/m = 1$) were found from equation (5.24).

The results clearly indicate that the effects of permeability variation upon well performance become more pronounced as the partial screening ratio (l_s/m) decreases. In terms of well design

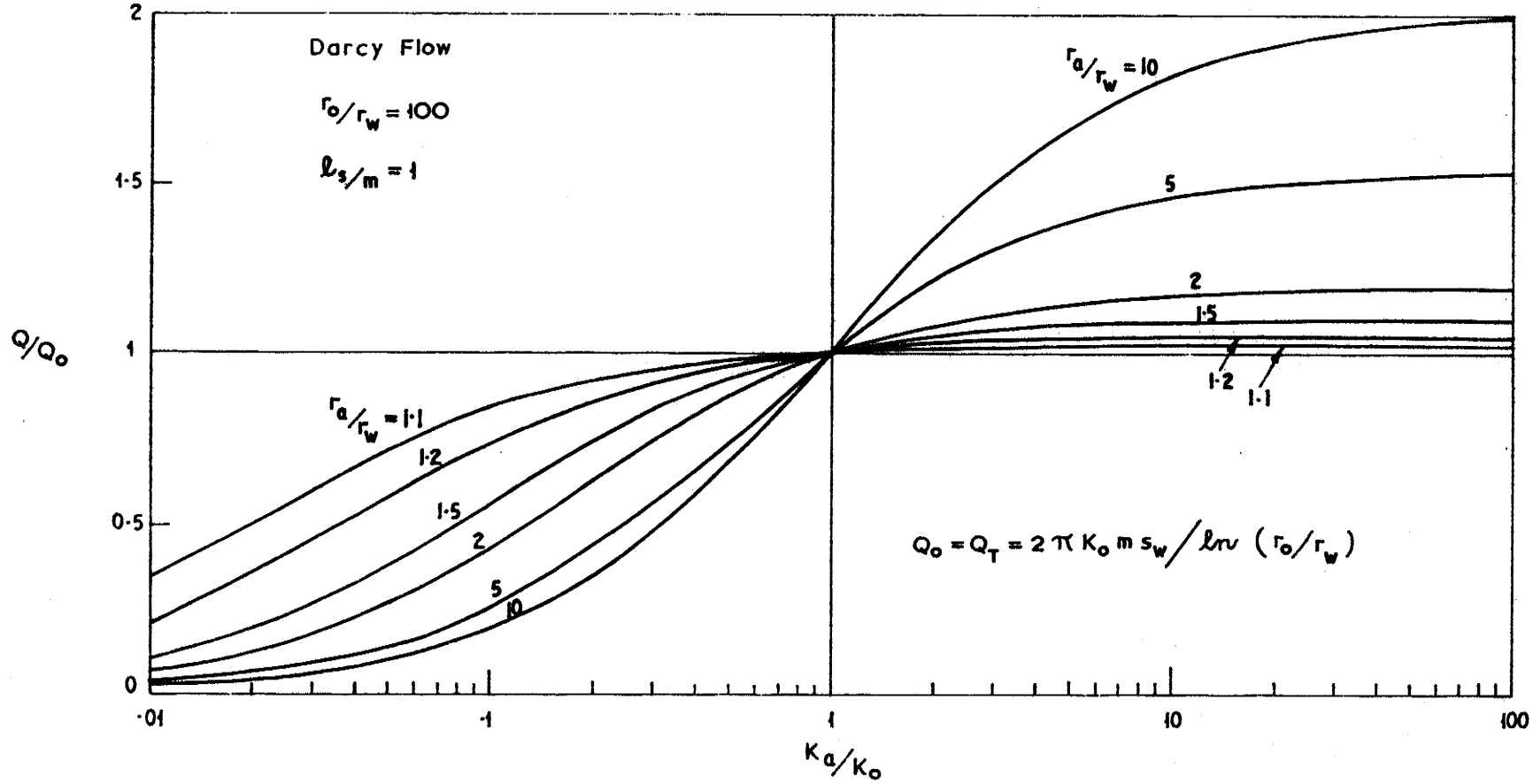

FIGURE 5·21: EFFECT OF RADIAL INHOMOGENEITY ON PERFORMANCE OF A FULLY SCREENED WELL IN A CONFINED AQUIFER

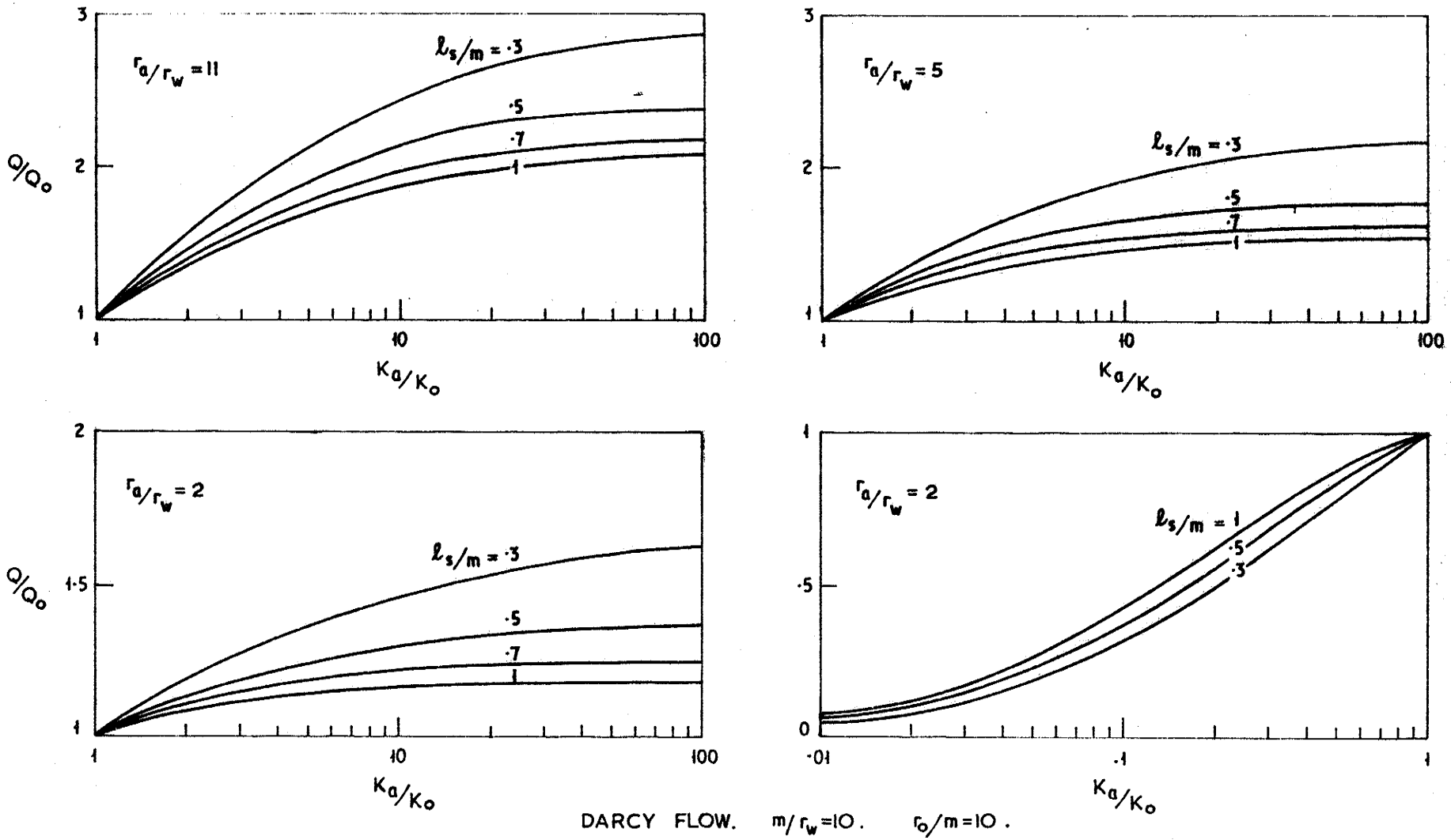

FIGURE 5·22: EFFECT OF RADIAL INHOMOGENEITY ON PERFORMANCE OF A PARTIALLY SCREENED WELL IN A CONFINED AQUIFER.

these findings are significant. Partial screening of an aquifer will therefore become respectively less or more detrimental to well performance according to the degree to which the permeability within the affected zone has been improved or reduced.

Table 5.8: Effect of Radial Inhomogeneity on Performance of a Partially Screened Well in a Confined Aquifer - Tabulated Values of Q/Q_o. Darcy Flow. $m/r_w = 10$. $r_o/r_w = 100$

r_a/r_w	K_a/K_o	l_s/m			
		.3	.5	.7	1
11	100	2.85	2.37	2.15	2.06
	10	2.46	2.14	1.97	1.88
	5	2.09	1.89	1.78	1.71
5	100	2.14	1.78	1.61	1.53
	10	1.92	1.67	1.53	1.46
	5	1.72	1.54	1.45	1.39
2	100	1.63	1.37	1.25	1.17
	10	1.45	1.30	1.22	1.16
	5	1.36	1.24	1.18	1.14
	1	1.00	1.00	1.00	1.00
	.3	0.63	0.68	0.71	0.74
	.1	0.32	0.37	0.40	0.42
	.03	0.12	0.14	0.16	0.17
	.01	0.04	0.05	0.06	0.06

5.6 "Fingering" Effects about a Well in a Confined Aquifer

Apparently uniform homogeneous aquifers often contain thin bands of low or high permeability material. These thin bands are not necessarily continuous and are generally limited in areal extent. The normal techniques of analysing pump test results average the aquifer properties over a large area and cannot detect the presence of variable bands of limited extent. Aquifer sampling during investigatory drilling, particularly rotary drilling, may not detect thin bands of variable material amidst a reasonably uniform aquifer layer. The producing well, when completed in what is assumed to be a homogeneous aquifer, may in fact

intersect one or more of such bands.

The improvement in well productivity resulting from a well intersecting an axi-symmetric "finger" of high permeability material was investigated using the developed finite element computer programs.

Consider the case of a fully screened well in a confined aquifer shown in Figure 5.23. The well intersects a "finger" of material more permeable than the bulk of the aquifer. The thickness and radial extent of the "finger" are m_f and r_f respectively. The flow is assumed to obey Darcy's law throughout the system. The hydraulic conductivities of the "finger" and the aquifer are K_f and K_o respectively.

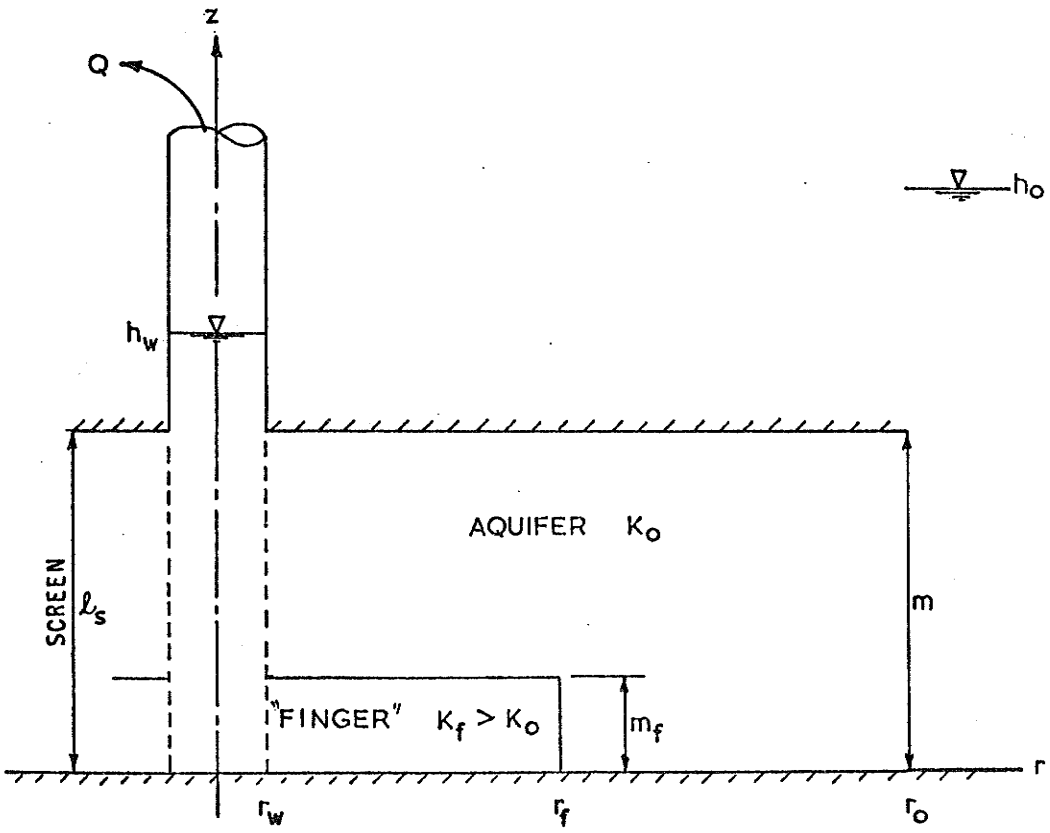

FIGURE 5·23: "FINGERING" EFFECTS ABOUT A WELL IN A CONFINED AQUIFER

The improvement in well performance due to the "finger" was gauged by the discharge ratio Q/Q_o, where Q is the discharge from the system including the "finger" and Q_o represents the discharge from the apparently homogeneous aquifer ignoring the "finger".

i.e. $$Q_o = 2\pi K_o m(h_o - h_w) \Big/ \ln(r_o/r_w)$$

The well performance can be fully described by the following set of dimensionless parameters.

$$\phi\left\{ \frac{Q}{Q_o}, \frac{m_f}{m}, \frac{r_f}{r_w}, \frac{K_f}{K_o}, \frac{m}{r_w}, \frac{r_o}{m} \right\} = 0 \qquad (5.26)$$

Accurate Q/Q_o results from the computer investigation for a range of the relevant controlling dimensionless parameters are presented in Table 5.9. Values in Table 5.9 for the limiting cases of regular aquifer variability where $r_f/r_w = r_o/r_w$ and $m_f/m = 1$ were calculated using the exact theory described in previous sections 5.4 and 5.5 for multi-layering and full depth radial inhomogeneity respectively.

The variation of Q/Q_o with K_f/K_o, m_f/m and r_f/r_w is shown for some typical cases in Figure 5.24.

For values of $r_f < m$, the well performance (Q/Q_o) improved with K_f/K_o but reached an upper limit where, for larger values of K_f/K_o, there was negligible further increase in Q/Q_o. At the high values of "finger" permeability the flow resistance of the "finger" becomes relatively negligible and the "finger" effectively becomes an extension of the well itself.

The investigation clearly indicated the possibility of substantial contributions to well performance arising from thin "fingers" of high

Table 5.9: Improvement in Performance of a Fully Screened Well in a Confined Aquifer due to "Fingering" Effects. Tabulated Values of Q/Q_o: Darcy Flow. $r_o/m = 2.$

m/r_w	K_f/K_o	r_f/r_w	m_f/m			
			1.0	0.5	0.2	0.1
20	10	2	1.20	1.14	1.07	1.06
		4	1.51	1.35	1.19	1.14
		6	1.78	1.55	1.31	1.22
		8	2.03	1.75	1.42	1.29
		r_o/r_w	10	5.5	2.8	1.9
	100	2	1.23	1.15	1.08	1.06
		4	1.59	1.43	1.25	1.19
		6	1.93	1.72	1.45	1.35
		8	2.26	2.02	1.67	1.54
		r_o/r_w	100	50.5	20.8	10.9
	1000	2	1.23	1.16	1.08	1.07
		4	1.60	1.44	1.26	1.20
		6	1.94	1.74	1.47	1.38
		8	2.29	2.06	1.71	1.59
		r_o/r_w	1000	500.5	200.8	100.9
10	10	2	1.26	1.16	1.08	1.06
		4	1.71	1.45	1.24	1.18
		6	2.17	1.84	1.45	1.30
		8	2.67	2.20	1.68	1.45
		r_o/r_w	10	5.5	2.8	1.9
	100	2	1.30	1.19	1.10	1.07
		4	1.85	1.62	1.38	1.28
		6	2.45	2.20	1.81	1.65
		8	3.20	2.85	2.32	2.00
		r_o/r_w	100	50.5	20.8	10.9
	1000	2	1.30	1.20	1.10	1.08
		4	1.86	1.67	1.40	1.30
		6	2.49	2.25	1.88	1.72
		8	3.26	2.91	2.50	2.20
		r_o/r_w	1000	500.5	200.8	100.9
5	10	2	1.37	1.25	1.13	1.07
		4	2.18	1.83	1.45	1.30
		6	3.34	2.55	1.75	1.45
		8	5.34	3.60	2.20	1.67
		r_o/r_w	10	5.5	2.8	1.9
	100	2	1.43	1.32	1.19	1.11
		4	2.48	2.19	1.81	1.60
		6	4.36	3.72	2.68	2.35
		8	9.44	7.20	5.10	4.00
		r_o/r_w	100	50.5	20.8	10.9
	1000	2	1.43	1.33	1.20	1.12
		4	2.51	2.20	1.88	1.75
		6	4.49	3.85	2.93	2.60
		8	10.22	8.00	6.20	5.30
		r_o/r_w	1000	500.5	200.8	100.9

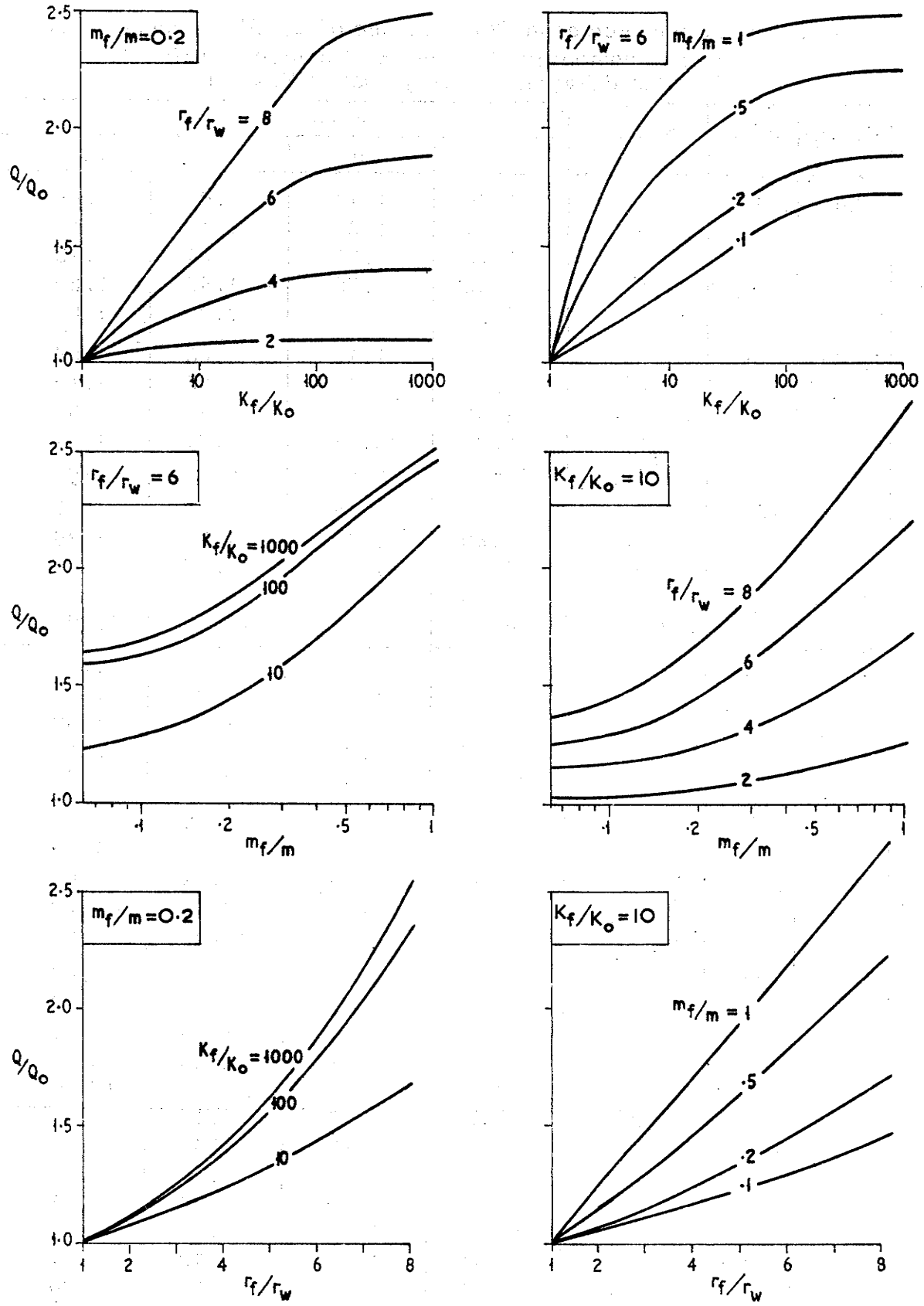

DARCY FLOW. FULLY SCREENED. $m/r_w = 10$, $r_o/m = 2$, $Q_o = 2\pi K_o m s_w / \ln (r_o/r_w)$

FIGURE 5·24: TYPICAL EFFECTS OF A HIGH PERMEABILITY "FINGER" ON THE PERFORMANCE OF A WELL IN A CONFINED AQUIFER.

permeability material of limited radial extent.

In practice non-linear flow may occur close to the well within a highly permeable "finger". In such cases the improvement in well performance would be less than the values indicated in Table 5.9 which assumed the flow to obey Darcy's law.

General solutions for the "finger" at the base of the aquifer shown in Figure 5.23 are equally applicable to a "finger" at the top of the aquifer. Well performance improvement in more complex "finger" problems may be solved by superposition techniques as illustrated in Figure 5.25.

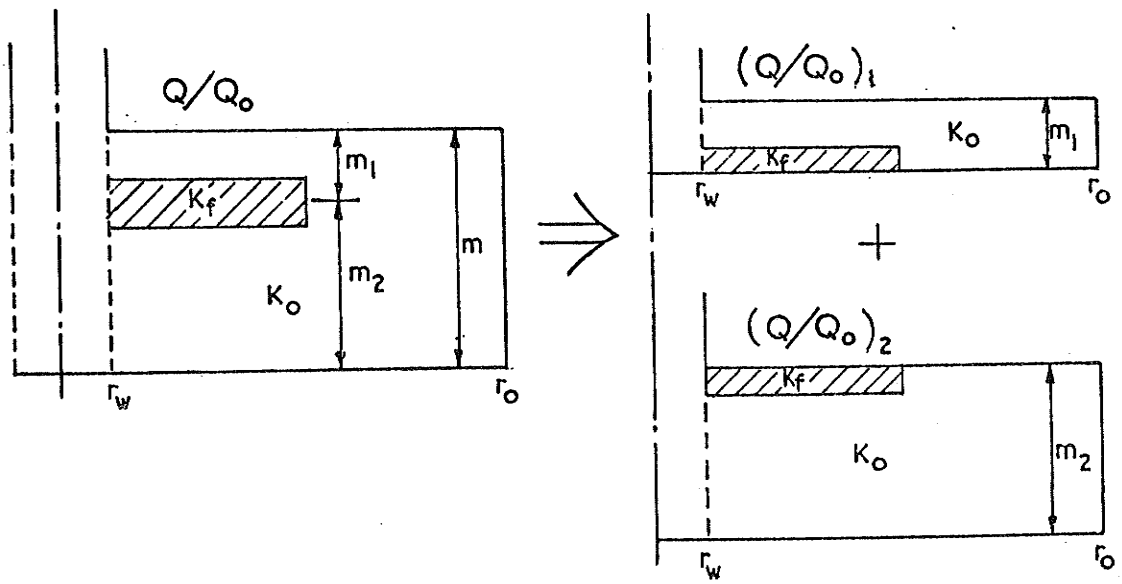

$$Q/Q_o = \frac{m_1}{m} (Q/Q_o)_1 + \frac{m_2}{m} (Q/Q_o)_2$$

FIGURE 5·25: COMPLEX PROBLEM SOLUTION BY SUPERPOSITION TECHNIQUES

5.7 Partially Screened Well in an Unconfined Aquifer

5.7.1 General

Exact analytical expressions for the flow behaviour around wells in unconfined aquifers are extremely difficult, if not impossible, to derive due to the complex boundary condition prevailing at the free surface.

The well-known and often used Dupuit equation,

$$h_o^2 - h^2 = Q \ln(r_o/r) / \pi K \qquad (5.27)$$

is an analytical solution based on the simplifying assumption that the flow obey's Darcy's law and is everywhere radial within the zone of influence (r_o) of a well that is screened throughout the entire original saturated thickness (h_o) of an unconfined aquifer. Muskat (1946) and Boulton (1951) have shown that although equation (5.27) closely represents the flow behaviour at $r > 1.5\ h_o$, it fails to represent the head distribution, (in particular the free surface) closer to the well. Based on experimental results, field experience and numerical analysis, various proposals have been made for the prediction of the seepage height where the free surface strikes such a fully screened well (Babbitt and Caldwell (1948), Boulton (1951), Hall (1955) Peterson (1957)). The Dupuit equation for well-discharge

$$Q_D = \pi K (h_o^2 - h_w^2) / \ln(r_o/r_w) \qquad (5.28)$$

has been rigorously validated by both analytical procedures (Chapman (1957) and Hantush (1964)) and experimental investigations (Boulton (1951), Hall (1955)). The contribution to well discharge arising from the existence of the capillary fringe above the phreatic surface has

been investigated by Muskat (1946) and Hall (1955) for a fully screened well. They proposed the following equations:-

Muskat (1946) $$\Delta Q/Q_0 = h_c/(h_o+h_w) \qquad (5.29a)$$

Hall (1955) $$\Delta Q/Q_0 = h_c/2h_o \qquad (5.29b)$$

where ΔQ is the well discharge contribution from the capillary fringe and h_c is the average thickness of the capillary layer.

Wells in unconfined aquifers are rarely screened throughout the full thickness of the aquifer and it is bad practice to do so since such a procedure results in dewatering of the screen with attendant corrosion and encrustation problems. Rather, the general practice is to partially screen the lower portion of a well which fully penetrates the aquifer as shown in Figure 5.26. The maximum design discharge for the well should be such that the corresponding drawdown will not cause the water level within the well to fall below the top of the screen.

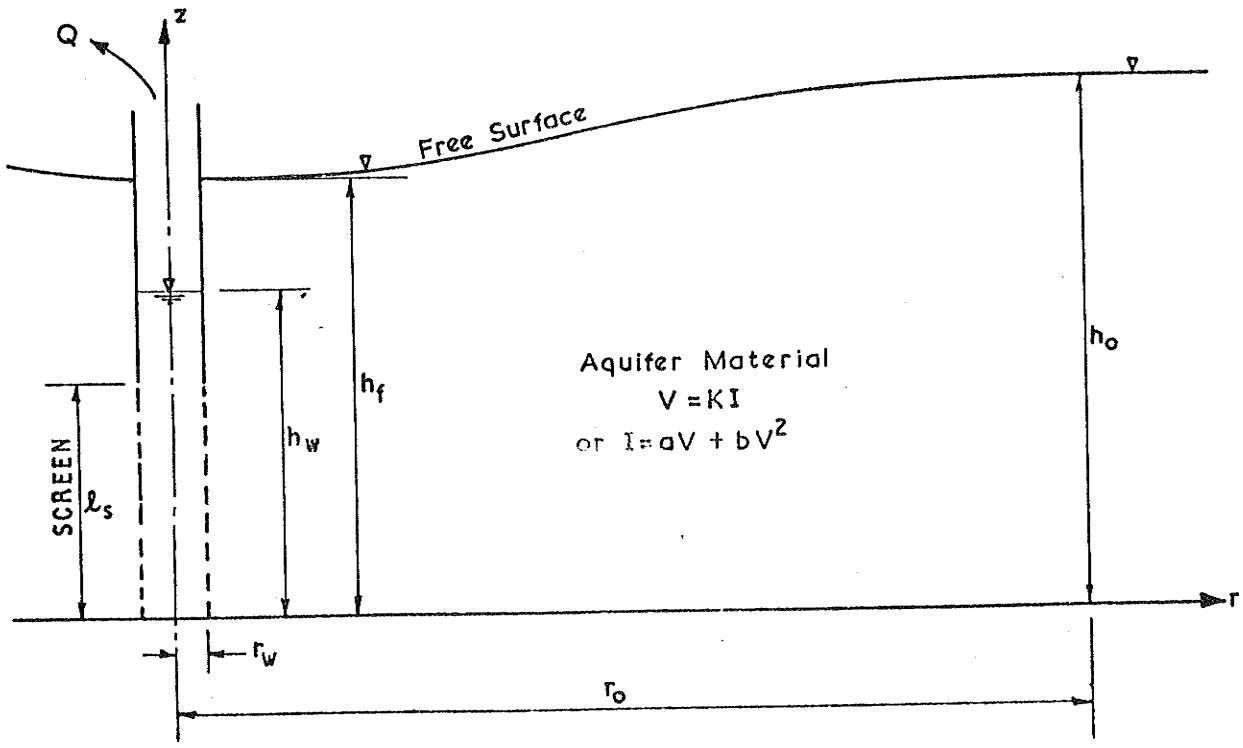

FIGURE 5·26: PARTIALLY SCREENED WELL IN AN UNCONFINED AQUIFER

No significant investigation of the more general practical well aquifer system shown in Figure 5.26 has been reported. Solutions incorporating the possibility of non-linear flow behaviour within the aquifer material do not exist even for the widely studied case of a fully screened well.

A two-dimensional axisymmetric finite element model was used to investigate problems of steady state Darcy and non-linear flow to partially screened wells in homogeneous isotropic unconfined aquifers as shown in Figure 5.26. In all cases, the capillary fringe was ignored since its contribution to the flow behaviour of the system would be even less significant than for the case of a fully screened well.

5.7.2 Dimensionless Parameters

Dimensional analysis of the problem variables of the system shown in Figure 5.26 was carried out to determine non-dimensional expressions for both the distribution of hydraulic head within the system and the well-discharge drawdown relationship for cases of Darcy and non-linear flow.

Darcy Flow

The drawdown distribution may be described by

$$\phi\left\{\frac{h_o-h}{h_o-h_w}=\frac{s}{s_w}\,,\ \frac{r}{h_o}\,,\ \frac{z}{h_o}\,,\ \frac{r_o}{h_o}\,,\ \frac{h_o}{r_w}\,,\ \frac{\ell_s}{h_o}\,,\ \frac{h_w}{h_o}\right\}=0 \qquad (5.30)$$

The well discharge drawdown relationship has the form

$$\phi\left\{\frac{Q}{K h_o^2}\,,\ \frac{r_o}{h_o}\,,\ \frac{h_o}{r_w}\,,\ \frac{\ell_s}{h_o}\,,\ \frac{h_w}{h_o}\right\}=0 \qquad (5.31)$$

Non-linear Flow

A complete description of the drawdown distribution and the well discharge drawdown relationship may be given by

$$\phi\left\{\frac{h_o-h}{h_o-h_w}, \frac{r}{h_o}, \frac{z}{h_o}, \frac{r_o}{h_o}, \frac{h_o}{r_w}, \frac{l_s}{h_o}, \frac{h_w}{h_o}, \frac{b}{a^2}\right\} = 0 \qquad (5.32)$$

$$\phi\left\{\frac{aQ}{h_o^2}, \frac{r_o}{h_o}, \frac{h_o}{r_w}, \frac{l_s}{h_o}, \frac{h_w}{h_o}, \frac{b}{a^2}\right\} = 0 \qquad (5.33)$$

As discussed in Chapter 2, the Forchheimer equation (5.4) with single valued coefficients a and b has been adopted to describe non-linear flow.

5.7.3 Finite Element Network Selection - Unconfined Aquifer

A typical finite element network for the solution of flow to a well in an unconfined aquifer is shown in Figure 5.27. The mesh is made up exclusively of triangular ring elements arranged to form several regions between which suitable transitions are interposed. As shown in Figure 5.27 each particular region is characterised by M_i and N_i the number of vertical and radial "tubes" of elements respectively. Network nodes are evenly spaced along vertical lines between the aquifer base and the free surface. The radial spacing between any two vertical lines is equal to the nodal spacing along the vertical line closer to the well. Along the well boundary ($r = r_w$) the nodal spacing scheme is altered slightly so that the nodes are evenly spaced over the two separate portions of the boundary given by $0 \leqslant z \leqslant l_s$ and $l_s \leqslant z \leqslant h_f$. The radial spacing of the vertical mesh lines in the final region of the network is adjusted to minimise distortion of the elements as the radius of influence is approached.

In solving a problem the correct location of the free surface is not known a priori. A trial free surface is assumed and subsequently adjusted by the overrelaxation iteration scheme described in Section 4.6 until the boundary condition $h = z$ along the free surface is sat-

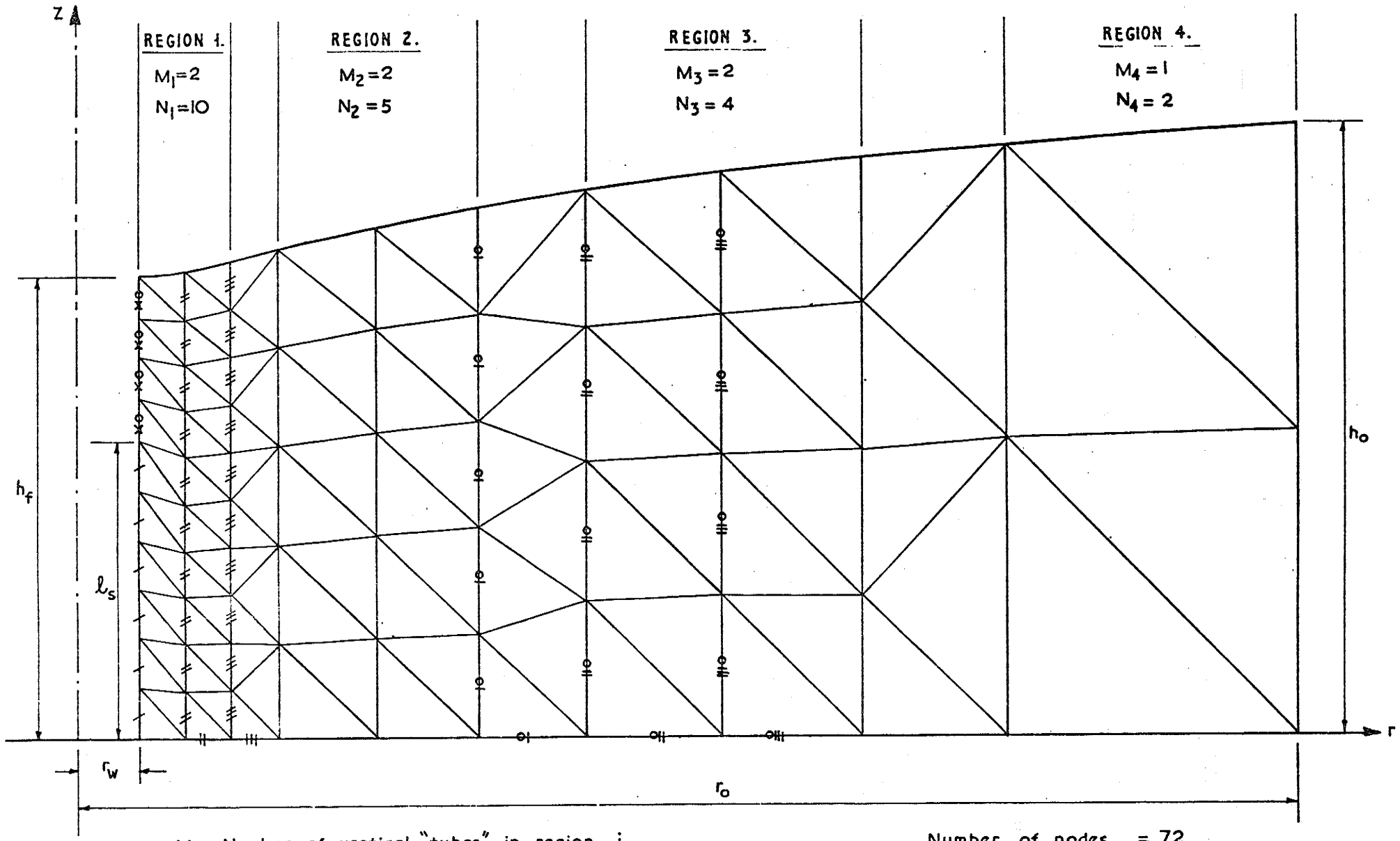

FIGURE 5·27: TYPICAL FINITE ELEMENT NETWORK – UNCONFINED AQUIFER

isfied within defined tolerance limits. For each iteration the finite element network is automatically generated by a subroutine within the computer program. Thus, the conditioning of the elements in the mesh is guaranteed at all stages of the solution process. The automatic mesh generation routines considerably reduce data preparation, an essential saving when considering the number of different problems to be investigated.

Based on the proposals of Hall (1955), the original assumed trial free surface in the solution of a problem was defined by the following equations

$$\frac{h_f - h_w}{h_o - h_w} = \left[1 - \left(\frac{h_w}{h_o}\right)^{2.4}\right] \Bigg/ \left[1 + \frac{\ln(r_o/r_w)}{50}\right]\left[1 + \frac{5 r_w}{h_o}\right] \qquad (5.34a)$$

$$\frac{z - h_f}{h_o - h_f} = 2.5\left(\frac{r - r_w}{r_o - r_w}\right) - 1.5\left(\frac{r - r_w}{r_o - r_w}\right)^{1.5} \qquad (5.34b)$$

Program trials were undertaken which indicated that the final problem solution afforded by the finite element analysis was negligibly affected by the assumed position of the original trial free surface. Various alternatives for the initial trial location of h_f and the form of the free surface were investigated but most rapid convergence of the free surface iteration scheme was attained with the adopted scheme given by equations (5.34).

As previously noted, the finite element model used overestimates both the well discharge and the drawdown (h_o-h) at any point within the aquifer and refinement of the element network improves the accuracy of solution. Program trials were carried out to determine the refinement of finite element network required for a given accuracy of solution. The accuracy of a particular network

was found to be influenced mainly, and most easily measured, by N_1, the number of radial "tubes" in the region of the mesh closest to the well. Negligible improvement in solution accuracy was achieved by increasing the number of vertical "tubes" above three for mesh regions near the well. As a general guideline this may be stated as

$$M_i = 2 \text{ or } 3 \quad \text{for} \quad i < 4$$

For a range of Darcy flow problems in which the water level within the well is drawn down to the top of the screen ($h_w = l_s$), the percentage overestimates in discharge (Q) and the percentage underestimates in the position of the free surface at the well (h_f) are given in Tables 5.10a and 5.10b respectively for various network refinements (as gauged by N_1 the number of radial "tubes" at the well). The values in Table 5.10 were obtained by solving each problem with progressively refined element networks until no significant change in solution accuracy occurred with further refinement.

Tables 5.10a and 5.10b clearly indicate that although the free surface (h_f) may be located quite accurately in the solution of a problem by a comparatively coarse network, the well discharge may be substantially overestimated by such a mesh. Generally, the discharge is of major importance in well design. The mesh accuracy testing results shown in Table 5.10a indicate that for a chosen network the percentage overestimate in well discharge decreases linearly with increase in l_s/h_o, $\log (h_o/r_w)$ and $\log (r_o/h_o)$. Thus the network refinement required to solve any particular problem

Table 5.10: Finite Element Network Errors for Flow to a Partially Screened Well in an Unconfined Aquifer

r_o/h_o	h_o/r_w	Network Refinement N_1	l_s/h_o .2	.4	.6	1
(a) Tabulated values of the percentage overestimate in well discharge Q to nearest $\frac{1}{2}$%.						
2	200	16	30	22	16	0
		32	12	9	6	
		48	$5\frac{1}{2}$	4	2	
		64	2	$\frac{1}{2}$	$\frac{1}{2}$	
2	100	16	21		11	0
		32	8		4	
		48	$3\frac{1}{2}$		$1\frac{1}{2}$	
		64	1		0	
2	50	16	$12\frac{1}{2}$	9	6	0
		32	4	3	2	
		48	$1\frac{1}{2}$	1	1	
		64	$\frac{1}{2}$	$\frac{1}{2}$	0	
4	100	16	19		9	
		32	7		$3\frac{1}{2}$	
		48	3		1	
8	200	16	$24\frac{1}{2}$		11	0
		32	9		$4\frac{1}{2}$	
		48	4		$1\frac{1}{2}$	
		64	1		0	
8	100	16	17	$12\frac{1}{2}$	$7\frac{1}{2}$	0
		32	6	$4\frac{1}{2}$	3	
		48	$2\frac{1}{2}$	$1\frac{1}{2}$	1	
8	50	16	9		$3\frac{1}{2}$	0
		32	$2\frac{1}{2}$		2	
		48	1		$\frac{1}{2}$	
(b) Tabulated values of percentage underestimate in value of h_f to nearest $\frac{1}{2}$%.						
2	200	16	3	3	3	0
		32	1	1	1	
		48	$\frac{1}{2}$	$\frac{1}{2}$	$\frac{1}{2}$	
		64	0	0	0	
2	100	16	$2\frac{1}{2}$	$2\frac{1}{2}$	$2\frac{1}{2}$	0
		32	1	1	1	
		48	$\frac{1}{2}$	$\frac{1}{2}$	$\frac{1}{2}$	
		64	0	0	0	
2	50	16	2	2	2	0
		32	$\frac{1}{2}$	$\frac{1}{2}$	$\frac{1}{2}$	
		48	0	0	0	
		64	0	0	0	
4	100	16	3		3	0
		32	1		1	
		48	$\frac{1}{2}$		$\frac{1}{2}$	
8	100	16	3		3	0
		32	$\frac{1}{2}$		$\frac{1}{2}$	
		48	0		0	

within specified limits of accuracy may be evaluated from Table 5.10a by interpolation or extrapolation.

The accuracy of the drawdown in the vicinity of the well screen closely follows the well discharge accuracy. As distance from the well screen increases, the percentage overestimate of drawdown rapidly decreases from the values of Table 5.10a.

Trial testing indicated that for finite element networks in which $N_1 \geqslant 32$ the accuracy estimates of Table 5.10 could be applied to cases involving less drawdown ($h_w > l_s$) and/or non-linear flow without introducing significant errors.

5.7.4 Finite Element Model Verification

Darcy Flow

The two dimensional axisymmetric finite element program for solution of Darcy flow to wells in unconfined aquifers was verified in the following manner. The partial screening problems described in Table 5.11 were solved by finite element analysis using a network having $N_1 = 32$ radial "tubes" at the well. Table 5.10 indicates that the expected solution accuracy should be better than 1%.

Table 5.11: Problem Data for Finite Element Model Verification
Darcy Flow to Partially Screened Well in an Unconfined Aquifer

$h_w = l_s$

Flow Case	h_o/r_w	r_o/h_o	l_s/h_o
1	10	2	0.75
2	10	2	0.50
3	10	2	0.25

In all three cases the finite element solutions compared extremely well with the analogous results obtained from experiments using an electrolytic tank apparatus. The apparatus and experi-

ments are described in Appendix 2.

Figures 5.28 and 5.29 show close agreement between the solutions obtained by the finite element analysis and the electrolytic tank results.

A discrepancy between the finite element and electrolytic tank solutions for the dimensionless distribution of drawdown shown in Figure 5.29 apparently exists in the upper portion of the aquifer close to the well. Within this region, accurate positioning of the head contours is difficult in both the finite element and electrolytic tank solutions since the flow velocities and hydraulic gradients are very small. The position of the drawdown contours may vary considerably without affecting the overall flow system.

Non-linear Flow

The Darcy flow finite element model was modified to solve problems involving non-linear flow as described by the Forchheimer relationship. The verification of this modified and more comprehensive finite element analysis by comparison with experimental results is specifically presented in Chapter 7.

5.7.5 Darcy Flow Solutions - Well Drawn Down to Top of Screen

For a partially screened well in an unconfined aquifer as depicted in Figure 5.26 ($h_w \geqslant l_s$), the case most relevant to well design is that of the water level within the well being drawn down to the top of the screen, i.e. maximum well drawdown before screen dewatering occurs ($h_w = l_s$).

A wide range of such problems involving Darcy flow were investigated using the verified finite element model.

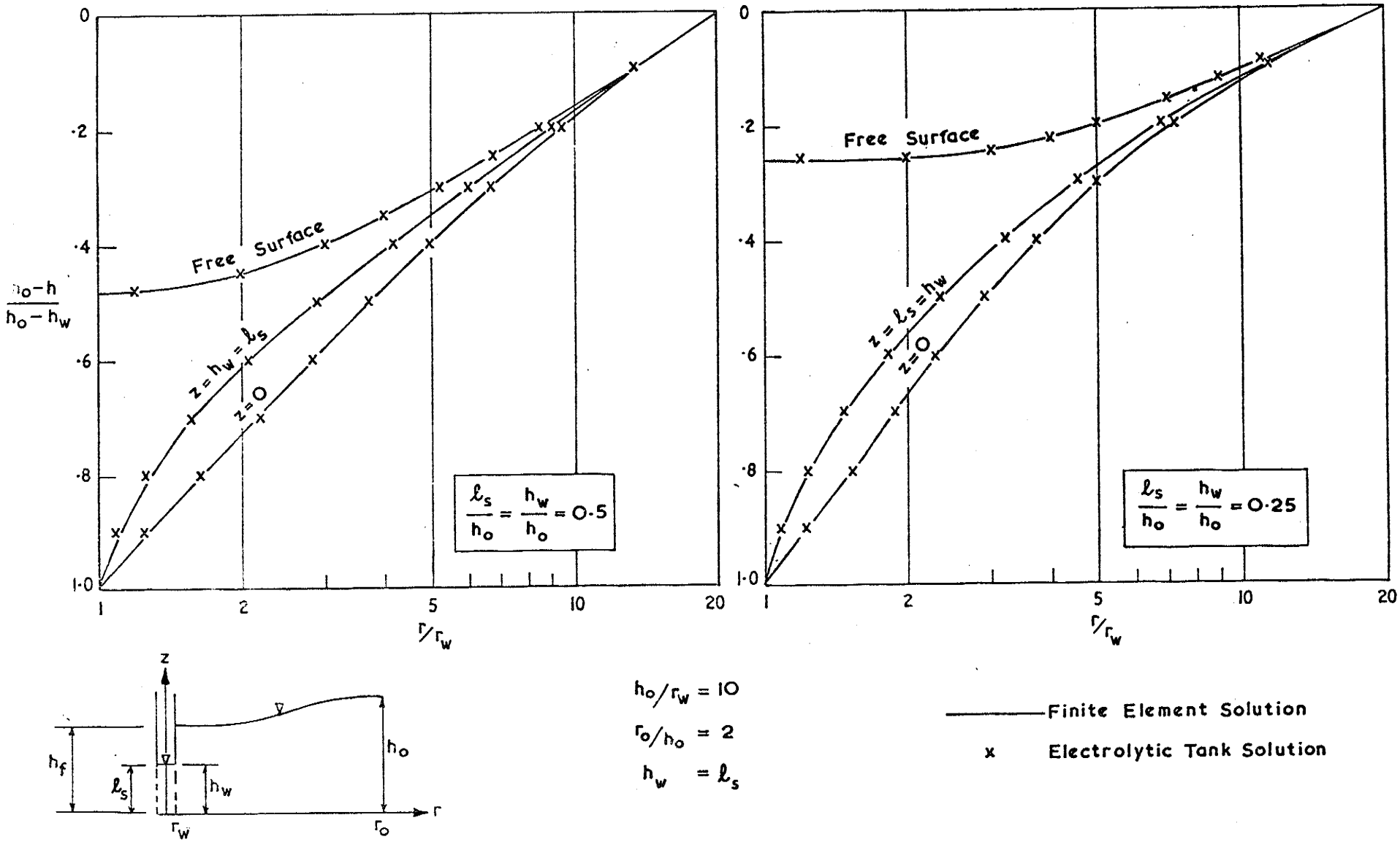

FIGURE 5·28: PARTIALLY SCREENED WELL IN AN UNCONFINED AQUIFER.
COMPARISON OF FINITE ELEMENT & ELECTROLYTIC TANK SOLUTIONS – DARCY FLOW

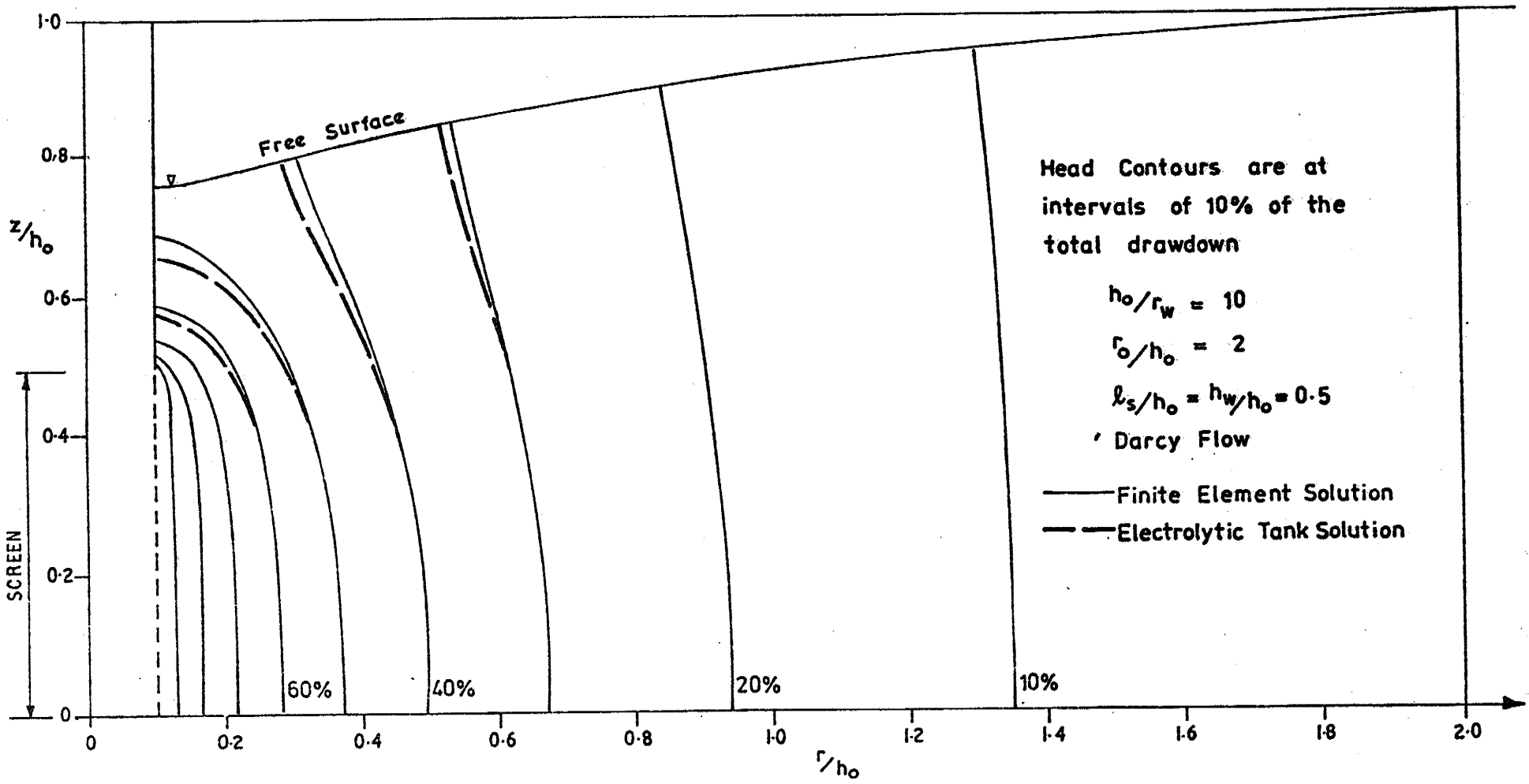

FIGURE 5·29: PARTIALLY SCREENED WELL IN AN UNCONFINED AQUIFER.

COMPARISON OF FINITE ELEMENT & ELECTROLYTIC TANK HEAD DISTRIBUTIONS - DARCY FLOW.

The program results indicating the relative effects of partial screening on well performance and free surface drawdown are presented in Table 5.12a and 5.12b respectively. Through successive refinement of the element networks, accurate solutions were available for the particular problems covered by Table 5.10. Values given in Table 5.12 for other problems were obtained by applying the relevant corrections, as estimated from Table 5.10, to the finite element solutions found using $N_1 = 32$ radial "tube" element meshes.

In Figure 5.30 the partial screening effects are presented for the typical case $r_o/h_o = 2$. The Dupuit expression (equation(5.28)) for discharge to the equivalent fully screened wells has been presented (dotted lines) in Figure 5.30 for comparison with the partially screened results. For values of $h_w/h_o \geqslant 0.7$ the Dupuit equation (5.28) for fully screened wells ($l_s = h_o$) is seen to give an accurate estimate of the well performance for the partially screened case ($l_s = h_w$). However, for partial screening where $l_s/h_o < 0.7$, the Dupuit equation overestimates the well discharge and the error rapidly increases with decrease in screen length for $l_s/h_o < 0.4$.

In all cases of prescribed h_o/r_w and r_o/h_o, both the maximum well discharge and free surface drawdown were obtained at values of $0.4 < h_w/h_o = l_s/h_o < 0.5$.

Figure 5.31 shows clearly the maximum values of well discharge and free surface drawdown attainable with partially screened wells in unconfined aquifers if dewatering of the screens is not to be allowed.

The drawdown distribution for the Darcy flow problem ($r_o/h_o = 2$ $h_o/r_w = 100$ $l_s/h_o = h_w/h_o = 0.5$) is shown in Figure 5.32.

Typical distributions of the drawdown along the free surface, the line $z = l_s$, and the base of the aquifer are given in Figure 5.33.

From the problems investigated, the following significant features were found to be characteristic of the hydraulic head distribution:-

(i) The flow was essentially radial one-dimensional for $r > h_o$ and beyond a distance h_o from the well the Dupuit equation (5.27) may be used to describe the flow distribution. For values of $h_o/r_w < 50$ the limiting radius from the well beyond which the flow may be described by equation (5.27) should be extended to $r > 1.5\ h_o$.

(ii) The flow was radially one-dimensional for $z < l_s/2$. Thus the base pressure head distribution is representative of the region within a height $l_s/2$ above the base.

(iii) Within the flow region ($r < l_s$, $z < l_s/2$) the expression

$$h - h_w = \left[\frac{Q \ln (r/r_w)}{2\pi K l_s}\right] \Big/ \left[\sqrt{2}\ \frac{h_f}{h_o}\right] \qquad (5.35)$$

predicted $h - h_w$ with an error not exceeding 3% for the range of problems $.15 < l_s/h_o = h_w/h_o < .65$, $40 < h_o/r_w < 250$, $r_o/h_o > 2$.

(iv) Near the well, the free surface remained very nearly horizontal as demonstrated by the following equations:-

$$h\ (r, \text{free surface}) - h_f = \epsilon \qquad (5.36a)$$

$$\epsilon \text{ was negligible for } r < 0.15\ (h_o - l_s) \qquad (5.36b)$$

$$\epsilon < (h_o/200) \text{ for } r < 0.3\ (h_o - l_s) \qquad (5.36c)$$

The discharge flux distribution along the screen length is presented in Figure 5.34 for several typical flow cases. In all problems solved the flux q equalled the uniform flux distribution value

$q^* = Q/l_s$ at the position $l/l_s = 0.75$ along the screen. In general the flux distribution became more uniform with increase in both l_s/h_o and h_o/r_w. The behavioural trends so exhibited are similar to those noted in Section 5.3.5 for partially screened wells in confined aquifers. The flux distributions for $r_o/h_o = 2$ as shown in Figure 5.34 are equally applicable for any larger radius of influence.

5.7.6 Non-linear Flow Solutions - Well Drawn Down to Top of Screen

The verified finite element program was used to examine a wide range of problems involving non-linear flow in partially screened unconfined aquifers as shown in Figure 5.26. The maximum allowable well drawdown case $h_w = l_s$ was solved since it is of major importance.

The program results indicating the effects of non-linear flow on well performance and free surface drawdown are presented in Tables 5.13a and 5.13b respectively. Tabulated values were found by applying the relevant corrections, as estimated from Table 5.10, to the finite element solutions obtained using $N_1 = 32$ radial "tube" element meshes.

Figure 5.35 presents the effects of non-linear flow and partial screening for the typical case $r_o/h_o = 2$, $h_o/r_w = 50$. With increasing non-linearity (measured by b/a^2) there is a dramatic reduction in well performance and free surface drawdown.

The critical screening ratio, $(l_s/h_o)_{crit.}$ at which maximum well discharge and free surface drawdown were obtained is seen in Figure 5.36 to increase with b/a^2. Also shown clearly in Figure 5.36 is the effect of non-linear flow on the maximum values of well

performance and free surface drawdown attainable without dewatering the well screen.

The typical drawdown distribution shown in Figure 5.37 for the case ($r_o/h_o = 2$, $h_o/r_w = 100$, $l_s/h_o = h_w/h_o = 0.5$, $b/a^2 = 1$) may be compared with the Darcy solution for the same geometry (Figure 5.32).

The distributions of drawdown along the free surface and the aquifer base are shown in Figure 5.38 for some typical cases of non-linear flow.

As for the Darcy flow case -

(i) the flow was radially one-dimensional for $z < l_s/2$,

(ii) partial screening effects were negligible and the flow was fully radial for $r > 1.5\ h_o$,

(iii) near the well the free surface remained essentially horizontal.

Non-linear flow effects were found to be negligible at $r=r_o=2h_o$ even for the extreme case of $b/a^2 = 100$. The flow could be described by the Dupuit equation (5.27) for Darcy flow ($K = 1/a$) for $r > 2h_o$.

The effects of non-linearity on the flux distribution along the screen are demonstrated in Figure 5.39. The flux distribution is seen to become more uniform with increasing non-linearity as measured by b/a^2 (this trend was also noted in Section 5.3.6 when confined aquifers were being considered). As for the Darcy flow cases considered in Section 5.7.5 the following effects were found to be applicable to cases of non-linear flow:-

(i) The flux q equals the uniform distribution flux, $q^* = Q/l_s$,

at $l/l_s = 0.75$.

(ii) The flux distribution becomes more uniform with increase in both l_s/h_o and h_o/r_w.

(iii) Flux distributions for $r_o/h_o = 2$ are representative for any larger radius of influence.

5.7.7 Solutions for Well Water Levels above the Screen

In the previous sections 5.7.5 and 5.7.6 solutions were presented for the respective cases of Darcy and non-linear flow to partially screened wells (see Figure 5.26) for the limiting condition of drawdown to the top of the screen ($h_w = l_s$).

In many cases a well may be operated with the water level in the well above the top of the screen. This condition, $h_w > l_s$, was investigated for Darcy flow using the finite element model.

The results for a range of problems are presented in Table 5.14. The values in Table 5.14 were obtained by applying corrections according to Table 5.10 to finite element solutions found using $N_1 = 32$ radial "tube" element networks.

The effects of h_w/h_o upon both well performance and free surface level (h_f) at the well are shown in Figure 5.40 for the typical case $r_o/h_o = 2$, $h_o/r_w = 50$.

In all cases, both the well performance and the free surface drawdown varied linearly with h_w/h_o between $h_w/h_o = l_s/h_o$ and $h_w/h_o = 1$. Thus, well performance and free surface drawdown at the well may be estimated for any value $h_w > l_s$ from the solutions for the limiting case ($h_w = l_s$) investigated in Section 5.7.5.

Table 5.12: Darcy Flow to a Partially Screened Well in an Unconfined Aquifer - Drawdown to Top of Screen

r_o/h_o	h_o/r_w	$h_w/h_o = l_s/h_o$ .2	.3	.4	.5	.6	.7
(a) Well performance - tabulated values of Q/Kh_o^2							
2	200	.27	.32	.34	.34	.31	.26
	100	.31	.36	.39	.38	.35	
	50	.39	.44	.46	.45	.41	.34
4	200	.26	.30	.32	.31	.28	
	100	.30	.34	.36	.35	.31	
	50	.37	.41	.42	.40	.36	
8	200	.25	.28	.30	.29	.26	
	100	.29	.32	.33	.32	.29	
	50	.35	.38	.39	.37	.33	
16	200		.27	.28	.27		
	100		.30	.31	.30		
	50		.36	.36	.33		
(b) Free surface location at the well - tabulated values of h_f/h_o							
2	200	.94	.93	.92	.91	.91	
	100	.93	.91	.90	.89	.89	
	50	.91	.89	.88	.87	.87	
4	200	.91	.89	.88	.87	.87	
	100	.90	.87	.86	.85	.85	
	50	.86	.84	.83	.82	.83	
8	200	.88	.86	.84	.84	.84	
	100	.86	.83	.82	.82	.83	
	50	.82	.80	.78	.78	.79	
16	200		.82	.81	.81		
	100		.79	.78	.78		
	50		.75	.74	.74		

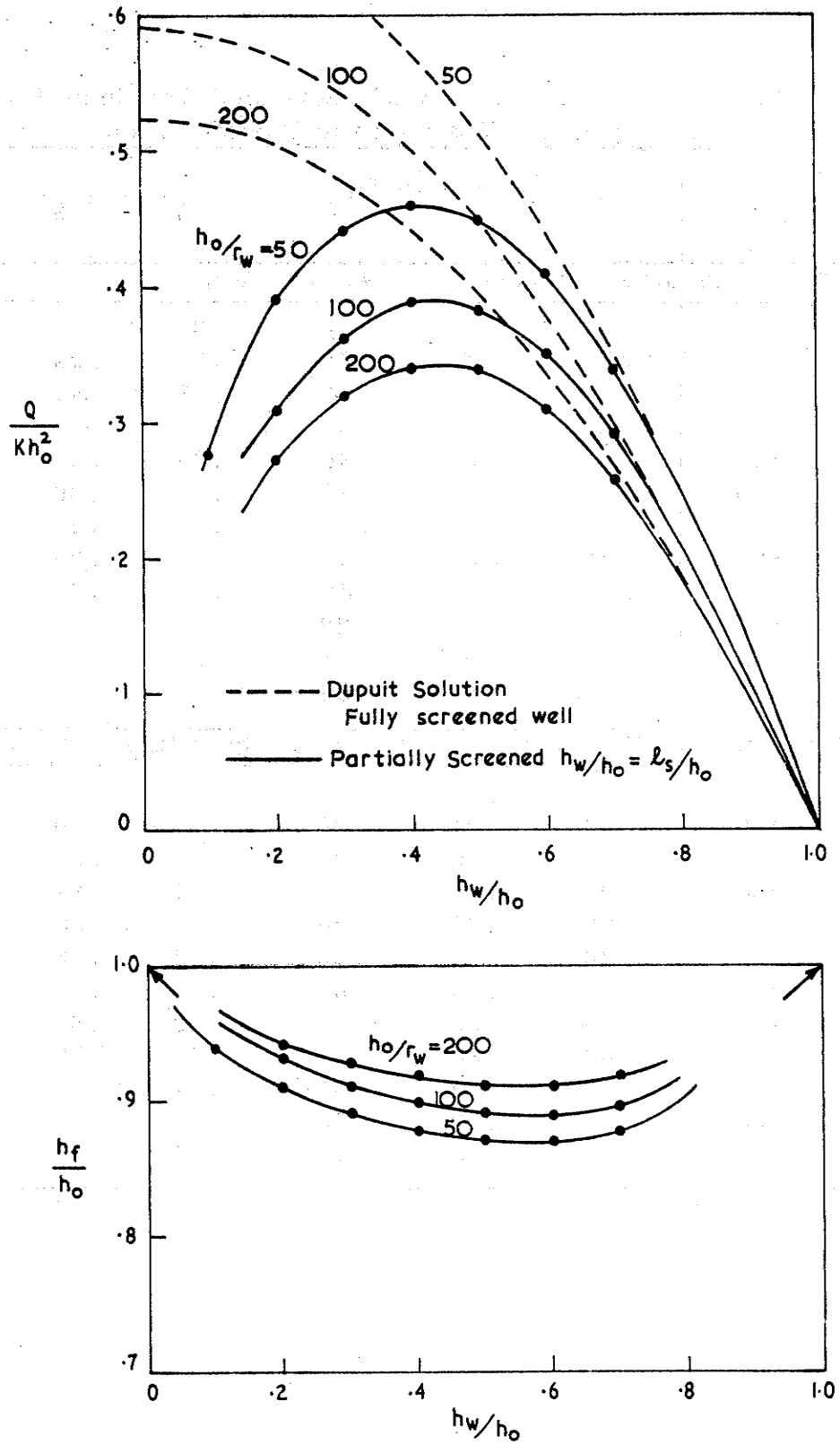

DARCY FLOW. $\ell_s = h_w$. $r_o/h_o = 2$

FIGURE 5·30: PARTIALLY SCREENED WELL IN AN UNCONFINED AQUIFER

TYPICAL EFFECTS FOR WELL DRAW-DOWN TO TOP OF SCREEN - DARCY FLOW.

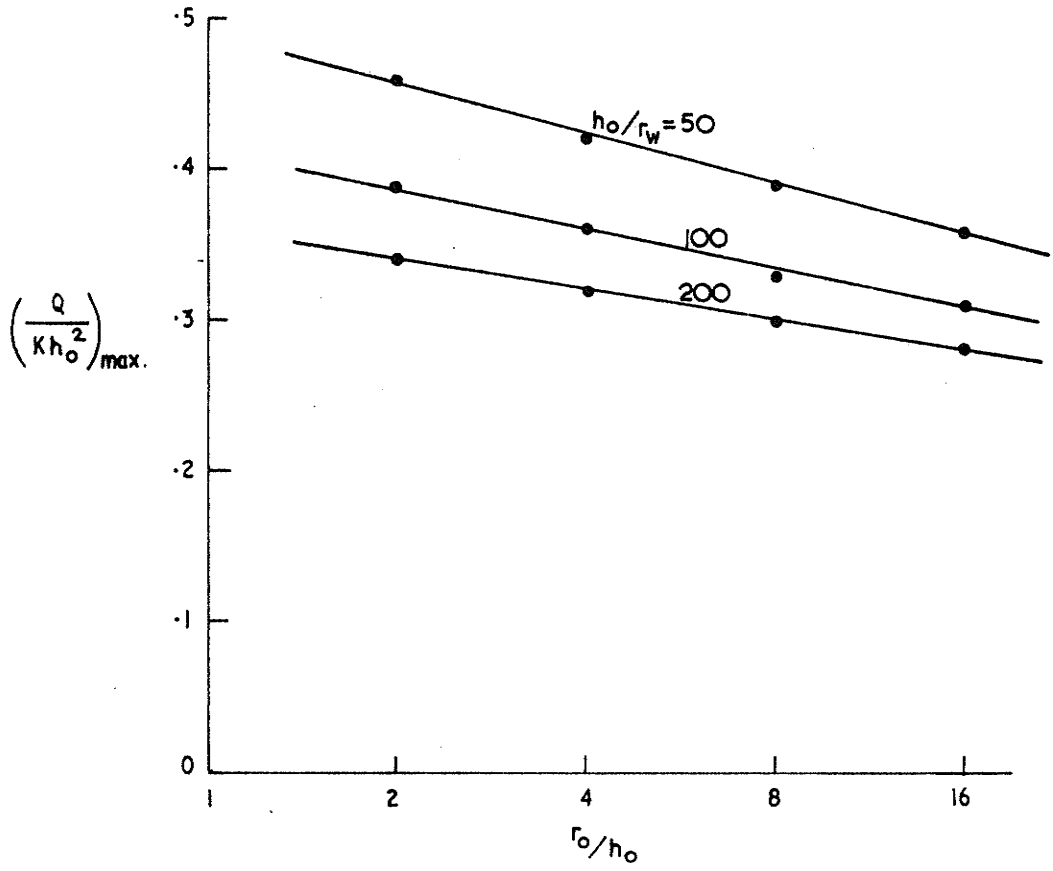

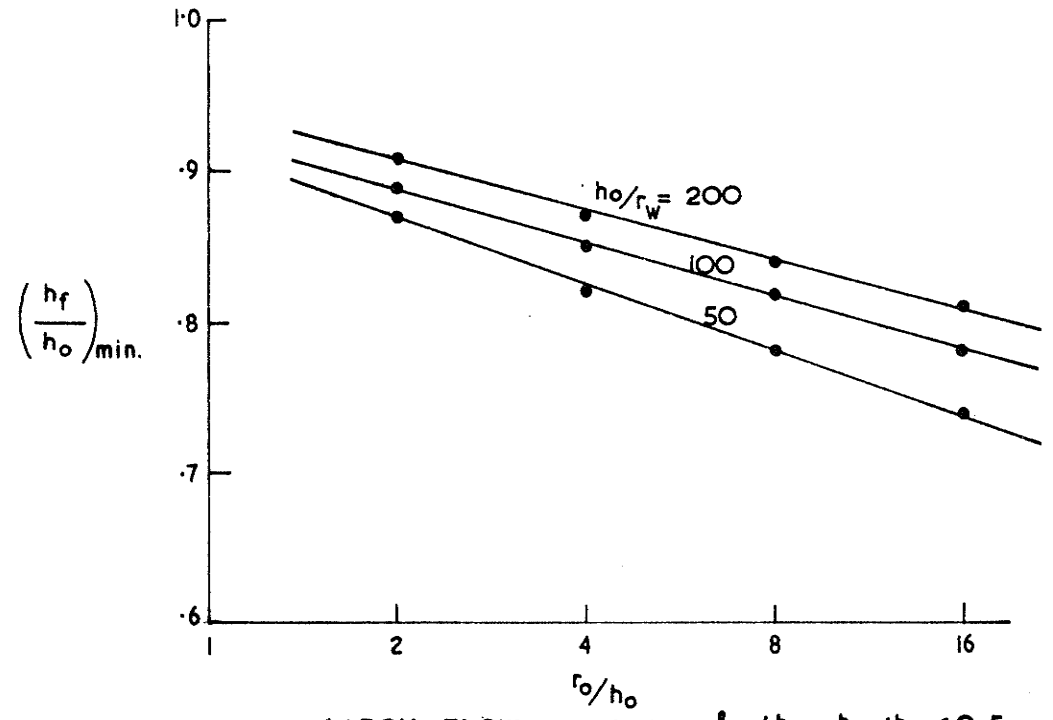

DARCY FLOW. $0.4 < \ell_s/h_o = h_w/h_o < 0.5$

FIGURE 5·31: PARTIALLY SCREENED WELL IN AN UNCONFINED AQUIFER.

MAXIMUM VALUES OF WELL DISCHARGE AND FREE SURFACE DRAWDOWN - NO SCREEN DEWATERING - DARCY FLOW

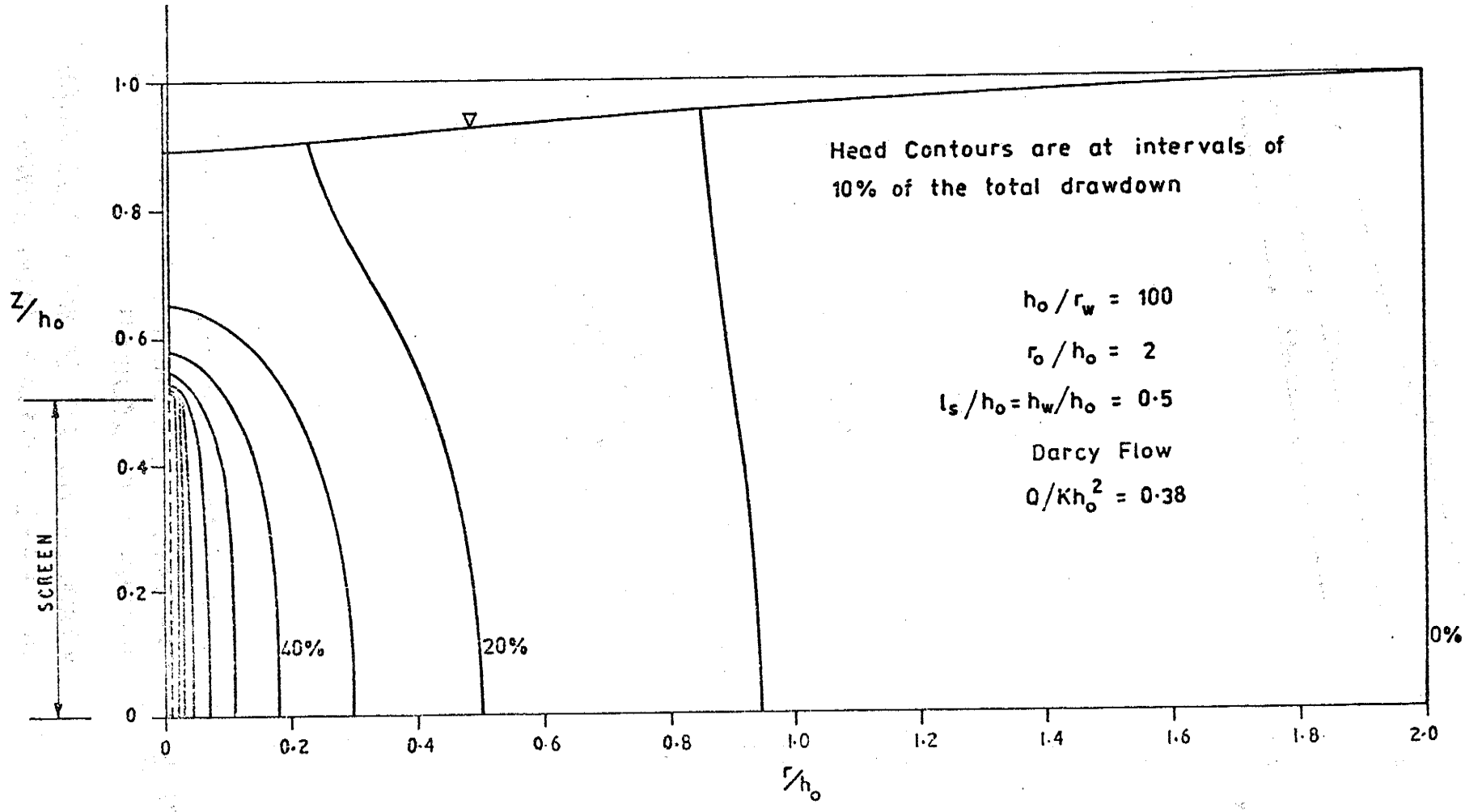

FIGURE 5·32: PARTIALLY SCREENED WELL IN AN UNCONFINED AQUIFER.
TYPICAL HEAD DISTRIBUTION FOR DARCY FLOW.

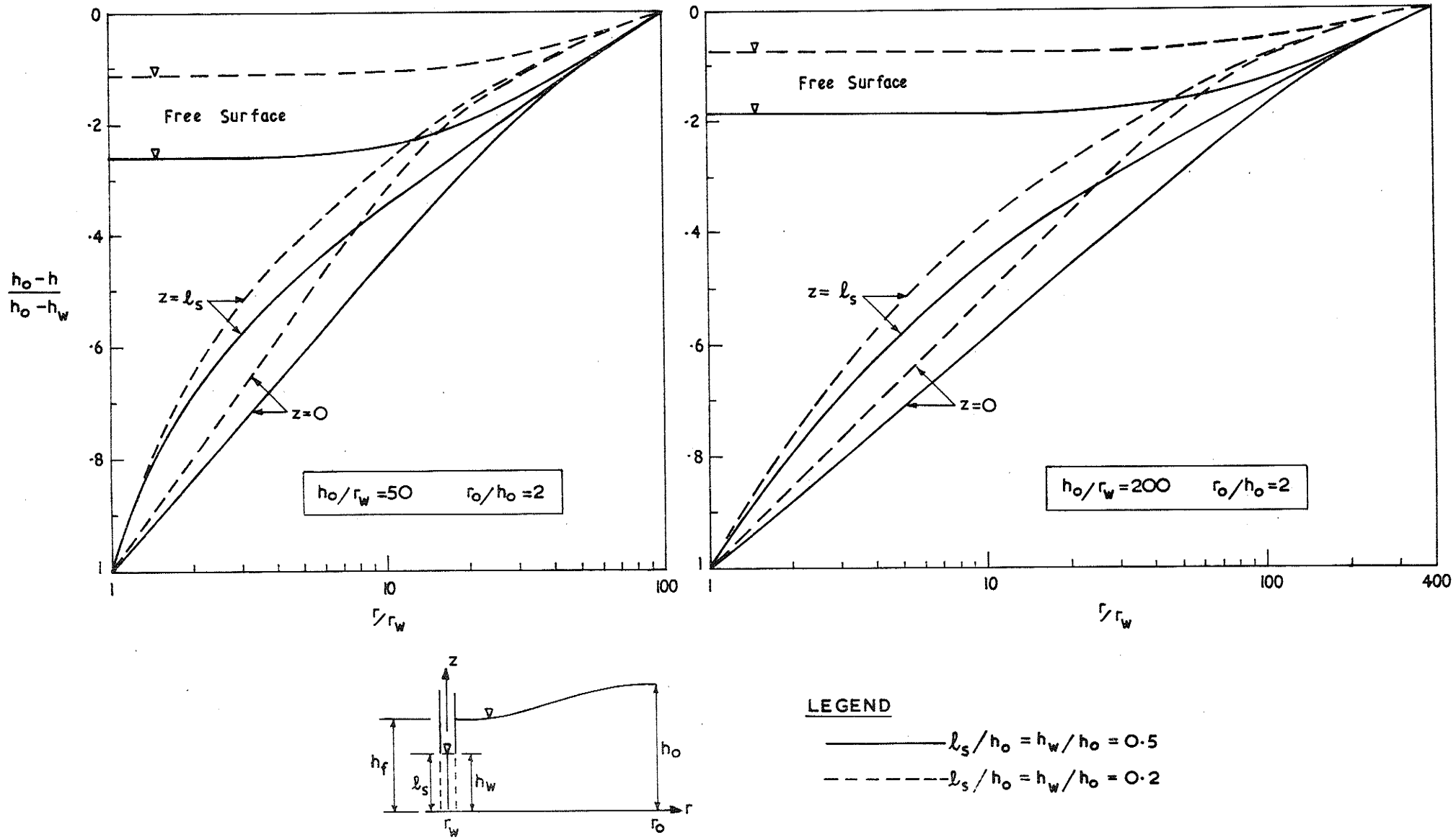

FIGURE 5·33: PARTIALLY SCREENED WELL IN AN UNCONFINED AQUIFER. TYPICAL DRAWDOWN DISTRIBUTIONS FOR DARCY FLOW.

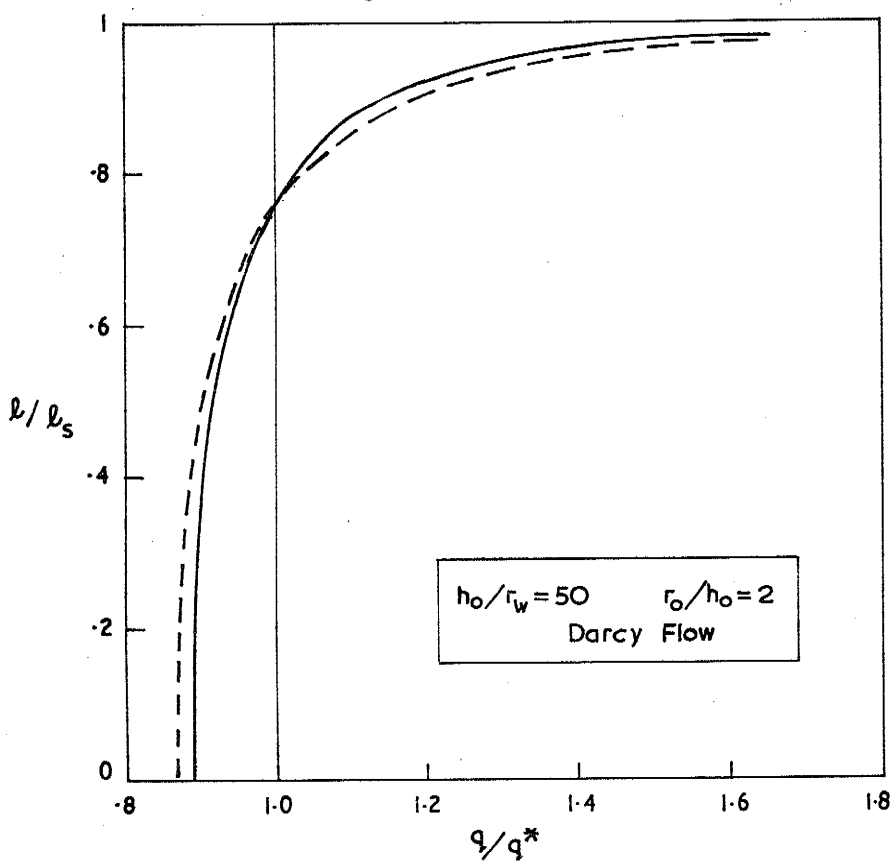

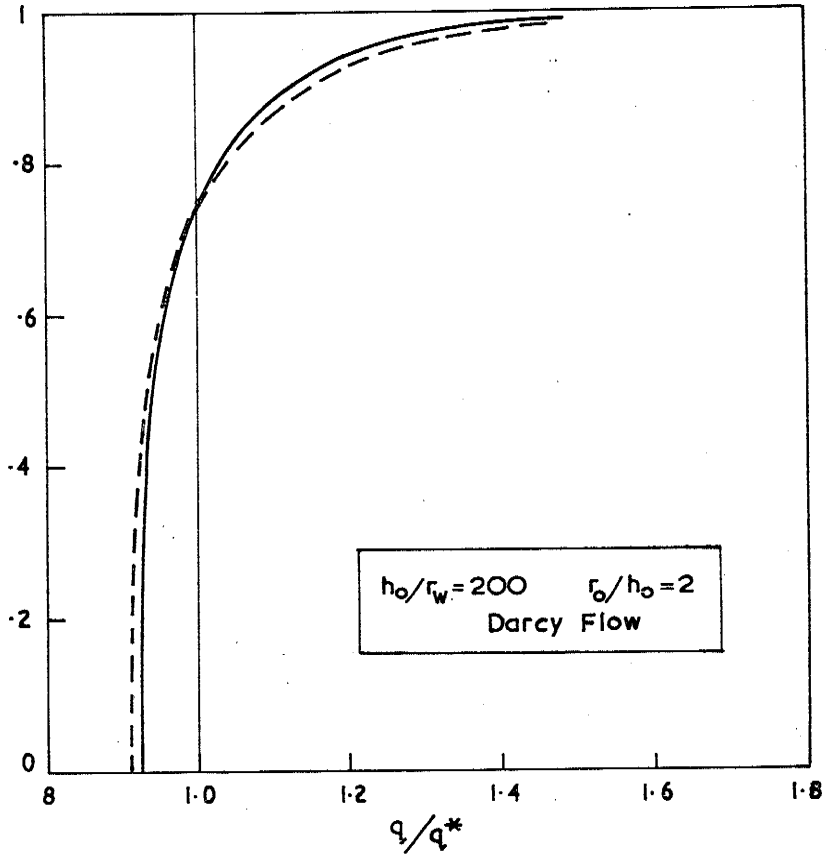

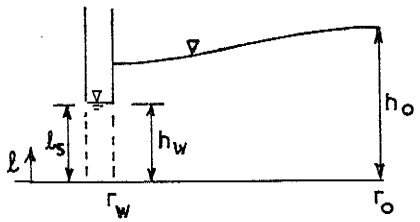

LEGEND

——— $\ell_s / h_o = 0.5$

– – – – – – $\ell_s / h_o = 0.2$

$q^* = Q / \ell_s$

$\ell_s = h_w$

FIGURE 5·34: PARTIALLY SCREENED WELL IN AN UNCONFINED AQUIFER. TYPICAL DISCHARGE FLUX DISTRIBUTIONS ALONG SCREEN - DARCY FLOW.

Table 5.13: Non-linear Flow to a Partially Screened Well in an Unconfined Aquifer-Drawdown to Top of Screen

r_o/h_o	h_o/r_w	b/a^2	$h_w/h_o = l_s/h_o$ .2	.3	.4	.5	.6	.7	.8
(a) Well Performance - Tabulated Values of $\frac{aQ}{h_o^2}$									
2	50	Darcy	.39	.44	.46	.45	.41	.34	
		.01		.43	.45	.44	.40		
		.1		.36	.39	.39	.37	.32	
		1		.20	.23	.24	.24	.22	
		10			.090	.099	.10	.10	.090
		100		.026	.031	.034	.036	.036	.033
2	100	Darcy	.31	.36	.39	.38	.35		
		.01		.35	.37	.37	.34		
		.1		.28	.31	.32	.31	.27	
		1		.15	.17	.19	.19	.18	
		10			.067	.074	.078	.077	.070
		100		.019	.023	.025	.027	.027	.025
2	200	Darcy	.27	.32	.34	.34	.31	.26	
		.01		.30	.32	.33	.30		
		.1		.24	.27	.28	.27	.24	
		1		.12	.14	.15	.16	.15	
		10			.054	.060	.064	.064	.058
		100		.015	.018	.020	.022	.022	.021
(b) Free Surface Location at the Well - Tabulated Values of h_f/h_o.									
2	50	Darcy	.91	.89	.88	.87	.87		
		.01		.89	.88	.87	.87		
		.1		.91	.89	.88	.88	.88	
		1		.95	.94	.93	.92	.92	
		10			.98	.97	.97	.96	.96
		100		.99	.99	.99	.98	.98	.98
2	100	Darcy	.93	.91	.90	.89	.89		
		.01		.91	.90	.89	.89		
		.1		.93	.92	.91	.90	.90	
		1		.96	.96	.95	.94	.94	
		10			.98	.98	.98	.97	.97
		100		.99	.99	.99	.99	.99	.99
2	200	Darcy	.94	.93	.92	.91	.91		
		.01		.93	.92	.91	.91		
		.1		.95	.94	.93	.92	.92	
		1		.98	.97	.97	.96	.96	
		10			1.00	.99	.99	.99	.99
		100		1.00	1.00	1.00	1.00	1.00	1.00

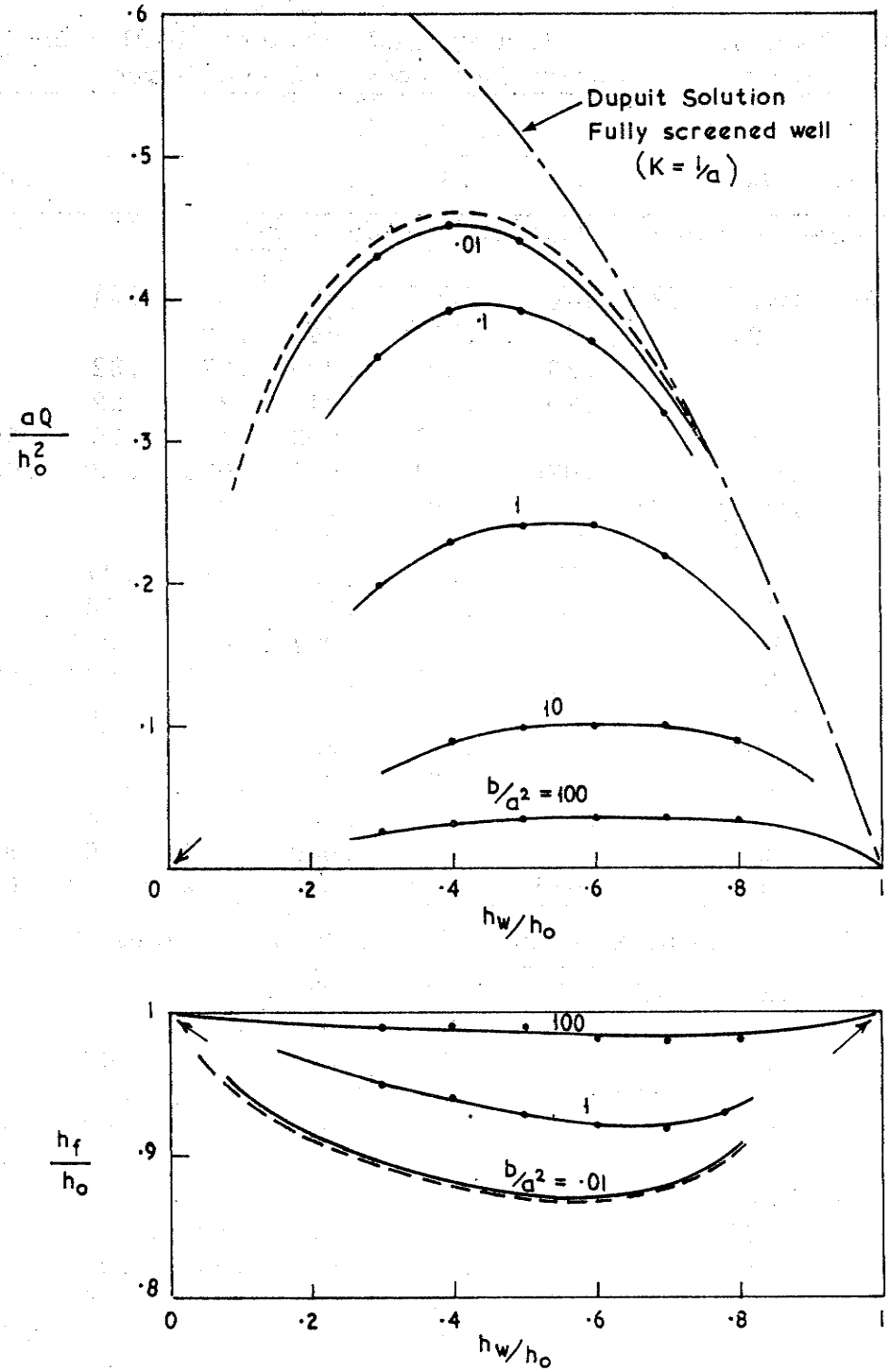

FIGURE 5·35: PARTIALLY SCREENED WELL IN AN UNCONFINED AQUIFER

TYPICAL EFFECTS FOR DRAWDOWN TO TOP OF SCREEN – NON LINEAR FLOW.

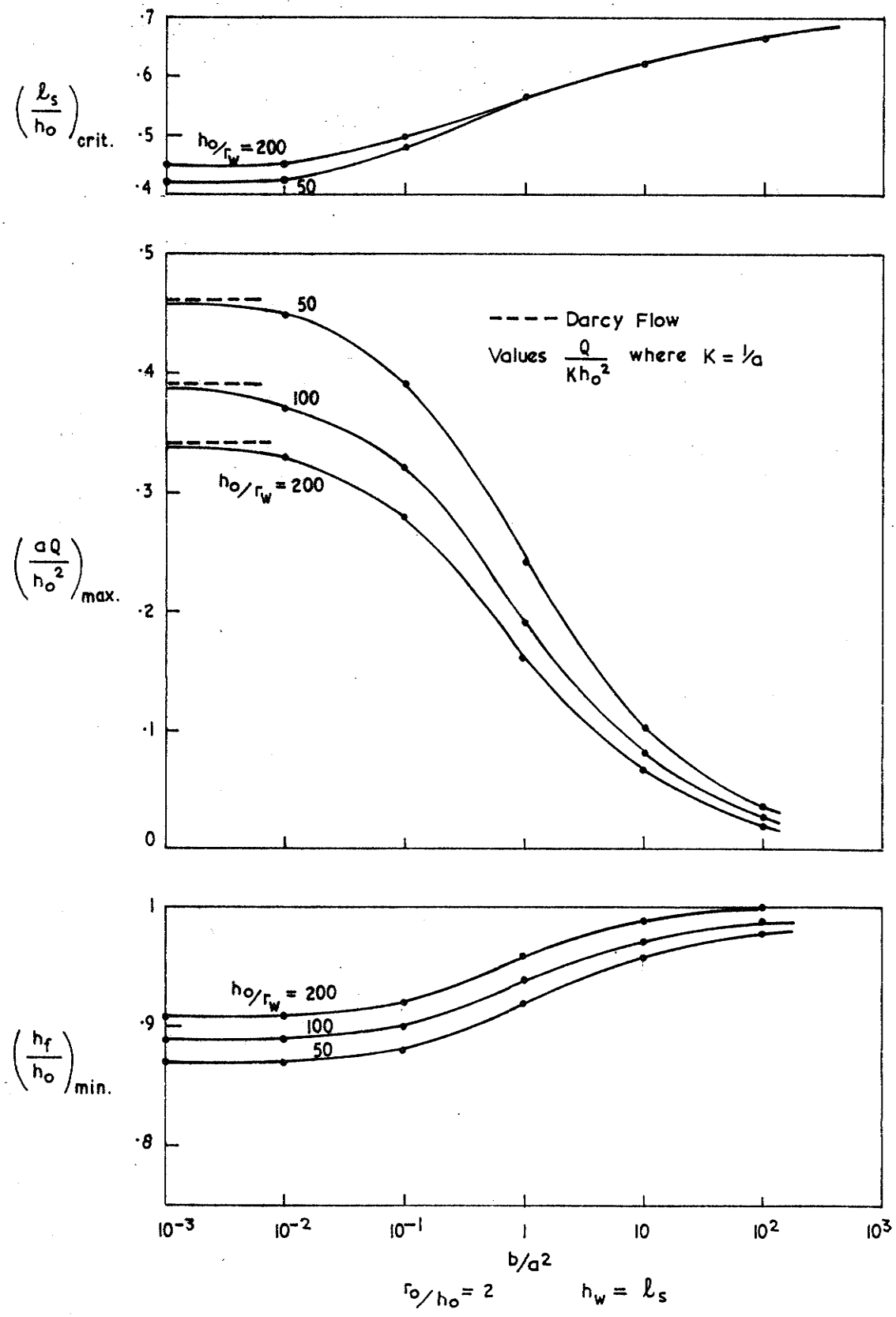

FIGURE 5·36: PARTIALLY SCREENED WELL IN AN UNCONFINED AQUIFER.

MAXIMUM VALUES OF WELL DISCHARGE AND FREE SURFACE DRAWDOWN - NO SCREEN DEWATERING - NON LINEAR FLOW

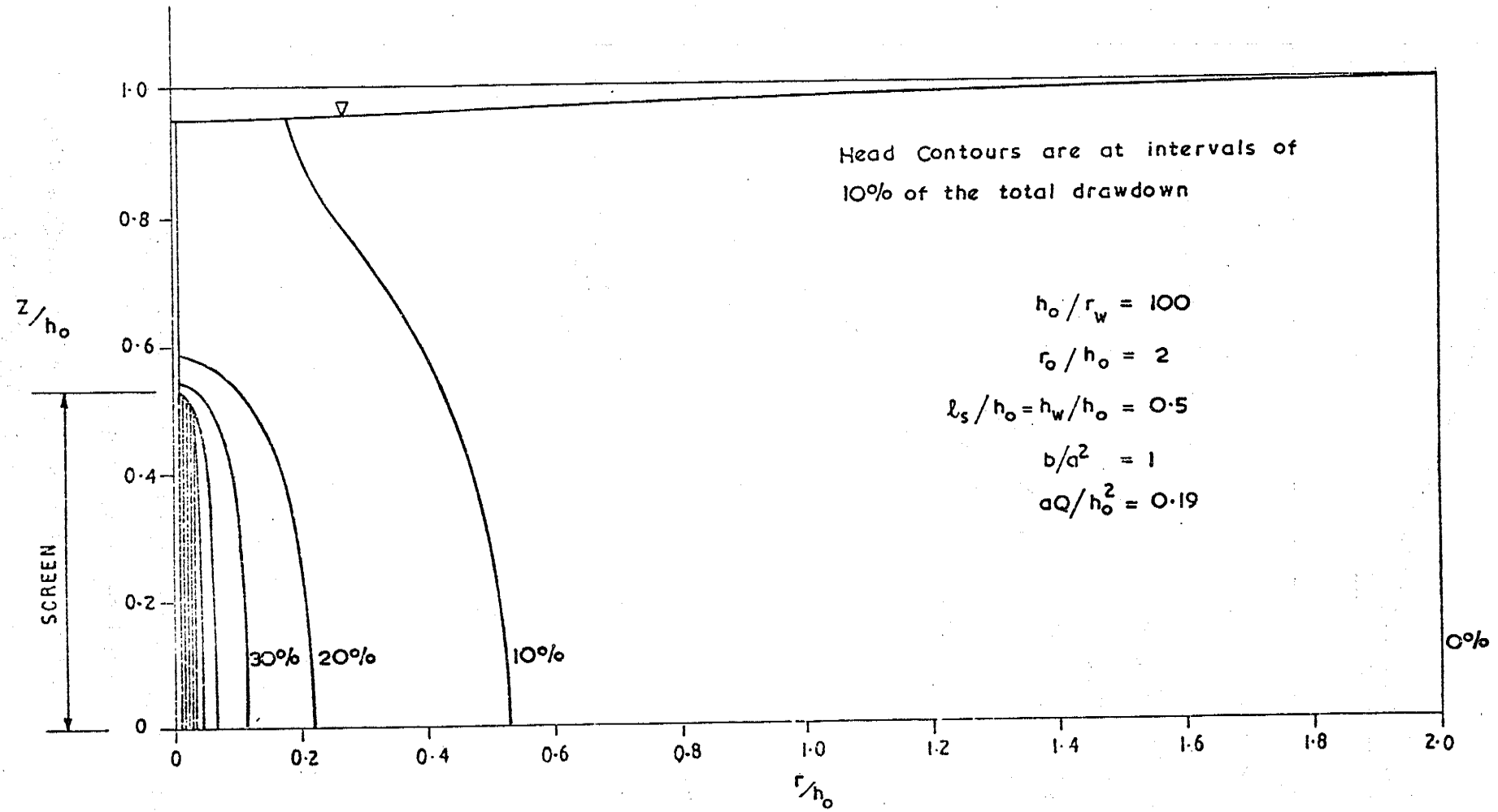

FIGURE 5-37: PARTIALLY SCREENED WELL IN AN UNCONFINED AQUIFER.
TYPICAL HEAD DISTRIBUTION FOR NON LINEAR FLOW.

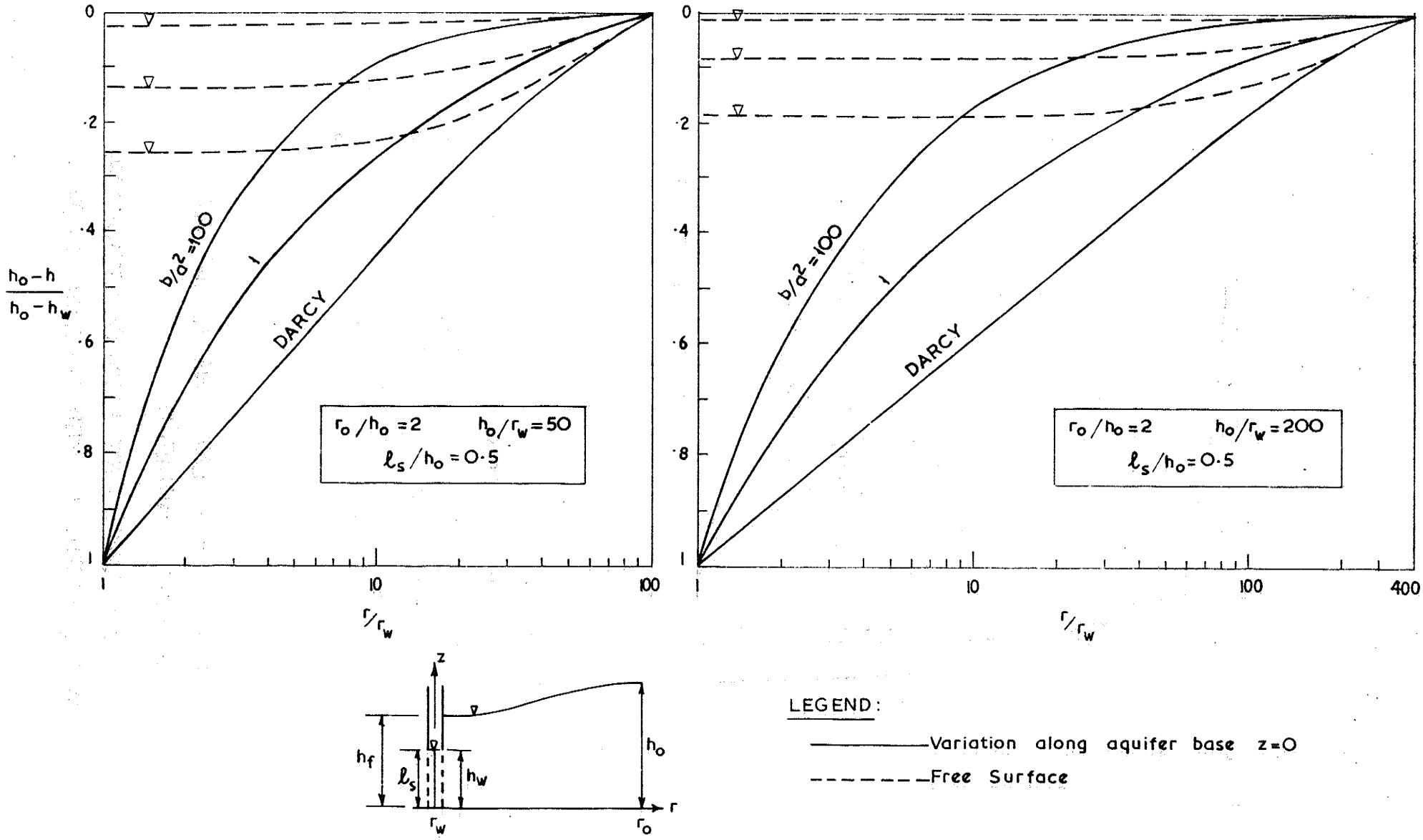

FIGURE 5·38: PARTIALLY SCREENED WELL IN AN UNCONFINED AQUIFER. TYPICAL DRAWDOWN DISTRIBUTIONS FOR NON LINEAR FLOW

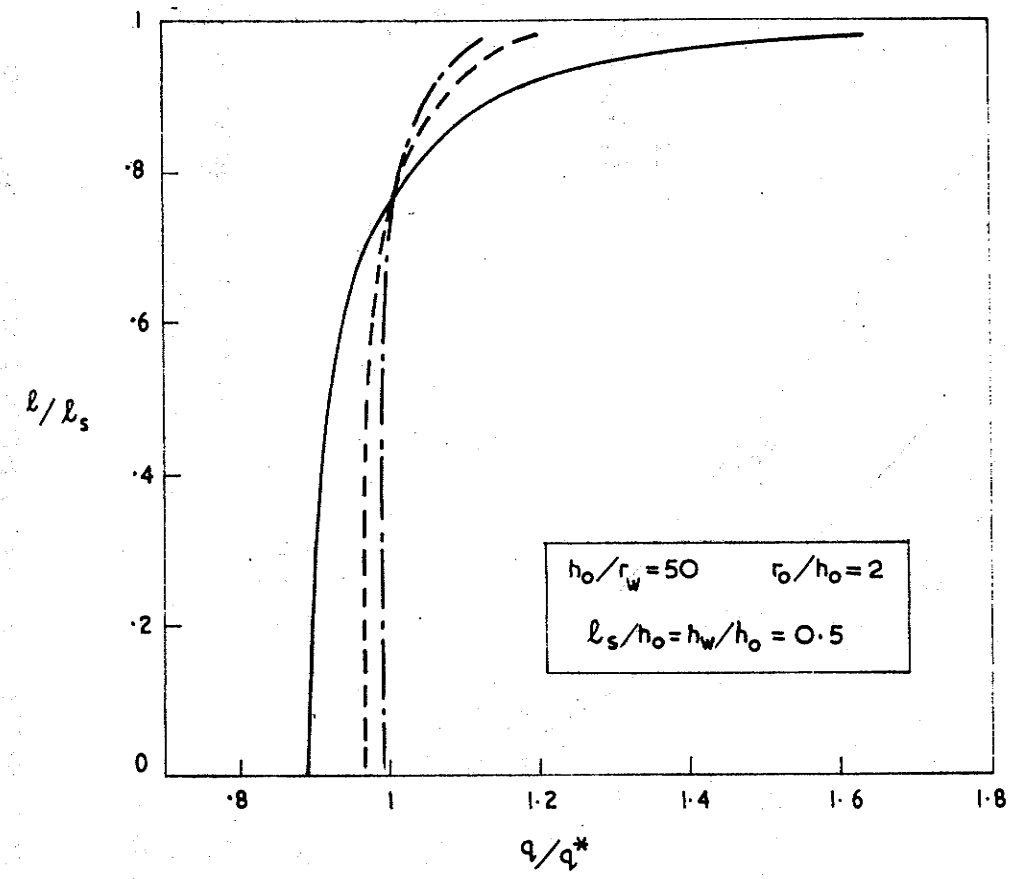

LEGEND:

——— $b/a^2 = 0$ Darcy

– – – – $b/a^2 = 1$

—·—·— $b/a^2 = 100$

$q^* = Q/\ell_s$

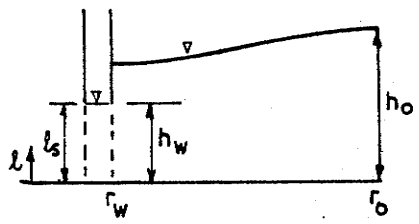

FIGURE 5·39: PARTIALLY SCREENED WELL IN AN UNCONFINED AQUIFER

TYPICAL DISCHARGE FLUX DISTRIBUTIONS ALONG SCREEN - NON LINEAR FLOW

Table 5.14: Partially Screened Well in an Unconfined Aquifer - Well Water Level Above the Screen - Tabulated Values of Q/Kh_o^2 and h_f/h_o

r_o/h_o	h_o/r_w	l_s/h_o	h_w/h_o	Q/Kh_o^2	h_f/h_o
2	50	0.2	0.2	.388	.908
			0.6	.194	.955
			0.8	.097	.978
			1	0	1
		0.4	0.4	.460	.874
			0.6	.308	.919
			0.8	.155	.962
			1	0	1
		0.6	0.6	.406	.863
			0.73'	.273	.915
			0.86'	.137	.960
			1	0	1
2	200	0.2	0.2	.268	.934
			0.6	.134	.967
			0.8	.067	.984
			1	0	1
		0.4	0.4	.337	.907
			0.6	.225	.939
			0.8	.113	.971
			1	0	1
		0.6	0.6	.311	.898
			0.73'	.208	.935
			0.86'	.104	.969
			1	0	1
8	50	0.2	0.2	.346	.824
			0.6	.175	.917
			0.8	.088	.960
			1	0	1
		0.4	0.4	.386	.782
			0.6	.260	.864
			0.8	.131	.936
			1	0	1
		0.6	0.6	.326	.795
			0.73'	.219	.874
			0.86'	.111	.941
			1	0	1

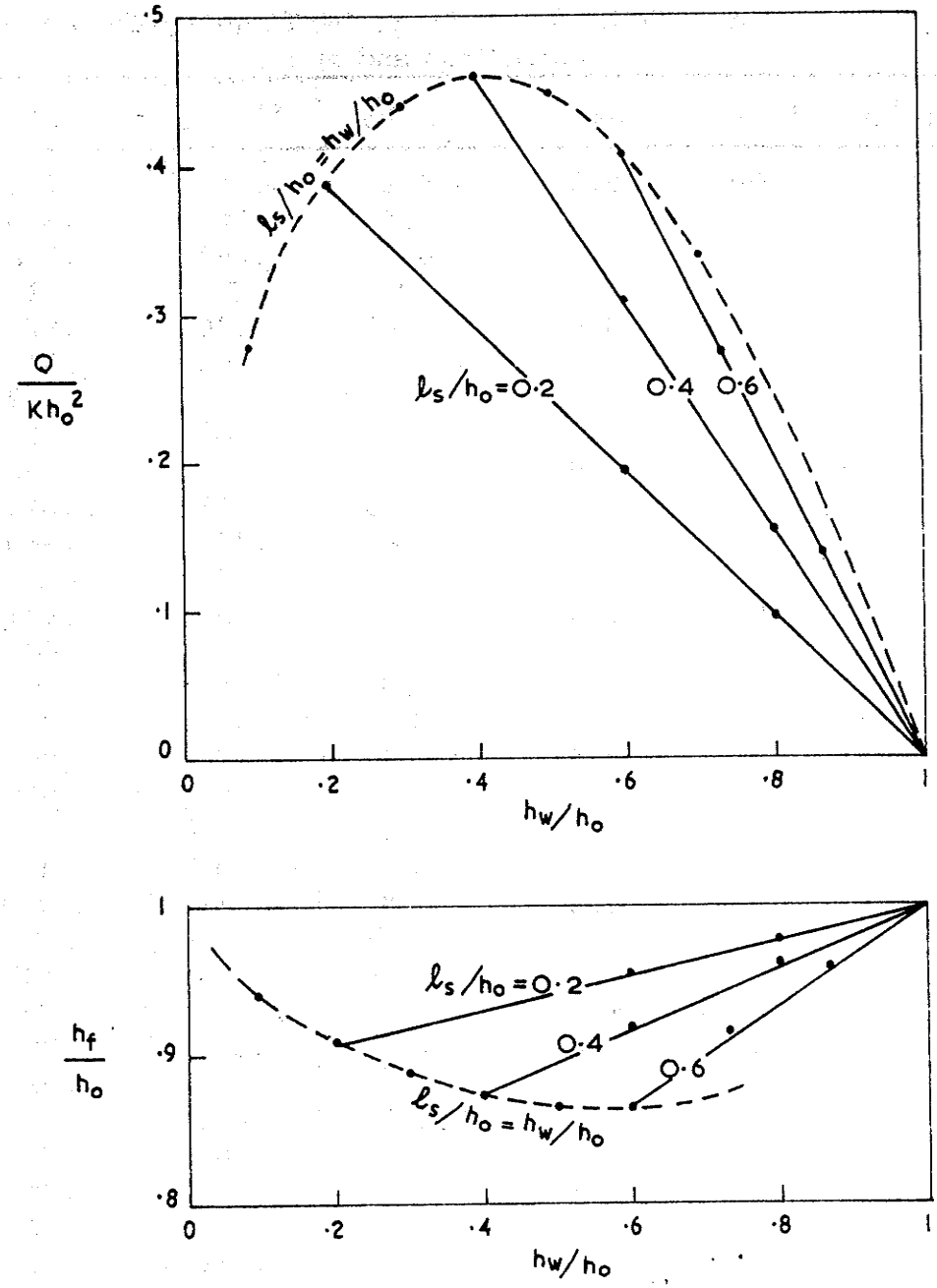

FIGURE 5·40: PARTIALLY SCREENED WELL IN AN UNCONFINED AQUIFER

NON-UTILIZATION OF FULL AVAILABLE DRAWDOWN – $h_w > \ell_s$ – DARCY FLOW

For any value $h_w > l_s$, both the distribution of dimensionless drawdown $\left(\frac{h_o - h}{h_o - h_w}\right)$ throughout the flow domain and the discharge flux variation along the well screen are the same as those for the limiting case ($h_w = l_s$) previously discussed in Section 5.7.5.

5.7.8 Well Screen Above Base of Aquifer

Consider the case of a partially screened well in an unconfined aquifer as shown in Figure 5.41. The well screen does not extend to the base of the aquifer and the well is pumped at the limiting discharge which causes the water level within the well to be drawn down to the top of the screen. The finite element model was used to investigate Darcy flow problems of this type.

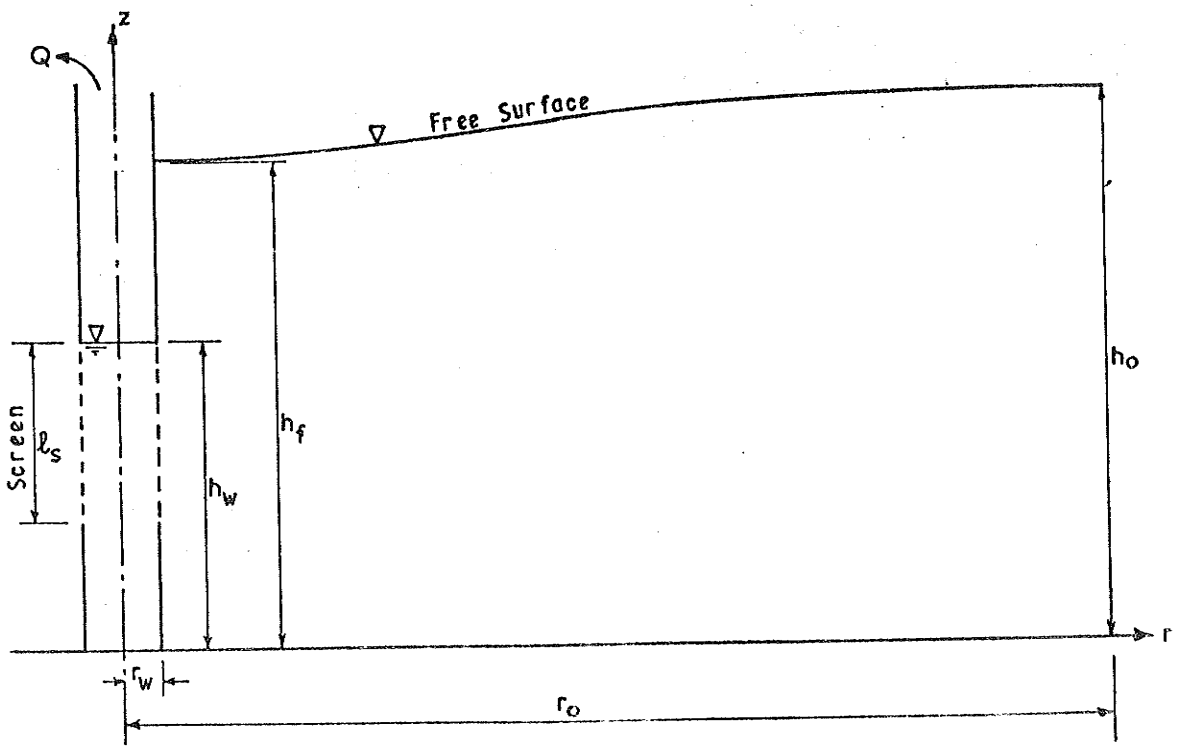

FIGURE 5·41: PARTIALLY SCREENED WELL IN AN UNCONFINED AQUIFER - WELL SCREEN ABOVE BASE OF AQUIFER.

Table 5.15: Darcy Flow to Partially Screened Well in an Unconfined Aquifer - Well Screen Above Base of Aquifer.

r_o/h_o	h_o/r_w	l_s/h_o	h_w/h_o							
			.1	.2	.3	.4	.5	.6	.7	.8
(a) Well Performance - Tabulated Values of Q/Kh_o^2										
2	50	0.1	.28	.31	.29	.25		.17		
		0.2		.39	.40	.36	.30	.24	.18	.12
		0.4				.46	.42	.35	.26	.17
		0.6						.41	.32	.22
4	50	0.2		.37	.37	.33	.28	.22	.17	.11
		0.4				.42	.38	.31	.24	.16
		0.6						.36	.29	
2	200	0.2		.27	.28	.24	.21	.16	.12	.08
		0.4				.34	.31	.25	.19	.13
		0.6						.31	.25	.17
4	200	0.2		.26	.26	.23	.19	.16	.12	.08
		0.4				.32	.29	.24	.18	.12
		0.6						.28	.23	.15
(b) Free Surface Location at the Well - Tabulated Values of h_f/h_o										
2	50	0.1	.94	.93	.93	.93		.93		
		0.2		.91	.90	.90	.90	.91	.91	.92
		0.4				.88	.88	.88	.89	.90
		0.6						.87	.87	.89
4	50	0.2		.86	.85	.86	.87	.88	.89	.90
		0.4				.83	.83	.84	.86	.88
		0.6						.83	.84	.86
2	200	0.2		.94	.93	.93	.94	.94	.94	.95
		0.4				.92	.92	.92	.93	.94
		0.6						.91	.92	.92
4	200	0.2		.91	.90	.91	.92	.92	.93	.94
		0.4				.88	.88	.89	.90	.92
		0.6						.87	.89	.91

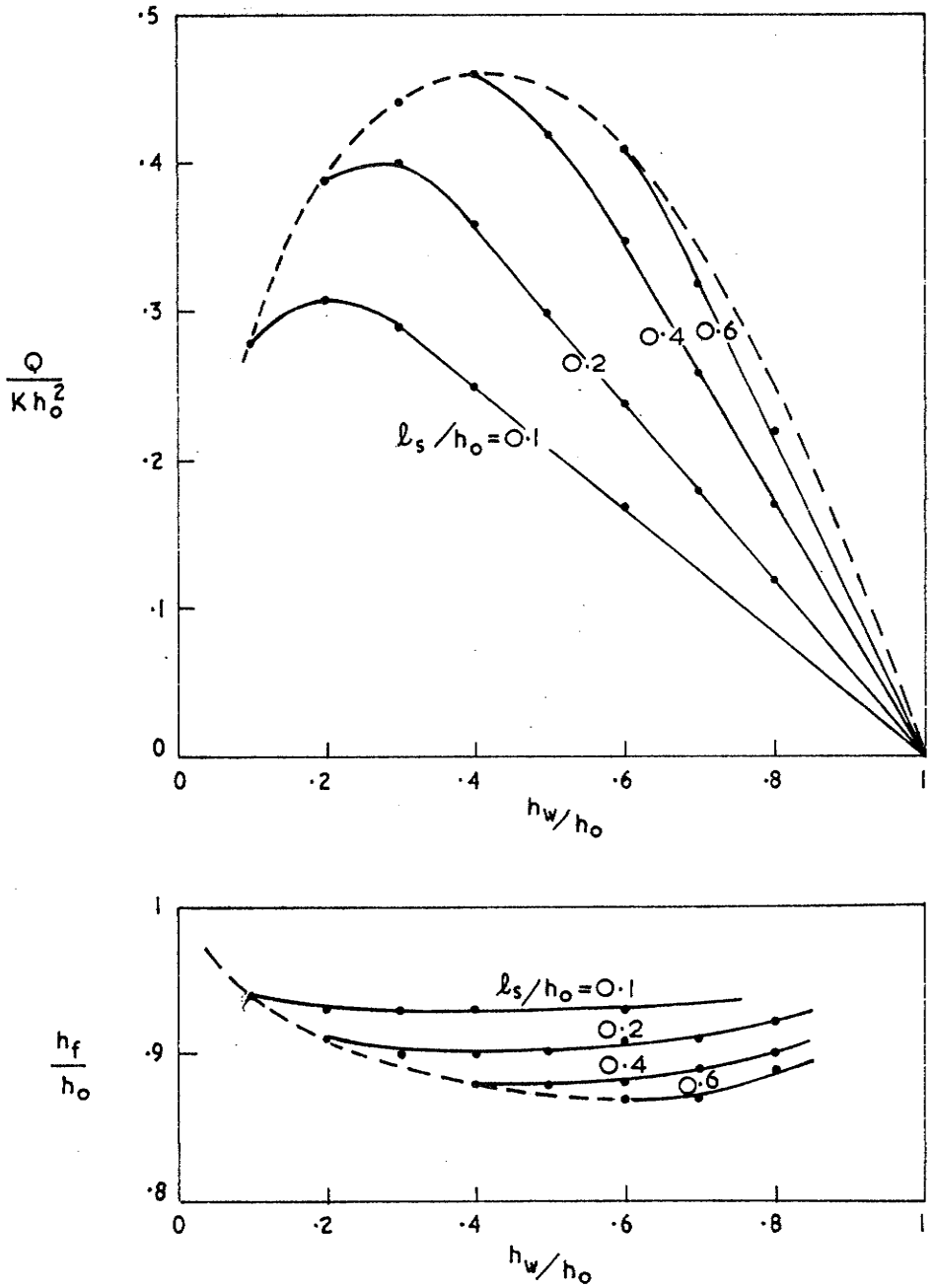

FIGURE 5·42: PARTIALLY SCREENED WELL IN AN UNCONFINED AQUIFER

WELL SCREEN ABOVE BASE OF AQUIFER - DARCY FLOW

The results indicating the effect of screen position on well performance and free surface drawdown are presented in Table 5.15 for a range of problems. The tabulated values were found by applying the relevant corrections, as estimated from Table 5.10, to the finite element solutions obtained using either $N_1 = 32$ or 64 radial "tube" element networks.

Figure 5.42 illustrates the effect of screen position upon well performance and free surface drawdown at the well for the typical case ($r_o/h_o = 2$, $h_o/r_o = 50$).

As shown in Figure 5.42, for small lengths of screen $l_s/h_o < 0.4$, optimum well performance results from placing the screen slightly above the base of the aquifer. As a general rule, for $l_s/h_o < 0.4$, the screen should be positioned mid-way between $z = 0$ and $z = 0.4h_o$.

5.8 Bottom Entry Large Diameter Well in an Unconfined Aquifer

The occurrence and general usage of large diameter wells (wells large enough for a man to enter and work) under Australian conditions has been discussed by Williamson (1967). These days such large diameter wells, whether they be dug by hand or machine, are rarely constructed to a depth greater than 20 metres. In highly permeable aquifers where the formation is coarse enough to be readily stabilised and not cause sand entry problems, such wells may be recommended for large scale water production for irrigation or town supply. Most large diameter wells are now constructed using concrete liners (1 to 2 metres diameter)and depend mainly upon bottom entry of the water.

Consider a large diameter well in a relatively shallow uncon-

fined aquifer as shown in Figure 5.43.

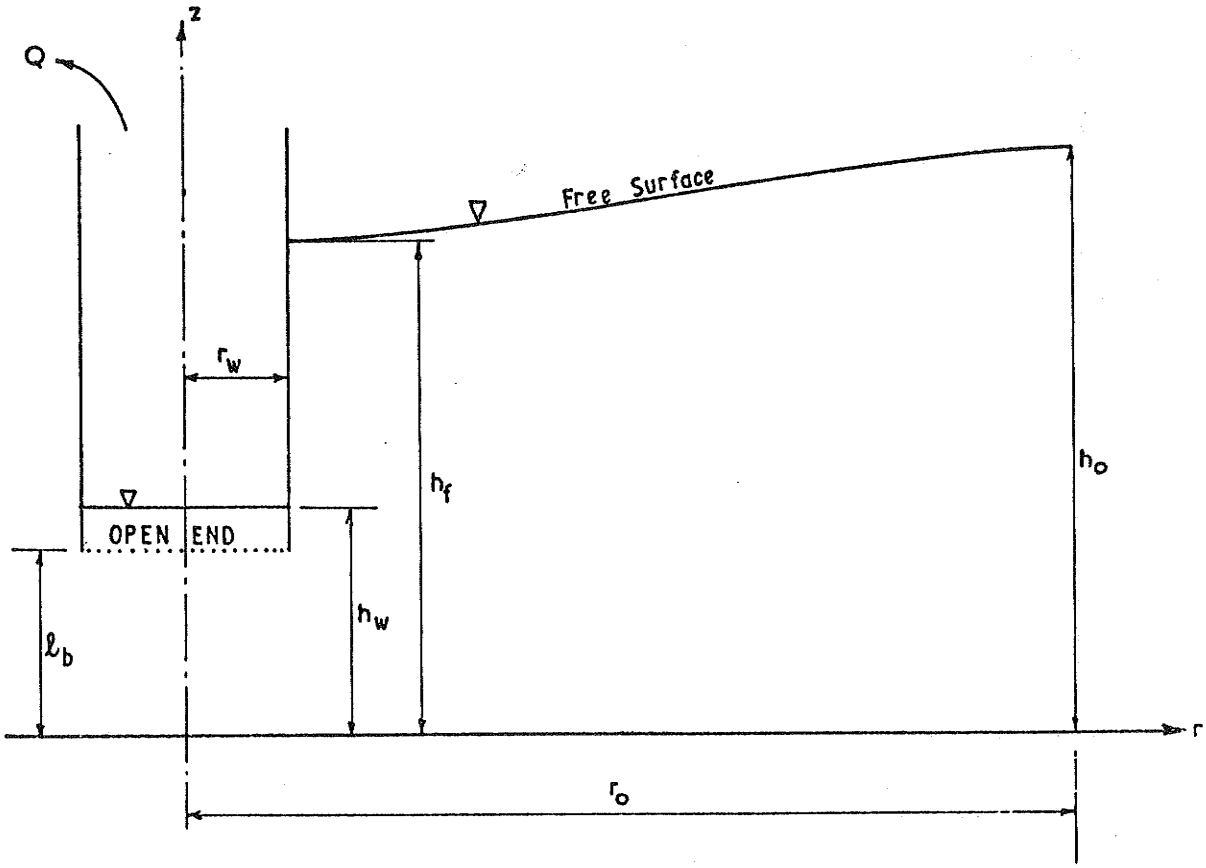

FIGURE 5·43: BOTTOM ENTRY LARGE DIAMETER WELL IN AN UNCONFINED AQUIFER.

The well is open ended and the water level may be drawn down to the base of the well. The aquifer material is assumed to be both homogeneous and isotropic but the flow behaviour may be either Darcy or non-linear. The finite element model was used to investigate a range of such problems.

In choosing appropriate finite element networks, it should be noted that the critical region of the flow occurs close to the well and below the open bottom end. For $r \geqslant r_w$ the finite element networks used followed the same notation and rules described in Section 5.7.3. As shown in Figure 5.44, the flow region beneath the well ($0 \leqslant r \leqslant r_w$, $0 \leqslant z \leqslant l_b$) was divided into triangular ring elements

in a manner to conform as closely as possible with the elements in the first network region beyond r_w.

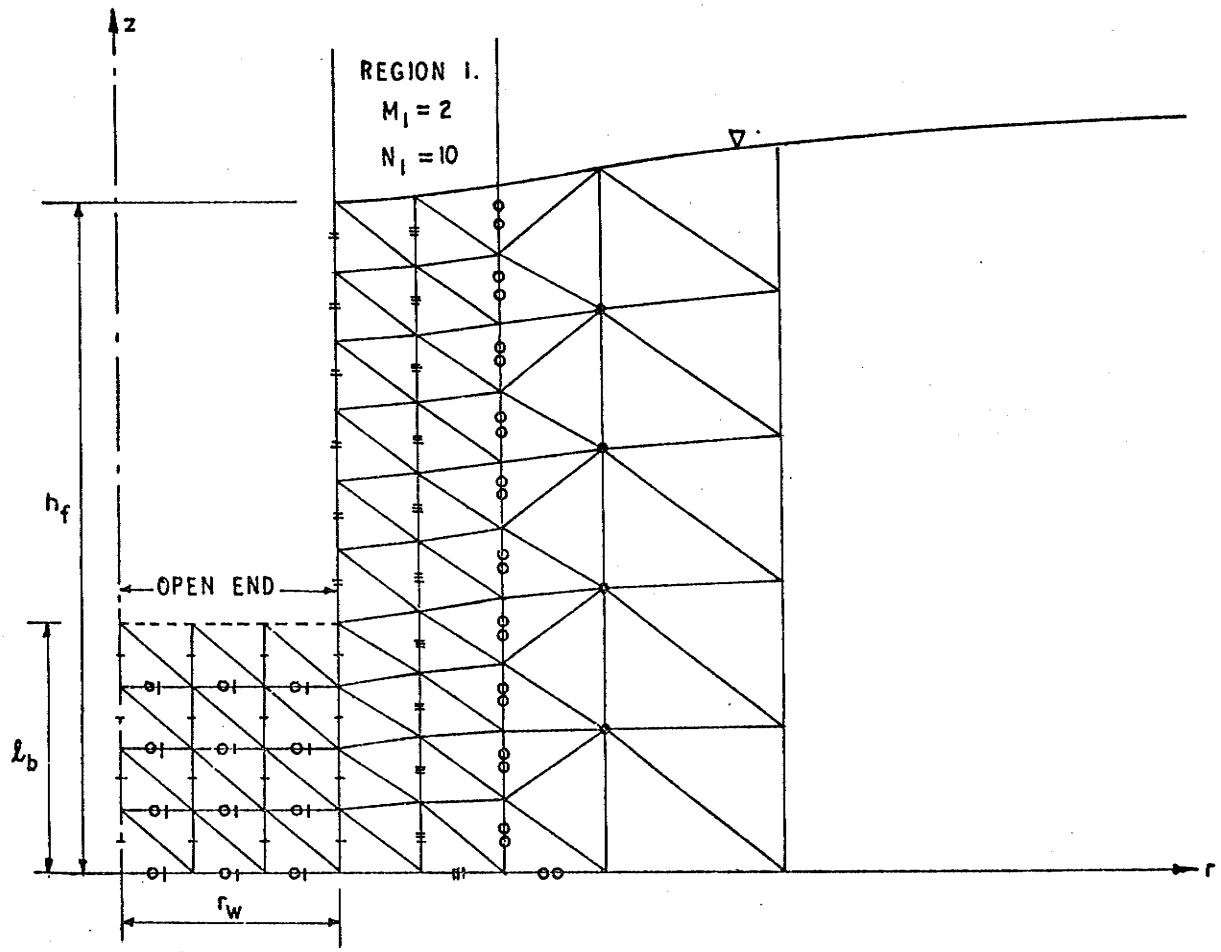

FIGURE 5·44: BOTTOM ENTRY LARGE DIAMETER WELL IN AN UNCONFINED AQUIFER-FINITE ELEMENT NETWORK.

Along the vertical line $r = r_w$, the network nodes were evenly spaced over the two separate distances defined by $0 \leqslant z \leqslant l_b$ and $l_b \leqslant z \leqslant h_f$.

Mesh testing was carried out to give a guide to network solution accuracy. The accuracy of a particular mesh solution was found to depend mainly upon the number of network nodes that fall along the open bottom entry section of the well. Results indicated that the solution accuracy of a selected network (as gauged by N_1 the number of radial "tubes" in the first network region $r \geqslant r_w$),

was effectively independent of all problem variables other than the dimensionless parameter h_o/r_w. Table 5.16 shows the overestimates in well discharge for selected networks.

Table 5.16: Finite Element Network Errors - Bottom Entry Large Diameter Well in Unconfined Aquifer

Percentage Overestimate in Well Discharge to Nearest 1%. $r_o/h_o \gg 2$ $h_w \gg l_b$

h_o/r_w	Network Refinement, N_1				
	16	24	32	48	64
5	9	4	2	0	
10		14	9	4	1
20			16	7	3

The finite element program results indicating the relative effects of l_b/h_o and h_w/h_o on well performance and free surface drawdown at the well are presented in Table 5.17 for various problems involving both Darcy and non-linear flow. Values given in Table 5.17 were found by applying corrections as estimated from Table 5.16 to finite element solutions obtained using networks with N_1 = 32, 48, 64 radial "tubes" for the respective problems h_o/r_w = 5, 10, 20.

For the important case of maximum drawdown to the bottom of the well, $l_b = h_w$, values of well performance and free surface level (h_f) at the well are shown in Figures 5.45 and 5.46 for typical cases of Darcy and non-linear flow. In all Darcy flow cases of prescribed h_o/r_w and r_o/h_o, both the maximum well discharge and free surface drawdown were obtained at values of $1/8 < l_b/h_o = h_w/h_o < \frac{1}{4}$. The critical penetration ratio $(l_b/h_o)_{crit}$ at which maximum well discharge and free surface drawdown were obtained is seen in Figure 5.46 to increase with non-linearity (b/a^2). The results demonstrate that

Table 5.17: Bottom Entry Large Diameter Well in an Unconfined Aquifer

r_o/h_o	h_o/r_w	Flow b/a^2	l_b/h_o	h_w/h_o 1/8	1/4	1/2	3/4	1
(a) Well Performance - Tabulated Values of Q/Kh_o^2 (K = 1/a)								
2	5	0(Darcy)	h_w/h_o	.81	.81	.58	.29	0
	10			.48	.48	.32	.16	0
	20			.29	.27	.19		0
2	5	1	h_w/h_o	.38	.41	.37	.20	0
		10		.15	.18	.18	.093	0
		100		.052	.057	.048	.034	0
2	10	1	h_w/h_o	.18	.18	.16	.088	0
		10		.070	.068	.060	.038	0
		100		.023	.023	.019	.014	0
2	10	0(Darcy)	1/8	.48	.41	.27	.14	0
			1/4		.48	.31	.15	0
			1/2			.32	.17	0
2	5	0(Darcy)	1/8	.81	.69	.46	.23	0
			1/4		.81	.54	.28	0
			1/2			.58	.34	0
4	5	0(Darcy)	h_w/h_o	.72	.71	.50	.25	0
8	5	0(Darcy)	h_w/h_o	.63	.62	.45	.22	0
(b) Free Surface Location at the Well - Tabulated Values of h_f/h_o								
2	5	0(Darcy)	h_w/h_o	.83	.82	.83	.85	1
	10			.90	.89	.90	.91	1
	20			.93	.94	.95		1
2	5	1	h_w/h_o	.92	.91	.90	.91	1
		10		.96	.95	.94	.95	1
		100		.98	.98	.98	.98	1
2	10	1	h_w/h_o	.96	.96	.95	.95	1
		10		.99	.99	.98	.98	1
		100		.99	.99	.99	.99	1
2	10	0(Darcy)	1/8	.89	.91	.94	.97	1
			1/4		.88	.93	.97	1
			1/2			.90	.95	1
2	5	0(Darcy)	1/8	.83	.86	.91	.96	1
			1/4		.82	.88	.94	1
			1/2			.83	.91	1
4	5	0(Darcy)	h_w/h_o	.74	.73	.75	.84	1
8	5	0(Darcy)	h_w/h_o	.66	.65	.71	.83	1

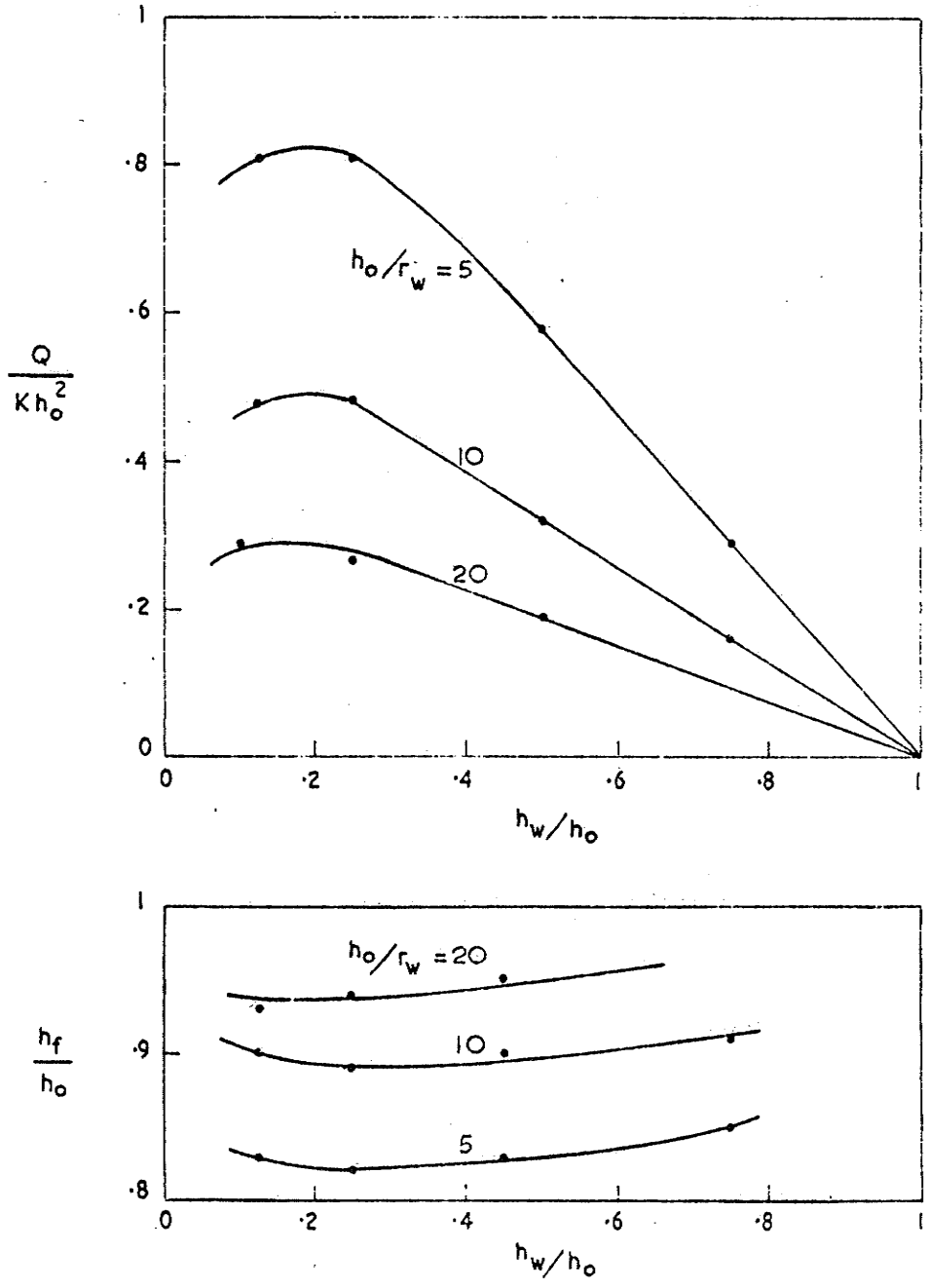

FIGURE 5·45: BOTTOM ENTRY LARGE DIAMETER WELL IN AN UNCONFINED AQUIFER

TYPICAL EFFECTS FOR DRAWDOWN TO BASE OF WELL - DARCY FLOW

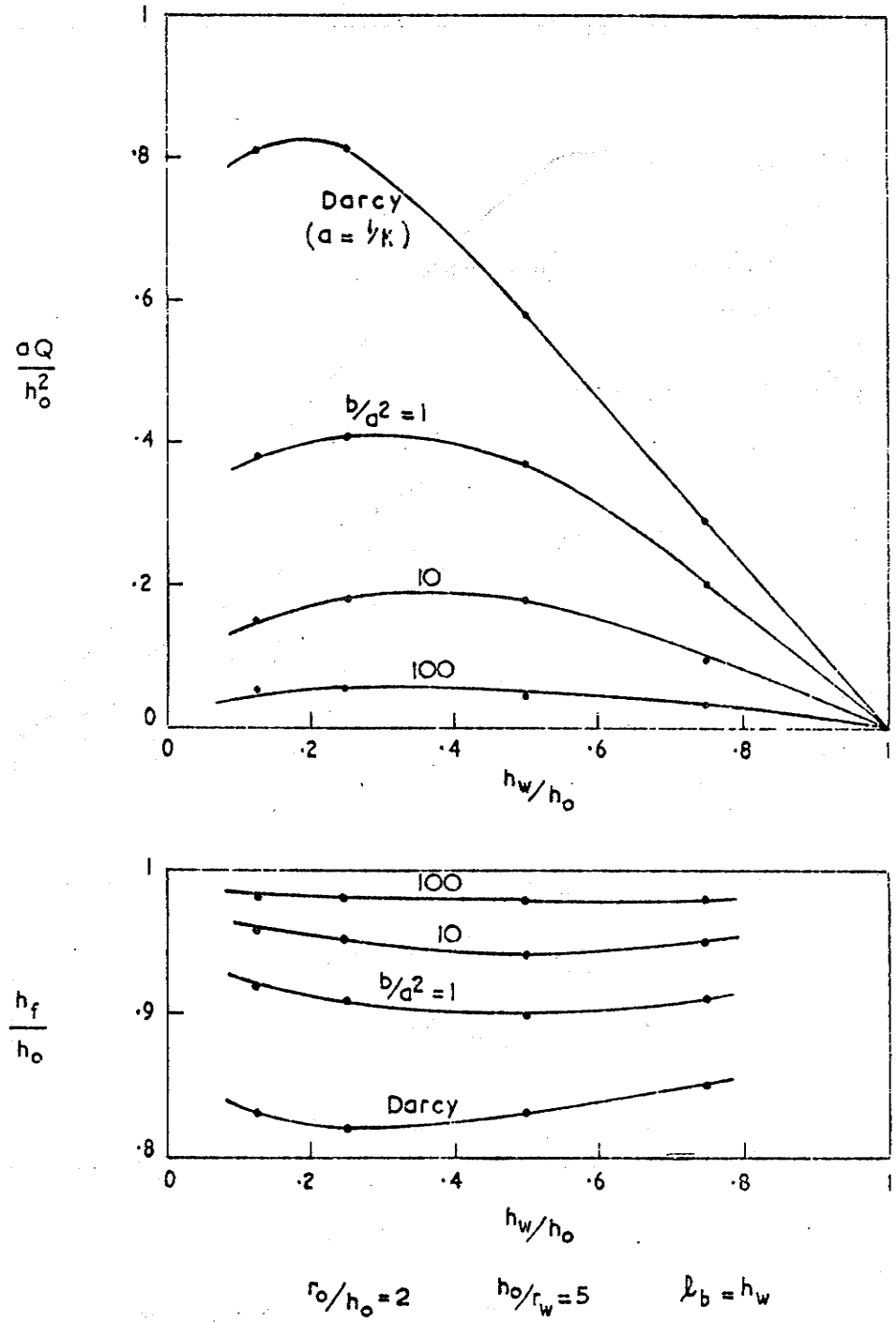

FIGURE 5·46: BOTTOM ENTRY LARGE DIAMETER WELL IN AN UNCONFINED AQUIFER

TYPICAL EFFECTS FOR DRAWDOWN TO BASE OF WELL – NON LINEAR FLOW

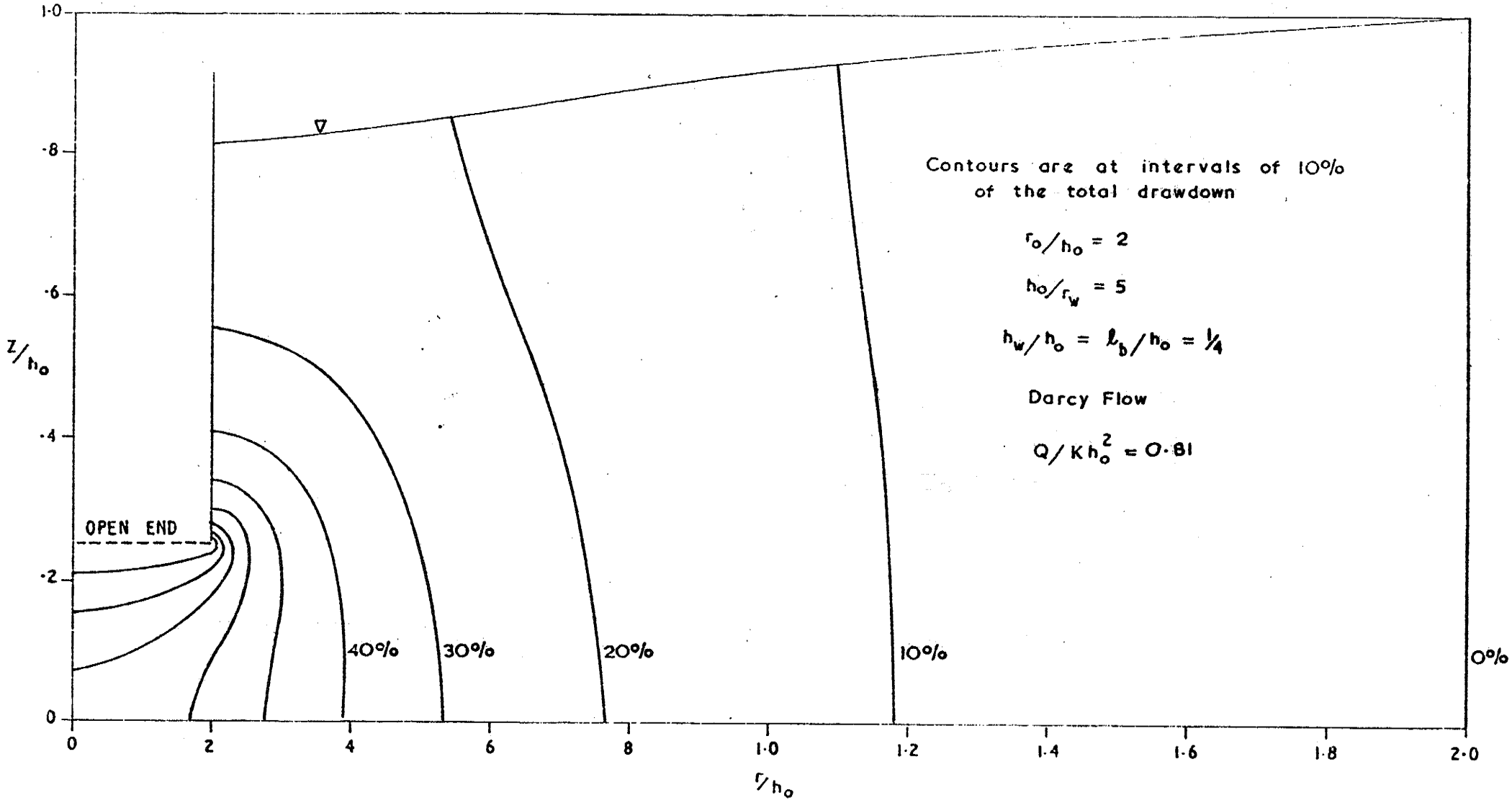

FIGURE 5·47: BOTTOM ENTRY LARGE DIAMETER WELL IN AN UNCONFINED AQUIFER
TYPICAL HEAD DISTRIBUTIONS FOR DARCY FLOW

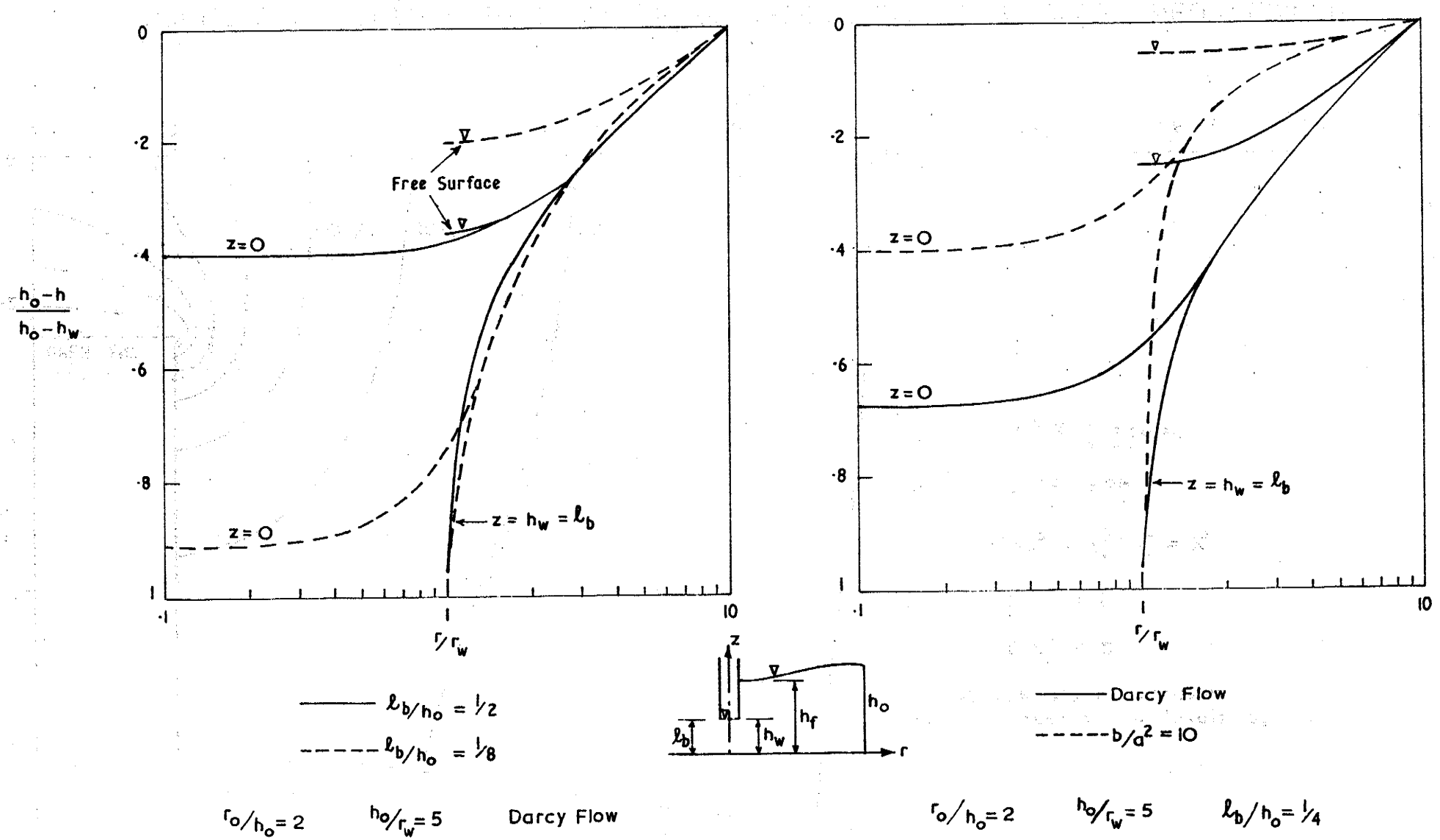

FIGURE 5·48: BOTTOM ENTRY LARGE DIAMETER WELL IN AN UNCONFINED AQUIFER
TYPICAL DRAWDOWN DISTRIBUTIONS

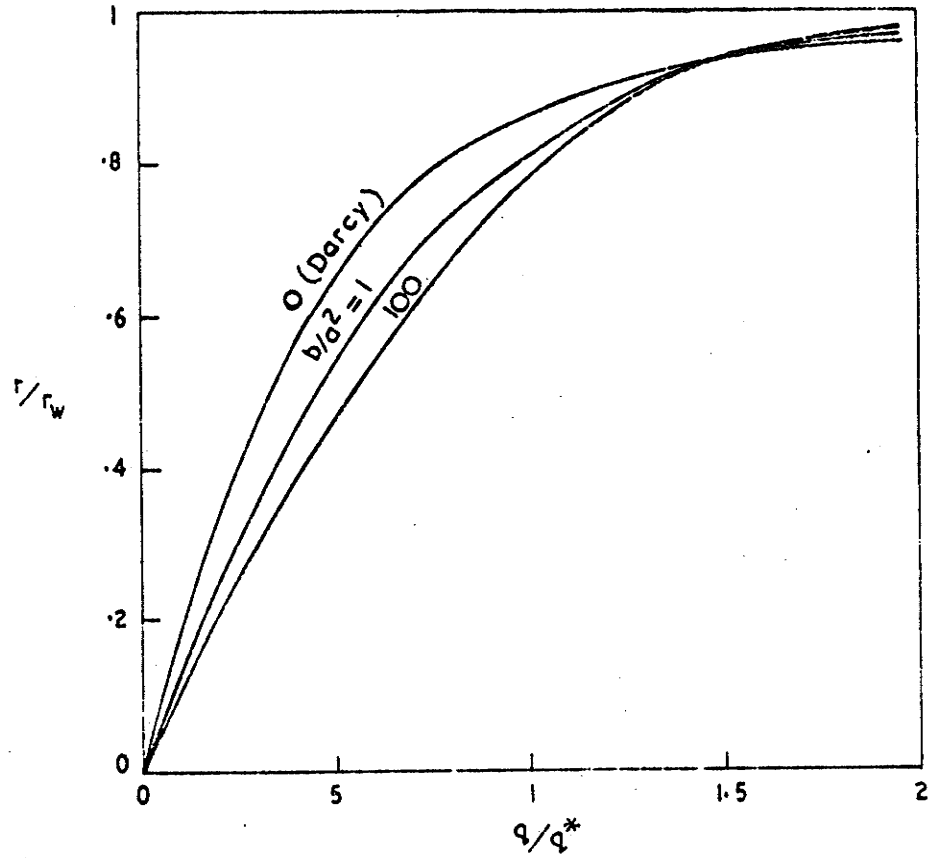

(a) $q^* = Q/r_w$

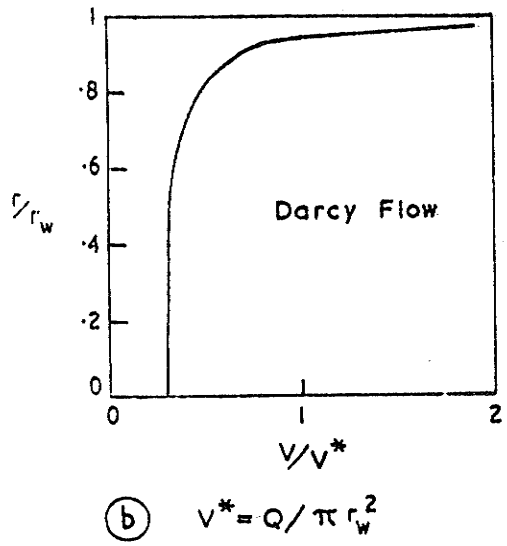

(b) $V^* = Q/\pi r_w^2$

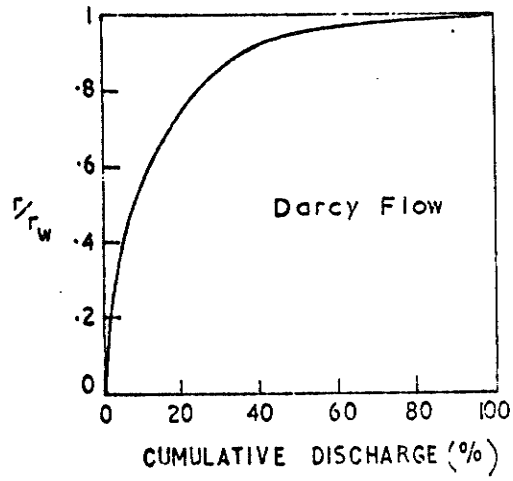

(c)

$r_o/h_o = 2$, $\quad 5 \leq h_o/r_w \leq 20$, $\quad \ell_b/h_o > 1/8$

FIGURE 5·49: BOTTOM ENTRY LARGE DIAMETER WELL IN AN UNCONFINED AQUIFER.
DISTRIBUTION OF DISCHARGE FLUX, VELOCITY AND CUMULATIVE WELL DISCHARGE ALONG BOTTOM ENTRY SECTION.

increasing non-linearity (as measured by b/a^2) may considerably reduce well discharge and free surface drawdown.

In all Darcy flow cases examined in which the full available drawdown was not utilised, both the well discharge and free surface water level at the well varied linearly with h_w between $h_w = l_b$ and $h_w = h_o$. These results are similar to those for conventional screened wells in unconfined aquifers discussed in Section 5.7.7. For any well water level $h_w > l_b$, the discharge and free surface position may be estimated by linear proportioning from the solution for the limiting condition of drawdown to the bottom of the well, $h_w = l_b$.

The drawdown distribution for the Darcy flow problem ($r_o/h_o = 2$, $h_o/r_w = 5$, $l_b/h_o = h_w/h_o = \frac{1}{4}$) is shown in Figure 5.47.

Distributions of the drawdown along the free surface, the line $z = l_b$, and the base of the aquifer are given in Figure 5.48 for typical cases of Darcy and non-linear flow.

For a specified degree of non-linearity (value of b/a^2), the discharge flux distribution along the open well bottom was found to be approximately independent of r_o/h_o, h_o/r_w and l_b/h_o within the range of values investigated (i.e. $r_o/h_o \geqslant 2$, $5 \leqslant h_o/r_w \leqslant 20$, $l_b/h_o > 1/8$). The discharge flux distributions are shown in Figure 5.49a for cases of Darcy flow and non-linear flow with $b/a^2 = 1$ and 100. Figure 5.49b shows the radial distribution of velocity along the bottom of the well for Darcy flow. It should be noted that high entrance velocities occur as r approaches r_w. This is very significant in relation to possible sand movement into the well. The cumulative well discharge distribution is shown in Figure 5.49c for Darcy flow.

6. Solutions to Transient Well Flow Problems - Confined Aquifers

6.1 General

Based on the theory outlined in Chapters 3 and 4, finite element computer programs were developed and used to solve a range of transient well flow problems in confined aquifers.

The transient finite element analysis was verified by comparison with known analytical solutions for various typical boundary value problems.

The finite element model was then used to investigate a range of problems previously insoluble by analytical techniques. In particular, the effects of well storage, partial penetration, non-linear flow and variable well pumping rate were considered. The results reported herein were oriented towards demonstrating the versatility of the developed finite element programs in handling a variety of conditions in transient flow problems to wells in confined aquifers.

In all cases the aquifer material was assumed to be isotropic and homogeneous unless stated otherwise.

6.2 Verification of Finite Element Solutions

6.2.1 General

The verification of the finite element analysis by comparison with known analytical solutions is now described.

Consider the general problem defined in Figure 6.1. Beginning from some initial time, t_o, a well in a uniform homogeneous isotropic confined aquifer is pumped at a constant rate $\bar{Q}$. The aquifer transmissivity, T, and storage coefficient, S, are defined

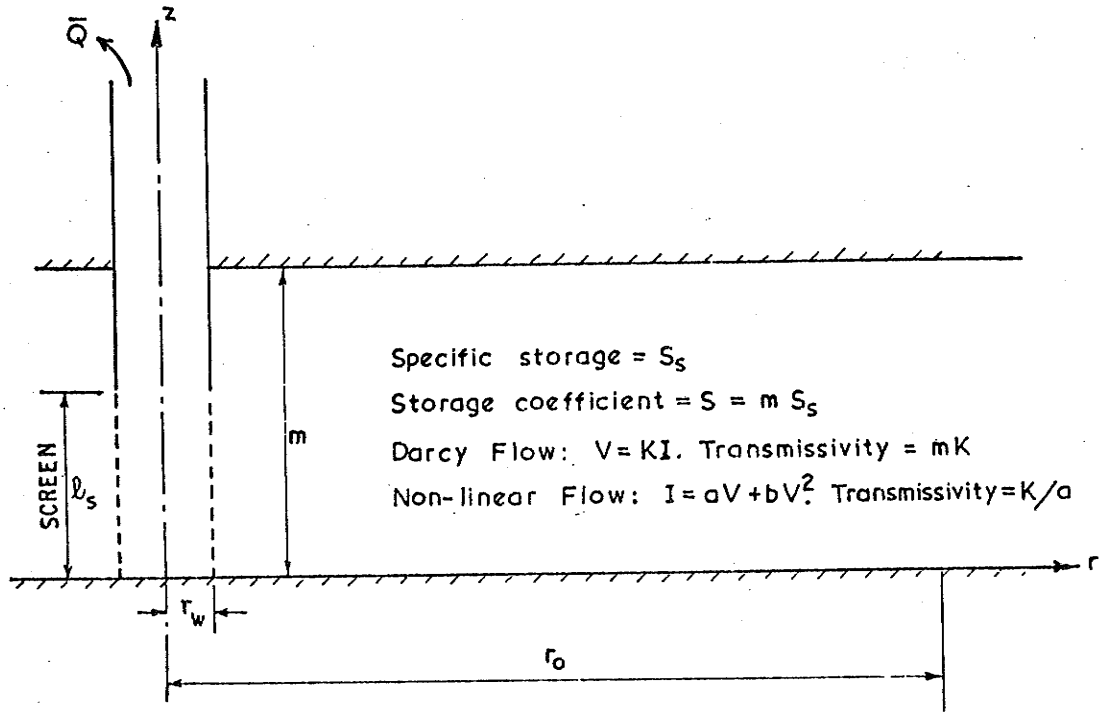

FIGURE 6·1: UNSTEADY FLOW TO A WELL IN A CONFINED AQUIFER.

in the figure. All other symbols have been defined previously.

In the following finite element model verification, well storage effects have been neglected since such effects are not included in any of the known analytical solutions used for comparative purposes.

As described in Section 4.5.4, the solution in time was carried out through a step-by-step mid-difference approximation. Within an individual time step, the accuracy of the solution depends upon the refinement of the finite element network over the flow region. Thus finite element networks were selected according to the guidelines and accuracy values given in Chapter 5 for the steady state analysis of flow to a well in a confined aquifer.

6.2.2 Stability of Step-by-Step Time Solution Procedure

The effect upon the finite element analysis of the specified steps in time was investigated by considering the case of fully radial one-dimensional Darcy flow.

The following problem was solved by a finite element model incorporating one-dimensional isoparametric ring elements:

$$r_w = 1 \qquad T = 3 \qquad S = 10^{-3} \qquad \bar{Q} = 10$$

The discharge ratio tolerance, ϵ_Q, was specified as 5% (see Section 4.5.6). The one-dimensional finite element network was chosen according to the guidelines of Section 5.2.4. The length of the element near the well was equal to the well radius ($r_w = 1$), and the mesh was graded such that the nodes were approximately evenly spread logarithmically with distance from the well. The mesh was extended to a specified radius of influence, $r_o = 2000$ where a prescribed head boundary condition was imposed.

The time domain, $10^{-2} \leqslant t \leqslant 10^{2}$, was divided into logarithmically evenly spaced time steps in the finite element analysis. Solutions based on the following four separate time step series were obtained:

(i) $t_{i+1} = t_i \times 10$

(ii) $t_{i+1} = t_i \times 10^{\frac{1}{2}}$

(iii) $t_{i+1} = t_i \times 10^{1/3}$

(iv) $t_{i+1} = t_i \times 10^{\frac{1}{4}}$

Figure 6.2 shows the drawdown versus time results for specific distances from the well, $r/r_w = 1, 10, 100$. The analytical

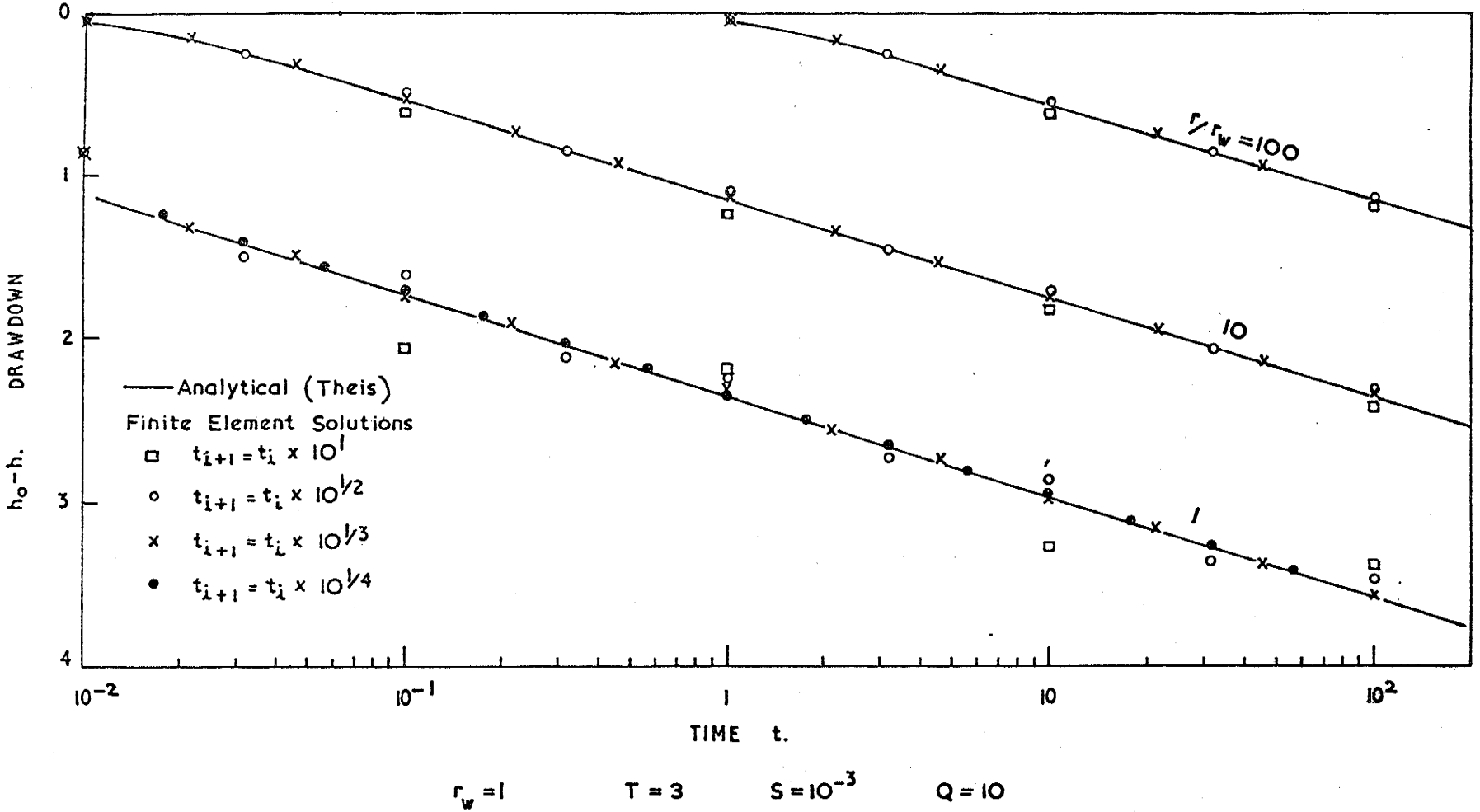

FIGURE 6·2: EFFECT OF TIME STEPS ON FINITE ELEMENT SOLUTION ACCURACY

Theis (1935) solution to the problem is shown in the figure for comparative purposes. Even for the most coarse time step series ($t_{i+1} = t_i \times 10$) in which the finite element results oscillate noticeably about the Theis solution, a mean fit through the program results only slightly overestimates the drawdown. With more time steps per logarithmic time cycle, the oscillations of the finite element results rapidly diminish and the lines of mean fit are not significantly different to the analytical solution. The finite element solution accuracy improves with radial distance from the well, irrespective of the time series chosen. Clearly, the mid-difference step-by-step time solution procedure is extremely stable. There would appear to be no advantage in specifying more than 3 time steps per logarithmic cycle in time, since the results for the time series, $t_{i+1} = t_i \times 10^{1/3}$, show negligible oscillation or deviation from the exact analytical Theis solution.

6.2.3 Fully Screened Well in an Infinite Aquifer

Consider the simple case of constant discharge Darcy flow to a fully screened well in a confined aquifer of infinite radial extent. The analytical solutions of Theis (1935) and Hantush (1964) are available for the respective problems of a well of zero radius (line sink) and a well of finite radius. Javandel and Witherspoon (1968) obtained good agreement with the analytical solutions by using a finite element solution based on triangular ring elements.

Since the flow is strictly radial one-dimensional, economical finite element computer solutions employing one-dimensional ring

elements were used by the author to solve the following problems:-

Line Sink $r_w = 0$ $T = 3$ $S = 10^{-3}$ $\bar{Q} = 10$

Finite Well Radius $r_w = 1$ $T = 3$ $S = 10^{-3}$ $\bar{Q} = 10$

The solution to the latter problem has already been referred to in Section 6.2.2 when discussing the stability of the transient solution procedure.

In both finite element problem solutions;

(i) the length of the element at the well was equal to 1 and the mesh nodes were spaced logarithmically with radial distance from the well;

(ii) the mesh extended to a radius of influence, $r_o = 2000$. This value was chosen since within the solution time domain, $10^{-5} \ll t \ll 1$, the drawdown at r_o is negligible and the aquifer behaves effectively as one of infinite extent;

(iii) the time step series was specified such that there were 3 time steps per logarithmic time cycle (i.e. $t_{i+1} = t_i \times 10^{1/3}$) as recommended in Section 6.2.2.

A comparison of the finite element and analytical solutions is shown in Figure 6.3 in terms of dimensionless drawdown, W(u), and dimensionless time, 1/u, where

$$W(u) = 4\pi T(h_o - h)/Q \qquad (6.1)$$

$$1/u = 4Tt/r^2S \qquad (6.2)$$

Q is the calculated well discharge and h_o is the original hydraulic head before pumping. For the finite well radius problem the results are presented for several values of dimensionless radius

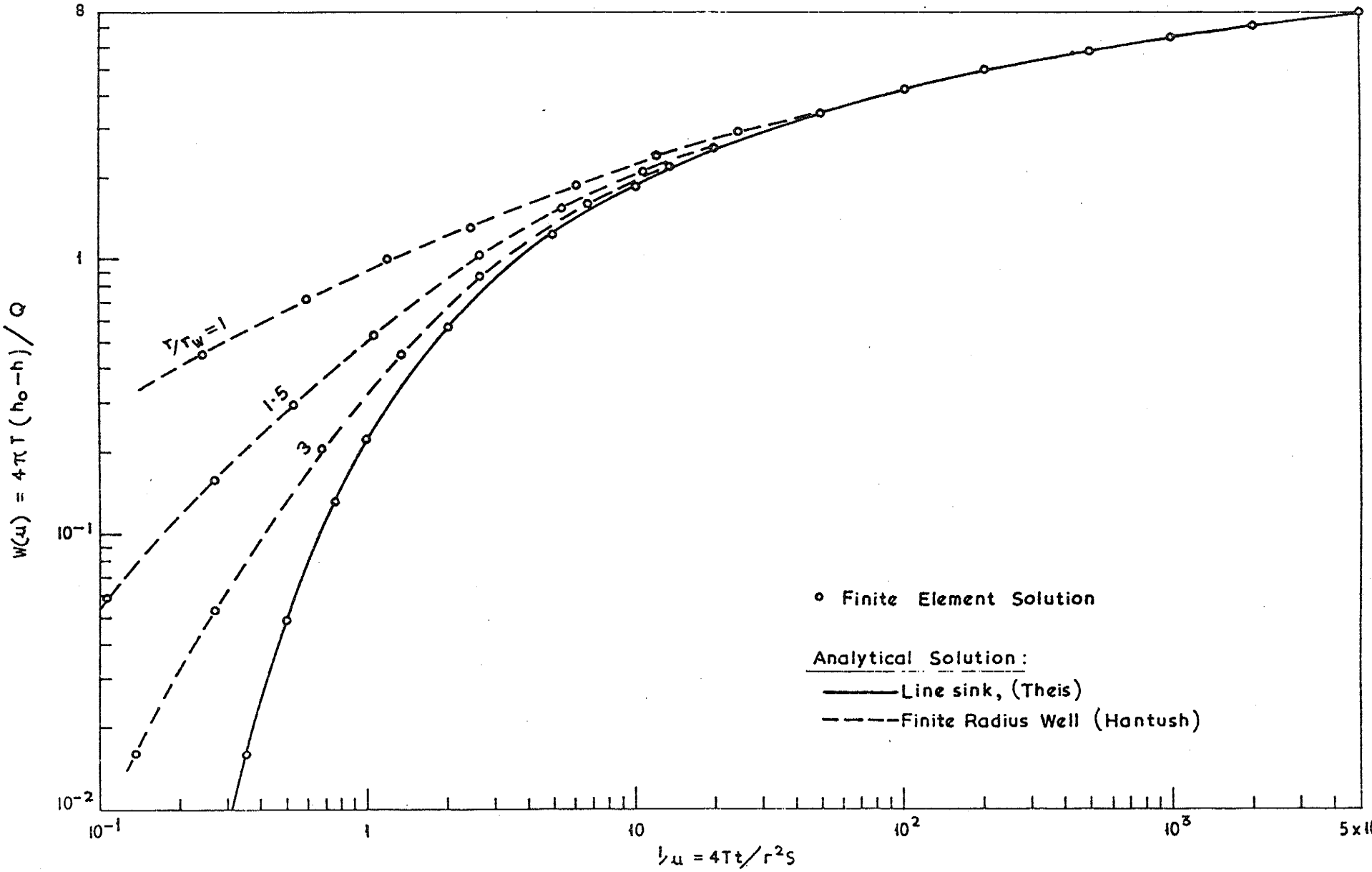

FIGURE 6·3: COMPARISON OF FINITE ELEMENT AND ANALYTICAL SOLUTIONS FOR FULLY SCREENED WELL IN AN INFINITE AQUIFER-CONSTANT DISCHARGE RATE.

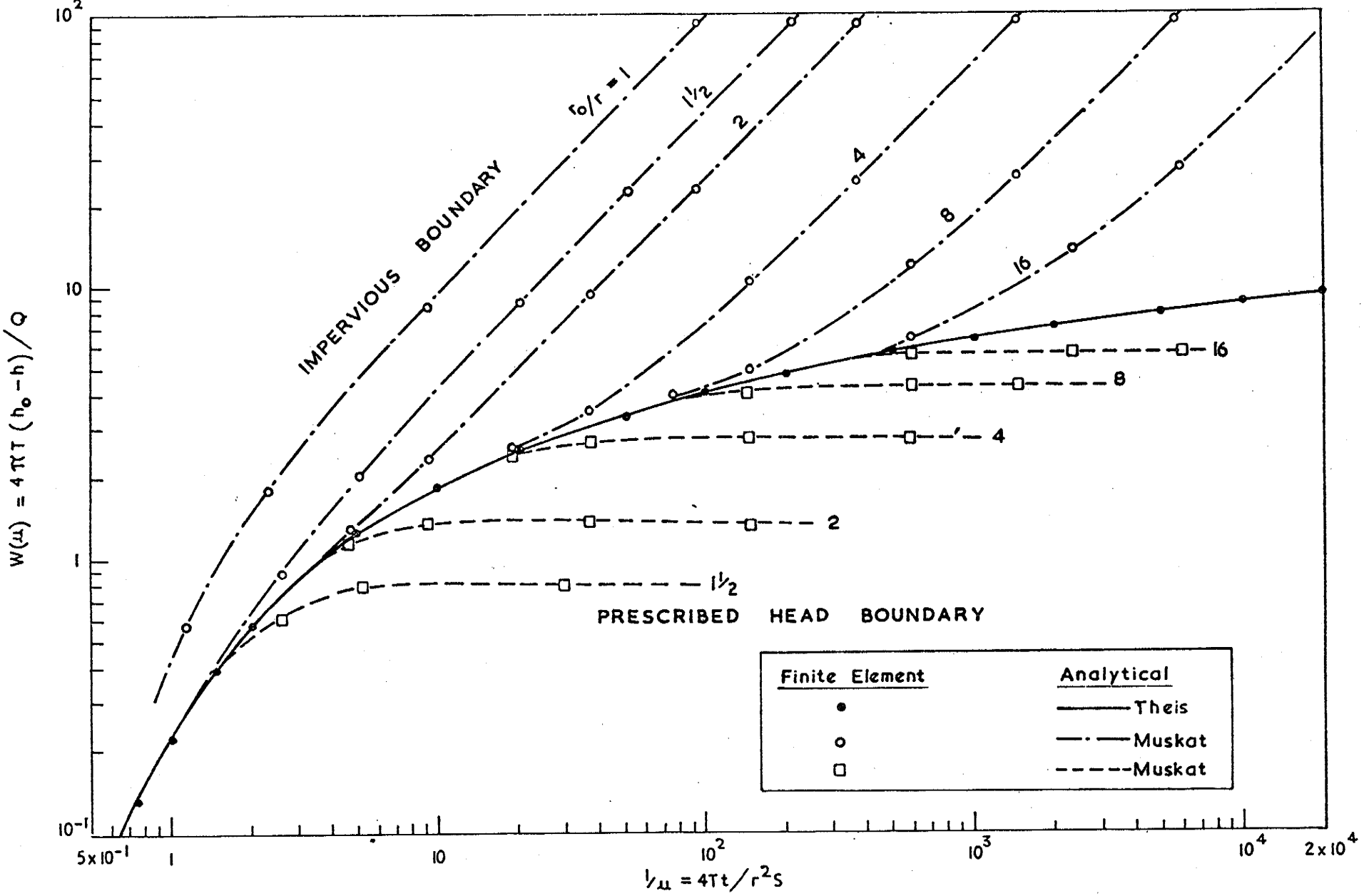

FIGURE 6·4: COMPARISON OF FINITE ELEMENT AND ANALYTICAL SOLUTIONS — FULLY SCREENED WELL IN A RADIAL BOUNDED CONFINED AQUIFER — CONSTANT DISCHARGE RATE

r/r_w. Excellent agreement between the finite element and analytical solutions is evident.

6.2.4 Fully Screened Well in a Radial Bounded Aquifer

Consider the case of constant discharge Darcy flow to a fully screened well in a confined aquifer which is bounded at the outer radius r_o. At the outer boundary, there may be either a prescribed head condition or an impervious boundary condition.

The line sink problem,

$$r_w = 0 \quad T = 1 \quad S = 10^{-3} \quad \bar{Q} = 50$$

was solved using a finite element model with a one-dimensional element network similar to that used in solving the line sink problem of Section 6.2.3 except that the mesh continued to an outer boundary of only $r_o = 400$. The time domain $10 \leqslant t \leqslant 10^4$ was divided into two steps per logarithmic time cycle, i.e. $t_{i+1} = t_i \times 10^{\frac{1}{2}}$. Solutions were obtained for the two separate possible imposed boundary conditions at r_o.

Figure 6.4 shows a comparison of the finite element results with the analytical solutions of Muskat (1946) for various dimensionless radii, r_o/r. As dimensionless time increases, the results diverge from the Theis solution as shown in the figure. Even with only two time steps per logarithmic time cycle, the finite element results compare very well with the analytical solutions.

6.2.5 Partially Screened Well

In problems of partial screening of the aquifer (Figure 6.1), the flow will not be purely radial and the simplified one-dimensional

finite element analysis so economically useful in previous fully screened solutions cannot be applied. A two-dimensional axisymmetric finite element program incorporating both rectangular and triangular ring elements was adopted for problems involving two-dimensional flow behaviour.

This two-dimensional finite element model was verified for Darcy flow in the following manner. The selection of the rectangular and triangular element networks was made according to the guidelines given in Section 5.3.4. A network of elements in which the radial spacing of nodes was the same as that previously employed in the verification of the one-dimensional finite element analysis (sections 6.2.2, 6.2.3, 6.2.4) was found to give identical solutions to those obtained by the one-dimensional program results. Thus the two-dimensional program's ability to solve the simplified one-dimensional radial flow problem was demonstrated.

To verify the program's ability to predict two-dimensional axisymmetric Darcy flow behaviour, the following problem of a partially screened well being pumped at constant rate was investigated:

$r_w = 1$ $\quad m = 40$ $\quad l_s = 20$

$K = 0.1$ $\quad S_s = 10^{-4}$

$\bar{Q} = 100$ $\quad \epsilon_Q = 5\%$

The time domain, $10^{-2} \leqslant t \leqslant 10^{2}$, was divided according to $t_{i+1} = t_i \times 10^{1/3}$. The two-dimensional element network was selected such that the network nodal spacing at the well, Δr_1, was

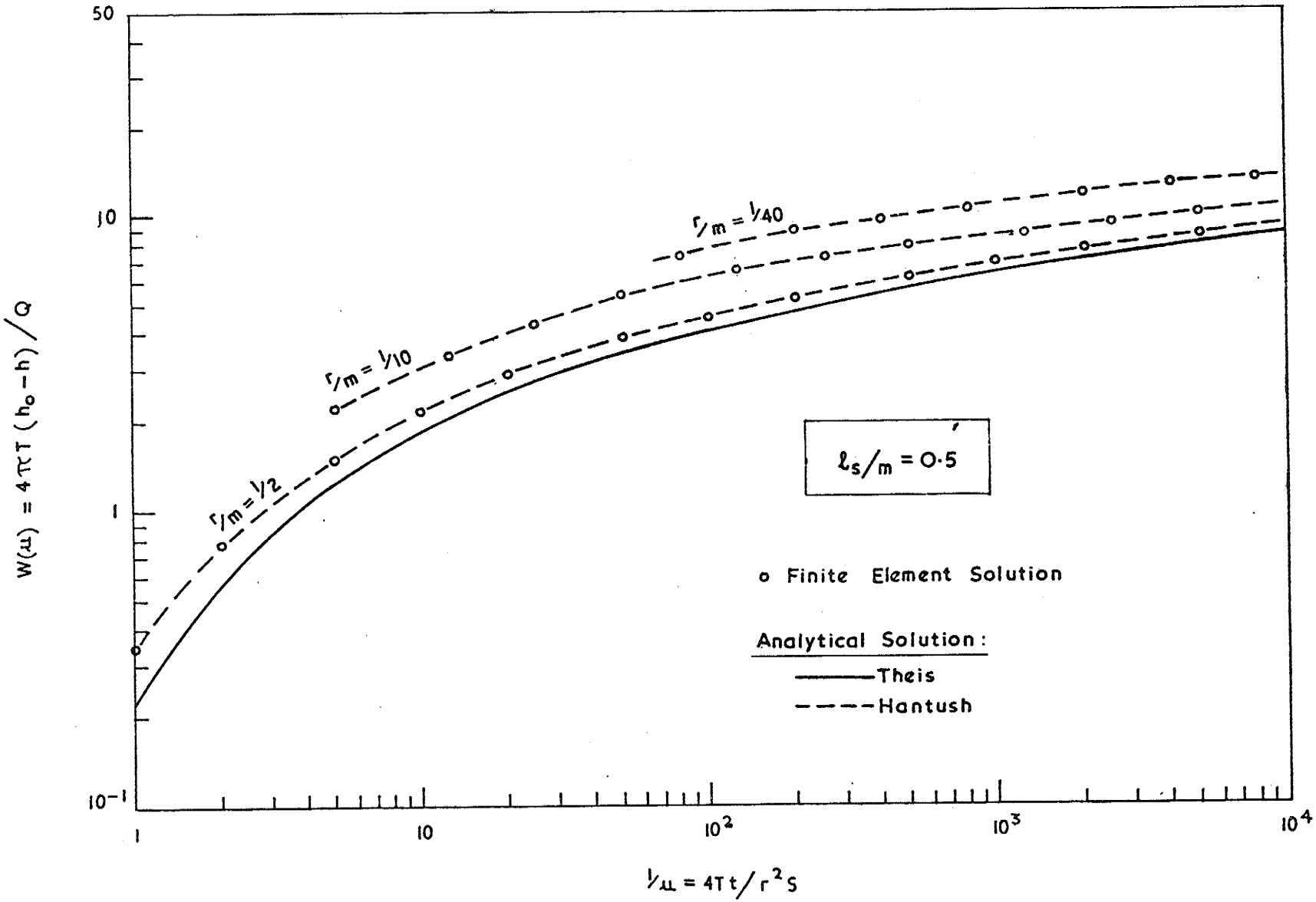

FIGURE 6·5: COMPARISON OF FINITE ELEMENT AND ANALYTICAL SOLUTIONS – PARTIALLY SCREENED WELL BEING PUMPED AT CONSTANT RATE.

equal to $r_w/2 = 0.5$. From Table 5.2, such a fine network should give extremely accurate results. The network was graded to a radius of influence $r_o = 1000$ where a prescribed head boundary condition was imposed.

The finite element solution resulted in a drawdown distribution that varied with depth for $r < 1.5$m. For $r \geq 1.5$m from the well the flow was essentially radial one-dimensional and the results obeyed the analytical Theis solution. The flow was also found to be purely radial for $z < l_s/2$ irrespective of the distance from the well. In Figure 6.5, the finite element results for the radial distribution of drawdown along the base of the aquifer are presented in the dimensionless form W(u) versus 1/u for values of r/m = 1/40, 1/10 and 1/2. The close agreement with the analytical solution of Hantush (1961) clearly evident in Figure 6.5 demonstrates the validity of the finite element analysis.

6.2.6 Discussion

In the previous sections, the transient finite element analysis has been verified for well flow problems involving Darcy flow. The unsteady solution procedure, so verified, relies on the application of a mid-difference time step scheme to essentially steady state solutions derived at particular instants in time. The extension of steady state finite element programs to include complex boundaries, aquifer inhomogeneity and non-linear flow behaviour has been demonstrated elsewhere (in particular chapters 5 and 7). It is considered, therefore, that if the previously verified time solution scheme

is applied to problems which include the abovementioned extensions, the transient finite element analyses should be correct.

A more complete verification of the analysis of transient non-linear flow problems would of necessity have to include experimental results from either laboratory and/or field testing since no analytical solutions are available. Such testing would need to be carefully controlled and would require extensive automatic electronic instrumentation if the results were to be meaningful in verifying both the original basic field equations and the finite element programs. (Huang (1973) encountered difficulties in obtaining reliable results in laboratory testing of the simpler Darcy well flow problem. The difficulty may be attributed mainly to a lack of adequate instrumentation).

Experimental testing of unsteady non-linear well flow was far beyond the limits imposed by both time and finance on the present study.

6.3 Effect of Well Storage on Flow Behaviour

As previously stated in Chapter 4, within the initial stages of pumping, the pump will draw mainly from the water standing within the well. Available analytical solutions ignore this effect and assume that the pump discharge is met fully by the aquifer. The effects of well storage upon the flow behaviour of a well-aquifer system being pumped at a constant rate were investigated using the developed finite element programs.

Consider the problem of a fully screened well in a confined aquifer being pumped at a constant rate. The flow obey's Darcy's

law and the effects of well storage are to be included. The following two problems were solved using one-dimensional isoparametric ring elements;

(i) Arbitrary Compatible Units

$r_w = 1$
$r_o = 2000$
$T = 1$
$S = 10^{-3}$
$\bar{Q} = 50$
$.01 \leqslant t \leqslant 100$

(ii) Typical Practical Problem

$r_w = 0.2$ metre
$r_o = 400$ metres
$T = 10^{-3}$ metre^2/sec.
$S = 1.5 \times 10^{-3}$
$\bar{Q} = 50$ litres/sec.
$.01 \leqslant t \leqslant 100$ minutes

In both problems the time steps were chosen to give 3 steps per logarithmic time cycle, i.e. $t_{i+1} = t_i \times 10^{1/3}$. The finite element network previously described in Section 6.2.2 was used in solving the first problem. The second problem was solved using a scaled version of the same network such that the element length at the well was equal to the well radius, $r_w = 0.2$ metre.

The results of the finite element analyses are presented in Figure 6.6 in the dimensionless form W(u) versus 1/u for specified values of r/r_w. The results clearly indicate that the well storage leads to substantial deviations from the analytical Theis solution for positions near the well at early times. The effects of well storage are seen to diminish with distance from the well. For $r/r_w > 500$ the effects are negligible and the flow obeys the Theis equation. As time increases, the contribution to pumping discharge derived from well storage decreases and eventually the aquifer meets the total flow requirements. This is evident in Figure 6.6 where the curves

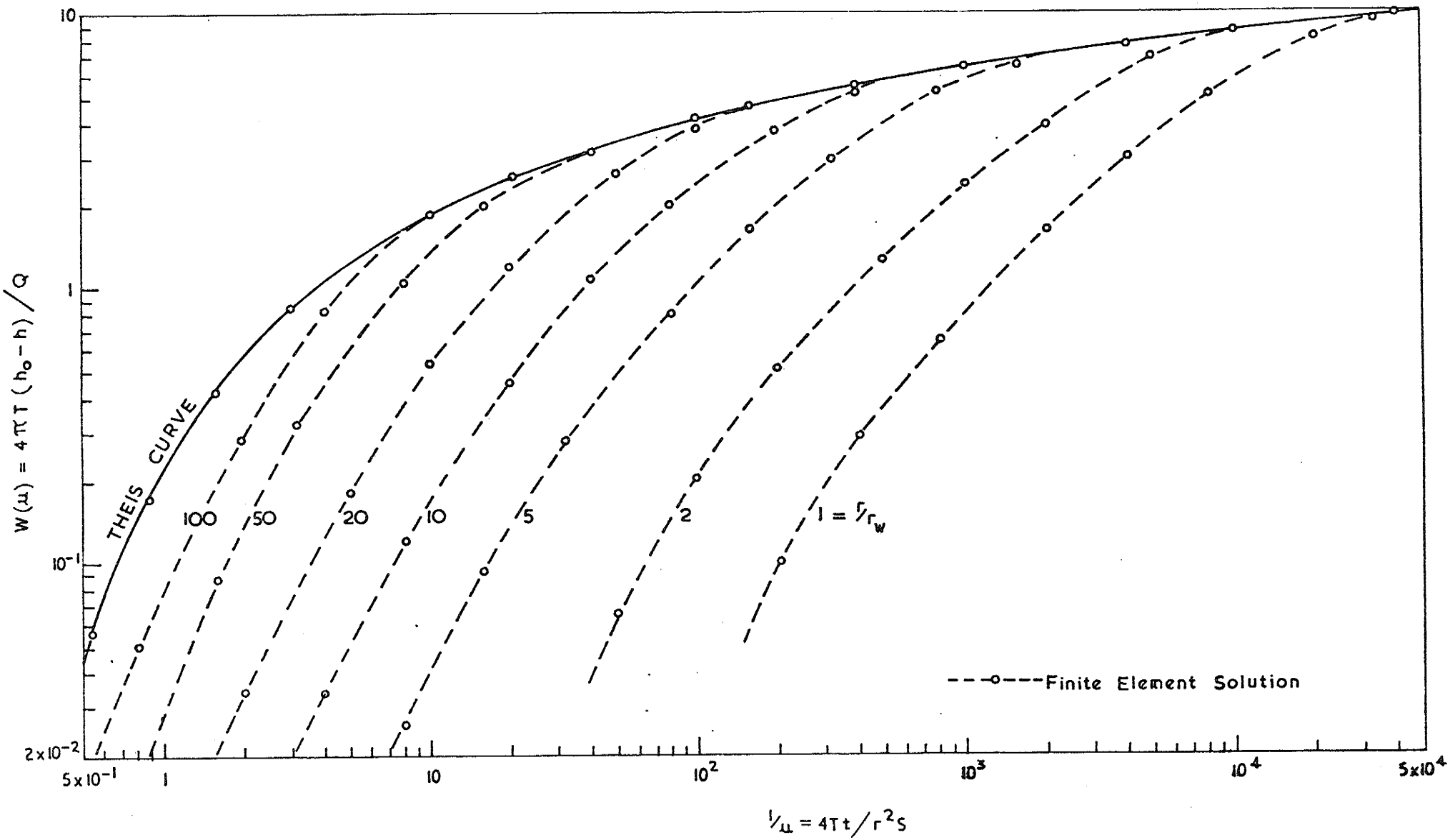

FIGURE 6·6: EFFECT OF WELL STORAGE - FULLY SCREENED WELL IN CONFINED AQUIFER-CONSTANT DISCHARGE RATE-DARCY FLOW.

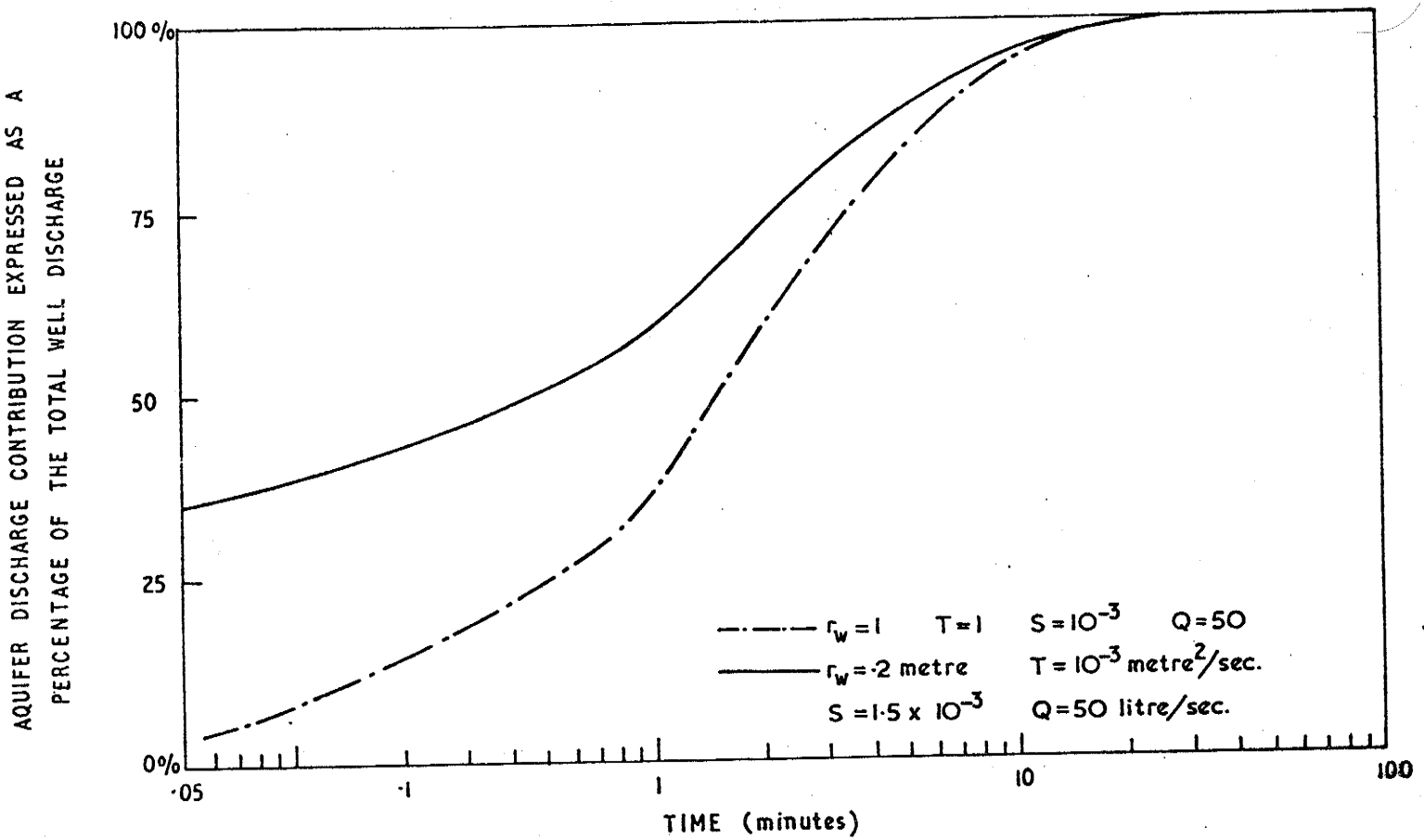

FIGURE 6·7: EFFECT OF WELL STORAGE - VARIATION OF AQUIFER DISCHARGE CONTRIBUTION WITH TIME.

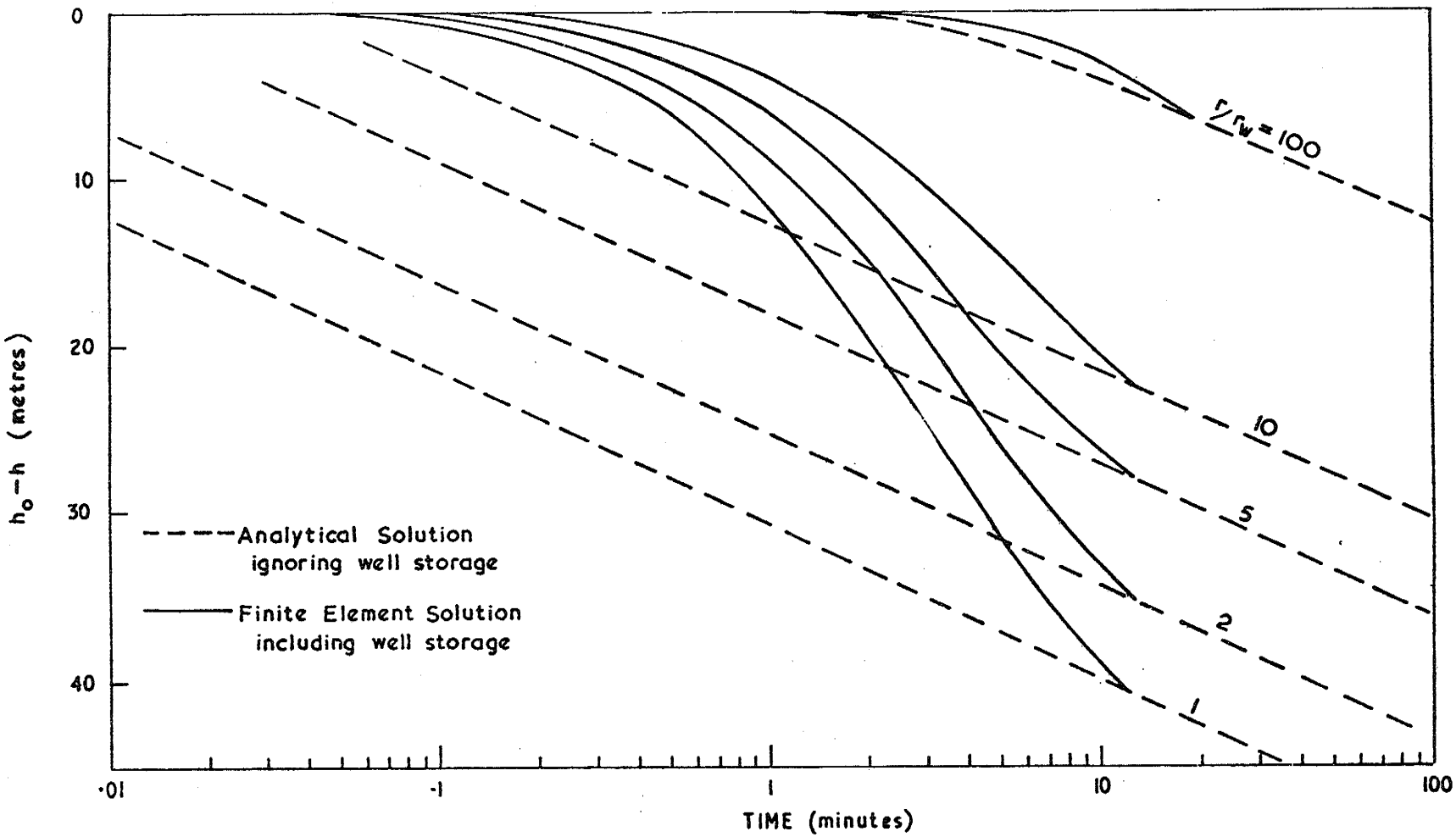

FIGURE 6·8: TYPICAL PROBLEM. EFFECT OF WELL STORAGE ON DRAWDOWN-TIME RELATIONSHIPS AT VARIOUS LOCATIONS.

for the different r/r_w values including well storage approach and merge with the analytical Theis solution as time increases.

The increase in the proportion of the pumped discharge attributable to the aquifer is shown in Figure 6.7 for both problems solved.

The second problem solved (metric unit values given) represents a typical practical well-aquifer system. The drawdown-time relationships for various r/r_w values are given in Figure 6.8 for this problem. For comparative purposes, the Theis analytical solution which ignores well storage is also shown. BothFigures 6.7 and 6.8 clearly demonstrate that well storage effects have dissipated after approximately 15 minutes of pumping for the typical practical problem discussed.

6.4 Non-Linear Flow Solutions

Analytical solutions for problems of transient non-linear well flow are unavailable in the literature even for the one-dimensional fully radial case. The finite element method was used to investigate the effects of non-linear flow on the near well behaviour of confined aquifer-well systems.

6.4.1 Fully Screened Well

The case of a fully screened well in a confined aquifer being pumped at constant rate was considered. Well storage effects were ignored. The following three problems were solved using the computer program employing one-dimensional isoparametric ring elements.

r_w = 0.1 metre m = 8 metres

a = 1 sec/cm b = 5 $(sec/cm)^2$

$S_s = 10^{-4}$ / metre

ϵ_Q = 5%

Problem (i) $\bar{Q}$ = 50 litres/sec.

Problem (ii) $\bar{Q}$ = 100 litres/sec.

Problem (iii) $\bar{Q}$ = 200 litres/sec.

The time domain $10^{-2} \leqslant t \leqslant 10^{4}$ seconds, was divided into steps according to $t_{i+1} = t_i \times 10^{1/3}$. All problems were solved using a finite element network which was selected to obey the rules of Section 5.2.4. The length of the element near the well was equal to the well radius, $r_w = 0.1$, and the mesh nodes were spaced logarithmically with radial distance from the well. The mesh extended to a radius of influence, r_o = 1000 metres, where a constant head boundary was imposed.

The results of the finite element solutions are shown in Figure 6.9 in which the drawdown-time relationships are presented in dimensionless form, W(u) versus 1/u. The dimensionless parameter $bQ/a2\pi mr$ previously derived in Section 5.2.2 was found to characterise the effect of non-linear flow on the transient drawdown behaviour within the confined aquifer. The dimensionless type curves for the non-linear flow cases all lie above the conventional Darcy flow Theis curve solution with the deviation from the Theis curve increasing with the value of $bQ/a2\pi mr$.

The radial distributions of drawdown at times t = 5, 50, 5000 seconds are shown in Figure 6.10 for the problems in which the

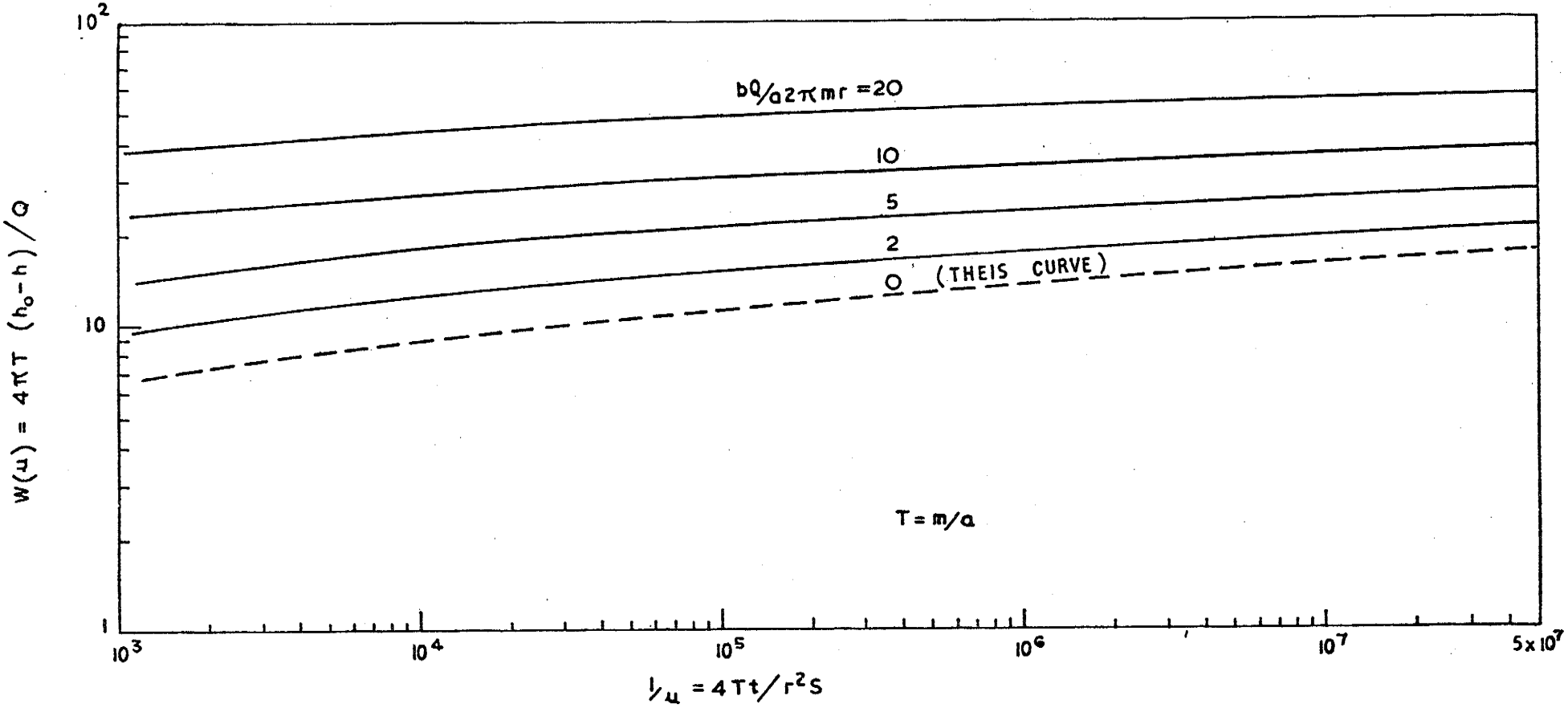

FIGURE 6·9: NON-LINEAR FLOW TO A FULLY SCREENED WELL.

DIMENSIONLESS DRAWDOWN-TIME RELATIONSHIPS.

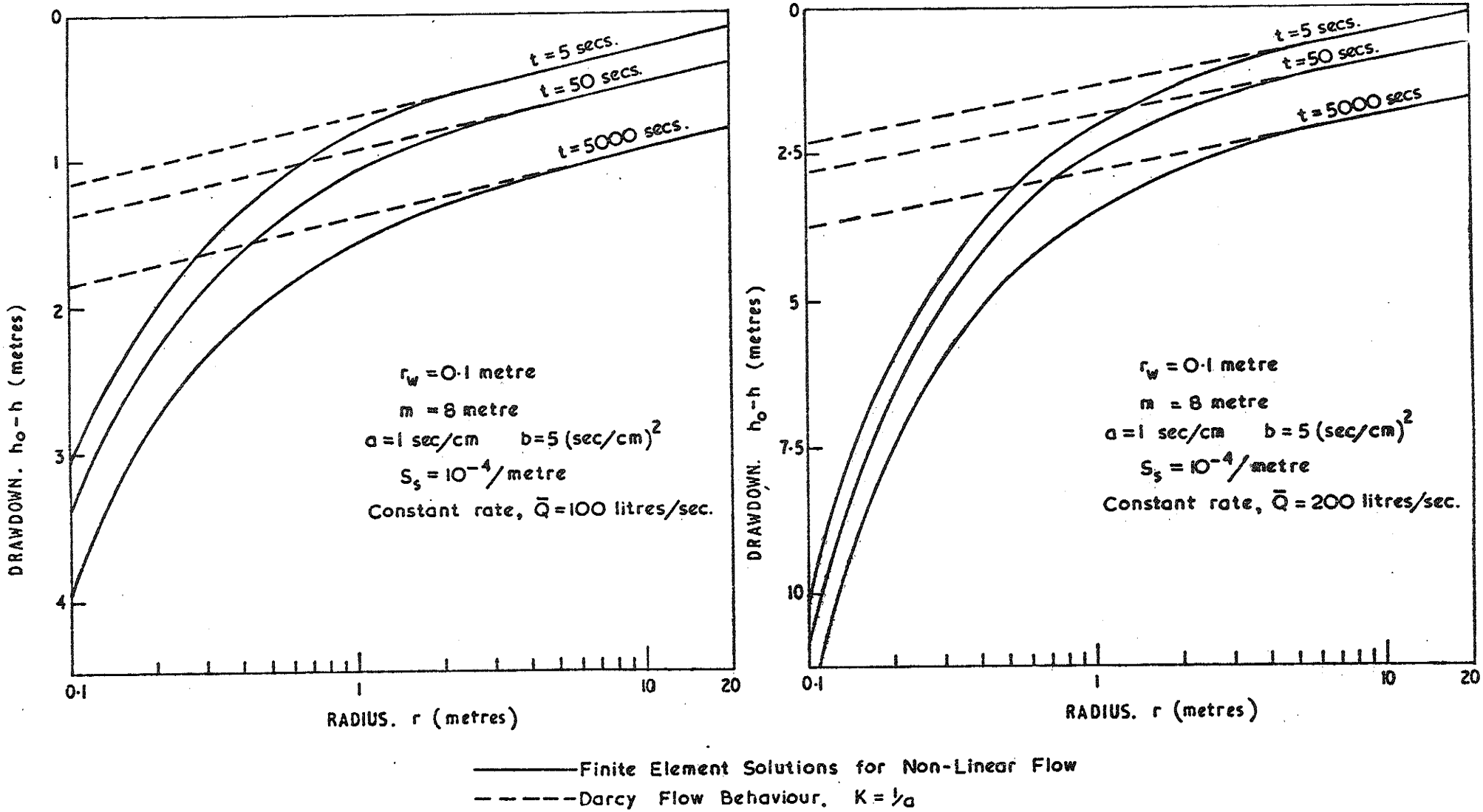

FIGURE 6·10: NON-LINEAR FLOW TO A FULLY SCREENED WELL – TYPICAL RADIAL DRAWDOWN DISTRIBUTIONS AT VARIOUS TIMES.

pumping rates were 100 and 200 litres/sec. The dotted lines represent the radial drawdown distributions for the equivalent Darcy flow behaviour in which the hydraulic conductivity is given by $K = 1/a$. As evidenced by the deviation of the non-linear flow results from the Darcy flow behaviour in Figure 6.10, the effect of non-linear flow is to cause additional drawdowns which increase with proximity to the well.

The variation of drawdown with time may be conveniently represented by two components -

$$s(r,t) = s(r,t)_{Darcy} + s(r,t)_{Non\ linear} \qquad (6.3)$$

$s(r,t)_{Darcy}$ is the component of drawdown based on the assumption of Darcy flow with $K = 1/a$.

$s(r,t)_{Non\text{-}linear}$ is the additional drawdown due to non-linear flow.

In all cases, after a short time, the additional drawdowns attributable to non-linear flow remained constant. The time for non-linear flow to become fully established and henceforth independent of time was of the order of a few seconds for the problems investigated. Figure 6.10 clearly demonstrates the time constancy of the additional drawdowns due to non-linear flow.

Once developed, the additional drawdown attributable to non-linear flow was found to be given by

$$s(r,t)_{Non\text{-}linear} = b\left(\frac{Q}{2\pi m}\right)^2\left(\frac{1}{r} - \frac{1}{r_o}\right) \qquad (6.4)$$

which is the expression derived in Section 5.2.2 (equation(5.3)) for the non-linear flow drawdown contribution for steady state well flow

in a confined aquifer.

6.4.2 Partially Screened Well

Several cases of a partially screened well in a confined aquifer being pumped at constant discharge were investigated using a two-dimensional finite element program. Well storage effects were ignored.

The basic problem described in Section 6.2.5 was solved for non-linear flow at three pumping rates as follows:-

$r_w = 1$ $\quad m = 40$ $\quad l_s = 20$

$a = 10$ $\quad b = 50$

$S_s = 10^{-4}$

$\epsilon_Q = 5\%$

Pumping rate (i) $\bar{Q} = 50$

(ii) $\bar{Q} = 100$

(iii) $\bar{Q} = 200$

Any consistent set of units can be applied to the above problems. The two-dimensional axisymmetric finite element network selected was the same as that previously described in Section 6.2.5. At the chosen radius of influence, $r_o = 1000$, a prescribed head boundary was imposed. The solution was carried out within the time domain, $10^{-1} \leqslant t \leqslant 10^{5}$, by selecting time steps according to $t_{i+1} = t_i \times 10^{1/3}$.

The finite element solutions for the dimensionless drawdown-time relationships, W(u) versus 1/u, for nodal points along the base of the aquifer and at radial distances $r = r_w = 1$ and $r = 4$ are plotted in Figure 6.11. The dimensionless parameter, $bQ/a2\pi mr$,

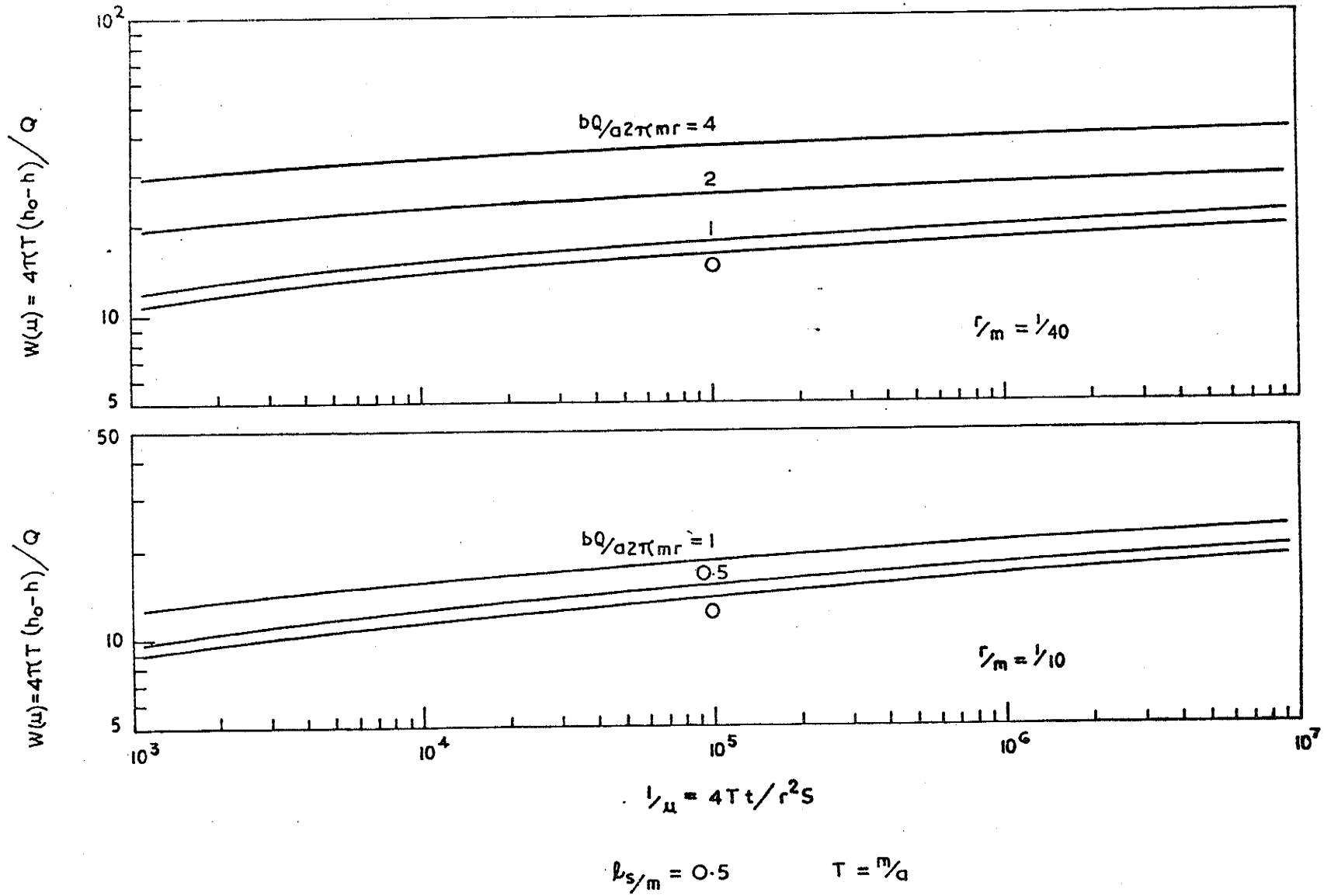

FIGURE 6·11: NON-LINEAR FLOW TO A PARTIALLY SCREENED WELL. DIMENSIONLESS DRAWDOWN-TIME RELATIONSHIPS FOR LOCATIONS ALONG THE CONFINED AQUIFER BASE.

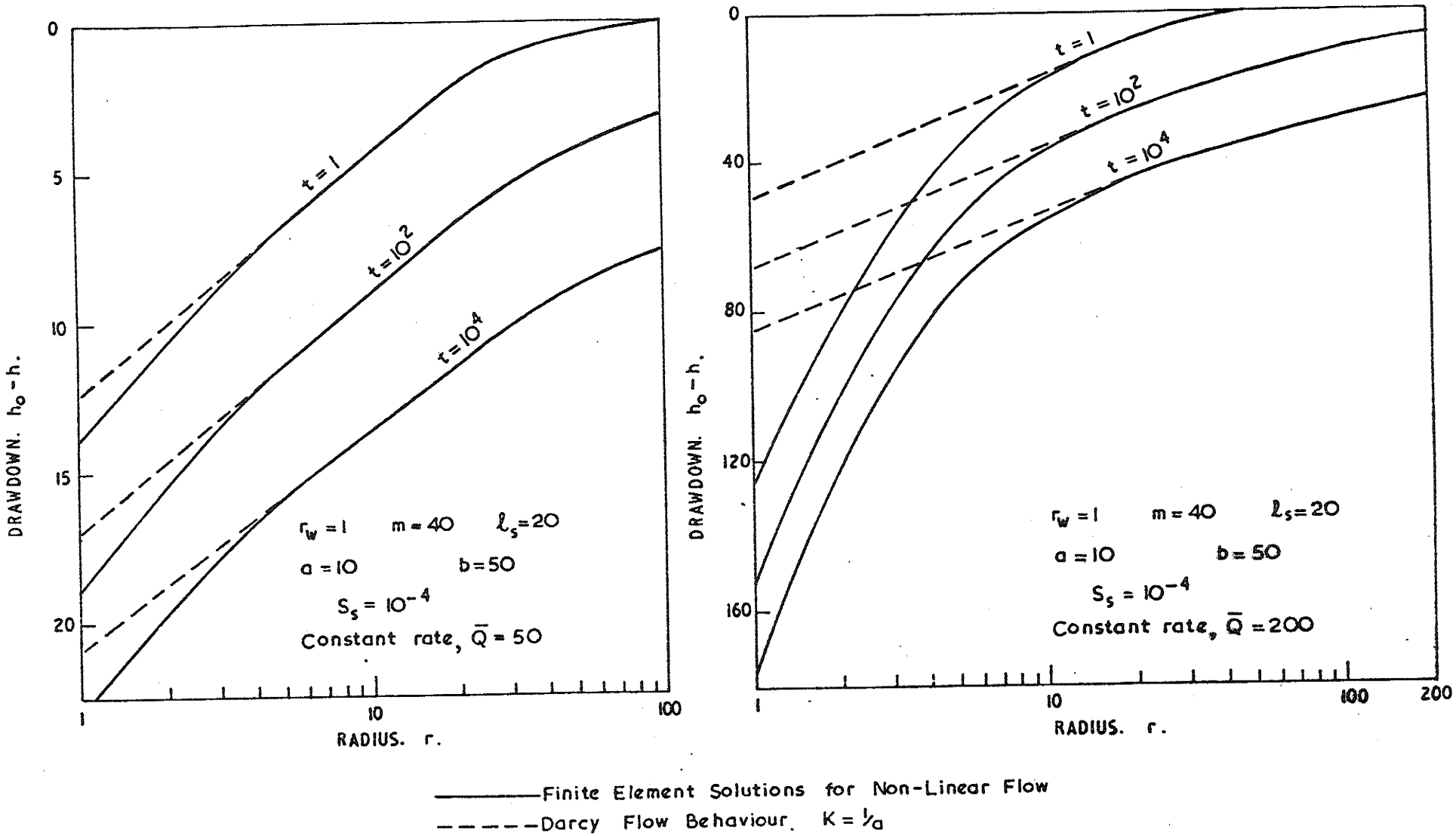

FIGURE 6·12: NON-LINEAR FLOW TO A PARTIALLY SCREENED WELL

TYPICAL AQUIFER BASE RADIAL DRAWDOWN DISTRIBUTIONS AT VARIOUS TIMES.

was used to characterise the non-linear flow behaviour. The type curves for the equivalent fully Darcy case K = 1/a are also included for comparative purposes. For both locations, r=1 and 4, the curves for the non-linear flow behaviour lie above the Darcy flow type curve, and the deviation from the Darcy curve becomes greater as the value of $bQ/a2\pi rmr$ increases.

The radial distributions of drawdown along the aquifer base at times t = 1, 10^2, 10^4 are shown in Figure 6.12 for the pumping rates $\bar{Q}$ = 50 and 100. The dotted lines represent the aquifer base radial drawdown distributions for the equivalent Darcy flow behaviour in which K = 1/a.

As for the fully screened purely radial flow case discussed in Section 6.4.1 -

(i) non-linear flow causes additional drawdown components which increase as the well is approached;

(ii) non-linear flow becomes fully developed within a relatively short period of time and henceforth the additional drawdowns attributable to non-linear flow remain constant.

Both the above effects are clearly demonstrated in Figure 6.12.

6.5 Variable Well Pumping Rate

In field testing of water well-aquifer systems, the pumping operation that is most practical, easiest to control and thus most widely used is that in which the well is pumped at a constant rate of discharge for a specific length of time. Step-drawdown tests in which the discharge is held constant for a certain period and then changed, held constant for another period, and so on, are also

commonly undertaken. The same basic procedures are used in analysing the results of both types of test.

In many field tests, the actual pumping rate may vary from the desired constant value for a multitude of reasons. Provided such variations are not excessive and occur at a time after the commencement of pumping long enough for the aquifer response to have slowed down, the errors introduced by assuming a constant discharge are small. In contrast, pumping rate variations within early times when the aquifer response is most pronounced may have considerable effects on the flow behaviour within the aquifer.

The finite element models developed in this study allow time variations of the discharge being pumped from the well to be considered. As an example, a problem of flow to a fully screened well with variable discharge was solved. The discharge rate was not instantaneously stepped at the start of pumping as is normally assumed. Rather, as shown in Figure 6.13, the discharge was allowed to gradually build up after pumping was commenced until it reached a value at which it remained constant for the remainder of the pumping period.

The remainder of the data for the problem solved using one-dimensional ring elements was as follows:-

$$r_w = 1 \qquad T = 3 \qquad S = 10^{-3}$$

The time domain, $10^{-2} \leqslant t \leqslant 10^{2}$, was divided into steps according to $t_{i+1} = t_i \times 10^{1/3}$ and the same network of elements as previously described in Section 6.2.2 was adopted. Solutions were obtained for the cases both including and ignoring the effects of well storage.

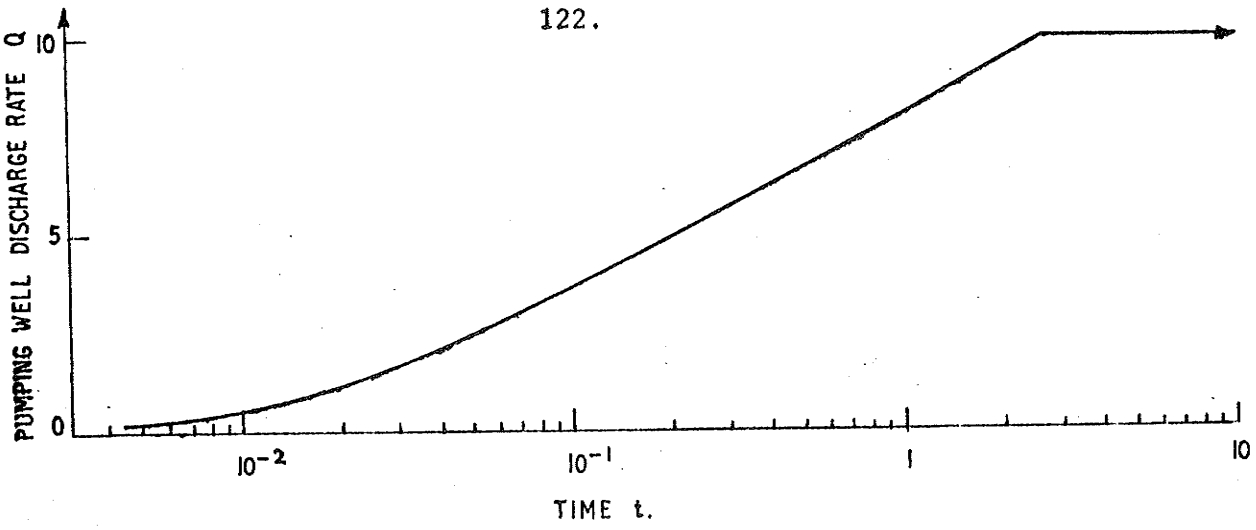

FIGURE 6·13: TIME BUILD UP OF WELL PUMPING RATE.

The drawdown-time results from the computer analyses are shown in Figure 6.14 for the locations r/r_w = 1 and 10. For comparative purposes the relationships for the more usual instantaneously constant pumping rate of $\bar{Q}$ = 10 as determined by the classical Theis solution are also shown in Figure 6.14. Although the deviations from the Theis curve are large in the early times in which the discharge is building up, the solutions rapidly converge to the Theis solution once a constant pumping rate is attained.

6.6 Aquifer Inhomogeneity

Several problems were solved to demonstrate that aquifer inhomogeneity can be readily incorporated into the developed finite element programs.

As previously discussed in Section 5.5 when considering steady

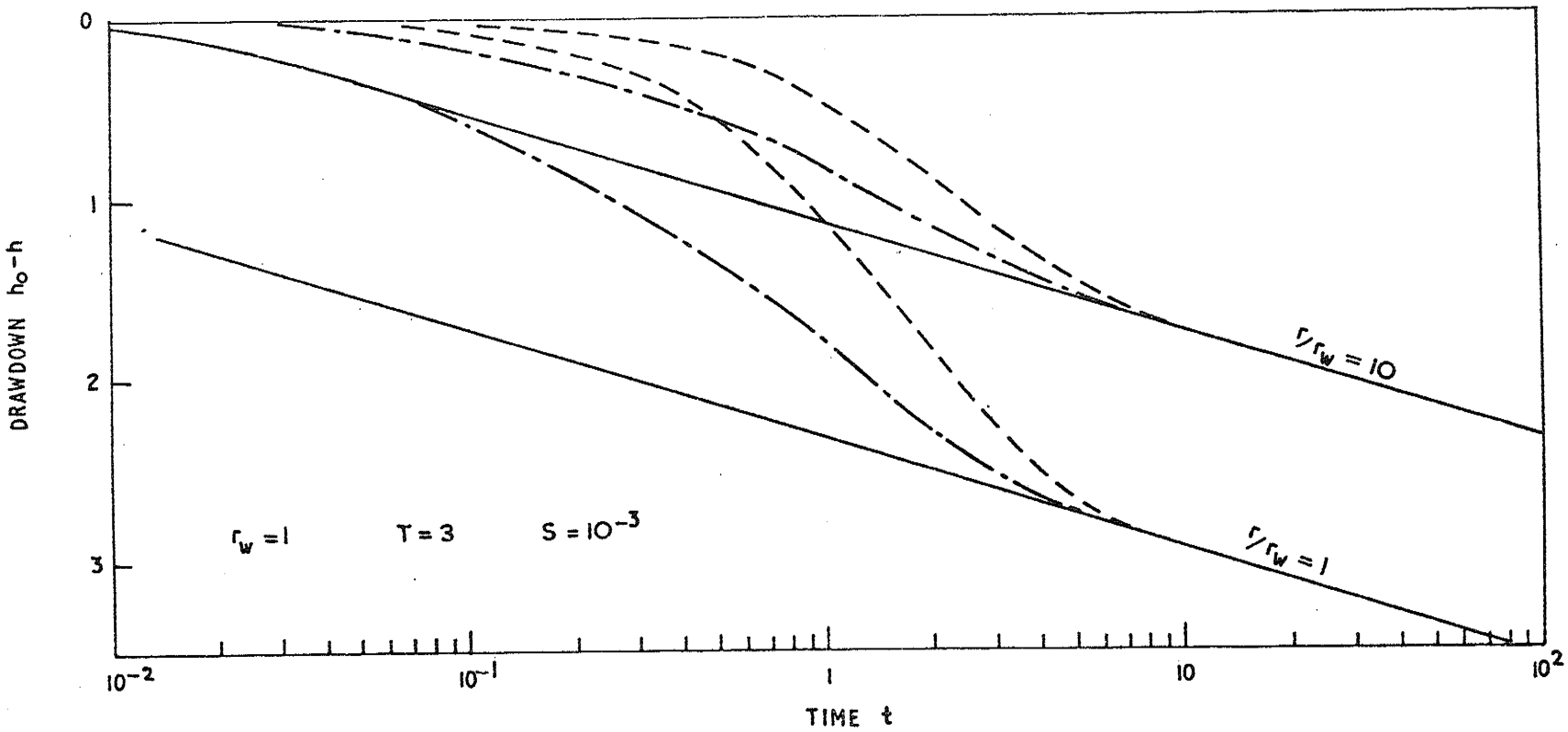

———— Instantaneously constant rate. $\bar{Q} = 10$. Theis solution.

Finite element solutions: buildup in well discharge as specified in Figure 6·13

—·—·— Well storage neglected

– – – – Well storage included

FIGURE 6·14: DRAWDOWN-TIME RELATIONSHIPS FOR SPECIFIC BUILDUP IN WELL DISCHARGE - FULLY SCREENED WELL - DARCY FLOW.

state performance, permeability variations which occur in a zone immediately surrounding the well may exert a marked influence on the flow behaviour. Theoretical analyses for flow to a fully penetrating well with permeability reduction or improvement have been presented in the petroleum industry literature (Van Everdingen (1953), Jones (1962), Van Poolen et al (1958)). Dudgeon and Huyakorn (1975) used finite element techniques to investigate this form of aquifer inhomogeneity for both fully and partially screened wells. The results for a typical problem solved by the author using the developed finite element programs are presented in Figure 6.15. In all cases examined -

(i) deviations from normal flow behaviour were confined to the affected zone around the well. As shown in Figure 6.15, the flow within the original unaffected aquifer material obeys the classical Theis equation;

(ii) as noted by Dudgeon and Huyakorn (1975), shortly after the commencement of pumping, the flow within the affected zone adjacent to the well becomes independent of time and is henceforth identical to the steady state flow behaviour. This applies to both fully and partially screened wells.

Aquifer inhomogeneity in the form of multi-layering was investigated by Javandel and Witherspoon (1968) who employed finite element programs using triangular ring elements. In an abbreviated investigation the author solved various unsteady well flow problems in multi-layered confined aquifers. The developed two-dimensional

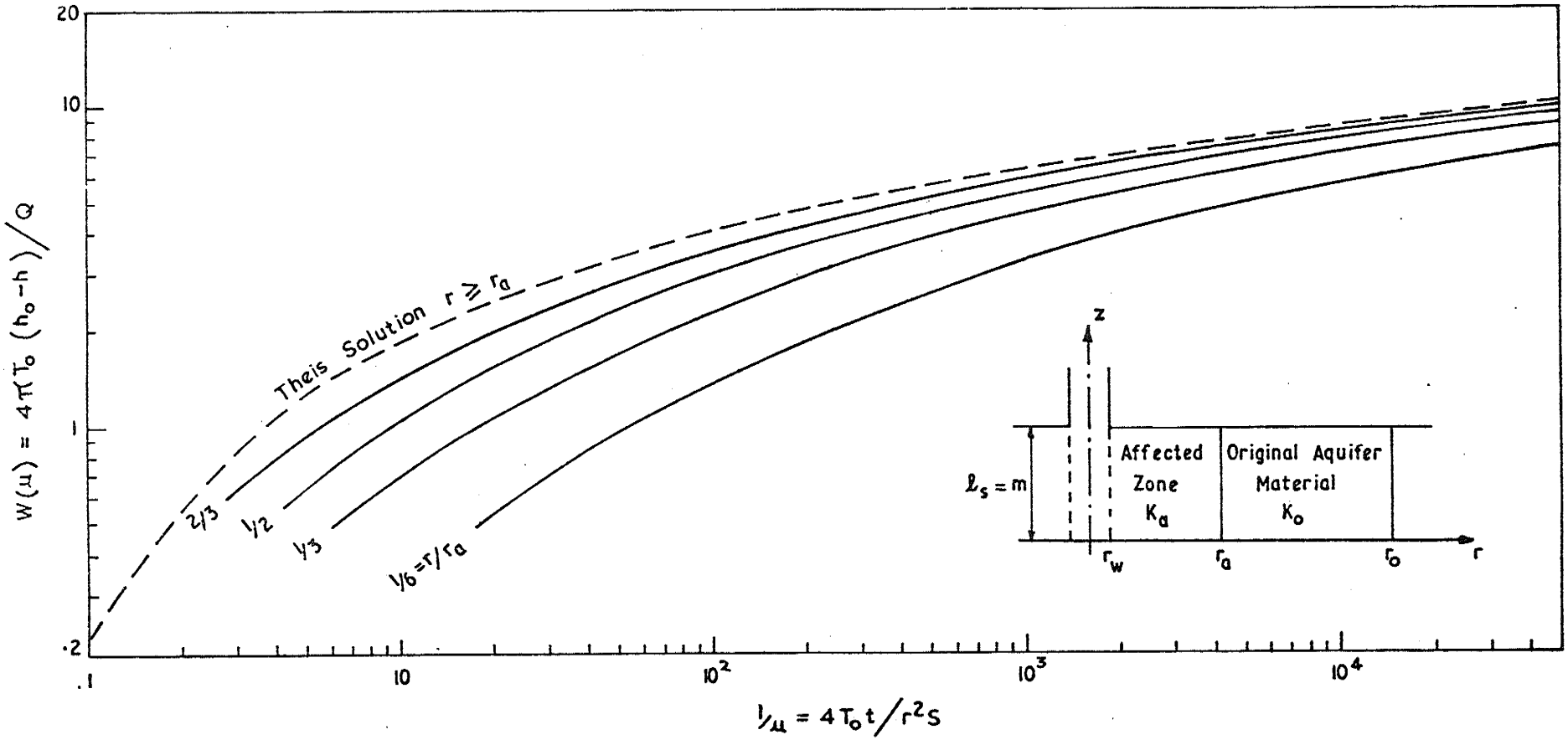

$r_w = 0.5$ $T_o = K_o m = 3$ $S_o = 10^{-3}$ $\bar{Q} = 10$

$r_a/r_w = 6$ $K_a/K_o = 10$

FIGURE 6·15: PERMEABILITY VARIATION ADJACENT TO A FULLY SCREENED WELL IN A CONFINED AQUIFER – TYPICAL PROBLEM.

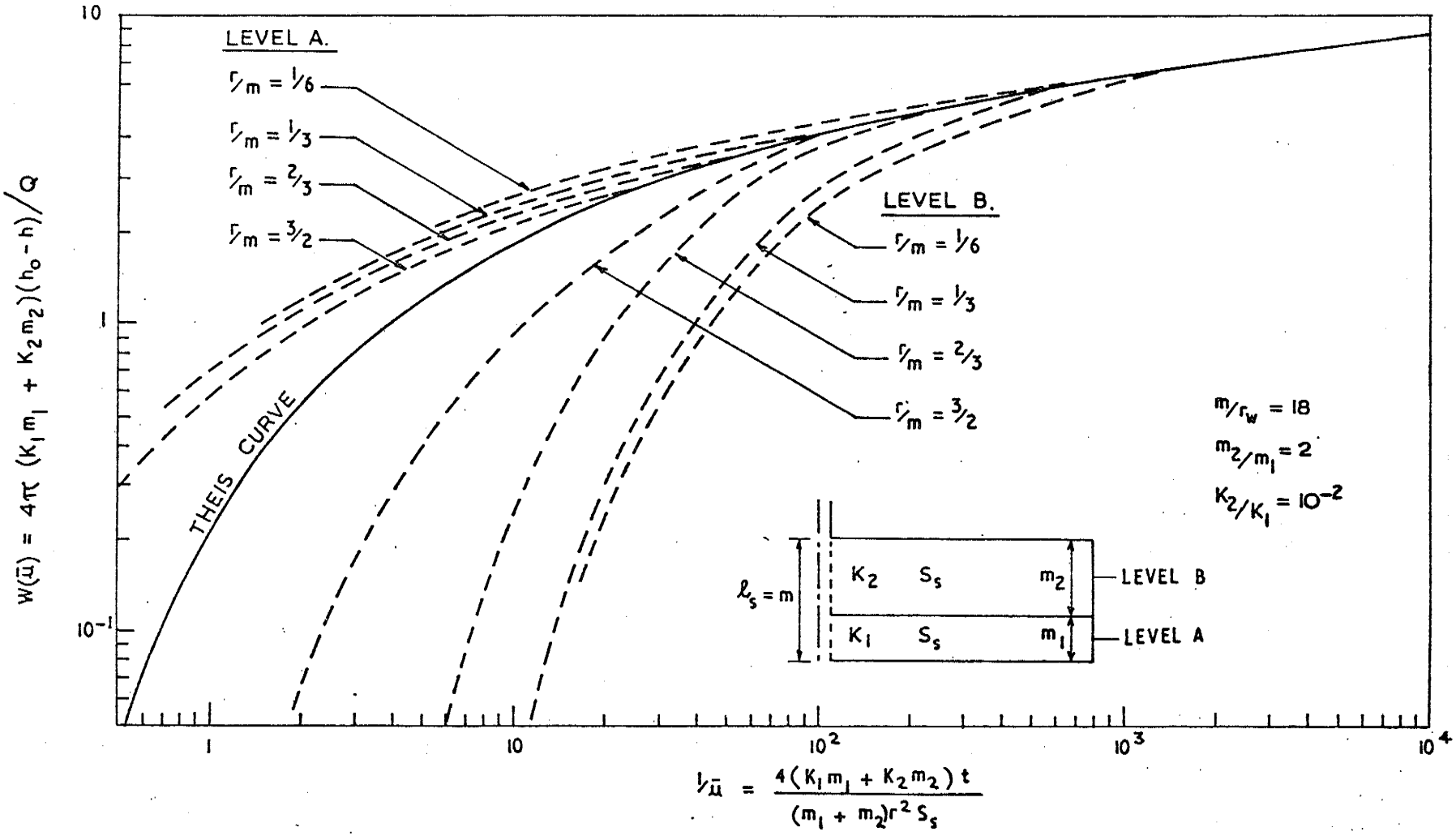

FIGURE 6·16: FULLY SCREENED WELL PUMPED AT CONSTANT RATE – MULTILAYERED AQUIFER – TYPICAL PROBLEM – DARCY FLOW – DIMENSIONLESS DRAWDOWN – TIME RELATIONSHIPS.

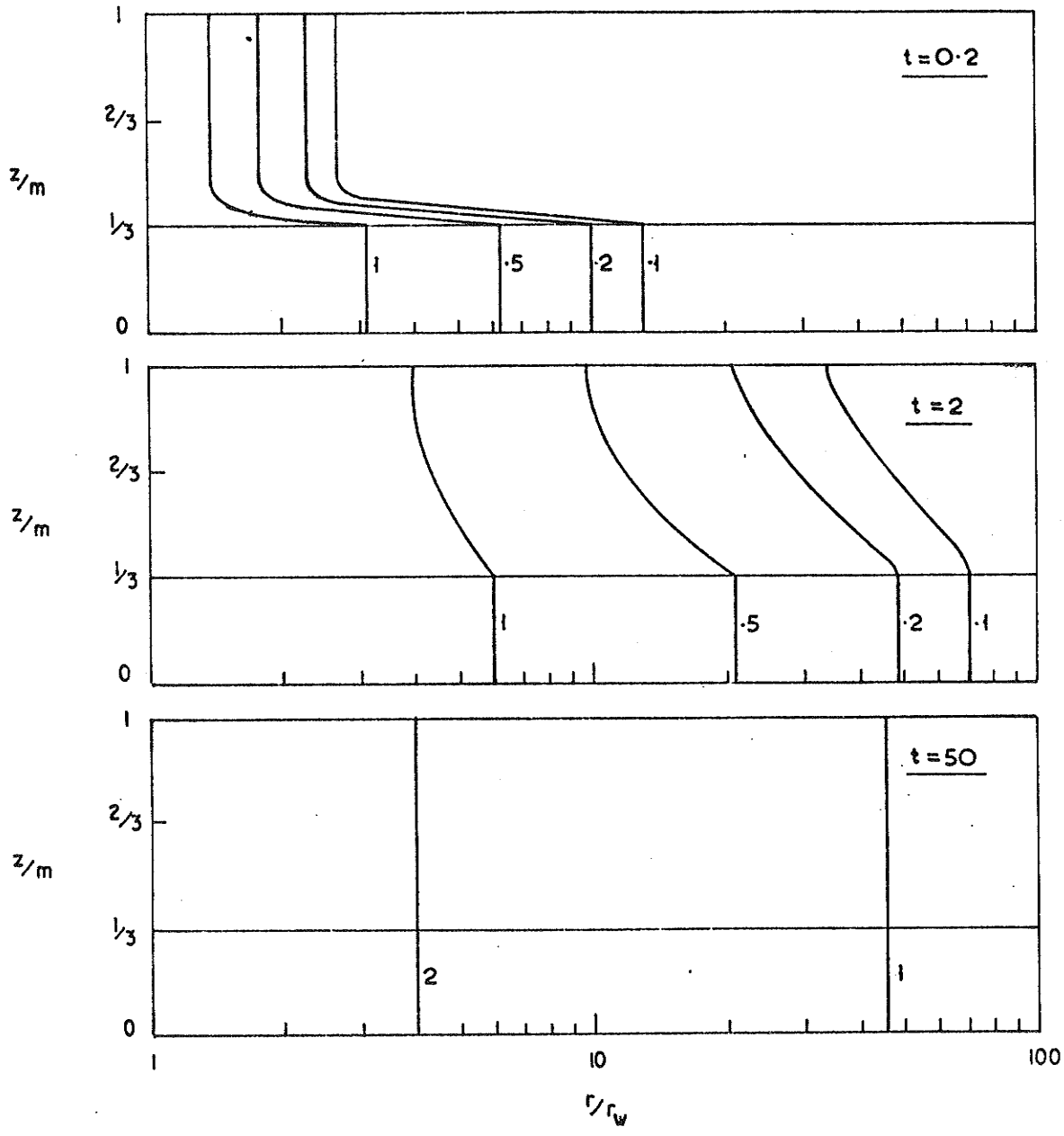

$m/r_w = 18$ $m_2/m_1 = 2$ $K_2/K_1 = 10^{-2}$. Drawdown contours are in arbitrary units

FIGURE 6·17: FULLY SCREENED WELL PUMPED AT CONSTANT RATE - MULTILAYERED AQUIFER - TYPICAL PROBLEM - DARCY FLOW — AQUIFER DRAWDOWN DISTRIBUTION CONTOURS.

finite element computer programs which employ mainly rectangular ring elements were used. The general conclusions drawn by Javandel and Witherspoon were supported by the results obtained. For completeness the relevant generalisations may be stated as:-

(i) Multi-layered confined aquifer systems may be considered equivalent to a single homogeneous layer only when the well is fully screened and enough time has elapsed since the start of pumping.

(ii) At distances less than twice the total thickness of the layered system, ($r < 2m$), the effects of both partial screening and inhomogeneity may be significant at early times. As time increases, the effects of inhomogeneity slowly diminish and the effects of partial screening dominate.

(iii) For $r > 2m$, the effects of partial screening are negligible for all times, and only the effects of inhomogeneity which slowly diminish with time must be considered.

Finite element results for a typical multi-layered aquifer problem solved by the author are presented in Figures 6.16 and 6.17.

6.7 Discussion

In this chapter, finite element computer programs have been verified and used to solve a range of unsteady well flow problems in confined aquifers. The capacity of the finite element analysis and developed computer programs to take into account effects not previously considered has been demonstrated. Substantial deviations from classical theoretical flow behaviour have been shown to occur.

In early times after the commencement of pumping, the flow

behaviour may be markedly affected by well storage, variable pumping rate, partial screening and aquifer inhomogeneity. Thus, little value can be gained, at present, from early time data if conventional interpretation procedures are employed. If early time data are to be meaningfully evaluated, then more rigorous analysis, most probably employing numerical solutions similar to those demonstrated herein, is essential. More thorough early time analysis will of necessity have to include the effects of non-linear flow, well screen loss and flow friction losses within the well in addition to the complicating effects already mentioned above. Field testing of wells in both Australia and New Zealand, where early time data ($t < 3$ minutes) was recorded, has resulted in pressure oscillations being observed in both pumping and observation wells. The possibility of phenomena similar to water hammer or surging suggests itself but as yet the pressure oscillations are unexplained, further shadowing the usefulness of early time data in determining aquifer properties.

Fortunately, deviations from the generally expected classical behaviour occur at early times and/or in the vicinity of the well. Thus, the accepted and well-known type curve fitting techniques may be used and are recommended for determining the overall aquifer characteristics, namely transmissivity T and storage coefficient S. The noted deviations should, however, be considered and the type curve techniques only used within the limits in which they are appropriate.

If the effects of non-linear flow and/or aquifer inhomogeneity

adjacent to the well are likely, the construction of an observation bore close to the well should be considered. Field information from such an observation bore in conjunction with planned geophysical logging may enable the aquifer characteristics in the vicinity of the well to be evaluated. A pressure sensing device attached to the outside of the well screen may also be of inestimable value in such cases since well screen losses may be specifically isolated. The interpretation of data collected from such locations close to the well is made easier by the fact that deviations from normal flow behaviour caused by non-linear flow and aquifer inhomogeneity rapidly become independent of time and equal to those for steady state flow.

7. Experimental Verification of Steady State Non-linear Flow Finite Element Solutions

7.1 General

The finite element analysis for two dimensional axisymmetric flow problems incorporating non-linear behaviour was experimentally verified using data obtained during a joint investigation in which the author participated. Some of the experimental results have been published (Dudgeon et al, 1972). The majority of the results are unpublished.

A large scale hydraulic model was used to investigate the flow towards partially screened wells in both confined and unconfined aquifers. A general description of the experimental model and testing procedures is included in the chapter.

Methods were developed by the author to determine the in-situ hydraulic characteristics, namely the Forchheimer equation coefficients a and b, of the aquifer material used in the experiments. The determined values of the hydraulic coefficients were used in obtaining finite element model solutions of flow problems for comparison with experimental results.

7.2 Experimental Test Facility

The test facility was constructed with funds made available by the Australian Water Resources Council Research Project 68/8. A rigorous discussion of the design, construction and use of the test facility has been given by Dudgeon et al (1972 pp. D2-D13), and only major points will be presented.

The facility was designed and constructed specifically for use in studying the hydraulics of flow into wells and practical aspects

associated with well drilling and development. The experimental facility, being quite large, enables test wells to be made from full sized commercially available products commonly employed in the field.

A reinforced concrete tank, square in plan, with internal dimensions approximately 16' x 16' x 11' forms the main component of the test facility. The square section chosen enables tests to be carried out on either a circular aquifer of 8 feet radius with a centrally located well, or on a quadrant of an aquifer of 16 feet radius with the well located in the corner of the tank. The general layout is shown in Figure 7.1.

The aquifer material is retained by outer barriers formed from framed sections of 16 gauge perforated metal sheeting having 15% open area. The inner retaining barriers of 4 feet radius enable the aquifer material close to the well to be removed without disturbing the bulk of the entire aquifer. The inner barriers were made from 16 gauge perforated metal sheet, curved and corrugated to allow it to resist compressive loads without buckling. The 45% open area of perforated sheeting used for inner barriers was sufficient to ensure negligible flow resistance.

The flexible arrangement of pipes shown in Figure 7.2 allows gravity driven or pumped water supplies to be fed to and drawn from wells placed at the centre or corner of the tank. A 6-inch centrifugal pump with a 20 HP motor capable of delivering 2 ft.^{3}/sec. against a head of 60 feet can be used for forced water circulations. Discharges are accurately measured by orifice plate meters man-

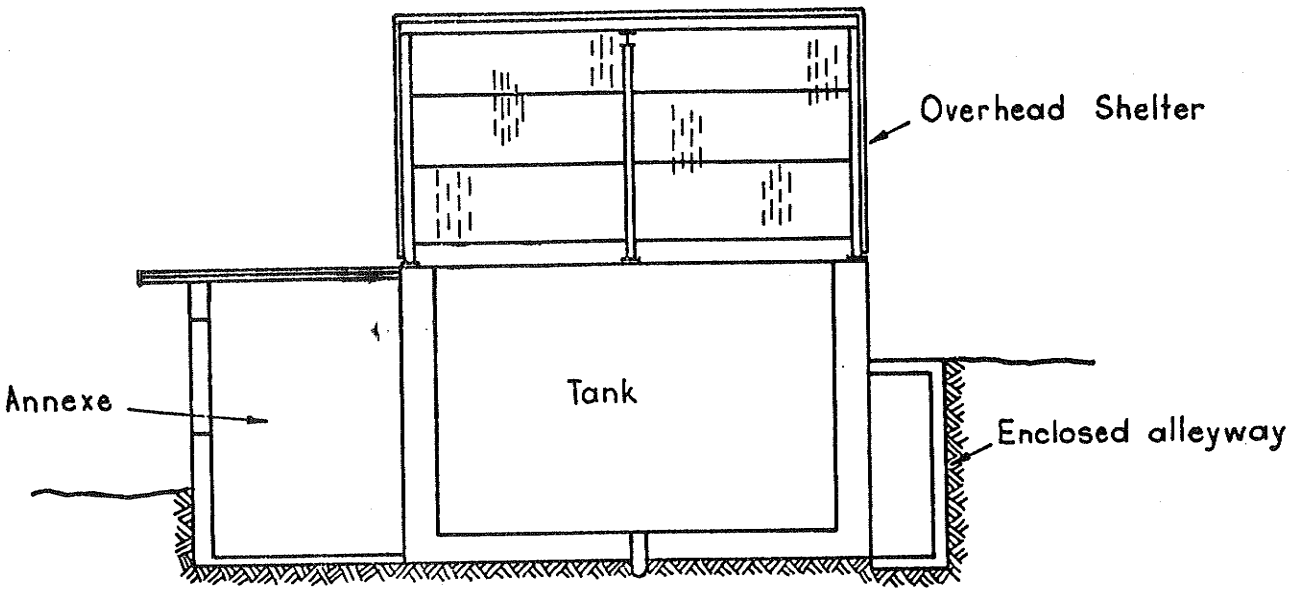

ELEVATION A-A

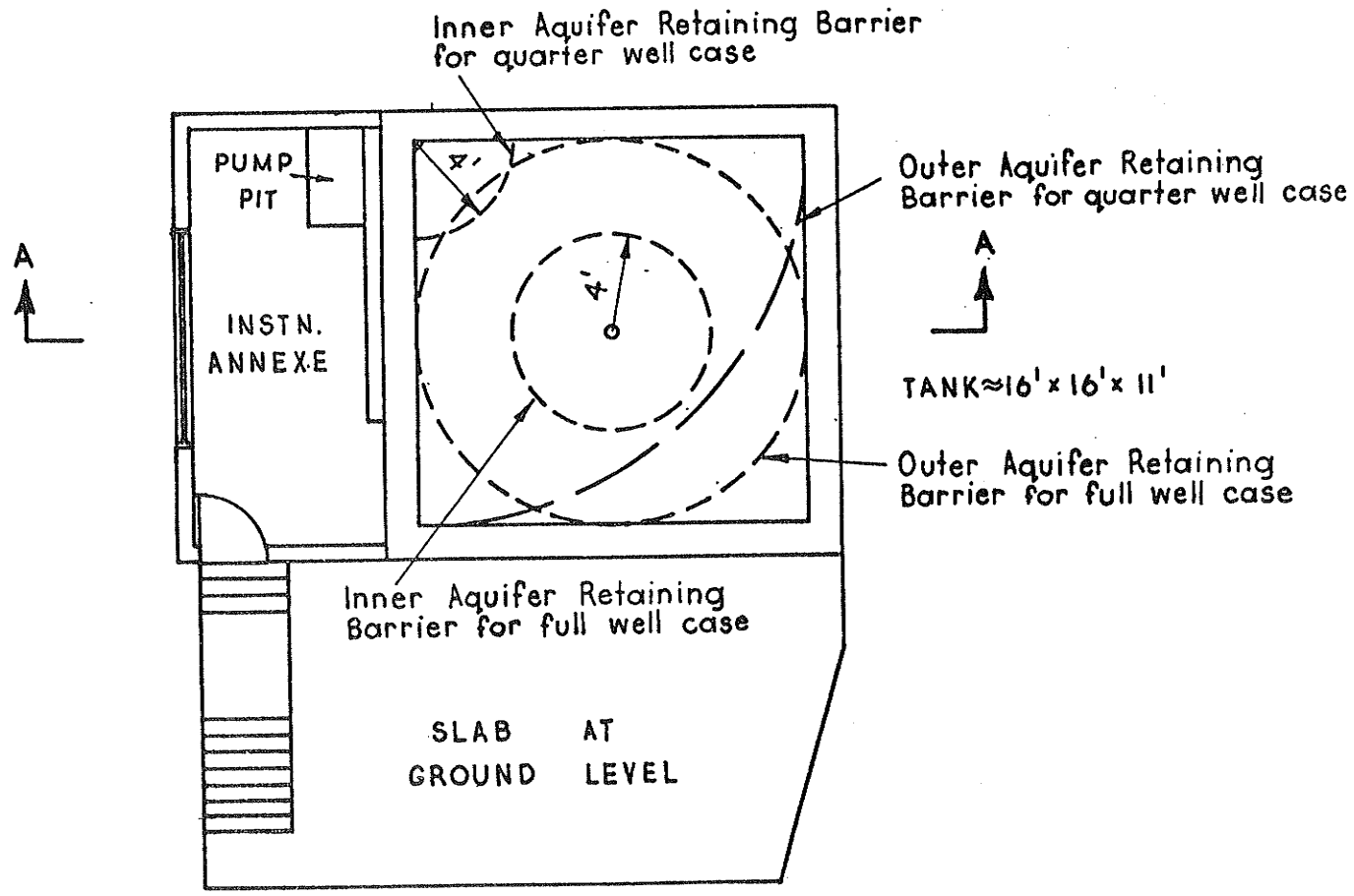

FLOOR PLAN

FIGURE 7·1 : WELL TESTING FACILITY

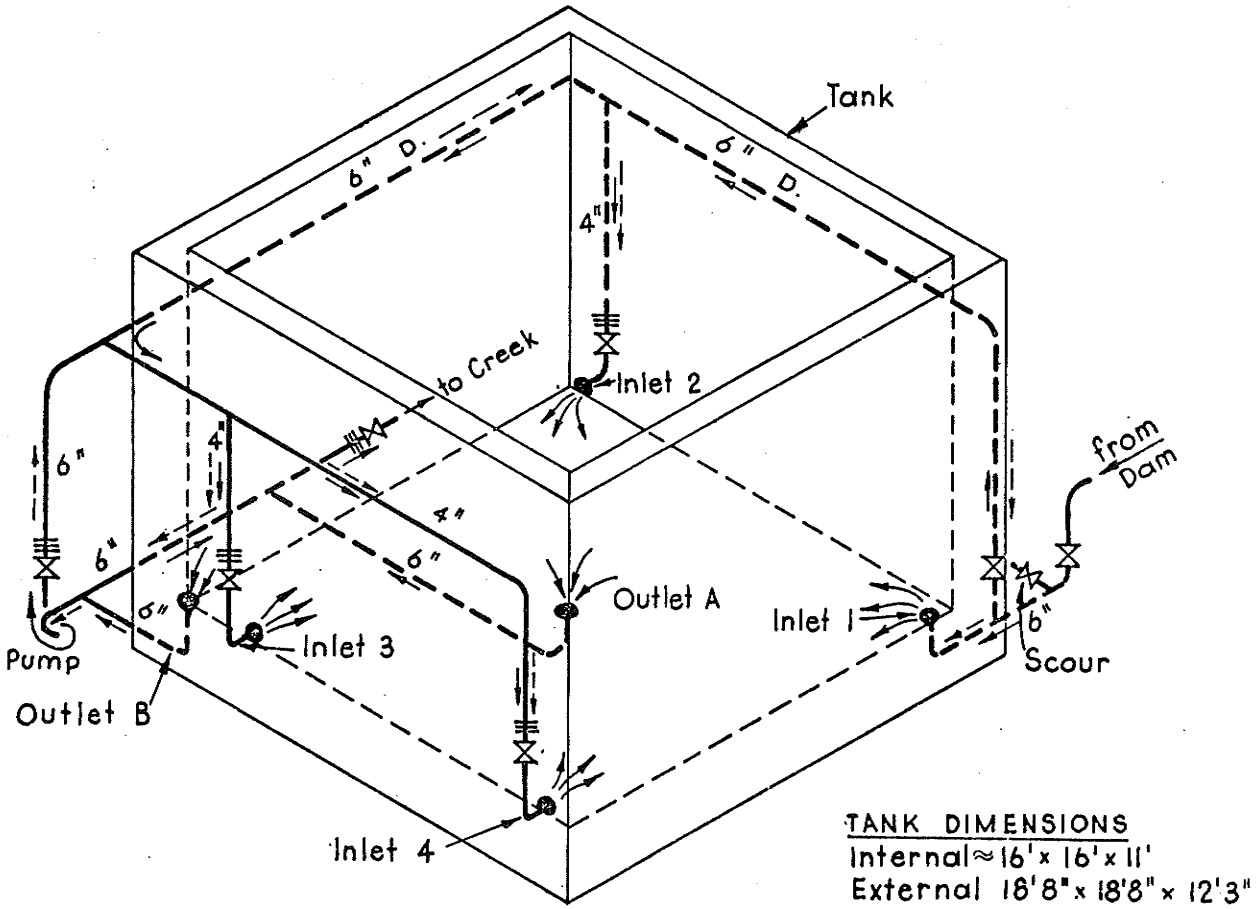

≡ Orifice Plates shown thus

1. With ¼ well under investigation Inlet 1 only to be used and Outlet A, to be blank flanged; valves on Inlets 2,3,4 to be enclosed.
2. With full well under investigation use all Inlets and blank flange outlet B
3. With pump in operation flow shown——►; gravitate——►

FIGURE 7·2: EXPERIMENTAL FACILITY
PIPEWORK AND FLOW DIAGRAM

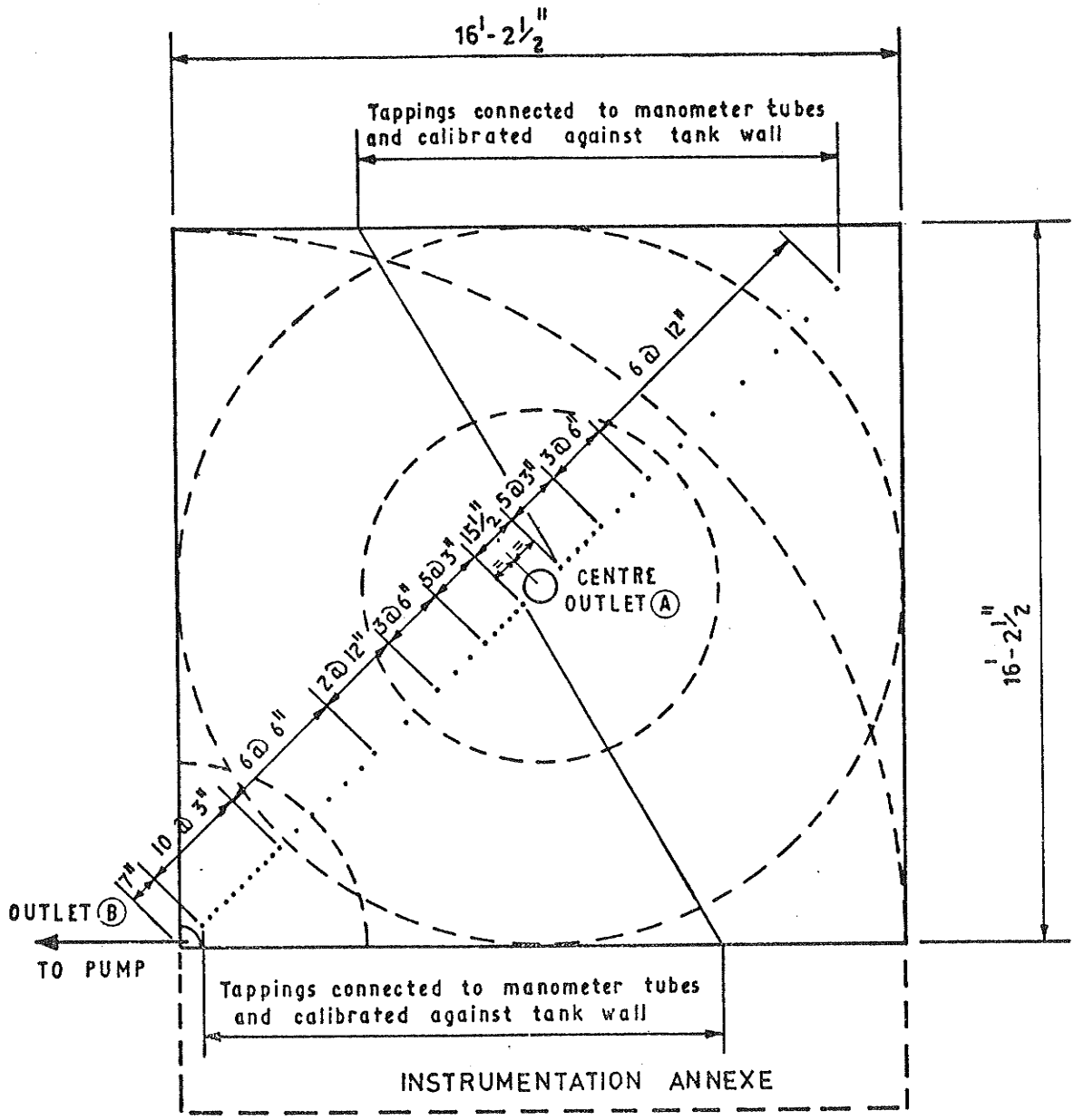

TOTAL NUMBER OF PIEZOMETER TAPPINGS = 42

FIGURE 7·3: LOCATION OF PIEZOMETER TAPPINGS SET IN TANK FLOOR

ufactured and calibrated to British standard specifications.

Piezometer tappings made from copper tubes are set into the floor of the tank on a radial line between the corner well outlet and the diagonally opposite corner. The positioning of the tappings is shown in Figure 7.3. Closer spacings near the well being pumped allows more accurate recording of steeper hydraulic gradients. The copper tubes extend to the outer edge of the tank base where a screwed brass tee enables simple connection of manometers, pressure gauges or transducers.

7.3 Hydraulic Model Testing

7.3.1 Model Description and Test Procedure

The test facility described in Section 7.2 was prepared for testing of a quadrant portion of a well-aquifer system (Figure 7.1).

The relevant length well screen was made from perforated metal sheet curved to form a quadrant of a 10 inch diameter circle, and installed in the corner of the test tank. The 4 mm diameter perforations (40% screen open area) were chosen according to general screen opening selection guidelines such that between 30% and 50% of the aquifer material (Figure 7.5) should be retained.

The aquifer material was placed in the test tank to a depth of 5 feet. Care was taken to avoid unnecessary compaction of the aquifer material during placement.

The vast majority of the air in the pores of the aquifer was removed when filling the test facility by proceeding very slowly. As a measure of aquifer uniformity the variation with depth of effective porosity of the aquifer material was determined by volume

measurement during the slow filling of the tank and aquifer model. All air was removed from the system before testing proceeded. This was achieved by forcing water through the aquifer and pipe network with subsequent bleeding until no air remained.

A pressure resisting cover has been designed such that flow in confined aquifers under pressures up to 50 feet of head may be simulated. At present, construction is incomplete and confined aquifer tests were carried out by covering the 5 feet thick quadrant aquifer with polythene sheeting held in position by several inches of aquifer material and sealed at the edges of the tank. The sheet simulates an overlying impermeable layer as shown in Figure 7.4. Water above the confining sheet applies additional force to hold the sheet down and at the same time provides the head to drive water through the aquifer from the outer barrier to the well, the top of which is left open to the air. Care was taken to avoid vertical leakage to the aquifer.

Unconfined tests were made by lowering the water level to below the polythene sheeting as indicated in Figure 7.4.

A steady state test was carried out by withdrawing water from the well and returning it via the recirculating pump to the inlet in the diagonally opposite corner from where it passes through the aquifer medium towards the well (see Fig. 7.2). The flow rate as measured by an orifice plate downstream of the pump was controlled by throttling the valve in the corner of the tank opposite the well. All piezometer tappings from the base of the tank were connected to manometer panels on two opposite walls of the tank (Figure 7.3). Base pressure head readings were recorded only after all fluctuations in

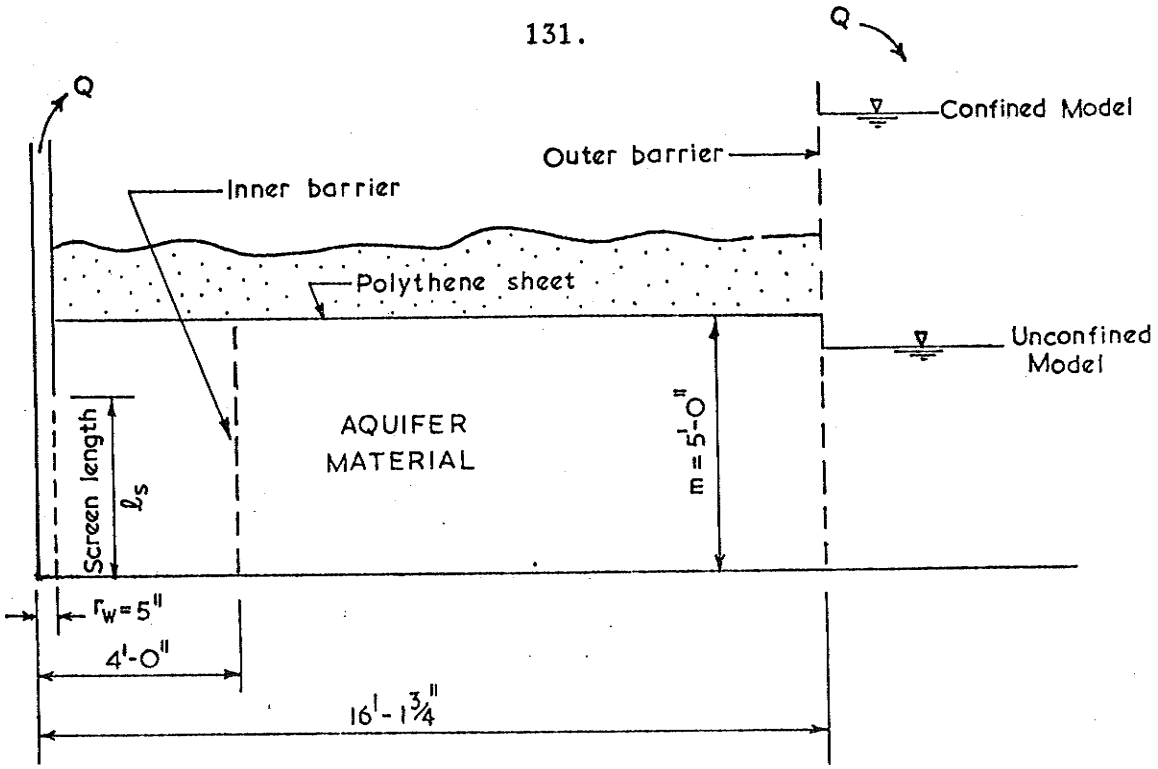

FIGURE 7·4: RADIAL CROSS SECTION OF WELL AQUIFER MODEL SHOWING ARRANGEMENT FOR TESTING

manometer levels had ceased.

Thus the basic experimental results of a test consisted of the discharge and the radial base pressure head distribution.

7.3.2 Further Pressure Measurements

To allow measurement of piezometric heads at various levels at a given radial position in the aquifer a multiple observation well was developed. This consisted of a length of P.V.C. tube with holes drilled at 1 foot intervals and a series of sliding valves which allowed the holes to be covered or uncovered as required without disturbing the piezometer tube or the surrounding aquifer material. The valves were operated by a rod inserted from the top of the tube. The pressure at the position in the aquifer of the opened valve was

given by the water level in the tube.

Probes made from lengths of P.V.C. tubing continuously perforated between 3 and 4.7 feet above the tank base were used to locate the free surface in unconfined aquifer tests. For flow in the unconfined aquifer systems tested, the vertical components of flow were relatively small in the upper portions of the aquifer (near the free surface). The head distribution along the perforated length of such a tube would be relatively uniform and the water level within such a probe a reliable indication of the position of the free surface.

An inexpensive stainless steel contact electrode using a low voltage battery, transistorised amplifier and indicator light was used for measuring water levels in the well itself, the observation well tubes and the free surface location probes.

7.3.3 Aquifer Material

A Nepean River gravel consisting of rounded particles was selected for the aquifer material to be used in the model. The grain size distribution of this material lies within the band shown in Figure 7.5 as determined by sieve analyses of various samples.

The grading of the material indicates an aquifer which would generally be more permeable than aquifers likely to be encountered in the field. However, the selection of such a coarse material ensured the occurrence of non-linear flow in the testing of the model and also guaranteed that capillary effects would be negligible for unconfined aquifer flow.

A single Forchheimer relationship was found to give a very good fit to each of two independent sets of results from permeameter testing

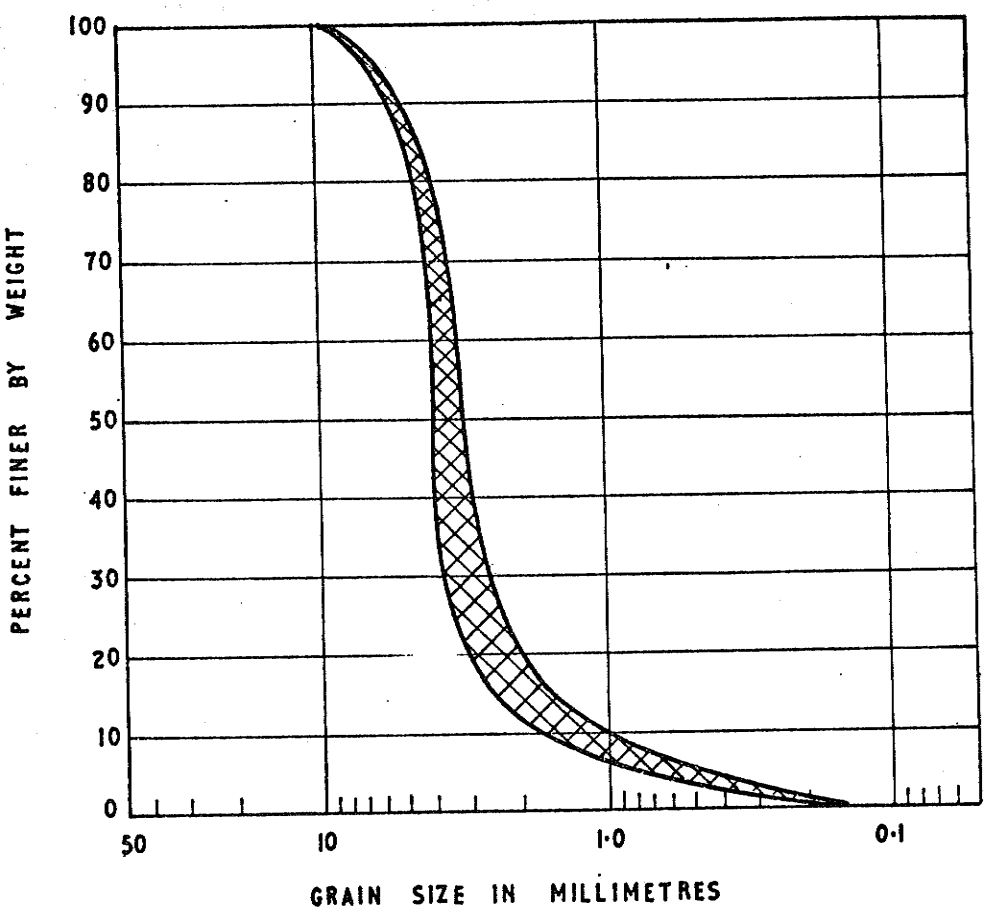

FIGURE 7·5: SIEVE ANALYSES OF AQUIFER MATERIAL USED IN EXPERIMENTAL TESTS

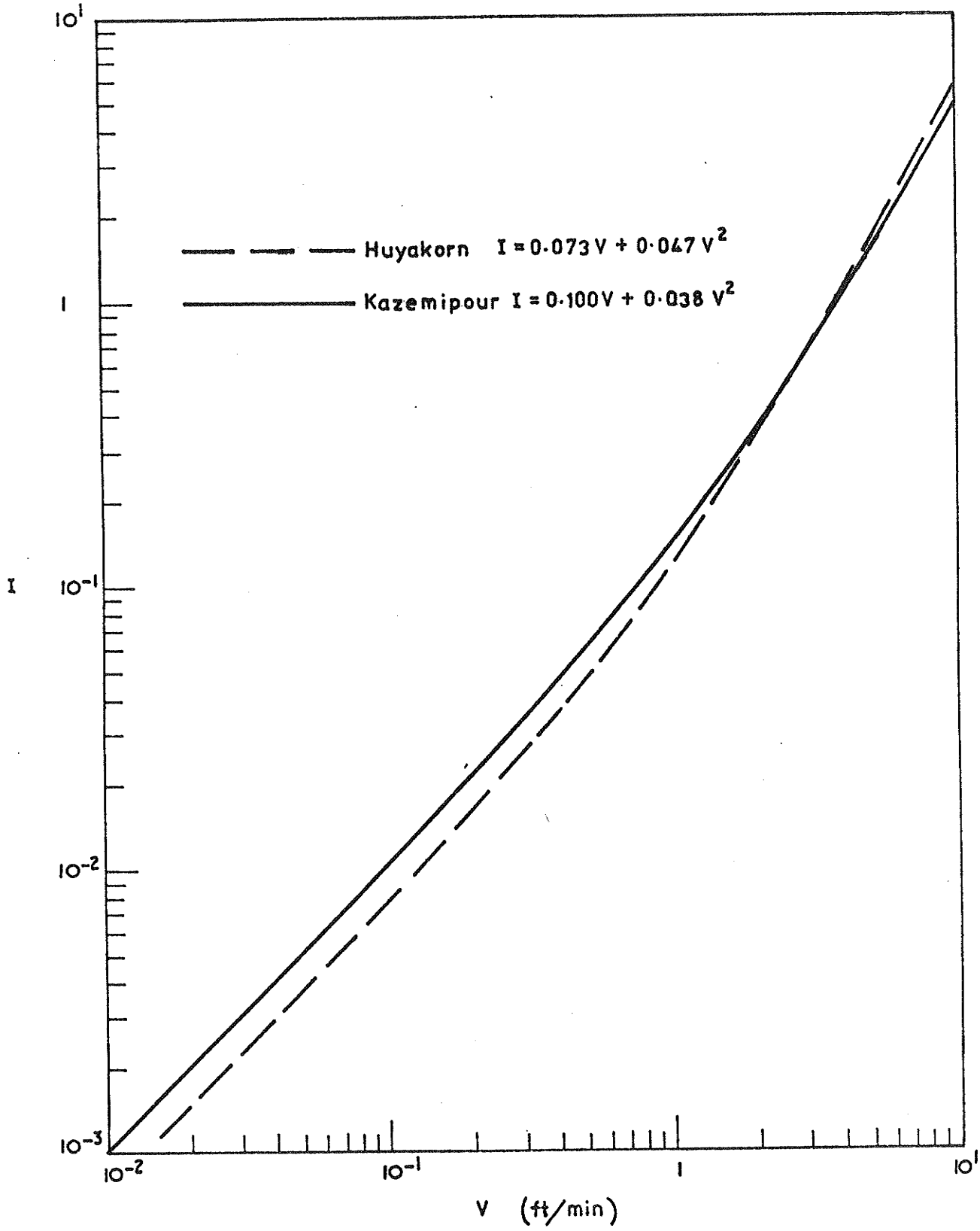

FIGURE 7·6: PERMEABILITY TESTS ON NEPEAN RIVER GRAVEL USED IN EXPERIMENTAL TESTS

of different samples of the aquifer material. Particulars of the results and the fitted Forchheimer constants are given in Table 7.1.

Table 7.1: Forchheimer Relationships fitted to Permeameter Tests of Aquifer Material

Data Source	Porosity of Tested Sample	Fitted Forchheimer Constants	
		a(min/ft.)	b(min^2/ft^2)
Huyakorn (1973)	35%	0.073	0.047
Kazemipour (1974)	40%	0.100	0.038

The sample tested by Kazemipour had considerably more fines than that tested by Huyakorn.

A comparison of the two fitted Forchheimer curves is shown in Figure 7.6.

7.3.4 Test Program

To study non-linear two dimensional axisymmetric flow, two series of tests for different partial well screenings were carried out for both the confined and unconfined aquifer models.

(i) The first series of tests was carried out with a 3 feet length of screen placed at the base of the aquifer. As generally shown in Figure 7.4 the remaining thickness of the aquifer was cased. Several tests were carried out to establish the well drawdown-discharge relationship for the confined aquifer model.

Before proceeding with the unconfined aquifer testing the water level in the tank was dropped below the polythene sheet and several days allowed to elapse to guarantee complete drainage of the now exposed upper aquifer material. Several tests were performed over a range of discharges and corresponding water levels within the well.

For each test in both the confined and unconfined models, the measurement of the piezometric heads at the floor tappings and the water level in the well were recorded. Measurements of the vertical variation in head at certain locations within the aquifer were made for some tests using the multiple observation well P.V.C. tubes. The position of the free surface was located at several radial positions for unconfined aquifer model tests.

In all confined model testing the water level within the well was not allowed to fall below the top of the aquifer, i.e. no dewatering of the confined aquifer occurred.

For all unconfined model testing the water level in the well was not allowed to fall below the top of the screened portion of the well, i.e. no exposure of the screen occurred.

(ii) After completion of all tests for the first partial screening geometry, the 3 feet screen was removed and replaced by a 1 foot screen length placed at the base of the aquifer with the casing again extending to the aquifer top. In carrying out this task, it was necessary to remove and backfill the aquifer material in the zone within the inner 4 feet barrier.

As for the first series testing, several tests were carried out for both the confined and unconfined aquifer models, in that order.

7.4 Comparison of Finite Element and Experimental Results

7.4.1 General

In comparing experimental results from a well-aquifer model with numerical solutions, it is essential that appropriate values of the hydraulic coefficients of the aquifer material be obtained and fed into the

numerical model.

Earlier workers (Volker (1969), Trollope et al (1971)), resorted to permeameter testing over a range of velocities comparable with those encountered during experimental model testing. While this approach may be justified in the absence of a more satisfactory procedure, it is unlikely that the physical properties of the permeameter sample will be similar to those of the model aquifer. Slight changes in such properties as effective porosity and packing of grains can alter considerably the Forchheimer flow equation coefficients a and b (Engelund (1953), Dudgeon (1964)).

The possibility of large variations in hydraulic coefficients is clearly illustrated by the results of two independent permeameter tests on samples of the aquifer material used in the experimental model (Section 7.3.3 and Table 7.1).

In the present work, non-linear hydraulic coefficients for the in situ material were determined by applying newly developed procedures to the results for each series of confined and unconfined aquifer tests. The so determined single valued Forchheimer coefficients (a and b) used in subsequent finite element flow solutions assume the aquifer material to be both homogeneous and isotropic. Despite such simplification, the analysis was verified by the close agreement between the finite element solutions and the experimental results.

7.4.2 Flow Towards a Partially Screened Well in a Confined Aquifer

The diagrammatic arrangement for the model testing is shown in Figure 7.4. Results were obtained for a sufficient number of

flows to establish the well discharge drawdown relationship for the two cases of confined aquifer partial screening considered. For each test, the total discharge from the full well, Q, was calculated as 4 times the measured test discharge from the quadrant well.

(a) Lower 3 Feet Screened

In the first series of tests the lower 3 feet of the 5 feet thick confined aquifer was screened.

To determine the in-situ hydraulic coefficients, the following procedures were applied to the results from the tests which gave total discharges of 63.6 ft^3/min. and 124 ft^3/min.

Method 1

The base piezometric head readings were converted to drawdowns (s) and plotted on a semi logarithmic scale in the dimensionless form s/s_w versus r/r_w, where r_w and s_w are the well radius and well drawdown respectively (see Figure 7.7). Beyond a radius of 8 feet from the well the drawdown distribution results plot closely along a straight line, thus indicating that any non-linear flow effects are negligible beyond this distance. The experimental results clearly become non-linear as the well is approached. A value of r/r_w from the linear portion of the experimental plot was selected and the corresponding value of the dimensionless drawdown s/s_w was read from Figure 7.7.

Using these values, the equivalent hydraulic conductivity of the aquifer material was calculated using the Thiem equation $Q_T = \frac{2\pi Km\, s}{\ln(r_o/r)}$.

Test A	Test B
Q = 63.6 ft^3/min.	Q = 124 ft^3/min.
s_w = 1.25 ft.	s_w = 3.23 ft.
r_w = 5 inches	r_w = 5 inches

r_o = 16.15 ft.
m = 5 ft.
l_s = 3 ft.

r_o = 16.15 ft.
m = 5 ft.
l_s = 3 ft.

Point on linear portion of plot - Figure 7.7.

$(r/r_w = 20.5,\ s/s_w = 0.1)$

Thus, r = 8.55, s = 0.125

and $K = \frac{63.6 \times \ln (16.15/8.55)}{2 \times \pi \times 5 \times .125}$

K = 10.31 ft/min.

$(r/r_w = 20,\ s/s_w = 0.08)$

r = 8.34, s = 0.258

$K = \frac{124 \times \ln (16.15/8.34)}{2 \times \pi \times 5 \times .258}$

K = 10.11 ft/min.

The non-linear Forchheimer flow equation coefficients (a and b) were then evaluated. The value of a was calculated as a = 1/K. A family of base pressure distribution curves for steady state non-linear flow applicable to the test model geometry of this series was prepared and superimposed on the experimental results plotted in Figure 7.7. The value of the non-linear flow parameter $\frac{bs_w}{a^2 r_w}$ for the best fitting curve was obtained and used to evaluate the coefficient b.

Test A

a = 1/K = 0.097 min/ft.

$\frac{bs_w}{a^2 r_w}$ = 6 (Figure 7.7)

$b = \frac{6 \times (.097)^2 \times .417}{1.25}$

$b = 0.019\ (\text{min/ft})^2$

Test B

a = 1/K = 0.099 min/ft.

$\frac{bs_w}{a^2 r_w}$ = 16

$b = \frac{16 \times (.099)^2 \times .417}{3.23}$

$b = 0.020\ (\text{min/ft})^2$

Method 2

An alternative procedure for determining the in-situ values of a and b was also applied.

From the superposition of the base pressure distribution of the test results and the family of curves for varying degrees of non-

linearity (Figure 7.7), the value of $\frac{bs_w}{a^2 r_w}$ for the best fitting curve was obtained. This value of $\frac{bs_w}{a^2 r_w}$ was then used to enter Figure 7.8 where the effects of non-linearity upon the well drawdown-discharge performance of the test model system are presented. The value of $c = Q/Q_T$ for the corresponding $\frac{bs_w}{a^2 r_w}$ was read from Figure 7.8 and then used in evaluating the aquifer hydraulic conductivity, K.

Test A		Test B
$Q = 63.6\ ft^3/min.$		$Q = 124\ ft^3/min.$
$s_w = 1.25$ ft.		$s_w = 3.23$ ft.
$\frac{bs_w}{a^2 r_w} = 6$	(Figure 7.7)	$\frac{bs_w}{a^2 r_w} = 16$
$c = \frac{Q}{Q_T} = 0.58$	(Figure 7.8)	$c = \frac{Q}{Q_T} = 0.44$

$$K = \frac{Q_T \ln (r_o/r_w)}{2 \pi m s_w} \qquad \text{(Thiem equation)}$$

$$K = \frac{63.6 \ln (16.15/.417)}{0.58 \times 2 \times \pi \times 5 \times 1.25} \qquad K = \frac{124 \ln (16.15/.417)}{0.44 \times 2 \times \pi \times 5 \times 3.23}$$

$K = 10.22$ ft/min. $\qquad K = 10.17$ ft/min.

The value of a was again calculated by $a = 1/K$, and b was found from the known value of $bs_w/a^2 r_w$.

$a = 1/K = 0.098$ min/ft. $\qquad a = 1/K = 0.098$ min/ft.

$$b = \frac{6 \times (.098)^2 \times .417}{1.25} \qquad b = \frac{16 \times (.098)^2 \times .417}{3.23}$$

$b = 0.019\ (min/ft)^2 \qquad b = 0.020\ (min/ft)^2$

Determined in situ values of $a = 0.098$ min/ft. and $b = 0.019\ (min/ft)^2$ were chosen and fed into the finite element model to obtain theoretical predictions of the experimental flow conditions. In the finite element analyses, the hydraulic heads along the well screen were prescribed as the measured water level in the well. In so doing, it

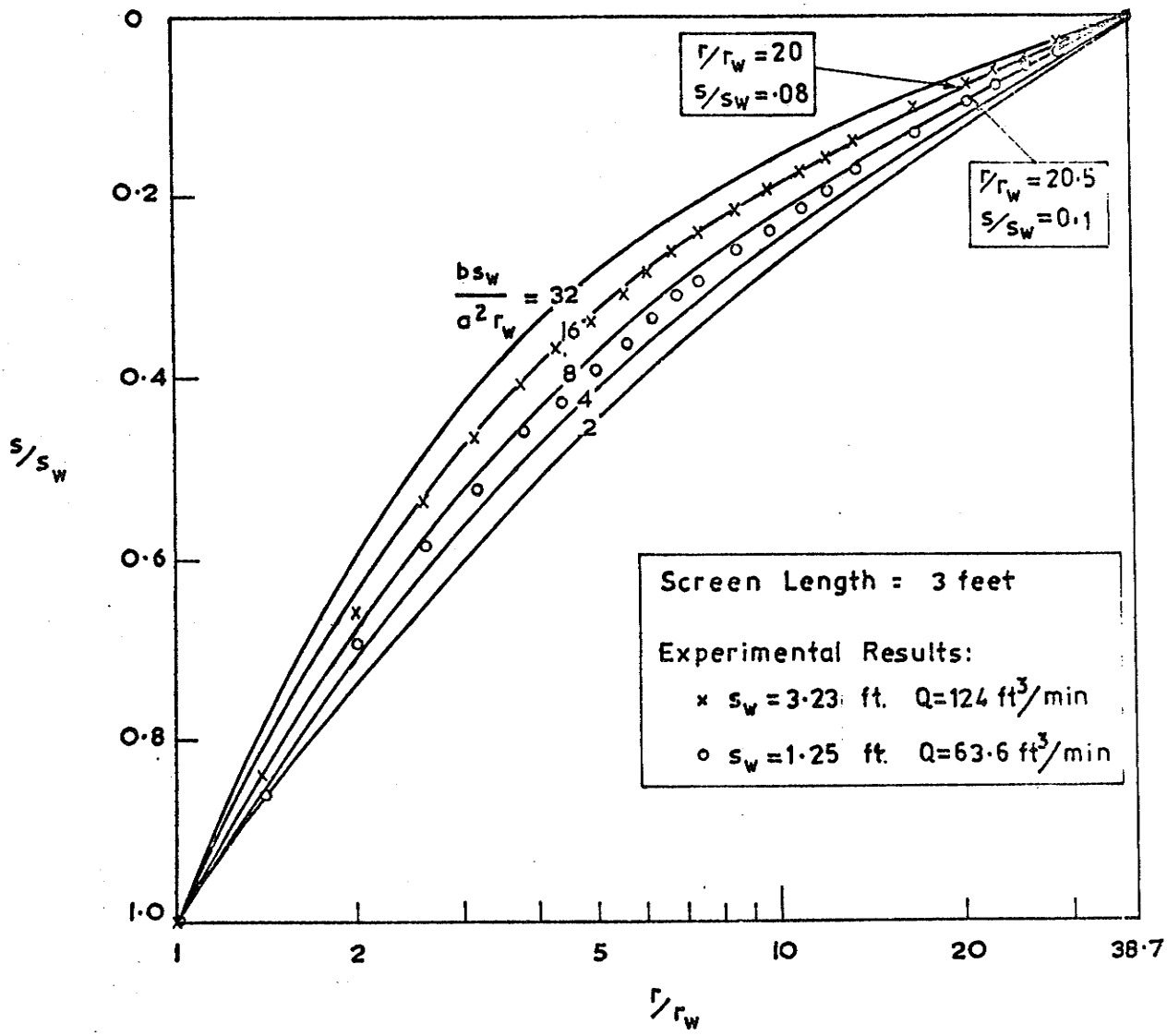

FIGURE 7·7: SUPERPOSITION OF EXPERIMENTAL RESULTS AND NON-LINEAR DRAWDOWN DISTRIBUTIONS ALONG THE BASE OF A CONFINED AQUIFER.

$$\left(\frac{\ell_s}{m} = 0{\cdot}6 \quad ; \quad \frac{m}{r_w} = 12 \quad ; \quad \frac{r_o}{m} = 3{\cdot}23\right)$$

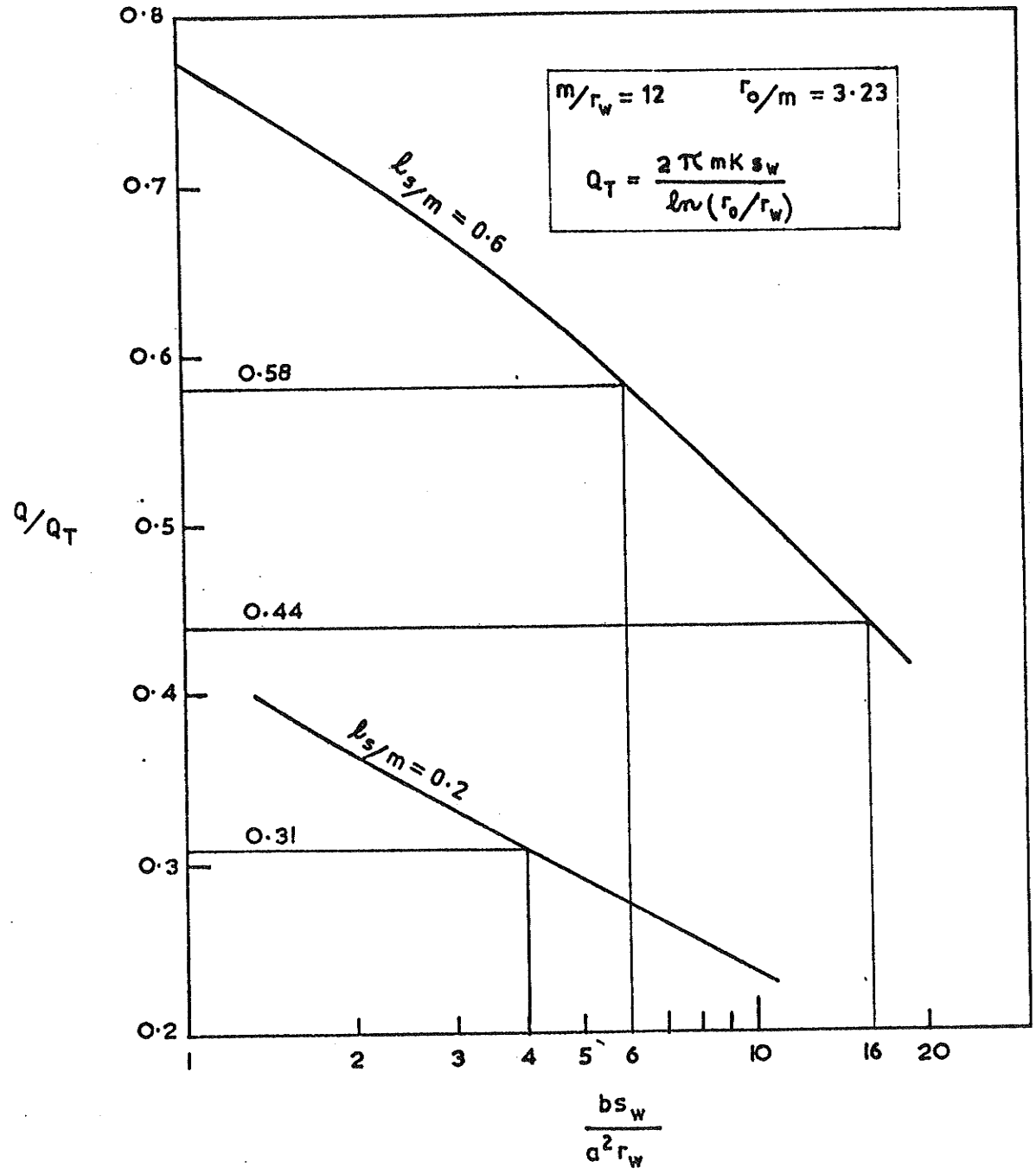

FIGURE 7·8 : EFFECTS OF NON-LINEAR FLOW ON PERFORMANCE OF PARTIALLY SCREENED CONFINED AQUIFER TEST MODELS.

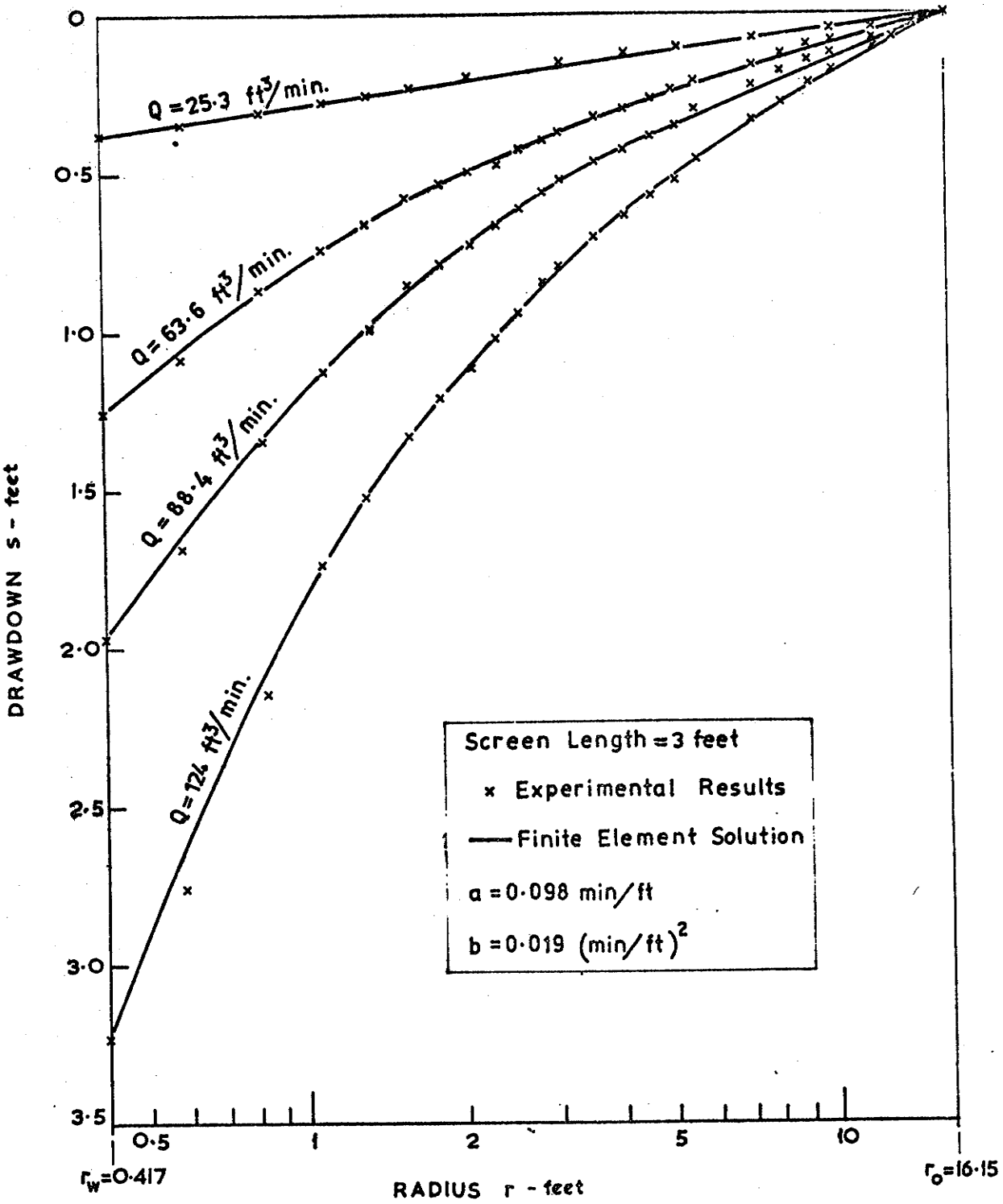

FIGURE 7·9: DRAWDOWN DISTRIBUTIONS ALONG BASE OF THE CONFINED AQUIFER MODEL. COMPARISON OF EXPERIMENTAL RESULTS AND FINITE ELEMENT SOLUTIONS.

$\left(\frac{\ell_s}{m} = 0.6\ ;\qquad \frac{m}{r_w} = 12\ ;\qquad \frac{r_o}{m} = 3.23\right)$

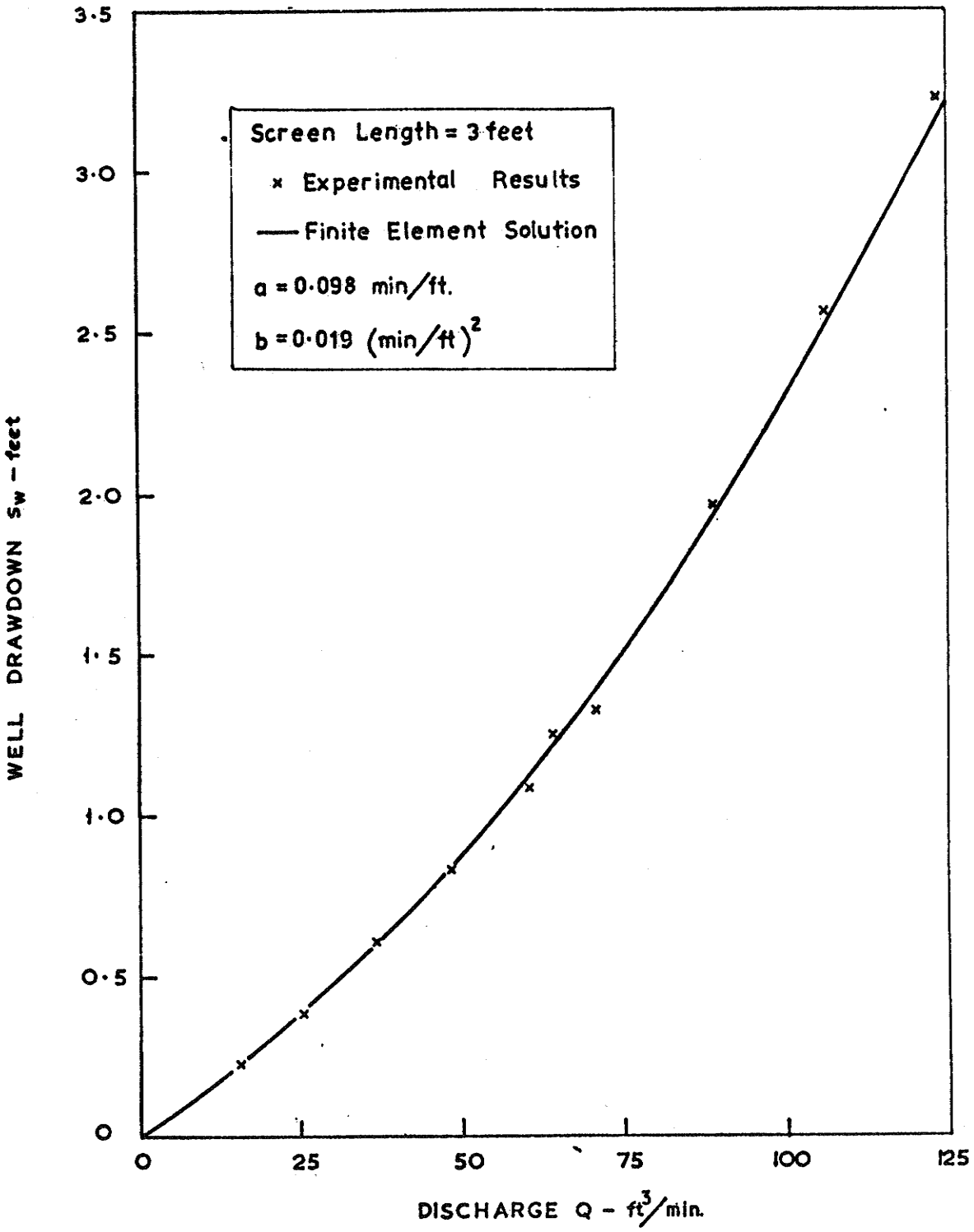

FIGURE 7·10: WELL DRAWDOWN-DISCHARGE RELATIONSHIP FOR CONFINED AQUIFER MODEL. COMPARISON OF EXPERIMENTAL RESULTS AND FINITE ELEMENT SOLUTIONS.

$\left(\frac{\ell_s}{m} = 0{\cdot}6\ ;\qquad \frac{m}{r_w} = 12\ ;\qquad \frac{r_o}{m} = 3{\cdot}23\right)$

was assumed that screen losses were negligible.

Figure 7.9 shows a comparison of the finite element solutions for the distribution of base pressure drawdown with the experimental results from four tests chosen to cover a good range of the well drawdown. The discharges listed are the experimental discharges. It can be seen that the determined coefficients, a and b, led to very good agreement between the theory and experiment.

The well drawdown-discharge relationship determined by the finite element analysis also compares very well with the experimental results shown in Figure 7.10. The discharges determined by finite element analyses are within 5% of experimental discharge results. This is good when it is noted that fluctuations in orifice plate manometer readings were such that for some tests the reliability of recorded discharge was only 5%.

(b) Lower 1 Foot Screened

In carrying out the series of tests in which the lower 1 foot of the 5 feet confined aquifer was screened, it was necessary to remove and backfill the aquifer material within the inner retaining barrier. This process could have lead to significant changes in aquifer hydraulic properties. Thus the in situ values of a and b were redetermined in a similar manner to that previously described. The test which gave a total discharge of 55.8 ft^3/min was considered in evaluating a and b.

Method 1

The experimental base pressure distribution results and the

superimposed family of curves for varying degrees of non-linearity are shown in Figure 7.11.

Method 1

$Q = 55.8\ ft^3/min.$ $\quad r_o = 16.15\ ft.$

$s_w = 1.85\ ft.$ $\quad m = 5\ ft.$

$r_w = 0.417\ ft.$ $\quad l_s = 1\ ft.$

Point on linear portion of plot - Figure 7.11 - ($r/r_w = 15.5$, $s/s_w = 0.08$)

Thus $K = \dfrac{55.8 \times \ln(16.15/6.46)}{2 \times \pi \times 5 \times .148} = 11.00\ ft/min.$

and, $a = 1/K = .091\ min/ft.$

$$\frac{bs_w}{a^2 r_w} = 4 \qquad \text{(Figure 7.11)}$$

$$b = \frac{4 \times (.091)^2 \times .417}{1.85} = .0074\ (min/ft)^2$$

Method 2

The variation in well discharge performance with increasing non-linearity for the test model system is shown in Figure 7.8 in the form of Q/Q_T versus $bs_w/a^2 r_w$.

$Q = 55.8\ ft^3/min.$ $\quad s_w = 1.85\ ft.$

$$\frac{bs_w}{a^2 r_w} = 4 \qquad \text{(Figure 7.11)}$$

$$c = Q/Q_T = 0.31 \qquad \text{(Figure 7.8)}$$

Thus, $K = \dfrac{55.8 \ln(16.15/.417)}{0.31 \times 2 \times \pi \times 5 \times 1.85} = 11.33\ ft/min.$

and, $a \doteq 1/K = 0.088\ min/ft.$

$$b = \frac{4 \times (.088)^2 \times .417}{1.85} = 0.0070\ (min/ft)^2$$

Values of $a = 0.090\ min/ft.$ and $b = 0.007\ (min/ft)^2$ were fed into the finite element model to obtain theoretical predictions of the ex-

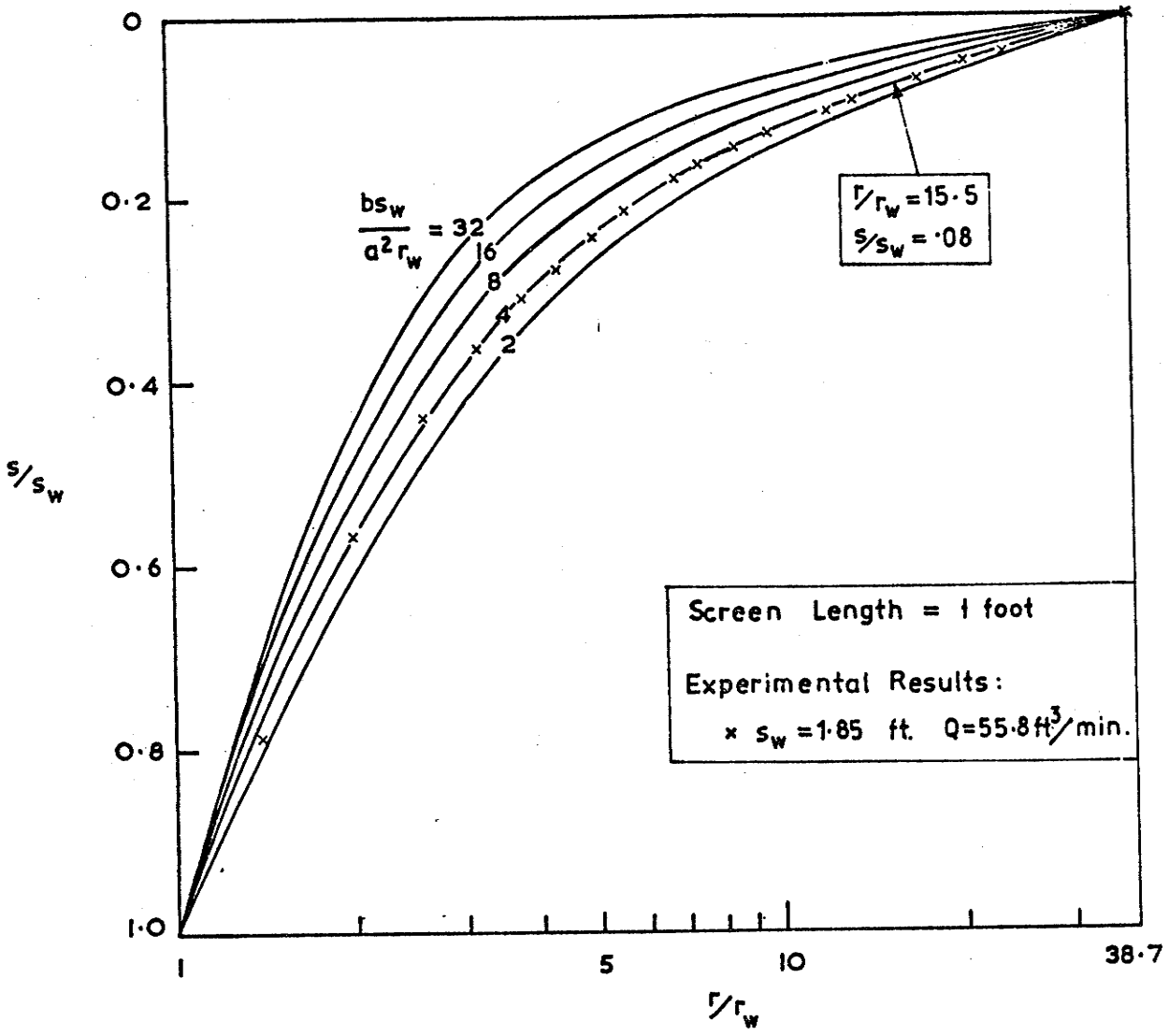

FIGURE 7·11: SUPERPOSITION OF EXPERIMENTAL RESULTS AND NON-LINEAR DRAWDOWN DISTRIBUTIONS ALONG THE BASE OF A CONFINED AQUIFER.

$$\left(\frac{\ell_s}{m} = 0{\cdot}2 \quad ; \quad \frac{m}{r_w} = 12 \quad ; \quad \frac{r_o}{m} = 3{\cdot}23\right)$$

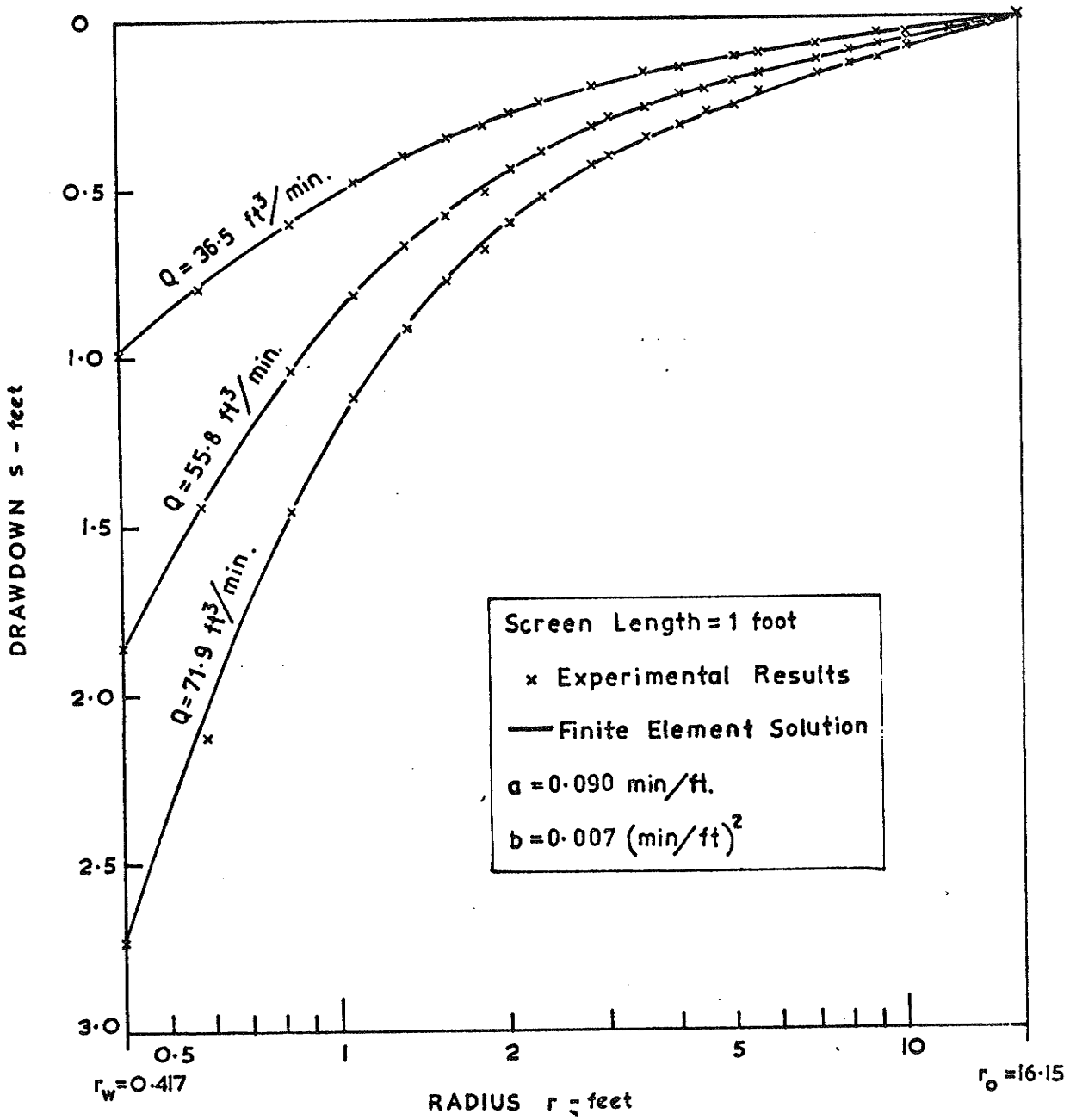

FIGURE 7·12: DRAWDOWN DISTRIBUTIONS ALONG BASE OF THE CONFINED AQUIFER MODEL. COMPARISON OF EXPERIMENTAL RESULTS AND FINITE ELEMENT SOLUTIONS.

$\left(\frac{\ell_s}{m} = 0.2 \; ; \qquad \frac{m}{r_w} = 12 \; ; \qquad \frac{r_o}{m} = 3.23 \right)$

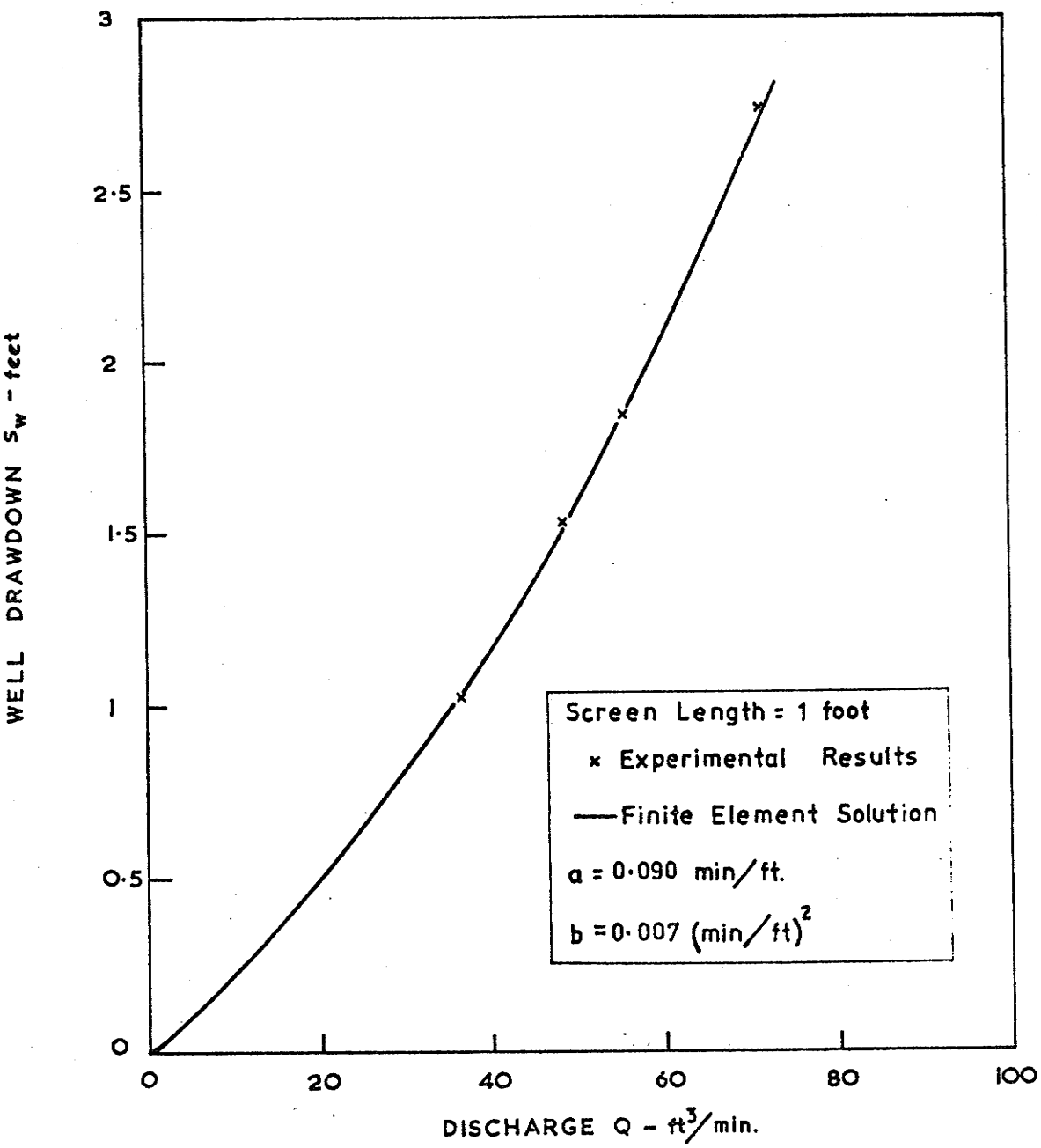

FIGURE 7·13: WELL DRAWDOWN-DISCHARGE RELATIONSHIP FOR CONFINED AQUIFER MODEL. COMPARISON OF EXPERIMENTAL RESULTS AND FINITE ELEMENT SOLUTIONS.

$\left(\frac{\ell_s}{m} = 0{\cdot}2\ ;\qquad \frac{m}{r_w} = 12\ ;\qquad \frac{r_o}{m} = 3{\cdot}23\right)$

perimental results. The newly determined coefficients which were assumed to be applicable throughout the entire aquifer are significantly different from those obtained for the 3 feet screened condition ($a = .098$ min/ft. and $b = .019$ $(\text{min/ft})^2$).

The aquifer material beyond the inner retaining barrier was unchanged in the two series of tests and thus the hydraulic properties of this bulk of the aquifer material should have been the same for both series. This would suggest a treatment of the problem in which the material characteristics within the first 4 feet from the well should be different from those for the aquifer beyond 4 feet and extending to the outer barrier. The refinement of a two zone radial treatment was unwarranted as the properties of the material within the inner 4 feet barrier are decisive in determining both the discharge and drawdown distributions. Approximately 85% of the total drawdown occurs within 4 feet of the well.

Figure 7.12 shows a plot of the base pressure distribution for three values of the prescribed well drawdown. It can be seen that once again the finite element solutions agree closely with the experimental results.

As a further check on the theoretical analysis, a plot of the well discharge drawdown relationship is shown in Figure 7.13. Good agreement between theory and experiment may again be observed with the maximum difference being only 5%.

7.4.3 Flow Towards a Partially Screened Well in an Unconfined Aquifer

The diagrammatic arrangement for the unconfined aquifer model

testing is shown in Figure 7.4 for the case where the water level beyond the outer retaining barrier is below the overlying polythene sheet. Results were obtained for a number of tests for each case of partial screening considered.

(a) Lower 3 Feet Screened

The series of unconfined aquifer tests for a 3 feet screen in the lower portion of the aquifer were carried out directly after the similarly screened confined aquifer test series. As the aquifer material was not physically disturbed, it might be assumed that the same hydraulic coefficients determined for the confined aquifer model should be equally applicable to this unconfined model series. Comparison of several finite element solutions with experimental results quickly showed such a premise to be in error and the following explanation is offered.

When filling the test tank the variation with depth of the effective porosity of the aquifer material was determined by volumetric measurements. This variation as shown in Figure 7.14 is quite substantial and indicates the distinct possibility of non-homogeneity of aquifer material. The determined values of hydraulic coefficients assume the aquifer to be homogeneous and as such are an average over the entire aquifer. In the confined aquifer testing the averaging has taken place over a constant aquifer thickness of 5 feet. For unconfined aquifer tests the averaging takes place over aquifer thicknesses varying between 3.5 and 4.5 feet. Under such circumstances it is not surprising to find the predetermined coefficients from the confined aquifer model inapplicable to the unconfined model tests.

A method of determining a set of in situ hydraulic coefficients for the unconfined aquifer model was derived and applied to the test for which the total derived discharge was 34.6 ft^3/min.

The experimental base pressure results were plotted in Figure 7.15. For the same problem geometry, a family of base pressure curves for varying degrees of non-linearity were prepared and superimposed on the test results (as shown in Figure 7.15). A point was chosen on the linear portion of the head distribution (far enough removed from the well for the flow to be essentially radial) and the effective hydraulic conductivity of the aquifer was determined by the Dupuit equation,

$$Q_D = \frac{\pi K (h_o^2 - h^2)}{\ln(r_o/r)}$$

The value of the non-linear Forchheimer constant, a, was calculated as $a = 1/K$. The value of b/a^2 for the curve which best fitted the experimental results (Fig. 7.15) was used to evaluate b.

$$Q = 34.6 \text{ ft}^3/\text{min}.$$

$$r_w = 0.417 \text{ ft.} \qquad r_o = 16.15 \text{ ft.}$$

$$h_w = 3.71 \text{ ft.} \qquad h_o = 4.36 \text{ ft.}$$

Point on linear portion of plot - Figure 7.15 - (r=7.0 ft., h = 4.23 ft.)

Thus, $K = \frac{34.6 \times \ln (16.15/7)}{\pi(4.36^2 - 4.23^2)} = 8.25 \text{ ft/min.}$

and, $a = 1/K = 0.121 \text{ min/ft.}$

From Figure (7.15) $b/a^2 = 0.5$ gives best fit.

Thus, $b = 0.5 \times (.121)^2 = 0.0073 \text{ (min/ft)}^2$.

Values of $a = 0.120$ min/ft. and $b = 0.007 \text{ (min/ft)}^2$ were fed into the finite element model and solutions obtained for comparison with experimental tests.

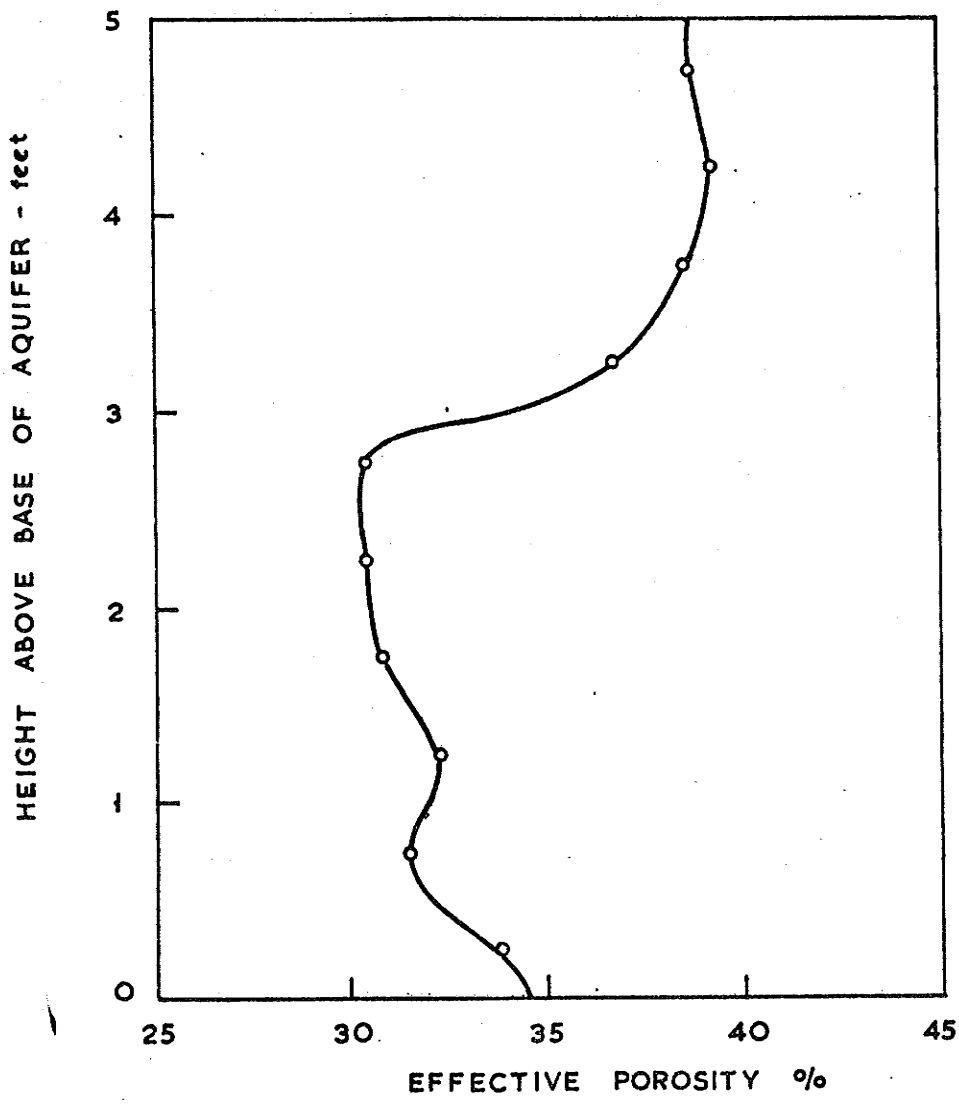

FIGURE 7·14: VARIATION OF EFFECTIVE POROSITY WITH DEPTH OF IN-SITU AQUIFER TEST MATERIAL

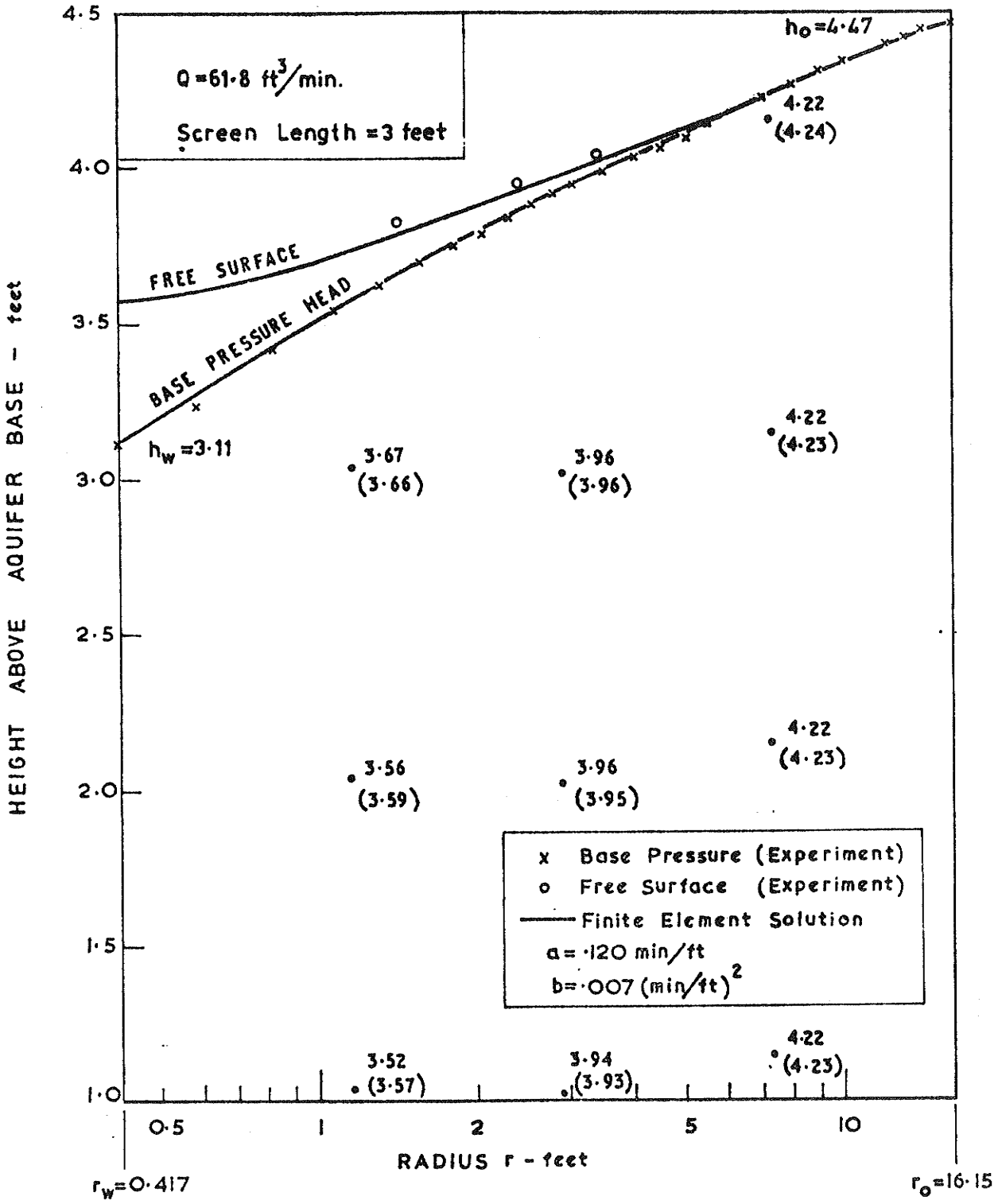

FIGURE 7·17.: COMPARISON OF EXPERIMENTAL RESULTS AND FINITE ELEMENT SOLUTIONS FOR DISTRIBUTION OF HEAD WITHIN UNCONFINED AQUIFER SCREENED IN LOWER 3 FEET. TEST Q = 61·8 ft³/min.

Since the water level beyond the radius of influence (as imposed beyond the outer aquifer retaining barrier) was not the same for all tests a well drawdown-discharge curve is meaningless since the geometric ratios defining the system were different for each test. A comparison of finite element and experimental resultant discharges is given in Table 7.2. In all cases the finite element analysis yielded discharge values which were closer than 6% to the actual experimental results.

Table 7.2: Comparison of Finite Element and Experimental Results for Unconfined Model Tests Screened in Lower 3 Feet.

	Well radius r_w = 0.417 ft. = 5 inches Radius of influence r_o = 16.15 ft.			
h_w (ft.)	h_o (ft.)	Total Well Discharge (ft^3/min)		Percentage Error
		Experiment	Finite Element	
3.80	4.28	26.9	25.3	-6%
3.71	4.36	34.6	33.4	-3½%
3.55	4.39	42.9	42.2	-1½%
3.40	4.45	50.4	51.2	1½%
3.44	4.53	53.2	54.5	2½%
3.11	4.47	61.8	64.9	5%

The base pressure head distributions obtained by finite element analysis agreed closely with actual experimental results for all six test cases.

The finite element solutions of head distribution and experimental results are presented together for comparison in Figures 7.16 and 7.17 for the tests having discharges of 34.6 ft^3/min. and 61.8 ^{3}/min. respectively. The base pressure head distribution and free surface are clearly shown. At various positions within the aquifer pressure heads were recorded during experimental testing. For comparative purposes,

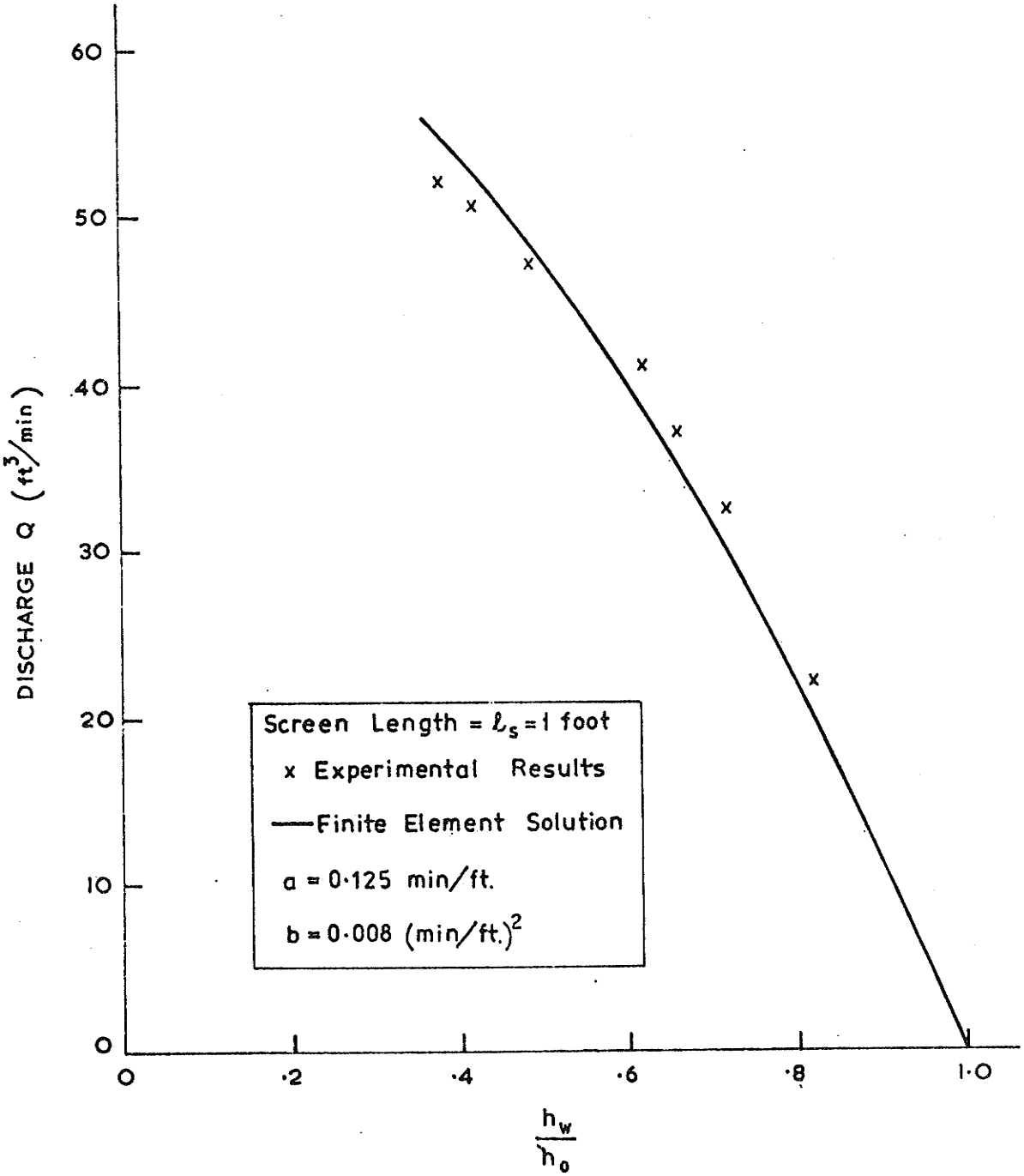

FIGURE 7·21: WELL DISCHARGE - DRAWDOWN RELATIONSHIP FOR UNCONFINED AQUIFER MODEL. COMPARISON OF EXPERIMENTAL RESULTS AND FINITE ELEMENT SOLUTIONS.

$\left(\frac{\ell_s}{h_o} = \cdot 245, \quad \frac{h_o}{r_w} = 9 \cdot 79, \quad \frac{r_o}{h_o} = 3 \cdot 96\right)$

chosen to cover the range of well discharge. The discharges listed are the experimental discharges.

The finite element solution of head distribution and the experimental results are presented together for comparison in Figure 7.20 for the test having a discharge of 50.3 ft^3/min. For comparative purposes, at points within the aquifer the experimental pressure head value is given above the point and the finite element solution below the point in brackets. The finite element solution is seen to closely predict the base pressure, the free surface and the head distribution throughout the flow domain.

The well drawdown-discharge relationship determined by finite element analysis compares favourably with the experimental results as shown in Figure 7.21. The fit is not as close as was obtained in other test series, but is still reasonable when the assumption of material homogeneity and isotropy in applying the finite element model and the likelihood of 5% errors in experimental discharge values, are considered.

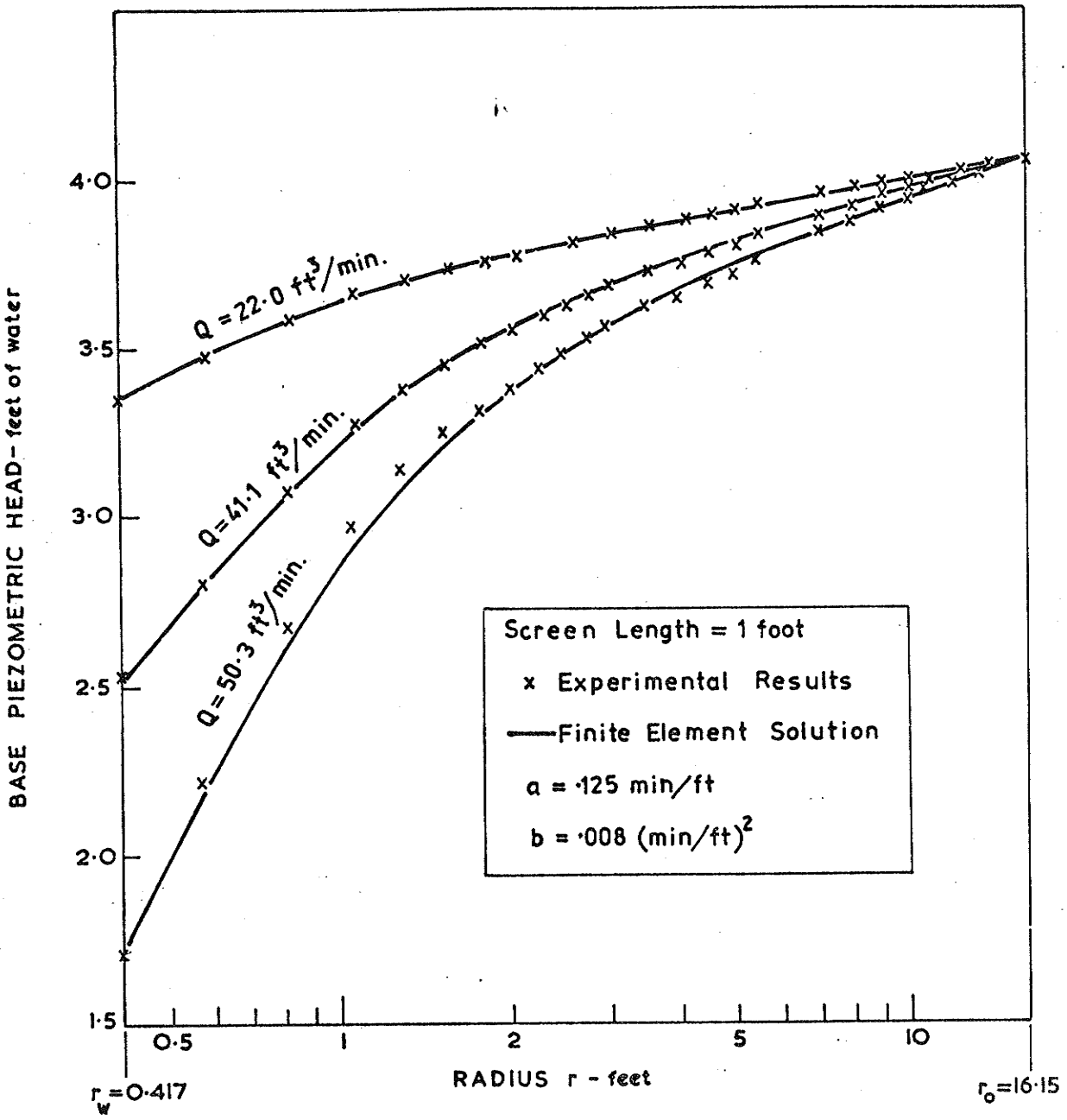

FIGURE 7·19: PRESSURE DISTRIBUTIONS ALONG BASE OF THE UNCONFINED AQUIFER MODEL. COMPARISON OF EXPERIMENTAL RESULTS AND FINITE ELEMENT SOLUTIONS.

$$\left(\frac{\ell_s}{h_o} = \cdot 245, \qquad \frac{h_o}{r_w} = 9 \cdot 79, \qquad \frac{r_o}{h_o} = 3 \cdot 96\right)$$

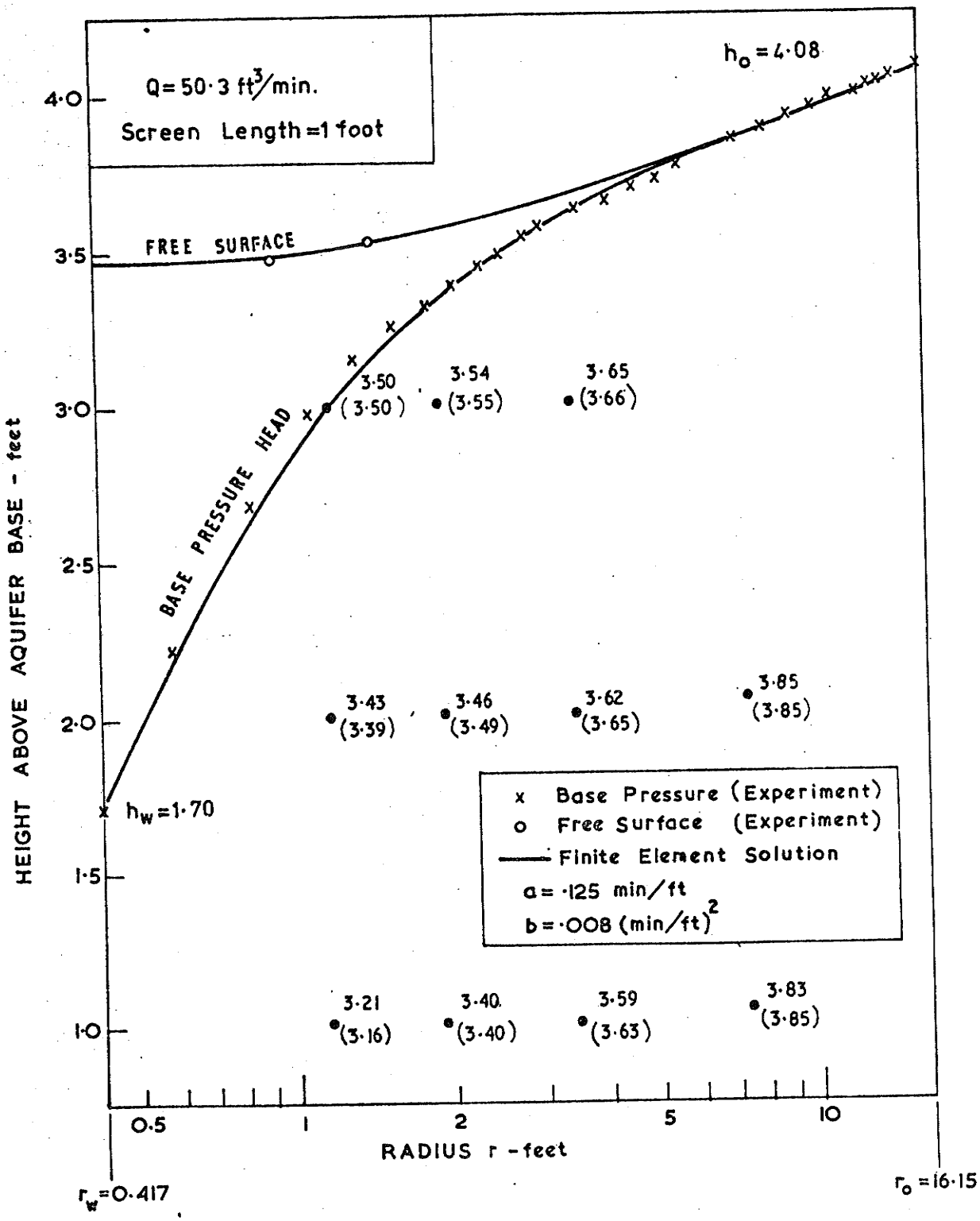

FIGURE 7·20: COMPARISON OF EXPERIMENTAL RESULTS AND FINITE ELEMENT SOLUTIONS FOR DISTRIBUTION OF HEAD WITHIN UNCONFINED AQUIFER SCREENED IN LOWER 1 FOOT.

TEST Q = 50·3 ft³/min.

at such points the experimental result is given above the point and the finite element solution below the point in brackets. As can be seen in Figures 7.16 and 7.17 the finite element solutions give good predictions of the experimental results throughout the flow domain.

(b) Lower 1 Foot Screened

For the series of tests in which the lower 1 foot of the unconfined aquifer was screened, the in situ values of a and b were redetermined in a similar manner to that previously described.

The test which gave a total discharge of 41.1 ft^3/min was considered in evaluating a and b. The experimental base pressure distribution results and the superimposed base pressure curves for varying degrees of non-linearity are shown in Figure 7.18.

Point on linear portion of plot - Figure 7.18 - (r=6.7 ft., h=3.90ft.).

r_w =.417 ft., r_o=16.15 ft., h_w= 2.55 ft., h_o = 4.08 ft.

$$\text{Thus, } K = \frac{41.1 \times \ln (16.15/6.7)}{\pi(4.08^2 - 3.90^2)} = 8.013 \text{ ft/min.}$$

and, $a = 1/K = 0.125$ min/ft.

From Figure 7.18 $b/a^2 = 0.5$ gives best fit

Thus, $b = 0.5\ (.125)^2 = 0.0078$ (min/ft.)^2

Values of $a = 0.125$ min/ft. and $b = 0.008$ (min/ft.)^2 were used in the finite element model to obtain solutions for comparison with experimental results.

The base pressure head distributions obtained by finite element analysis agreed closely with actual experimental results in all cases. Figure 7.19 shows a comparison of the finite element solutions of base pressure distribution with the experimental results from three tests

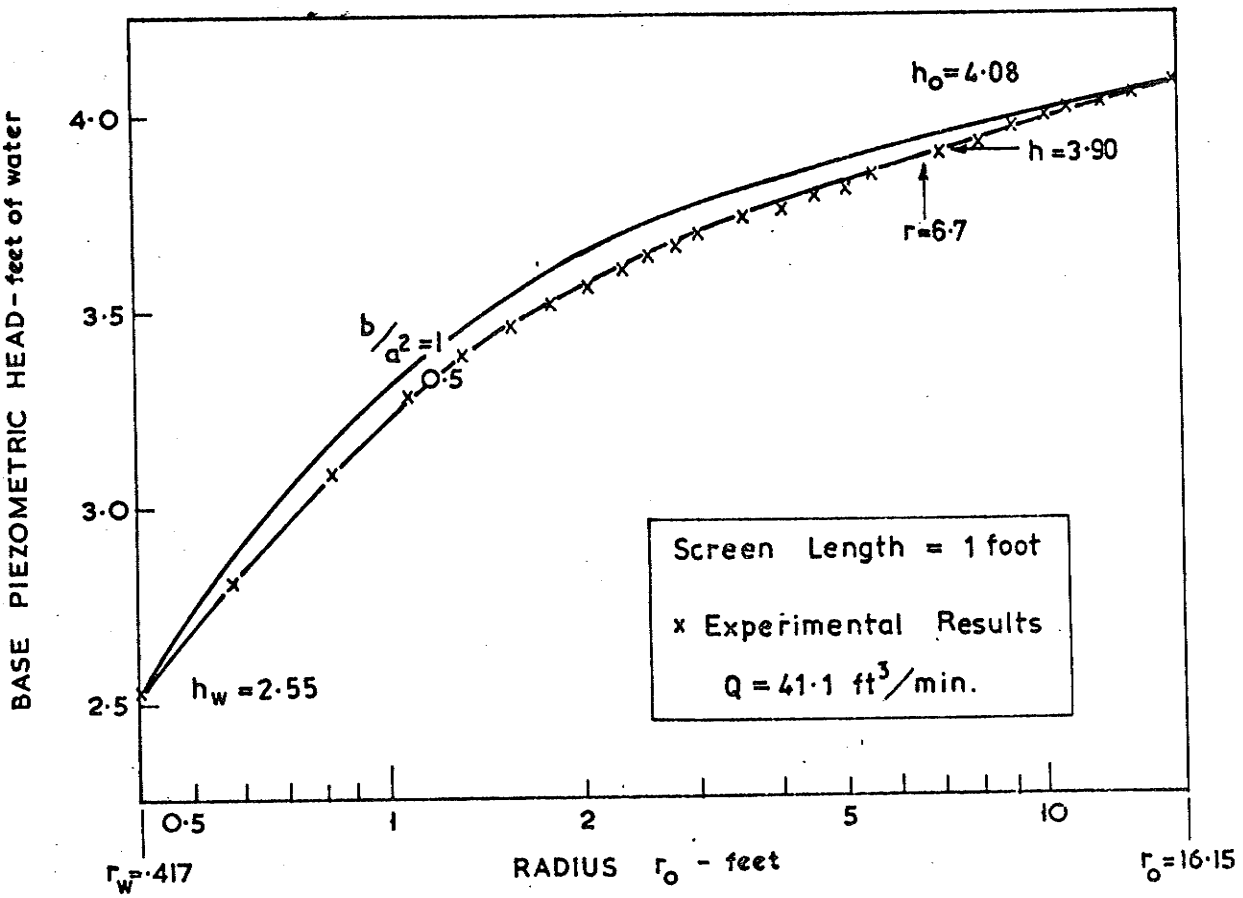

FIGURE 7·18: SUPERPOSITION OF EXPERIMENTAL RESULTS AND NON-LINEAR HEAD DISTRIBUTIONS ALONG THE BASE OF UNCONFINED AQUIFER MODEL.

$$\left(\frac{\ell_s}{h_o} = \cdot 245\ ;\ \frac{h_w}{h_o} = \cdot 625\ ;\ \frac{h_o}{r_w} = 9 \cdot 79;\ \frac{r_o}{h_o} = 3 \cdot 96\right)$$

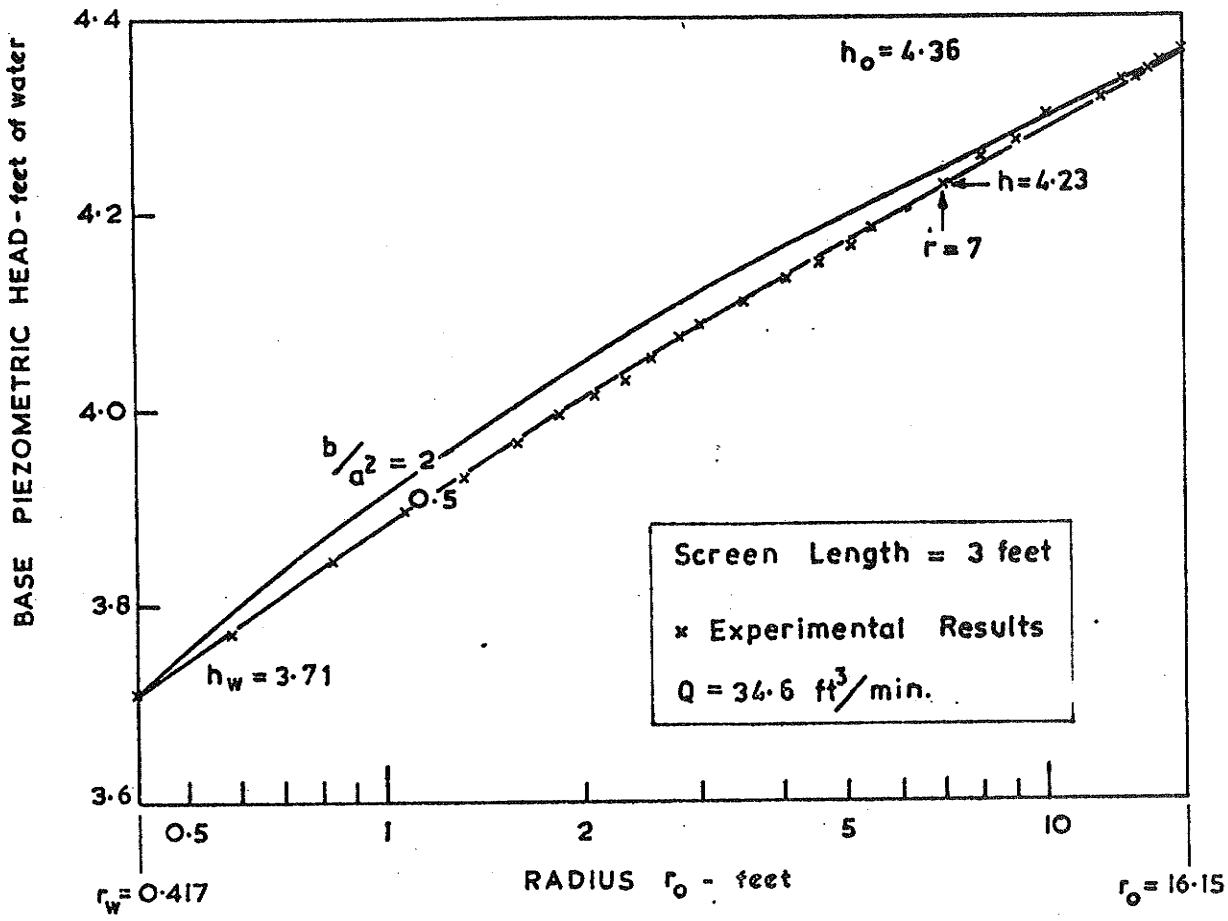

FIGURE 7.15: SUPERPOSITION OF EXPERIMENTAL RESULTS AND NON-LINEAR HEAD DISTRIBUTIONS ALONG THE BASE OF UNCONFINED AQUIFER MODEL.

$$\left(\frac{\ell_s}{h_o} = 0.688;\ \frac{h_w}{h_o} = 0.851;\ \frac{h_o}{r_w} = 10.46;\ \frac{r_o}{h_o} = 3.70\right)$$

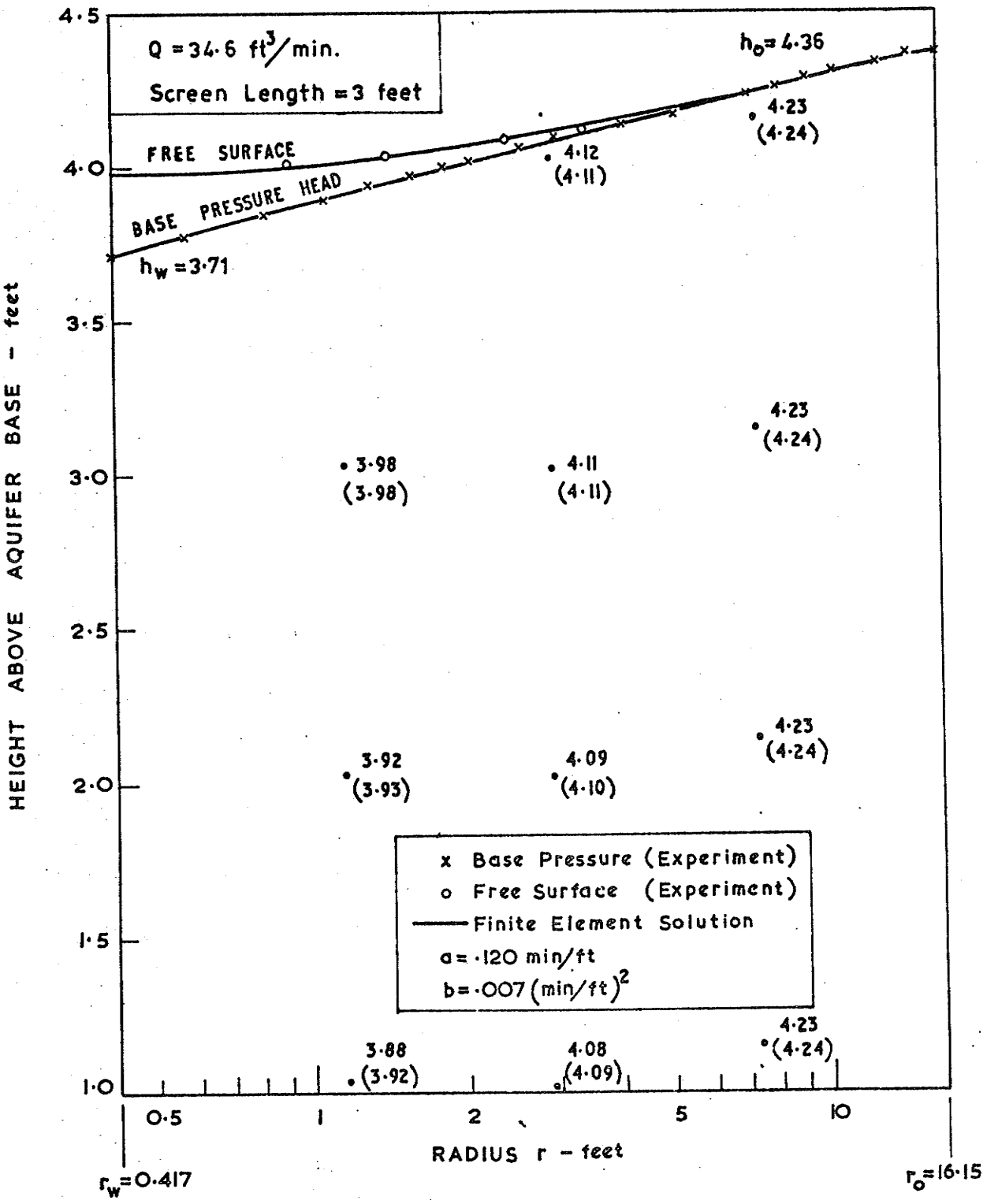

FIGURE 7·16: COMPARISON OF EXPERIMENTAL RESULTS AND FINITE ELEMENT SOLUTIONS FOR DISTRIBUTION OF HEAD WITHIN UNCONFINED AQUIFER SCREENED IN LOWER 3 FEET. TEST Q = 34·6 ft³/min.

8. Discussion - Application of Results in Well Design

8.1 General

Finite element numerical procedures have been formulated to solve problems of flow to pumped wells. Ccmputer programs were developed and verified by comparison with known analytical solutions and experimental results from an electrolytic tank analogue and a large scale sand-box type model. The proven programs were then used to investigate a wide range of axisymmetric well flow problems for which no previous solutions existed. Cases involving unsteady flow in confined aquifers and steady flow in both confined and unconfined aquifers were solved.

For unsteady flow to a well in a confined aquifer, the deviations from the normally assumed theoretical flow behaviour arising from non-linear flow, well storage, partial penetration, variable pumping rate and aquifer inhomogeneity were investigated and discussed in Chapter 6. The above effects were shown to exert considerable influence upon the flow behaviour during early times and in the vicinity of the well. However, the determination of overall aquifer transmissivity and storage coefficients (T and S) by normal type curve analysis of field pumping test data was shown to be satisfactory provided the generally accepted limits of applicability are not exceeded. Regional aquifer characteristics are required for effective aquifer management if safe yields are to be determined. A reliable estimate of transmissivity derived from unsteady field testing data is also required for the design of wells.

Since well design is based upon steady state (long term) pumping

behaviour and a major objective of this thesis was to provide new information for optimising design considerably more effort was devoted to steady rather than unsteady flow problems. An extensive study of steady state well performance in both confined and unconfined aquifers under various conditions was completed. Particular emphasis was placed on the effects of near well flow behaviour. The results in general dimensionless terms enable the hydraulic performance of many well-aquifer systems to be estimated. With these results, optimum well design becomes possible. For a given aquifer, alternative well configurations may be considered, the performance of each estimated and the optimum well selected on an economic basis which will be peculiar to the particular locality.

The performance of simple well-aquifer systems may be predicted by available analytical methods. These solutions have been incorporated in the presented design figures and tables.

For cases not covered, further sets of design data could be prepared using the finite element programs. However, for complex systems the multitude of controlling dimensionless parameters may make the preparation of design charts impractical because of the large number of graphs required. In such cases, individual use of the finite element programs is recommended for solving specific problems.

In concluding this thesis, a general review of the relevant design variables will be given, followed by specific discussion of the results obtained in previous chapters in regard to their relevance to optimising well design. The discussion has been divided along conventional lines

into sections dealing with confined and unconfined aquifers. The well drawdown-discharge relationship has been emphasised rather than the distributions of head and velocity within the aquifer. Brief mention is made of these distributions where considered particularly relevant.

8.2 Well Design Variables

8.2.1 Aquifer Properties

In selecting a well for a given location many of the relevant variables are beyond the control of the designing groundwater hydrologist. These variables relate to the type, thickness, extent and flow properties of the aquifer system.

Drill sampling, geophysical investigation, well logging and field pumping tests may be undertaken to ascertain such aquifer variables. As previously stated, conventional type curve analysis of field data is adequate for determining overall "average" aquifer flow characteristics S, T and K.

Near well aquifer properties exert a disproportionately large effect on well performance. Current testing and analysis procedures do not normally allow such local properties as non-linear flow and aquifer inhomogeneity constants to be evaluated. As discussed in Chapter 6, relatively simple analyses can be undertaken to evaluate near well properties provided additional field test data from observation pressure tappings close to and/or adjacent to the well are available. In general very few wells warrant the cost and extra difficulties associated with obtaining this additional information. The alternative is to estimate near well aquifer characteristics from experience or published data and the normally obtained data from drilling logs and

samples.

Non-linear Flow Characteristics

In this thesis, particular importance was placed upon examining the effects of non-linear flow on the behaviour of well-aquifer systems. A Forchheimer non-linear velocity-hydraulic gradient relationship with single valued coefficients a and b was chosen and was shown to give a close representation of material flow behaviour for a wide range of flows involving both Darcy and non-linear regimes (Chapter 2).

It should be noted that non-linear flow effects are normally not likely to be significant beyond a radius of several metres from the well. Beyond this distance, which varies with the aquifer material and well geometry and drawdown, the non-linear term bV^2 in the Forchheimer equation becomes insignificant and the flow may, if required, be described by Darcy's law $I = aV$ or $V = KI$.

Lindquist (1933), Ergun (1952), Schneebeli (1955) and Irmay (1964) have all offered specific expressions for the determination of a and b in terms of porosity, fluid viscosity and some characteristic length term of the porous medium matrix. Ward (1964) and Sunada (1965) obtained general relationships in terms of viscosity alone that gave a as being proportional to b^2 and $b^{5/3}$ respectively. All the above expressions are of little practical significance since they were derived from limited flow range permeameter testing of either idealised porous media or media of limited size and/or uniformity.

Both Dudgeon (1964) and Kazemipour (1975) have permeameter tested unconsolidated porous media over extended velocity ranges

covering both the Darcy and non-linear regimes. The materials tested by these two workers included river gravels and sands, crushed dolerites and marbles. Typical of a wide range of unconsolidated aquifer sediments, the tested materials varied in both the size and distribution of the grains. The combined range of materials tested may be most easily described by,

$$0.25 \leqslant d_{10} \leqslant 90\text{mm}$$

$$1 \leqslant d_{60}/d_{10} \leqslant 12$$

$$10^{-1} \leqslant K=1/a \leqslant 10^{4} \text{ cm/sec.}$$

where: d_{10} is the diameter that 10 per cent of the material is finer than;

d_{60}/d_{10}, the uniformity coefficient, is an index of the variation of particle size grading within the material;

and K is the hydraulic conductivity obtained from the Darcy flow portion of the test results.

For each material tested by either Dudgeon or Kazemipour, a single Forchheimer expression ($I = aV + bV^2$) was fitted to the permeameter velocity-gradient results in the manner described in Chapter 2. These values of a and b are plotted against one another in log-log form in Figure 8.1. The straight line drawn through the points in Figure 8.1 obeys the equation,

$$a = 2.5\, b^{4/3} \qquad (8.1)$$

where the units are centimetres and seconds. At low flow velocities, where Darcy's law is valid, the expression $a = 1/K$ applies since the

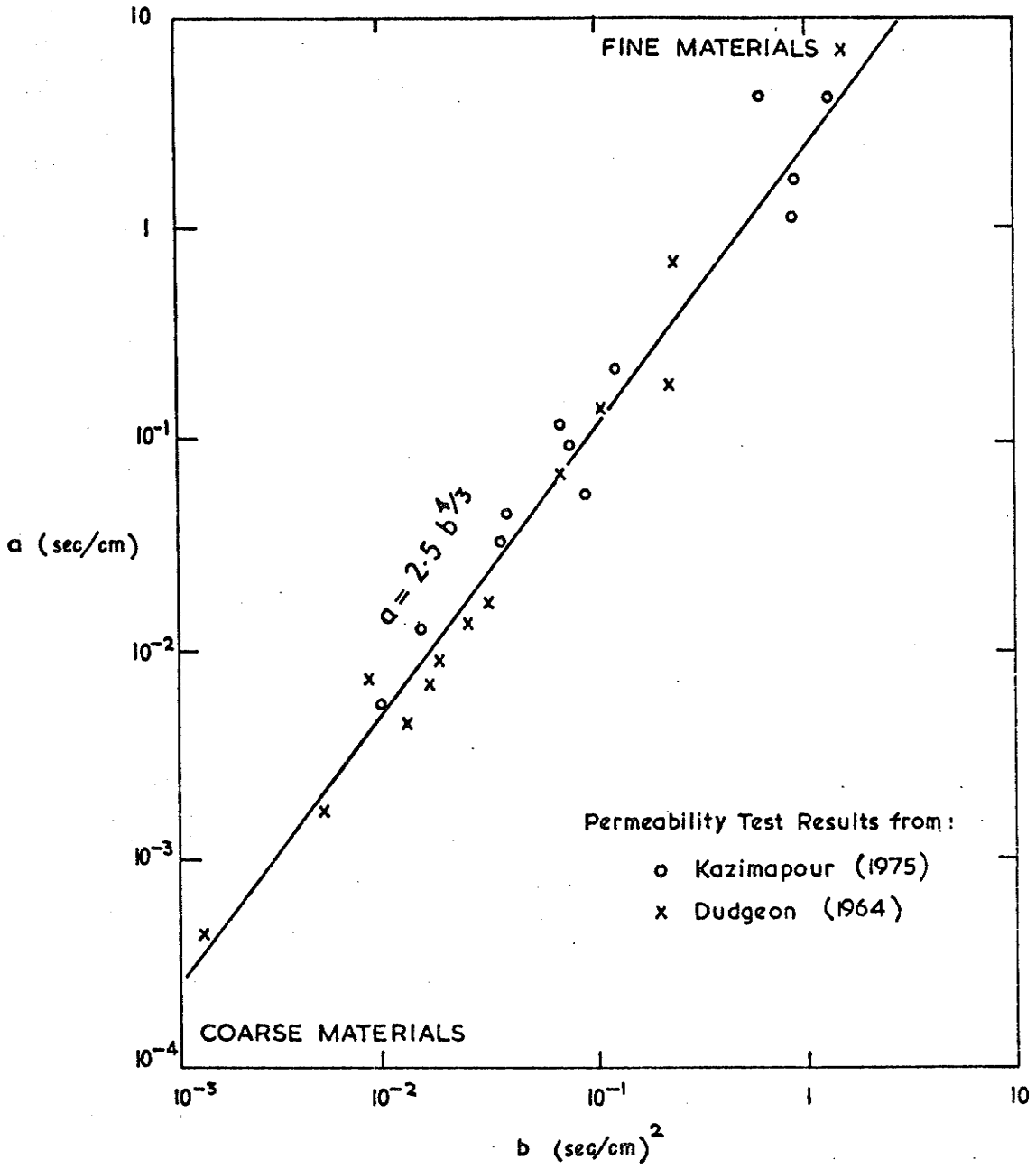

FIGURE 8·1: RELATIONSHIP BETWEEN FORCHHEIMER NON-LINEAR EQUATION COEFFICIENTS a AND b FOR UNCONSOLIDATED MATERIALS.

non-linear component bV^2 becomes negligible. The relationship,

$$b/a^2 = 0.5\ K^{5/4} \qquad (8.2)$$

(K in centimetre/sec)

may thus be used to estimate the dimensionless severity of non-linear flow in terms of the hydraulic conductivity of the aquifer. The value of K will in general be determined from conventional field testing and type curve analysis or may be estimated by experienced personnel.

The importance of equation (8.2) cannot be overemphasised. An estimate of the non-linear flow dimensionless parameter, b/a^2, may be made merely on the basis of the aquifer hydraulic conductivity. The reliability of this estimate is adequate for unconsolidated aquifer sediments since in most cases, a considerable error in the value of b/a^2 will not materially affect the choice of an optimal design.

8.2.2 Well Variables

The designer has almost complete control over well variables which include the type of construction, the diameter and the type, size, location and length of the intake sections of the well. These variables interact to determine the well drawdown-discharge performance for a given set of aquifer variables. In general the available alternatives will be limited by such things as the capability of drilling plant, the range of accessible commercial well components and the available power supply facilities.

During construction of a producing well, the hydraulic characteristics of the aquifer material immediately surrounding the well may be significantly altered. The degree to which such near well

inhomogeneities affect well performance depends upon such factors as the well geometry and the extent and type of screens and gravel packs. The possible effects of drilling and development on the properties of the aquifer close to the well should be given careful consideration when the predicted performance of trial designs are being compared. Reference should be made to Dudgeon and Cox (1975) and Dudgeon and Huyakorn (1975) for information on this subject.

8.2.3 Radius of Influence

In estimating steady state well-aquifer performance, some value for a radius of influence, r_o, beyond which the original hydraulic head levels are virtually unaffected by pumping, must be assumed. The radius of influence is governed by both the aquifer properties and the rate at which the particular well is pumped.

For confined aquifers of infinite extent, the concept of a radius of influence is theoretically unjustified since the cone of depression will continually expand ad infinitum. However, practical and commonly assumed values of $1000 < r_o < 5000$ metres are accepted as reasonable for confined aquifers whilst values $100 < r_o < 500$ metres suffice for unconfined aquifer single well flow problems.

Although the choice of radius of influence affects the predicted drawdown-discharge relationship, the effect is not large for practical values and the relative performance of different designs and thus the selection of the optimum are virtually unaffected.

8.2.4 Practical Range of Variables

When ascertaining the practical range of the relevant well design variables that needed investigation, particular attention was given to

Australian conditions. An Australia wide survey of existing production wells was undertaken with detailed reviews being made for the Eastern States from which data were more readily accessible. Only wells in the many aquifers formed by unconsolidated sedimentary formations which include alluvium of coastal and inland rivers, coastal sediments, lacustrine and some aeolian deposits were considered.

Wells in fractured and porous rock aquifers were not considered in deriving the ranges of the variables for design investigation. This, however, does not mean that the presented design information is inapplicable to such aquifers. It merely means that the range of the design data may not directly cover well flow problems in rock aquifers. Reasonable extrapolation of the presented design data may be used to solve such problems which lie outside the range for which solutions have been obtained.

Important aspects of the Australia wide data review will now be discussed.

(a) The range of aquifer material flow properties encountered was found to fall within normally quoted worldwide values:

(i) $10 < \text{Transmissivity, } T < 10^{4}$ metre^{2}/day

(ii) $10^{-3} <$ Hydraulic Conductivity, $K < 10$ cm/sec

(iii) $10^{-5} <$ storage coefficient, $S < 10^{-3}$ for confined aquifers.

For unconfined aquifers storage coefficients are in the main approximately equal to the specific yield and range between 0.1 and 0.3.

(b) Several significant points relating to current well construction practice were noted. Approximately 70% of wells employ wire wound screens whilst of the remaining 30%, most use slotted casing. Gravel

packing is used in about 35% of completed wells.

(c) Screen and casing diameters normally do not exceed 0.4 metres except for gravel packed wells which are generally limited to 0.6 metre diameter. As discussed in Section 5.8, in highly permeable coarse unconfined aquifers large diameter (up to 2 metres) wells may be found.

(d) Well depths generally do not exceed 150 metres.

(e) Well discharges rarely exceed 200 litres/sec. Yields between 25 and 100 litres/sec are most common.

(f) The occurrence of both confined and unconfined aquifers is common within Australia whilst individual regions may have predominantly more of one type than the other.

The following points of interest were noted as pertaining to confined aquifers:

(i) Confined aquifer thickness rarely exceeds 65 metres.

(ii) Current practice heavily favours tapping the full thickness of the aquifer or at least a high proportion of it as the following breakdown of the reviewed data illustrates;

Screen Ratio, l_s/m	Proportion of Wells
1 fully screened	65%
.75 - 1	15%
.5 - .75	15%
.25 - .5	5%
< .25	Negligible

Although this trend to high screening ratios is current practice, it is not necessarily good practice. Further discussion is to be found in Section 8.3.4.

(iii) In most cases (90 - 95%) the aquifer thickness to well radius ratio, m/r_w, is less than 160. Solutions obtained by the author, $10 \leqslant m/r_w \leqslant 80$, may be readily extrapolated to $m/r_w = 160$ and thus the available design results cover most eventualities.

(iv) In a detailed review of 150 wells in confined unconsolidated sedimentary river basins within the State of New South Wales, the well drawdown-radius ratio, s_w/r_w, varied between 15 and 700. The non-linear term b/a^2, estimated from the hydraulic conductivity K of the aquifer by equation (8.2), was combined with s_w/r_w for each well to obtain the parameter bs_w/a^2r_w. Values of bs_w/a^2r_w varied between 0.1 and 25 whilst the majority fell within the range 0.5 to 7. The effects of non-linear flow are significant for values of bs_w/a^2r_w as low as 1. Thus substantial non-linear flow effects are a distinct possibility in many Australia confined aquifer situations.

The following pertinent points were noted for wells in unconfined aquifers:-

(i) Unconfined aquifer thickness ranges between 5 and 150 metres.

(ii) The lower portion of the well is generally screened. The most common practice is to drill to the base of the aquifer and screen the lower $\frac{1}{2}$ to 1/3 of the aquifer. This is in line with normal world practice in unconfined aquifers.

(iii) For conventional screened wells, the undisturbed water level height to well radius ratio, h_o/r_w lies within the range 25 to 400. Solutions obtained by the author, $50 \leqslant h_o/r_w \leqslant 200$, cover a more practical abbreviated range and may be readily extrapolated to cover all cases.

(iv) For bottom entry large diameter wells (see Section 5.8), the value of h_o/r_w rarely exceeds 50. Well performance in the majority of such cases may be estimated by extrapolation of the trends obtained by the author when investigating such problems within the range $5 \leqslant h_o/r_w \leqslant 20$.

(v) Hydraulic conductivity values of $K > 0.075$ cm/sec are common. Corresponding values of the non-linear dimensionless term b/a^2, estimated from equation (8.2) for such unconsolidated aquifer materials, can thus be expected frequently to exceed 0.02. As shown in Figure 5.36, non-linear flow exerts a considerable influence upon unconfined aquifer well flow performance for values of $b/a^2 > 0.02$. Thus it is important to consider non-linear flow in designing wells for unconfined aquifers. Under Australian conditions, non-linear flow to wells in unconsolidated unconfined aquifers may be the norm and wholly Darcy flow the exception rather than the more commonly assumed situation in which the flow is considered fully Darcy in the majority of cases.

8.3 Design Criteria for Wells in Confined Aquifers

8.3.1 Uniform Homogeneous Aquifer - Single Screen in Top or Base

The effects upon well performance of partial screening and non-linear flow were investigated in Sections 5.2 and 5.3 for flow to a well in a uniform homogeneous isotropic confined aquifer. Partial screening as considered was in the form of a single length of screen adjacent to either the top or the base of the aquifer.

Deviations from Darcy one-dimensional radial flow attributable to either partial screening and/or non-linear flow were negligible

at the chosen value of radius of influence r_o = 10m and for $r > 10$m the flow could be described by the Thiem equation,

$$s = h_o - h = Q \ln(r_o/r)/2\pi K m \qquad (8.3)$$

where $K = 1/a$

Based on the results obtained for r_o = 10m, well performance at values of $r_o/m > 10$ was evaluated by a simple process in which the Thiem equation was applied in extending the flow beyond r_o = 10m. A comprehensive series of hydraulic design graphs was prepared in this manner and is presented in Appendix 3 (Figures A3.1 to A3.24). The figures are presented in terms of the dimensionless variables Q/Q_T, bs_w/a^2r_w, l_s/m, m/r_w, r_o/m. The discharge Q_T with which the predicted well discharge is compared is the Thiem equation discharge assuming fully radial Darcy flow, i.e. $Q_T = 2\pi Kms_w/\ln(r_o/r_w)$. Well performance, Q/Q_T, is plotted as a function of bs_w/a^2r_w for various partial screening ratios l_s/m. Individual figures apply for specific values of m/r_w and r_o/m within the ranges $10 \leqslant m/r_w \leqslant 80$ and $10 \leqslant r_o/m \leqslant 500$.

The relatively simple cases of full screening and/or Darcy flow are incorporated in the design figures.

In the past there has been considerable debate, with confusing and conflicting opinions being offered, as to the circumstances in which non-linear flow may substantially affect well performance. The importance of the composite non-linear dimensionless term, bs_w/a^2r_w should thus be stressed. The material non-linear flow behaviour dimensionless term b/a^2 is seen from equation (8.2) to

increase with the hydraulic conductivity. The values of well drawdown and radius are however equally as important as the material behaviour term b/a^2. None of the component terms, b/a^2, s_w or r_w may be discussed in isolation, since their effects are all closely interwoven. It is the complete composite term bs_w/a^2r_w which governs the magnitude of the deviations from normally assumed Darcy flow behaviour. A relatively large diameter well in a coarse gravel material (high b/a^2 value) may exhibit significant non-linear flow deviations at low drawdown. Alternatively, a well in a fine aquifer material (low b/a^2 value) may exhibit similarly significant non-linear deviations due to high drawdown and/or small well radius.

To illustrate the use of the design figures of Appendix 3 for comparing the performance of alternative well designs, a typical problem was investigated in which the effects of well diameter, partial screening and non-linear flow were considered. The basic aquifer data assumed for the problem were $m = 8$ metres and $K = 10^{-1}$ cm/sec. A value of $r_o = 1600$ metres was chosen and the well discharge for a drawdown of $s_w = 30$ metres was evaluated for three well radii, $r_w = 0.1$, 0.2 and 0.4 metres and three partial screening ratios, $l_s/m = 0.2$, 0.6, 1. Well discharges were evaluated for non-linear flow by using equation (8.2) to estimate $b/a^2 = 0.028$ from $K=10^{-1}$cm/sec. and then combining this value of b/a^2 with s_w/r_w to give the term bs_w/a^2r_w required to enter the relevant figure. For comparative purposes the well discharges assuming fully Darcy flow were also evaluated. The resultant estimates of discharge for the various well configurations are given in Table 8.1.

Table 8.1: Values of Well Discharge for Typical Example of Alternative Well Configurations.
$m = 8$ metres $K = 10^{-1}$ cm/sec $r_o = 1600$ metres
$s_w = 30$ metres.

For non-linear flow: $b/a^2 = 0.5K^{5/4} = 0.028$

r_w metres	m/r_w	r_o/m	$\frac{bs_w}{a^2 r_w}$	Reference Figure	Q_T (litre/sec)	Values of Q (litre/sec) l_s/m 0.2	0.6	1
0.1	80	200	Darcy	A3.23	156	75	131	156
0.2	40			A3.17	168	93	146	168
0.4	20			A3.11	182	109	161	182
0.1	80	200	8.4	A3.23	156	58	115	145
0.2	40		4.2	A3.17	168	80	137	160
0.4	20		2.1	A3.11	182	97	155	177

It can be seen that for small screening ratios and/or non-linear flow, the improvement in well discharge caused by doubling the well diameter can be significantly greater than the commonly quoted value of 8% which applies only for Darcy flow to a fully screened well. In this example, doubling the well radius from 0.1 to 0.2 metres for a partial screening ratio $l_s/m = 0.2$ when non-linear flow is considered results in increasing the well discharge from 58 to 80 litres/sec., i.e. an improvement of 38%.

Sufficient data can be extracted from the design figures to enable drawdown-discharge curves to be plotted for particular well geometries and aquifer characteristics. Each drawdown is taken in turn and the corresponding discharge calculated in the manner described in the above example. In this manner quite elaborate comparison between alternative well designs can be accomplished and the optimal well selected for various sets of constraints.

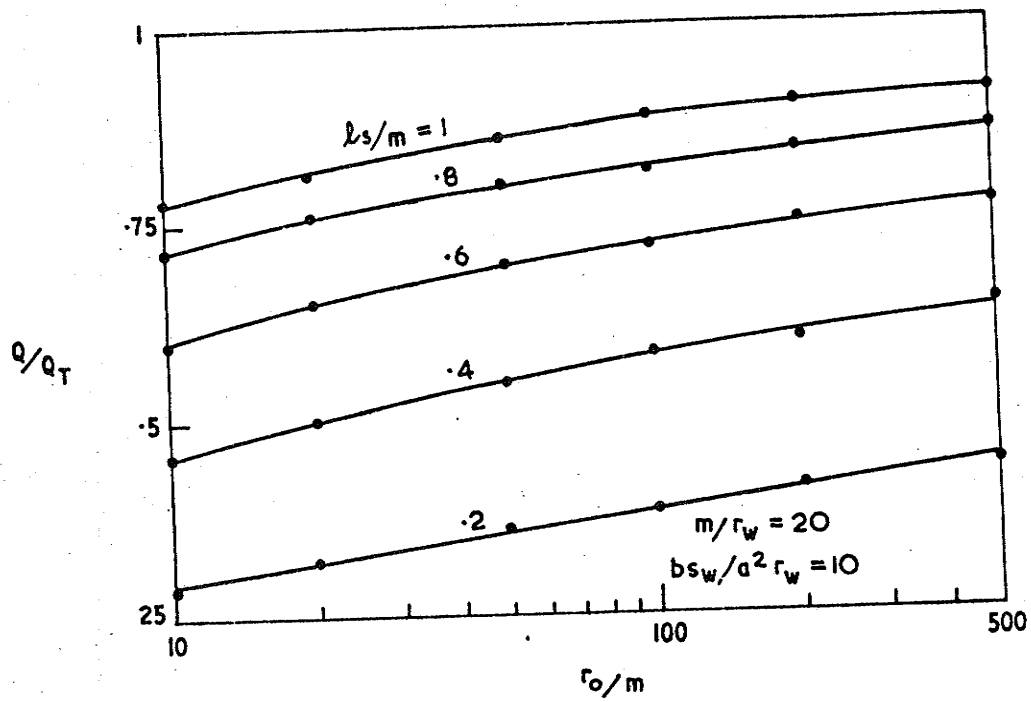

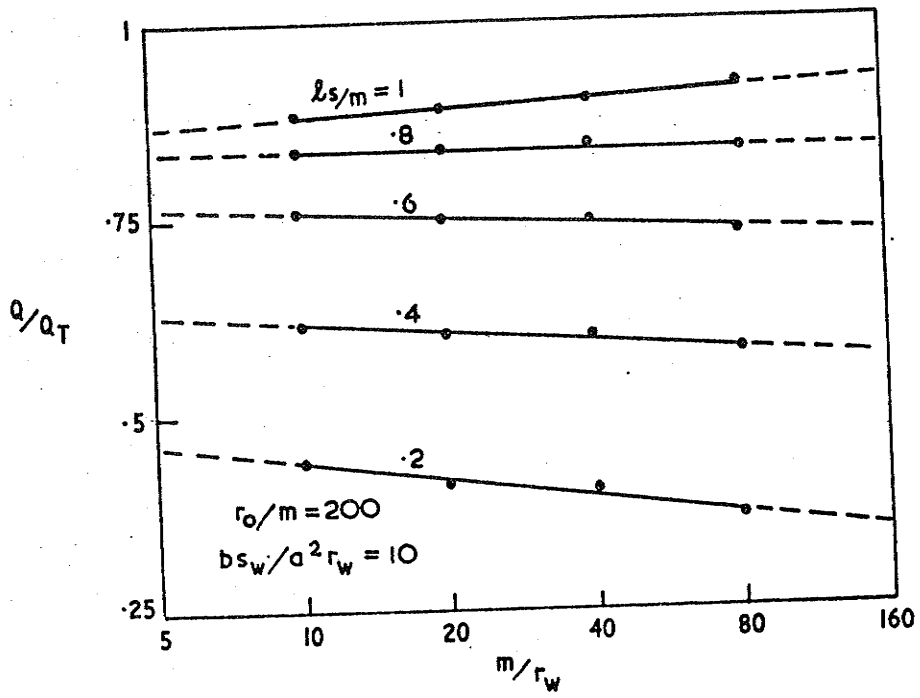

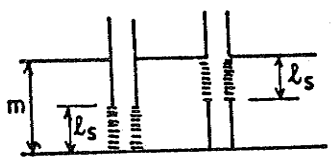

$$Q_T = \frac{2\pi K m s_w}{\ell n (r_o/r_w)} \qquad (K = 1/a)$$

FIGURE 8·2: TYPICAL EFFECTS. WELL PERFORMANCE OF A PARTIALLY SCREENED WELL IN A CONFINED AQUIFER FOR NON-LINEAR FLOW

From the overall general design Figures A3.1 to A3.24, particular results may be extracted and graphs drawn to illustrate the effects of specific variables upon well performance. For instance, the effects of partial screening (l_s/m) and well radius (m/r_w) may be isolated as shown in Figure 5.8 for fully Darcy flow to a well with $r_o/m = 10$. Typical non-linear flow cases illustrating the effects of both m/r_w and r_o/m are shown in Figure 8.2. By extrapolation on this type of specific graph, the ranges of the variables covered by the design figures of Appendix 3 may be readily extended.

As previously noted, the distribution of discharge flux and hence velocity at the intake portion of the well is important in regard to sand entry and corrosion/encrustation aspects of screen design. Typical flux distributions into partially screened wells are given in Figures 5.11 and 5.15 for Darcy and non-linear flow respectively. In all cases, the average discharge flux, Q/l_s, and thus the average velocity occurs at a point $0.75\ l_s$ along the screen from the end adjacent to a confining bed. The maximum discharge flux occurs at the end of the screen most removed from a confining bed and can exceed twice the average Q/l_s value for small values of the partial screening ratio l_s/m. The distribution becomes more uniform as complete aquifer screening ($l_s/m = 1$) is approached. When non-linear flow occurs, the greater the degree of non-linearity of the flow (as measured by bs_w/a^2r_w) the more uniform the distribution becomes, all other things being equal.

8.3.2 Radial Inhomogeneity

The effect of a zone of altered permeability around a well in an otherwise homogeneous aquifer was investigated in Section 5.5.

This inhomogeneity may be natural, artificially created by a gravel pack or may result from drilling or development during completion of the well.

As described in Section 5.5.2, analytical solutions can be obtained for the special case of flow to a fully screened well irrespective of whether the flow be Darcy or non-linear within either the affected zone close to the well or the bulk of the homogeneous aquifer. The well performance was shown to be substantially decreased by permeability reduction in a zone adjacent to the well. The severity of such permeability damage upon well performance clearly stresses the need for care in drilling, construction and development of the well. In particular, damage due to mud invasion may be both extensive and severe (Dudgeon and Cox (1975)). The improvement in well performance due to a zone of increased permeability of specific radial extent was shown to approach an upper limit at large values of K_a/K_o, the ratio of the permeability in the altered zone to the overall permeability. This upper limit for improvement in well performance was shown to correspond to an effective increase in well radius to the radius of the effected zone.

Analytical solutions do not exist for partially screened wells surrounded by a zone of altered permeability. Finite element solutions for such cases in which the flow obeys Darcy's law throughout the aquifer system were obtained and discussed in Section 5.5.3. The effects of near well permeability variation upon well performance were shown to become more pronounced with decrease in the partial screening ratio l_s/m. Thus permeability improvement or reduction

within the affected zone should respectively encourage or discourage the designer to adopt small partial screening ratios.

The more general case of non-linear flow to partially screened wells with radial inhomogeneity has not been treated. A very great number of graphs would have to be provided to cover such cases.

8.3.3 High Permeability "Fingers"

The improvement in well performance attributable to the presence of "fingers" (thin bands of material of limited areal extent) of high permeability material intersected by the well was investigated in Section 5.6. Only wholly Darcy flow to fully screened wells was considered.

The results clearly indicated the likelihood of substantial contributions to well discharge arising from such thin "fingers" of high permeability material. Values given in Table 5.9 may be used as a guide to the relative significance of the variables involved.

The investigation indicates that it is important to exercise care during drill sampling and geophysical logging so that thin high permeability bands are detected.

More complex cases involving non-linear flow and/or partial screening warrant individual numerical computer solution. The computation cost for such cases would be relatively high because of the fine network required in the finite element analysis.

8.3.4 Multiple Screens - Alternative Placement of Partial Screening Sections

In previous sections 8.3.1 - 8.3.3, partially screened well problems were concerned with the screen being placed at either the top or the base of the aquifer. If alternative screen placements and/or

multiple screened lengths are used, the total discharge for a given drawdown in the well can be predicted by subdividing the aquifer by horizontal planes drawn through mid-points of screens and midway between adjacent screens as shown in Figure 8.3.

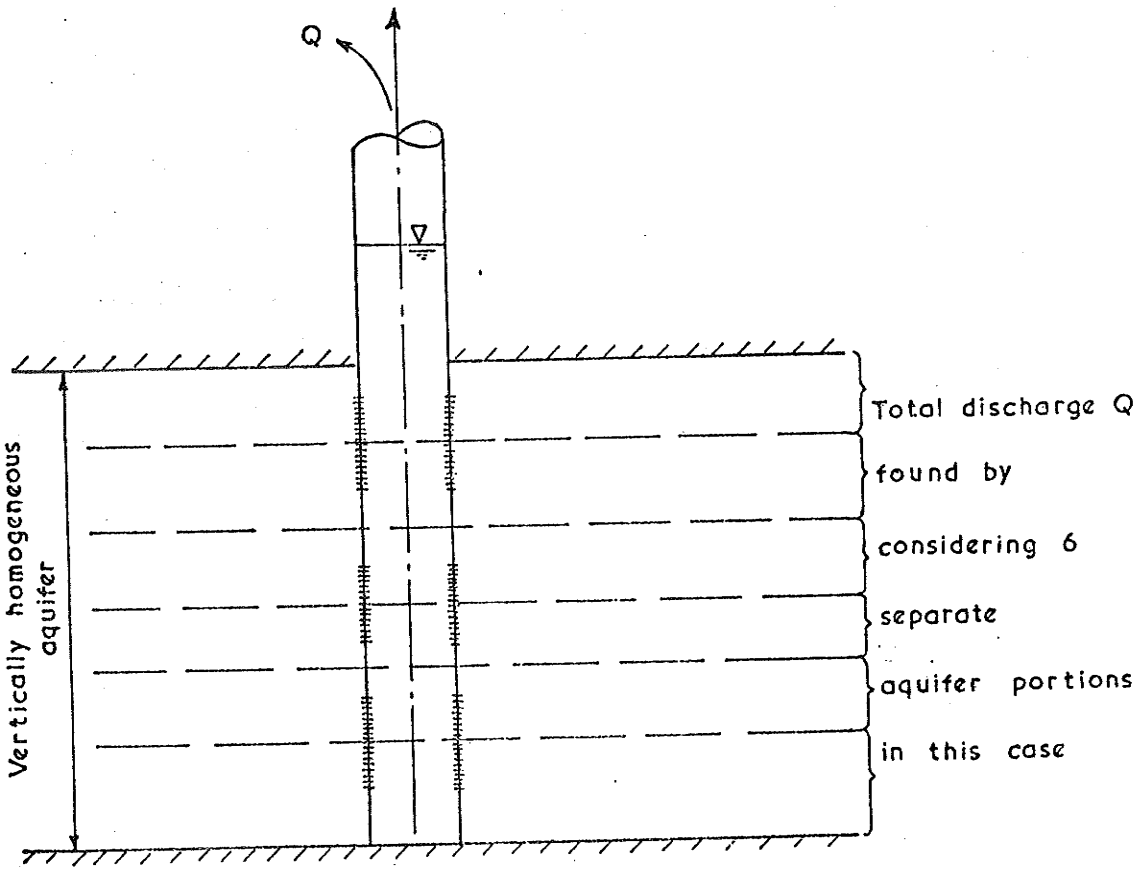

FIGURE 8·3: MULTIPLE SCREENING - CONFINED AQUIFER SUBDIVISION

Each portion of the aquifer can then be treated as a separate aquifer using the information provided in previous sections. Superposition will give the total well discharge.

The technique described has been used to examine the effect of placing a partial screen at the mid-point of the aquifer rather than at the top or bottom. The method was checked by comparing results with finite element solutions obtained by direct use of the computer

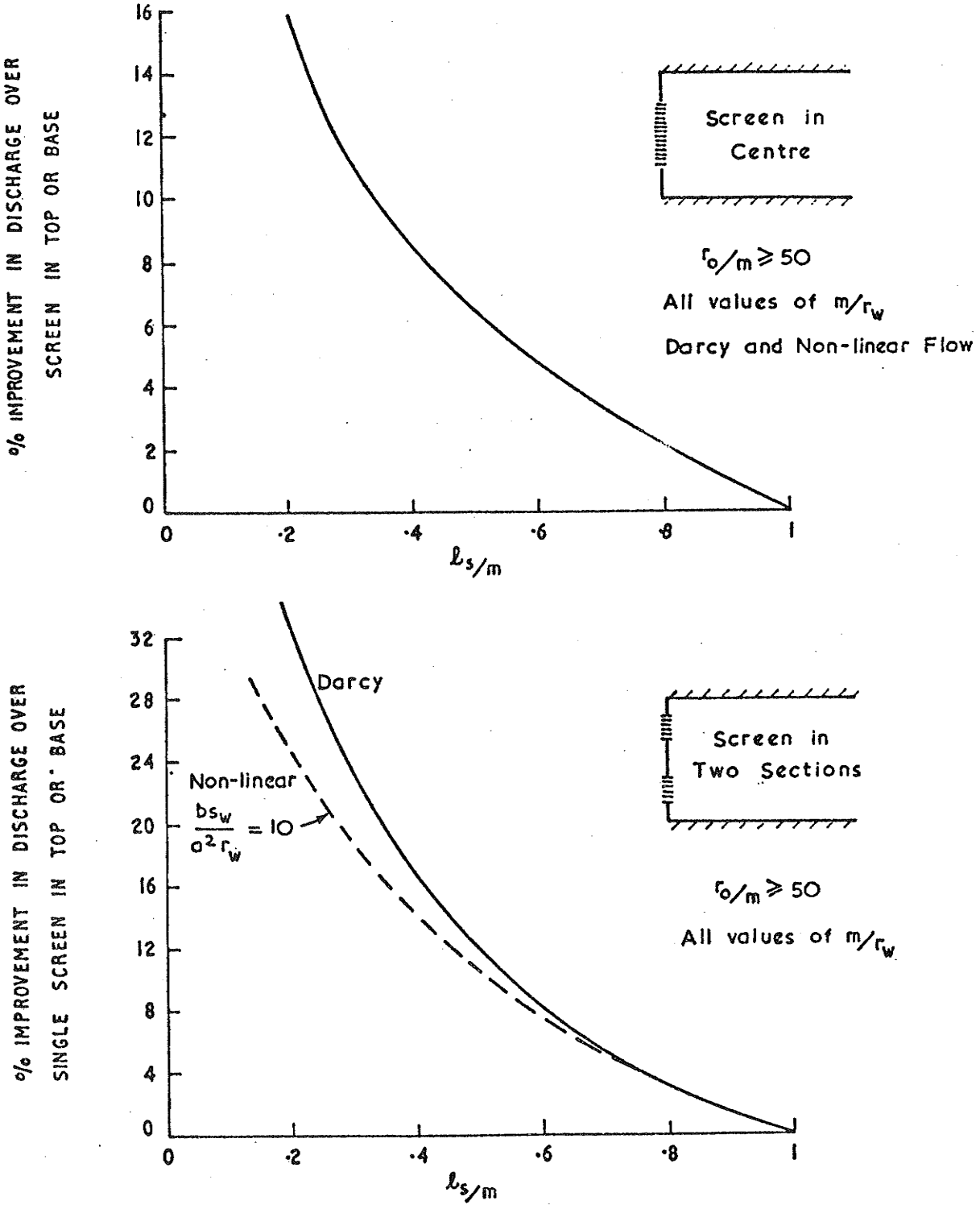

FIGURE 8·4: IMPROVEMENT IN WELL PERFORMANCE ARISING FROM MULTIPLE SCREENING OF A CONFINED AQUIFER.

programmes for several of such cases. Results were found to be identical. Similarly, the effect of dividing a screen into two portions was investigated. The resulting improvements in well performance over a single screen at the top or bottom of the aquifer are shown in Figure 8.4 for both alternative screen configurations studied. For values of $r_o/m > 50$, the condition usually met in practice, the improvement over a single screen at top or bottom was found to be independent of m/r_w. For the centrally screened condition the improvement was also independent of the degree of non-linearity of the flow.

As shown in Figure 8.4, the improvement in discharge is relatively insignificant when more than 75% of the aquifer is screened (currently the normal practice in Australia as discussed in Section 8.2.5) but rapidly increases with decreasing screen length. The high percentage improvement in discharge for small values of the screening ratio l_s/m should encourage the designer to consider multiple screening of minor portions of confined aquifers.

8.3.5 Multi-layered Aquifers

Problems involving flow to a well screened through a portion of a multi-layered confined aquifer system were investigated in Section 5.4.

For the simplified case of wholly Darcy flow to a well that fully screens all aquifer layers, the total discharge for a given drawdown can be calculated by adding the discharge from each layer treated as a separate aquifer. The flow will be everywhere radial

and may be described by the Thiem equation within each layer (see Section 5.4.1).

As discussed in Section 5.4.2, if the flow within any of the aquifer layers is non-linear, the flow will not be everywhere radial even for the fully screened case. Complex multi-layered aquifer problems involving non-linear flow may be solved by direct application of the computer programs. To give an indication of the importance of the relevant variables, an investigation of fully screened two-layered aquifer systems involving non-linear flow in the upper layer was made using the finite element programs. It was shown that the error in well discharge caused by adding the discharges from individual layers determined by assuming radial flow is not significant for the following practical range of cases,

$$10 < m/r_w < 100,\ r_o/m > 10,\quad 0.2 < m_2/m < 0.8,\ bs_w/a^2 r_w < 25$$

where m_2 is the thickness of the layer in which non-linear flow occurs whilst m is the total aquifer thickness.

In problems concerned with partial screening of multi-layered confined aquifers, particular cases must be solved by direct use of the computer programs since the number of variables is too great to allow the majority of cases to be covered by a reasonable number of dimensionless plots. For the special case of wholly Darcy flow in a two layer aquifer-aquitard system in which the more permeable aquifer layer is fully screened and the aquitard layer is unscreened (see section 5.4.3), the effect of the unscreened aquitard layer on the flow can be ignored if $m_1K_1/mK_2 > 10$. The symbols have been defined in Figure 5.18. The results of this aquifer-aquitard

investigation may be used as a guide to the relative importance of various layers in more complex multi-layered aquifers. Clearly thin low permeability (aquitard) layers may be ignored and in general should not be screened since the discharge contributed will be negligible.

8.4 Design Criteria for Wells in Homogeneous Unconfined Aquifers

8.4.1 Well Partially Screened at the Base of the Aquifer- Drawdown to Top of Screen

As noted in Section 5.7.1, wells in unconfined aquifers should not be screened throughout the entire thickness of the aquifer since such a procedure results in dewatering of the screen with attendant corrosion and encrustation problems. The general practice is to screen the lower portion of a well which fully penetrates the aquifer. Drawdowns which expose the screen should be avoided. Thus, the limiting and most important problem is that in which the water level within the well is drawn down to the top of the screen. This case results in maximum values of well discharge and free surface drawdown and was investigated in Sections 5.7.5 and 5.7.6 for Darcy and non-linear flow respectively. The unsaturated zone was neglected in the reported studies since its contribution to the flow to water supply wells is insignificant. In problems of land drainage, however, the unsaturated or capillary zone may be important.

Particular expressions and general guidelines for free surface profiles and drawdown distributions within the aquifer were discussed in the relevant sections 5.7.5 and 5.7.6 to which the reader is referred.

The discharge flux distribution at the well screen is important in relation to practical screen selection. Typical flux distributions for partially screened wells in unconfined aquifers are given in Figures 5.34 and 5.39 for Darcy and non-linear flow respectively. The trends in flux distribution behaviour are similar to those for partially screened wells in confined aquifers:

(i) The average discharge flux, Q/l_s, and thus the average velocity occurs at a point $0.75\ l_s$ above the base of the screen.

(ii) The maximum flux occurs at the top of the screen and can exceed twice the average value Q/l_s.

(iii) The flux distribution becomes more uniform with increase in both l_s/h_o and h_o/r_w.

(iv) The flux distribution becomes more uniform as the degree of non-linearity (measured by b/a^2) increases, all other things being equal.

(v) Flux distributions for $r_o/h_o = 2$ are representative for any larger radius of influence.

In the investigation of wells in unconfined aquifers reported in Chapter 5, major consideration was given to the determination of well discharge and free surface water level just outside the well. The estimation of such values will now be separately discussed for Darcy and non-linear flow.

(a) Darcy Flow

Table 5.12 gives data which allows the discharge and free surface level at the well to be calculated if the well is drawn down level with the top of the screen, there is no head loss through

the screen and the flow is wholly Darcy. The results are presented in terms of the dimensionless variables,

$$Q/Kh_o^2,\ h_f/h_o,\ r_o/h_o,\ h_o/r_w,\ l_s/h_o = h_w/h_o$$

The effects of partial screening can be plotted for specific cases in a manner similar to that shown in Figure 5.30. In all cases, the Dupuit expression,

$$Q_D = \pi K (h_o^2 - h_w^2)/ \ln(r_o/r_w) \qquad (8.4)$$

was found to give a reasonably accurate estimate of the well discharge only if 70% or more of the aquifer is screened.

Maximum values of well discharge and free surface drawdown were found to occur when between 40% and 50% of the aquifer is screened. Figure 5.31 shows these maximum possible values for a practical range of h_o/r_w and r_o/h_o values.

Reasonable extrapolation beyond the range of the variables covered by Table 5.12 can be made, preferably by graphical means.

In all cases, the flow was essentially radial one-dimensional for $r > 1.5\ h_o$ and beyond this distance from the well the Dupuit equation

$$h_o^2 - h^2 = Q \ln (r_o/r)/\pi K \qquad (8.5)$$

could be used to describe the flow. Thus a simple arithmetic procedure exists for extending the results obtained in Table 5.12 for $2 \leqslant r_o/h_o \leqslant 16$ to a wider radius of influence $r_o > 16\ h_o$ if required. Such a process in which the Dupuit equation (8.5) is applied in extending the flow beyond a given radius has been verified by deriving the results for $r_o/h_o > 2$ from the values at $r_o/h_o = 2$ and comparing them with the finite element results of Table 5.12.

(b) Non-Linear Flow

When non-linear flow occurs near the well the discharge will be less than that for the comparable wholly Darcy flow case. Data which allows the discharge and free surface water level outside the well to be calculated are given in Table 5.13.

The results are presented in terms of the dimensionless variables,

$$aQ/h_o^2,\ h_f/h_o,\ r_o/h_o,\ h_o/r_w,\ l_s/h_o = h_w/h_o,\ b/a^2.$$

A typical plot of part of the data of Table 5.13 is given in Figure 5.35. With increasing non-linearity as measured by b/a^2 there is a dramatic reduction in well performance and free surface drawdown.

The critical screening ratio at which maximum discharge and free surface drawdown occur increases with b/a^2 (see Figure 5.36). Figure 5.36 also clearly shows the maximum possible values of discharge and free surface drawdown for non-linear flow to partially screened wells drawn down to the top of the screen for the condition $r_o/h_o = 2$.

As discussed in Section 8.2.5, unconsolidated aquifer material properties within Australia are such that values of the dimensionless non-linear term b/a^2 greater than 0.02 are frequently encountered. Figure 5.36 clearly illustrates the increasingly marked influence that non-linear flow may exert upon unconfined aquifer well flow behaviour for values of $b/a^2 > 0.02$. The importance of the data of Table 5.13 in aiding the designer to estimate well performance including non-linear flow for partially screened wells is apparent.

Non-linear flow effects were found to be negligible at $r = r_o = 2h_o$ even for the extreme case $b/a^2 = 100$. The flow could be described by the Dupuit equation (8.5) for Darcy flow ($K = 1/a$) for $r > 2h_o$. Thus extrapolation of the data of Table 5.13 to larger values of r_o/h_o can be made arithmetically assuming Dupuit flow beyond $r_o = 2h_o$. The procedure is similar to that discussed for the Darcy flow case.

8.4.2 Well Partially Screened at the Base of the Aquifer— Well Not Drawn Down to Top of Screen

If the maximum drawdown without screen dewatering is not utilized the discharge will be lower than that for the limiting case of drawdown to the top of the screen discussed in Section 8.4.1. A range of such cases was investigated for Darcy flow in Section 5.7.7. The well discharge and free surface water level results may be found in Table 5.14. In all cases, there was a linear variation of well discharge and free surface drawdown with h_w/h_o between $h_w = l_s$ and $h_w = h_o$. Thus the well discharge and free surface water level just outside the well may be predicted by linear proportioning from the data for drawdown to the top of the screen. This is demonstrated in Figure 5.40.

The distributions of both dimensionless drawdown $(h_o-h)/(h_o-h_w)$ and discharge flux in such cases $h_w > l_s$ are the same as for the limiting condition of drawdown to the top of the screen $h_w = l_s$.

The case of non-linear flow has not been examined in detail but it is considered that an approximation to the well discharge can be obtained by the method described above for Darcy flow. Such

estimates would be conservative. For more precise evaluation, individual problems can be solved by use of the computer programs.

8.4.3 Well Partially Screened above the Base of the Aquifer

Table 5.15 gives data from which both well performance and free surface drawdown at the well can be predicted if the screen is situated above the base of the aquifer and the well is drawn down to the top of the screen. Only fully Darcy flow has been considered. Optimum well performance results from placing the screen at the base of the aquifer except for small screen ratios $l_s/h_o < 0.4$. For such small screen lengths, the optimum placement is midway between the base of the aquifer and a point $0.4\ h_o$ above the base.

8.4.4 Bottom Entry Large Diameter Well

As discussed in Section 5.8, in shallow unconfined aquifers it may be a practical proposition to construct large diameter wells up to 2 metres in diameter with open bottoms. Non-linear flow in such situations can be frequently expected and was shown to considerably reduce well performance. Data to allow the prediction of well performance for various conditions including the likelihood of non-linear flow are provided in Table 5.17.

Maximum discharge and free surface drawdown for fully Darcy flow conditions occur when the well is drawn down to the open bottom of the well, the bottom being located between 1/8 to 1/4 of the saturated thickness h_o above the base of the aquifer, i.e. $1/8 < h_w/h_o = l_b/h_o < 1/4$. For non-linear flow the critical value of $l_b/h_o = h_w/h_o$ at which maximum discharge occurs increases with the degree of non-linearity as measured by b/a^2.

The discharge and free surface location for a well water level above the base ($h_w > l_b$) may be estimated by linear proportioning from the values for drawdown to the bottom of the well ($h_w = l_b$). This result is similar to that for non-utilisation of available drawdown noted in Section 8.4.2 for conventional screened wells in unconfined aquifers.

As shown in Figure 5.49, the distribution of discharge flux at the open bottom entry portion of the well is significantly non-uniform. Velocities greater than twice the average value ($V^* = Q/\pi r_w^2$), may occur at the well radius.

9. List of References

1. Adams, W.C.
On the forms of equipotential curves and surfaces and lines of electric force.
Proc. Roy.Soc. (London), 23, 280-284, 1875.

2. Aguado, E. and Remson, I.
Ground-water hydraulics in aquifer management.
A.S.C.E., Jour., 100, HY1, 103-118, Jan., 1974.

3. Ames, W.F.
Numerical methods for partial differential equations.
Thomas Nelson and Sons Ltd., London, 1969.

4. Anandakrishnan, M., Varadarajulu, G.H.
Laminar and turbulent flow of water through sand.
A.S.C.E. Jour., 89, SM5, 1-15, 1963.

5. Anderson, K.E.
Water Well Handbook.
Missouri Water Well Drillers Assoc. 2nd Edn. 1963.

6. Babbitt, H.E., Caldwell, D.H.
The free surface around and interference between gravity wells.
Univ. Illinois Bull. Eng. Expt. Sta., No. 374, 1948.

7. Bakhmeteff, B.A., Feodoroff, N.V.
Flow through granular media.
Jour. Applied Mechanics 4A, 97-104, 1937.

8. Barry, J.M.
Application of the finite element method to elliptic problems.
The Aust. Computer Jour., 6, 2, July, 1974.

9. Baturic-Rubcic, J.
An electrical analog for some cases of non-linear flow through porous media.
Jour. of Hydraulic Research, 4, 2, 1-20, 1966.

10. Baturic-Rubcic, J.
The study of non-linear flow through porous media by means of electrical models.
Jour. of Hydraulic Research, 7, 1, 31-65, 1969.

11. Bear, J.
Dynamics of fluids in porous media.
American Elsevier, N.Y. 1972.

12. Blair, A.H.
Well screens and gravel packs.
Groundwater, 8, 1, 10-21, Jan.-Feb., 1970.

List of References (cont'd.)

13. Boulton, N.S.
The flow pattern near a gravity well in a uniform water bearing medium.
Jour. Inst. Civil Engrs. (U.K.), 36, 534-550, 1951.

14. Boulton, N.S.
Unsteady radial flow to a pumped well allowing for delayed yield and storage.
I.A.S.H. General Assembly of Rome, 2,37, 472-77, 1954.

15. Boulton, N.S.
Analysis of data from non-equilibrium pumping tests allowing for delayed yield from storage.
I.C.E. (U.K.) Proc., 26, 469-482, 1963.

16. Boulton, N.S.
Analysis of data from pumping tests in unconfined anisotropic aquifers.
Jour. of Hydrology, 10, 369-378, 1970.

17. Brutsaert, W.F.
Numerical solution of multiphase well flow.
A.S.C.E., Jour., 99, HY11, 1981-2001, Nov., 1973.

18. Brutsaert, W.F., et al.
Computer analysis of free surface well flow.
A.S.C.E. Jour., 97, IR3, 405-420, Sept., 1971.

19. Chapman, T.G.
Analytical derivation of the Dupuit equations for ground-water flow.
Geotechnique, 7, 142-143, 1957.

20. Childs, E.C.
An introduction to the physical basis of soil water phenomena.
John Wiley and Sons Ltd., N.Y., 1969.

21. Childs, E.C., et al
Permeability measurements in the field as an assessment of anisotropy and structure development.
Jour. of Soil Science, 8, 1, 27-41, 1957.

22. Cohen De Lara, G.
Ceofficient de Perte de Charge en Milieu Poreux Base 1'Equilibre Hydrodynamique d'un Massif.
La Houille Blanche, 2, 167-176, April 1955.

23. Cooley, R.L.
A finite difference method for unsteady flow in variably saturated porous media: application to a single pumping well.
Water Resources Research, 7, 6, 1607-25, 1971.

List of References (cont'd.)

24. Cooley, R.L., Case, C.M.
Effect of a water table aquitard on drawdown in an underlying pumped aquifer.
Water Resources Research, 9, 2, 434-447, 1973.

25. Cooper, H.H. Jr.
The equation of groundwater flow in fixed and deforming co-ordinates.
Jour.Geophys. Res., 71, 20, 1966.

26. Cooper, H.H. (Jr.), et al.
Response of a finite-diameter well to an instantaneous charge of water.
Water Resources Research, 3, 1, 263-9, 1967.

27. Curtis, R.P.
Flow over and through rockfill banks.
Univ. of Melbourne, Dept. of Civil Eng., Dec., 1965.

28. Davis, D.N., De Wiest, R.J.M.
Hydrogeology
John Wiley and Sons, N.Y., 1966.

29. Desai, C.S., Abel, J.F.
Introduction to the finite element method, a numerical method for engineering analysis.
Van Nostrand Reinhold Co., N.Y., 1972.

30. De Wiest, R.J.M.
Geohydrology
John Wiley & Sons, N.Y., 1965.

31. De Wiest, R.J.M.
On the storage coefficient and the equations of groundwater flow.
Jour.Geophys.Res., 71, 4, 1966.

32. Dudgeon, C.R.
Flow of water through coarse granular materials.
Univ. of New South Wales, Water Research Laboratory Report No. 76, Dec. 1964.

33. Dudgeon, C.R.
An experimental study of the flow of water through coarse granular media.
La Houille Blanche, 21, 7, 785-801, 1966.

34. Dudgeon, C.R., Cox, R.J.
Drilling mud invasion of unconsolidated aquifer materials.
A.W.R.C. Tech.Paper No. 17, 1975.

List of References (cont'd.)

35. Dudgeon, C.R., Huyakorn, P.
Effects of near-well permeability variation on well performance.
A.W.R.C. Tech. Paper No. 18, 1975.

36. Dudgeon, C.R., et al.
Hydraulics of flow near wells in unconsolidated sediments.
Univ. of N.S.W., Water Research Lab. Report No. 126, Vols. 1 and 2, 1972, 1973.

37. Einstein, P.A.
Factors affecting the accuracy of electrolytic plotting tanks.
Brit. Jour.Appl. Phys., 2, 49-55, 1951.

38. Emery, A.F., Carson, W.W.
An evaluation of the use of the finite element method in the computation of temperature.
A.S.M.E. Trans., Jour. of Heat Transfer, 136-145, May, 1971.

39. Engelund, F.
On the laminar and turbulent flows of ground water through homogeneous sand.
Trans. Dan.Acad.Tech.Sci. No.3, Contr. Hydraulic Lab. Tech., Univ. of Denmark Bull. No.4, 1953.

40. Ergatoudis, O.C., et al.
Curved isoparametric quadrilateral elements for finite element analysis.
Int. Jour. Solids Struct., 4, 31-42, 1968.

41. Ergun, S.
Fluid flow through packed columns.
Chem. Eng. Prog., 48, 89-94, 1952.

42. Escande, L.
Experiments concerning the infiltration of water through a rock mass.
Rep. Proc. Minnesota Inter. Hydraulics Conv., 1953.

43. Finn, W.D.L.
Finite element analysis of seepage through dams.
A.S.C.E., Jour., 93, SM6, 41-48, Nov. 1967.

44. Forchheimer, P.H.
Wasserbewegung durch Boden.
Zeitschrift, Verein Deut. Ing. 49, 1901.

45. Fox, C.
An introduction to the calculus of variations.
Oxford University Press, N.Y., 1950.

List of References (cont'd.)

46. France, P.W., et al
Numerical analysis of free surface problems.
A.S.C.E. Jour., 97, IR1, 165-179, 1971.

47. Freeze, R.A.
Theoretical analysis of regional groundwater flow.
Inland Waters Branch, Dept. of Energy, Mines and Resources, Ottawa, Canada, Scientific Series No.3, 1969.

48. Freeze, R.A.
Three-dimensional, transient, saturated-unsaturated flow in a groundwater basin.
Water Resources Research, 7, 2, 347-366, April, 1971.

49. Frind, E.O., Pinder, G.F.
Galerkin solution of the inverse problem for aquifer transmissivity.
Water Resources Research, 9, 5, 1397-1410, Oct., 1973.

50. Gatlin, C.
Petroleum engineering-drilling and well completions.
Prentice-Hall, Englewood Cliffs N.J. 1960.

51. Givan, C.V.
Flow of water through granular materials - initial experiments with lead shot.
A.G.U. Trans. 15, 572-579, 1934.

52. Grcic, J.A.
Model test of steady flow toward a well.
I.A.H.R. 9th Conv. Proc., 591-600, 1961.

53. Guymon, G.L., et al.
A general numerical solution of the two-dimensional diffusion-convection equation by the finite element method.
Water Resources Research, 6,6, 1611-7, Dec. 1970.

54. Hall, H.P.
An investigation of steady flow toward a gravity well.
La Houille Blanche, 10, 8-35, 1955.

55. Hancock, R.R.
Development of wells.
A.M.F., 4th Groundwater School, Adelaide, May, 1973.

56. Hansen, V.E.
Unconfined groundwater flow to multiple wells.
A.S.C.E. Trans., 118, 1098-1130, 1953.

57. Hantush, M.S.
Drawdown around a partially penetrating well.
A.S.C.E., Jour., 87, HY4, 83-98, July, 1961.

List of References (cont'd.)

58. Hantush, M.S.
Hydraulics of wells.
Advances in Hydroscience, Editor Ven te Chow., Academic Press, N.Y., Vol. 1, 1964.

59. Hazel, C.P.
Groundwater hydraulics.
A.W.R.C., Groundwater School, Adelaide, 1973.

60. Huang, Y.H.
Unsteady flow toward an artesian well.
Water Resources Research, 9, 2, 426-433, April, 1973.

61. Hubbert, M.K.
Darcy law and the field equations of the flow of underground fluids.
A.I.M.M.E. Trans., 207, 222-239, 1956.

62. Huisman, L.O.
Groundwater recovery.
Macmillan Press Ltd., London, 1972.

63. Hunt, B.W.
Exact flow rates from Dupuits approximation.
A.S.C.E., Jour., 96, HY3, 633-42, March 1970.

64. Huyakorn, P.
Finite element solutions of two-regime flow towards wells.
Univ. of N.S.W., Water Res. Lab.Report No. 137, (Ph.D. Thesis), 1974.

65. Huyakorn, P.S., Dudgeon, C.R.
Groundwater and well hydraulics. An annotated bibliography.
Univ. of N.S.W., Water Res. Lab.Report No. 121, Feb., 1972.

66. Instn. of Water Engrs., (U.K.)
Efficiency of well screens and gravel packs.
Institution of Water Engineers (U.K.), Jour., 23, 6, 355-68, Aug. 1969.

67. Instn. of Water Engrs. (U.K.)
Observation bore holes:- Construction and use.
Inst. Water Engrs. (U.K.), Jour., 23,6, 396-401, Aug. 1969.

68. Irmay, S.
On the theoretical derivation of Darcy and Forchheimer formulas.
A.G.U., Trans., 39, 4, 702-7, Aug. 1958.

69. Irmay, S.
Theoretical models of flow through porous media.
R.I.L.E.M. Symp.Transfer of Water in Porous Media, Paris, 1964.

List of References (cont'd.)

70. Jacob, C.E.
Flow of ground water.
Engineering Hydraulics, Chapter 5, John Wiley and Sons, N.Y., 1950.

71. Javandel, I., Witherspoon, P.A.
Analysis of transient fluid flow in multi-layered systems.
Uni. of California, Berkeley, Dept. of Civil Engineering, Water Resources Centre Contribution No. 124, March 1968.

72. Johnson, E.E. Inc.
Groundwater and wells.
Saint Paul, Minnesota, 1966.

73. Johnstone, D.I.
The construction of large diameter water wells using the "gravel packed, mud stabilised, open hole" technique with cable tool rigs.
N.W.W.A. Conf. Drill 74, Broadbeach, Queensland, Nov., 1974.

74. Jones, P.
Permeability and radius of a skin.
The Oil and Gas Jour., 60, 25, 114-119, 1962.

75. Karadi, G., Nagy, I.V.
Investigations into the validity of the linear seepage law.
I.A.H.R., 9th Convention, Proc., Dubrovnik, 556-566, 1961.

76. Karanjac, J.
Well losses due to reduced formation permeability.
Groundwater, 10, 4, 42-49, 1972.

77. Karplus, W.J.
Analog simulation solutions of field equations.
McGraw Hill, N.Y., 1958.

78. Karplus, W.J., Soroka, W.W.
Analog methods - computation and simulation.
McGraw Hill, N.Y., 1959.

79. Kazemipour, A.K.
Prediction of hydraulic characteristics of aquifer materials.
Univ. of N.S.W., M.Eng. Sc. Thesis, 1974.

80. Kipp, K.L. Jr.
Unsteady flow to a partially penetrating finite radius well in an unconfined aquifer.
Water Resources Research, 9, 2, 448-462, 1973.

List of References (cont'd.)

81. Kirkham, C.E.
Turbulent flow in porous media. An analytical and experimental model study.
Water Research Foundation of Australia, Bull. No.11, Feb., 1967 (also Univ. of Melbourne, Dept. of Civil Eng., Report, Feb. 1967).

82. Kirkham, D.
Exact theory of flow into a partially penetrating well.
Jour. Geophys. Res., 64, 1317-1327, 1959.

83. Koenig, L.
Relation between aquifer permeability and improvement achieved by well stimulation.
AWWA, Jour., 53,5, 652-798, May 1961.

84. Kozeny, J.
Theorie und Berechnung der Brunnen
Wasserkraft and Waserwirtschaft, 2, 101-105, 1933.

85. Liebmann, G.
Electrical analogues.
Brit.Jour.Appl. Phys., July, 1953.

86. Lindquist, E.
On the flow of water through porous media.
Rep. First Cong. on Large Dams, 5, 81-101, 1933.

87. Lohman, S.W.
Manual on ground-water hydraulics.
A.W.R.C., Ground-water School, Adelaide, May, 1970.

88. Luthin, J.N., Scott, V.H.
Numerical analysis of flow through aquifers toward wells.
Agric.Engng., 33, 279-282, May, 1952.

89. McCorquodale, J.A.
Variational approach to non-Darcy flow.
A.S.C.E. Jour., 96, HY-11, 2265-78, Nov. 1970.

90. McCorquodale, J.A., Ng, H.C.
Non-Darcy flow solved by finite element analysis.
I.A.H.R., 13th Congress, Kyoto, Proc., 4, Sub. D, 347-355, 1969.

91. Mauersberger, P.
The use of variational methods and of error distribution principles in groundwater hydraulics.
Int. Assoc. of Sci. Hydrol., Bull., 13, 2, 169-186, June 1968.

List of References (cont'd.)

92. Murray, W.A., Monkmeyer, P.L.
Validity of Dupuit-Forchheimer equation.
A.S.C.E. Jour., 99, HY9, 1573 - 1583, Sept., 1973.

93. Muskat, M.
The flow of homogeneous fluids through porous media.
McGraw Hill, N.Y., 1937.
(2nd Printing, Edwards, Ann Arbor, Michigan, 1946).

94. Neuman, S.P.
Effect of partial penetration on flow in unconfined aquifers considering delayed gravity response.
Water Resources Research, 10, 2, 303-312, 1974.

95. Neuman, S.P., Witherspoon, P.A.
Variational principles for confined and unconfined flow of groundwater.
Water Resources Research, 6, 5, 1376-82, Oct. 1970.

96. Neuman, S.P., Witherspoon, P.
Finite element method of analysing steady seepage with a free surface.
Water Resources Research, 6, 3, 889-97, June 1970.

97. Neuman, S.P., Witherspoon, P.A.
Analysis of nonsteady flow with a free surface using the finite element method.
Water Resources Research, 7, 3, 611-623, 1971.

98. Neuman, S.P. and Witherspoon, P.A.
Field determination of the hydraulic properties of leaky multiple aquifer systems.
Water Resources Research, 8,5, Oct., 1972.

99. Oden, J.T.
Finite elements of nonlinear continua.
McGraw Hill, N.Y., 1972.

100. Parekh, C.J.
A finite element solution of time dependent field problems.
M.Sc.Thesis, Univ. of Wales, Swansea, 1967.

101. Parkin, A.K.
Rockfill dams with inbuilt spillways - hydraulic characteristics.
Univ. of Melbourne, Dept. of Civil Eng., 1963.

102. Peterson, D.F.
Hydraulics of wells.
A.S.C.E. Trans., 122, 502-517, 1957.

List of References (cont'd.)

103. Peterson, J.S., et al
Effect of well screens on flow into wells.
A.S.C.E. Trans., 120, 563-585, 1955.

104. Pinder, G.F., Frind, E.O.
Application of Galerkin's procedure to aquifer analysis.
Water Resources Research, 8, 1, 108-120, Feb., 1972.

105. Polubarinova-Kochina, P.Ya.
Theory of filtration of liquids in porous media.
Advances in Applied Mechanics, 2, pp. 207, 1951.

106. Polubarinova-Kochina, P.Ya.
Theory of ground water movement.
Princeton Univ. Press, Princeton N.J., 1962.

107. Ponter, A.R.S.
The application of dual minimum theorems to the finite element solution to potential problems with special reference to seepage.
Int. Jour. for Numr. Meth. in Eng., 4, 85-93, 1972.

108. Prakash, D., et al
Effect of well screens and gravel envelopes on the movement of sand into wells and discharges.
Irrig. Res. Inst., Roorkee, Uttar Pradesh, Feb., 1962.

109. Prickett, T.A., Lonnquist, C.G.
Selected digital computer techniques for groundwater resource evaluation.
Illinois State Water Survey, Urbane, Illinois, Bull. 55, 1971.

110. Remson, I., et al
Numerical methods in subsurface hydrology, with an introduction to the finite element method.
Wiley-Interscience Book Co., N.Y., 1971.

111. Rose, H.E., Rizk, A.M.
Further researches in fluid flow through beds of granular material.
Inst. Mech, Engrs. (U.K.), Proc., 160, 493-511, 1949.

112. Scheidegger, A.E.
The physics of flow through porous media.
Macmillan Co., N.Y., 1960.

113. Schneebeli, G.P.
Experiences sur la limite de validite de la loi de Darcy et l'apparition de la turbulence dans un ecoulement de filtration.
La Houille Blanche, 10, 2, 141-149, 1955.

List of References (cont'd.)

114. Schreurs, R.L.
The health and care of wells.
A.W.W.A., Jour., 62, 7, 434-6, July, 1970.

115. Sheahan, N.T.
Type-curve solution of step-drawdown test.
Ground Water, 9, 1, 25-29, 1971.

116. Smith, R.C.
Relation of screen design to the design of mechanically efficient wells.
A.W.W.A. Jour., 55, 609-614, 1963.

117. Softky, S., Jungerman, J.
Electrolytic tank measurements in three dimensions.
Rev. Sci. Instr., 23, 306-307, 1952.

118. Stanley, D.J.
Drilling techniques.
A.M.F., 4th Groundwater School, Adelaide, May, 1973.

119. Stark, K.P., Volker, R.E.
Non-linear flow through porous materials. Some theoretical aspects.
Uni. College of Townsville, Queensland, Australia
Dept. of Engineering, Research Bull. No. 1, April 1967.

120. Sternberg, Y.M.
Some approximation solutions of radial flow problems.
Jour. of Hydrology, 7, 2, 158-166, Jan. 1969.

121. Streltsova, T.D.
Flow near a pumped well in an unconfined aquifer under nonsteady conditions.
Water Resources Research, 9, 1, 227-235, Feb., 1973.

122. Sunada, D.K.
Turbulent flow through porous media.
University of California, Berkeley, Water Resources Centre, Contribution No. 103, 1965.

123. Swift, G.W., Kiel, O.G.
The prediction of gas-well performance including the effect of non-Darcy flow.
Jour. Pet. Tech., 14, 791-798, July, 1962.

124. Taylor, R.L.
On completeness of shape functions for finite element analysis.
Int. Jour. for Numr. Meth. in Eng., 4, 17-22, 1972.

List of References (cont'd.)

125. Taylor, G.S., Luthin, J.N.
Computer methods for transient analysis of water-table aquifers.
Water Resources Research, 5,7, 145-52, Feb. 1969.

126. Taylor, R.L., Brown, C.B.
Darcy flow solutions with a free surface.
A.S.C.E., Jour. 93, HY2, 25-33, March 1967.

127. Tek, M.R.
Development of a generalised Darcy equation.
A.I.M.M.E. Trans., 210, 45, 1957.

128. Tek, M.R., et al.
The effect of turbulence on flow of natural gas through porous reservoirs.
Jour. Pet.Tech., 14, 799-806, July, 1962.

129. Terman, F.E., Pettit, J.M.
Electronic measurements.
McGraw Hill, N.Y., 1952.

130. Theis, C.V.
The relationship between the lowering of piezometric surface and the rate and duration of discharge using ground-water storage.
A.G.U. Trans., 519-524, 1935.

131. Todd, D.K.
Ground water hydrology.
John Wiley, N.Y., 1959.

132. Todsen, M.
On the solution of transient free-surface flow problems in porous media by finite difference methods.
Journal of Hydrology, 12,3, 177-210, 1971.

133. Trollope, D.H., et al.
Complex flow through porous media.
James Cook Univ. of North Queensland, Dept. of Eng., Res. Bull. No. C2, May, 1970.
Aust. Geomechanics Jour., 61, 1-10, 1971.

134. Vachaud, G., et al.
Etude expérimentale du drainage et de la recharge des nappes à surface libre dan un modèle bidimensionnel.
Univ. de Grenoble, Lab. de Mec. des Fluides, 1,2, 1971.

135. Van Everdingen, A.F.
The skin effect and its influence on the productive capacity of a well.
A.I.M.M.E. Trans., 198, 305-324, 1953.

List of References (cont'd.)

136. Van Poolen, H.K., et al
Hydraulic fracturing: fracture flow capacity vs. well productivity.
A.I.M.E. Pet. Trans., 213, 91-95, 1958.

137. Verma, R.D., Brutsaert, W.F.
Unconfined aquifer seepage by capillary flow theory.
A.S.C.E. Jour., 96, HY6, 1331-44, June, 1970.

138. Verruijt, A.
Theory of groundwater flow.
Macmillan and Co., London, 1970.

139. Volker, R.E.
Nonlinear flow in porous media by finite elements.
A.S.C.E., Jour., 95, HY6, 2093-111, Nov. 1969.

140. Walton, W.C.
Groundwater resource evaluation
McGraw Hill, N.Y., 1970.

141. Ward, J.C.
Turbulent flow in porous media.
A.S.C.E., Jour., 90, HY5, 1-12, Sept. 1964.

142. Watson, K.K.
The permeability of an idealised two-dimensional porous medium using the Navier-Stokes equations.
Proc. 4th Aust. N.Z. Conf. on Soil Mech. and Found. Eng. 37-40, 1963.

143. White, A.M.
Trans. Amer. Inst. Chem. Eng., 31, pp. 390, 1935.

144. Wienstock, R.
Calculus of variations.
McGraw Hill, N.Y., 1952.

145. Wilkins, J.K.
Flow of water through rock fill and its application to the design of dams.
N.Z. Eng., 382-387, Nov., 1955.

146. Williamson, W.H.
Groundwater extraction techniques.
A.W.R.C. Groundwater School, Adelaide, May, 1967.

147. Wilson, E.L., Nickell, R.E.
Application of the finite element method to heat conduction analysis.
Nuclear Eng. & Design, North Holl. Publ. Co., 4, 276-86, 1966.

List of References (cont'd.)

148. Wright, D.E.
Non linear flow through granular media.
A.S.C.E., Jour., 94, HY3, 851-72, July 1968.

149. Yalin, S., Franke, L.
Experimental investigation of the laws of filter flow.
I.A.H.R., 9th Convention, Proc., Dubrovnik, 324-31, 1961.

150. Young, R.A.
Safe yield of aquifers: An economic reformulation.
A.S.C.E., Jour., 96, IR4, 377-84, Dec. 1970.

151. Zienkiewicz, O.C.
The finite element method in engineering science.
McGraw Hill, London, 1971.

152. Zienkiewicz, O.C., Cheung, K.K.
Finite elements in the solution of field problems.
The Engineer (U.K.), pp.220, Sept., 1965.

153. Zienkiewicz, O.C., Cheung, K.K.
The finite element method in structural and continuum mechanics.
McGraw Hill, London, 1967.

APPENDIX 3

DESIGN FIGURES FOR WELLS IN CONFINED AQUIFERS - PARTIAL SCREENING - DARCY AND NON-LINEAR FLOW

This appendix contains design figures for estimating the performance of a well that is only partially screened in either the top or the base of a uniform homogeneous isotropic confined aquifer. The flow may be Darcy or non-linear.

An example of the use of the design figures is given in Section 8.3.1.

As discussed in Section 8.3.4, the design figures may be used to estimate the performance of more complex multi-screened wells.

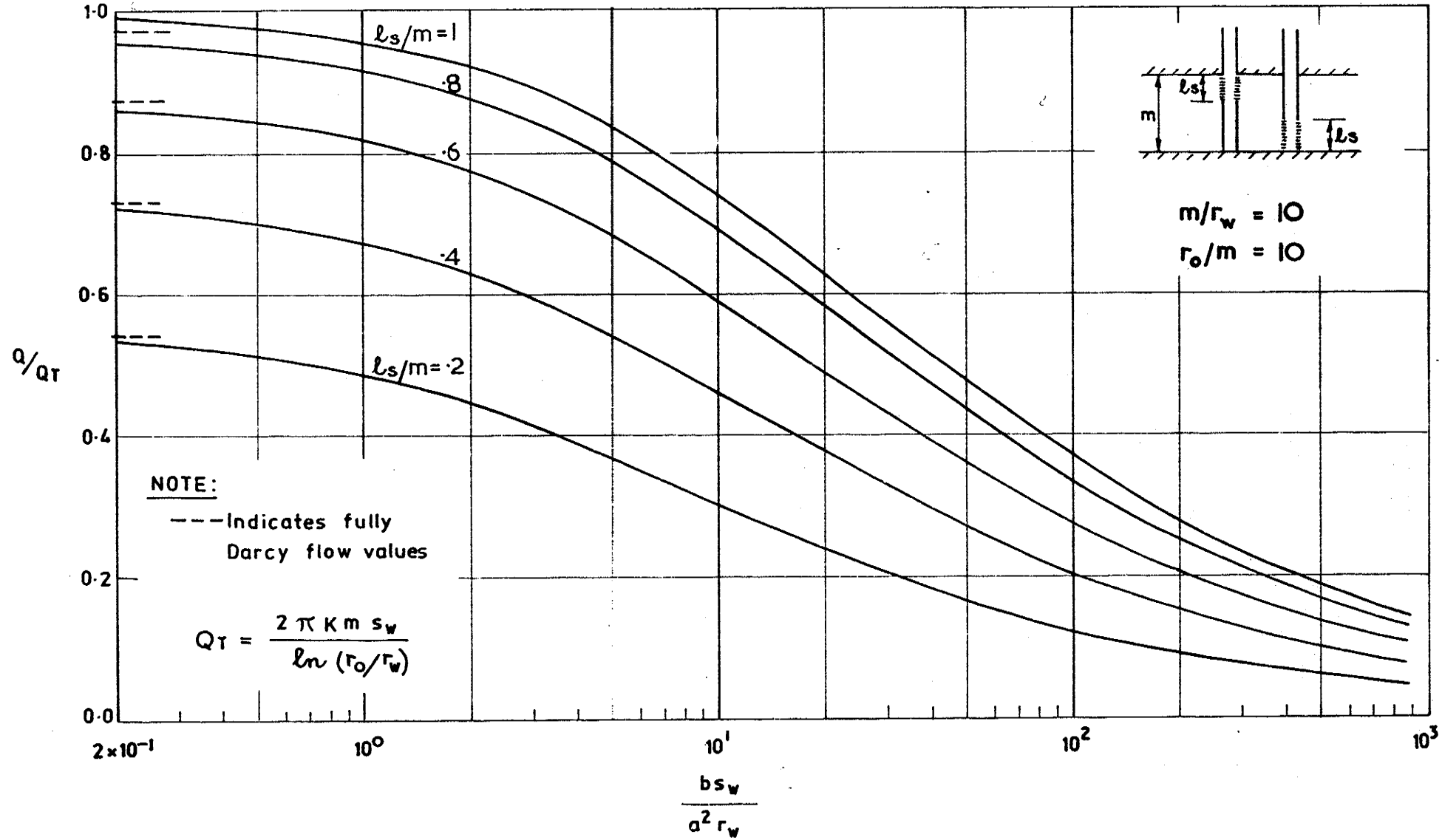

FIGURE A3·1: EFFECT OF NON-LINEAR FLOW ON WELL DRAWDOWN-DISCHARGE RELATIONSHIP. CONFINED AQUIFER

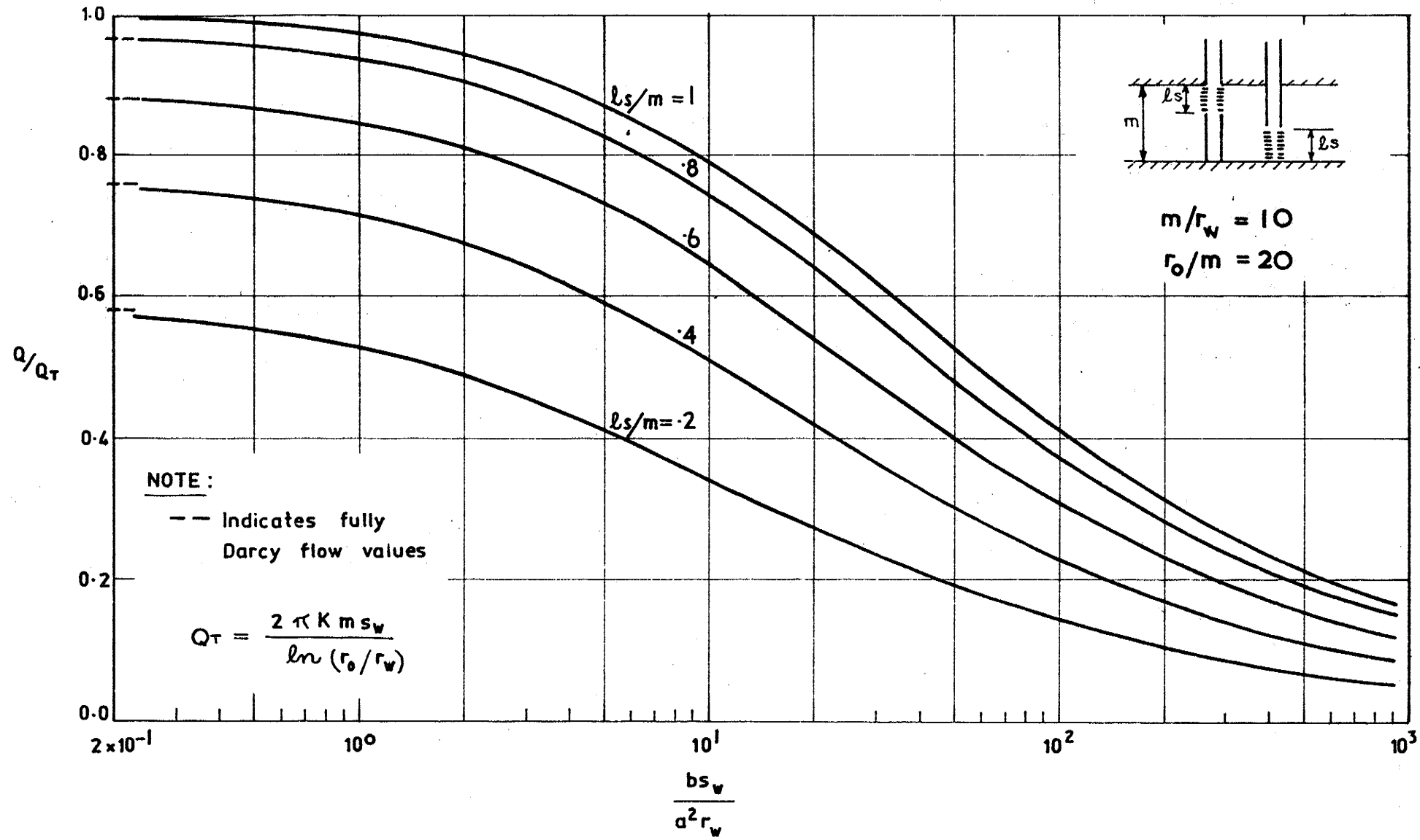

FIGURE A3·2: EFFECT OF NON-LINEAR FLOW ON WELL DRAWDOWN - DISCHARGE RELATIONSHIP. CONFINED AQUIFER

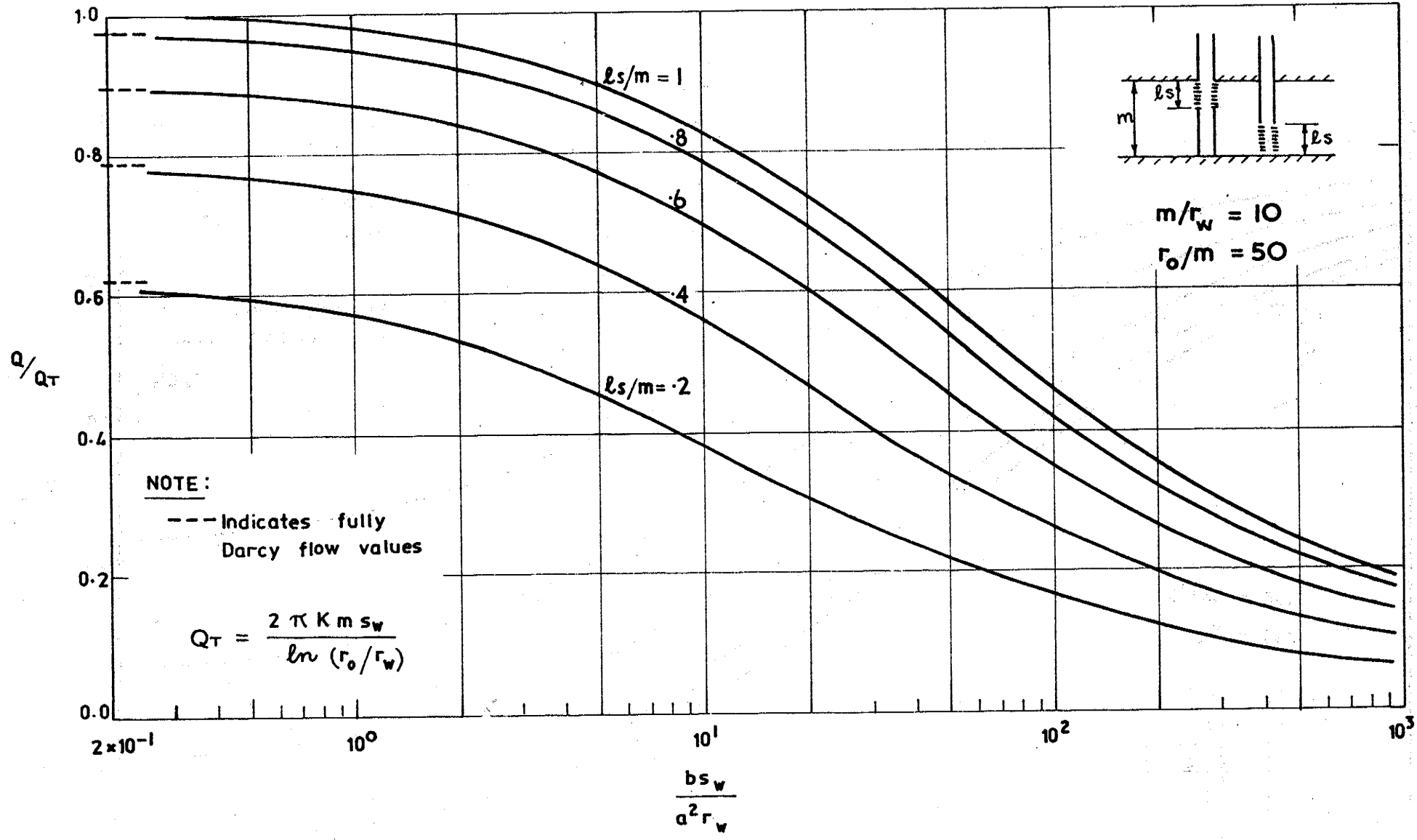

FIGURE A3·3: EFFECT OF NON-LINEAR FLOW ON WELL DRAWDOWN - DISCHARGE RELATIONSHIP. CONFINED AQUIFER

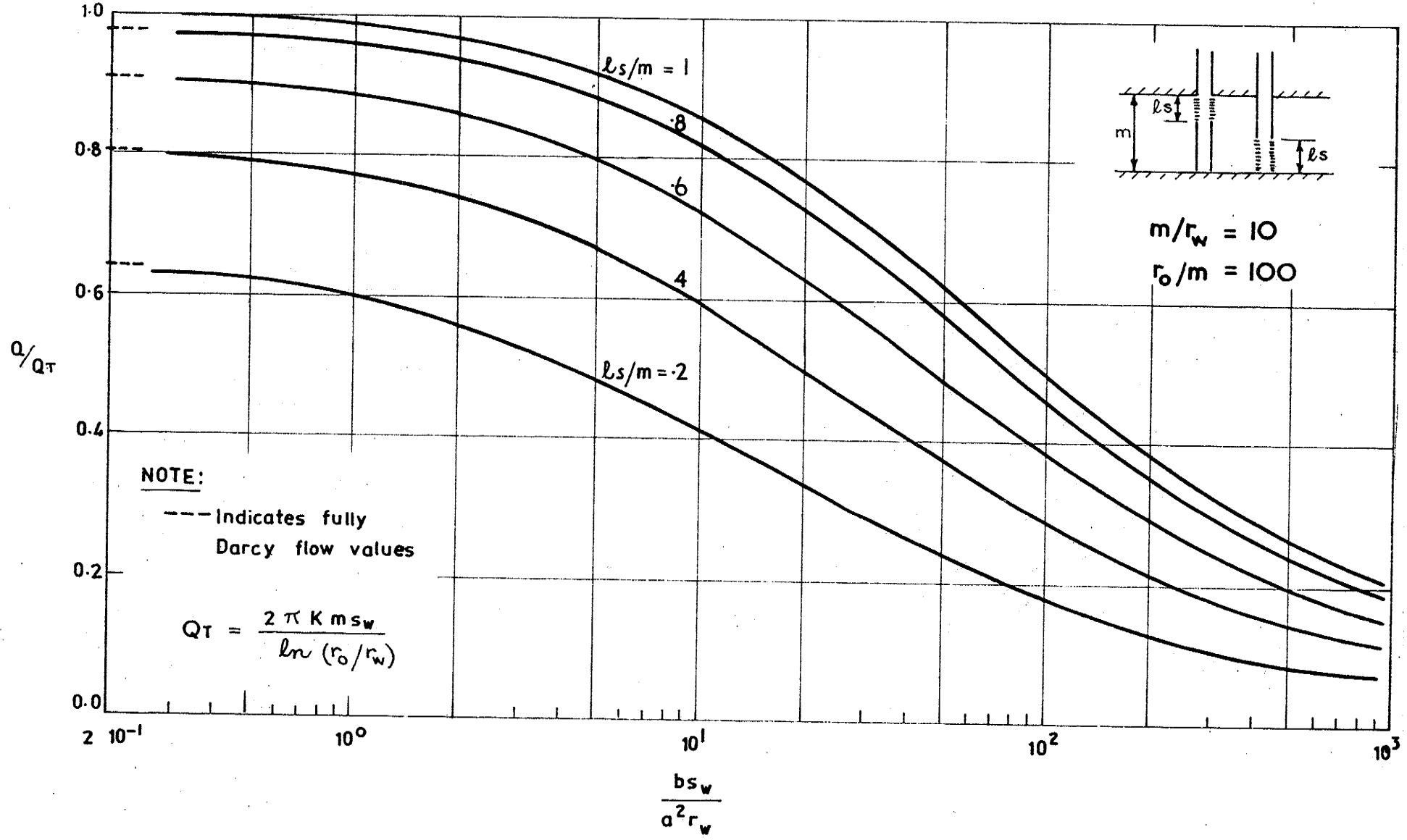

FIGURE A3·4: EFFECT OF NON-LINEAR FLOW ON WELL DRAWDOWN-DISCHARGE RELATIONSHIP. CONFINED AQUIFER

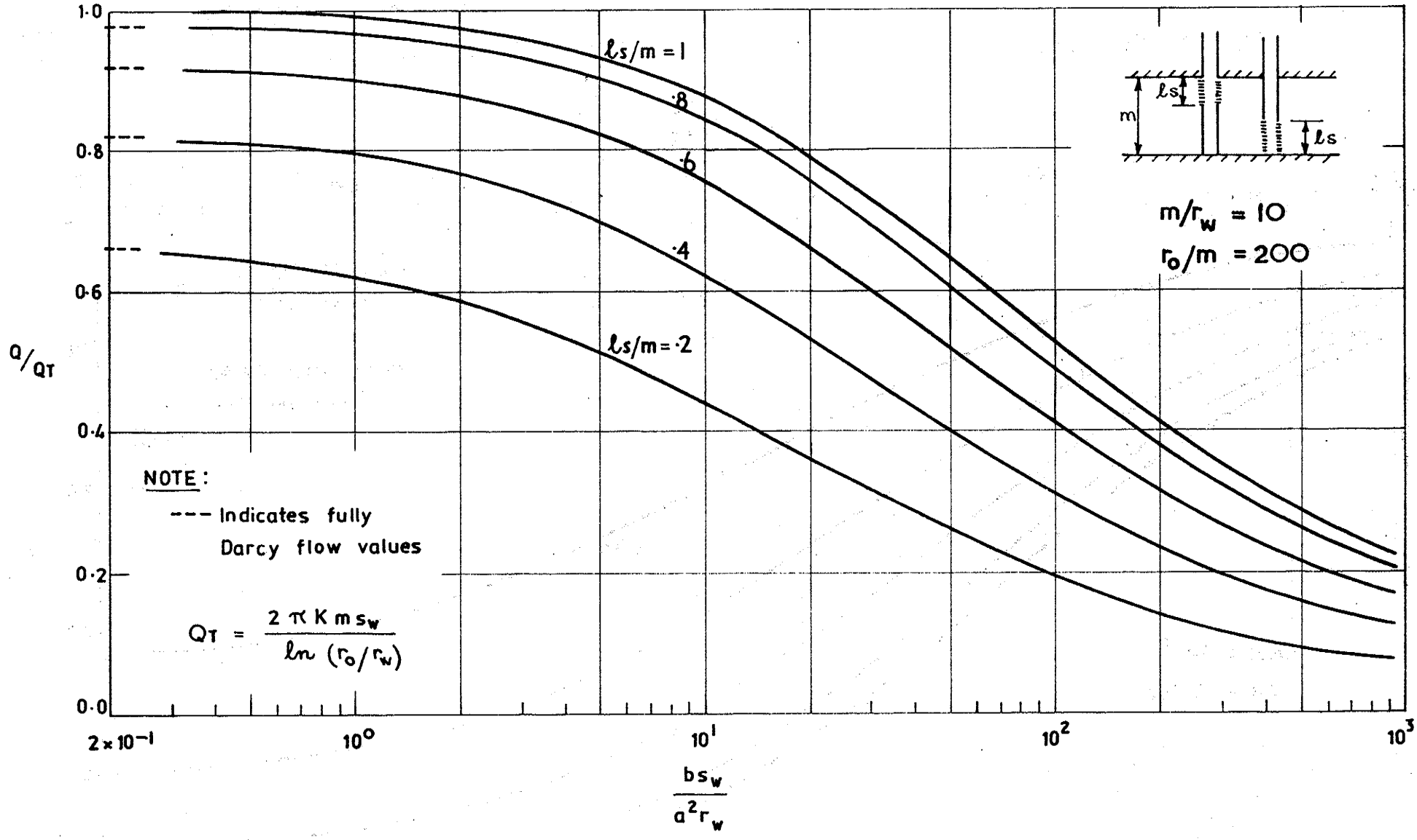

FIGURE A3·5: EFFECT OF NON-LINEAR FLOW ON WELL DRAWDOWN-DISCHARGE RELATIONSHIP. CONFINED AQUIFER

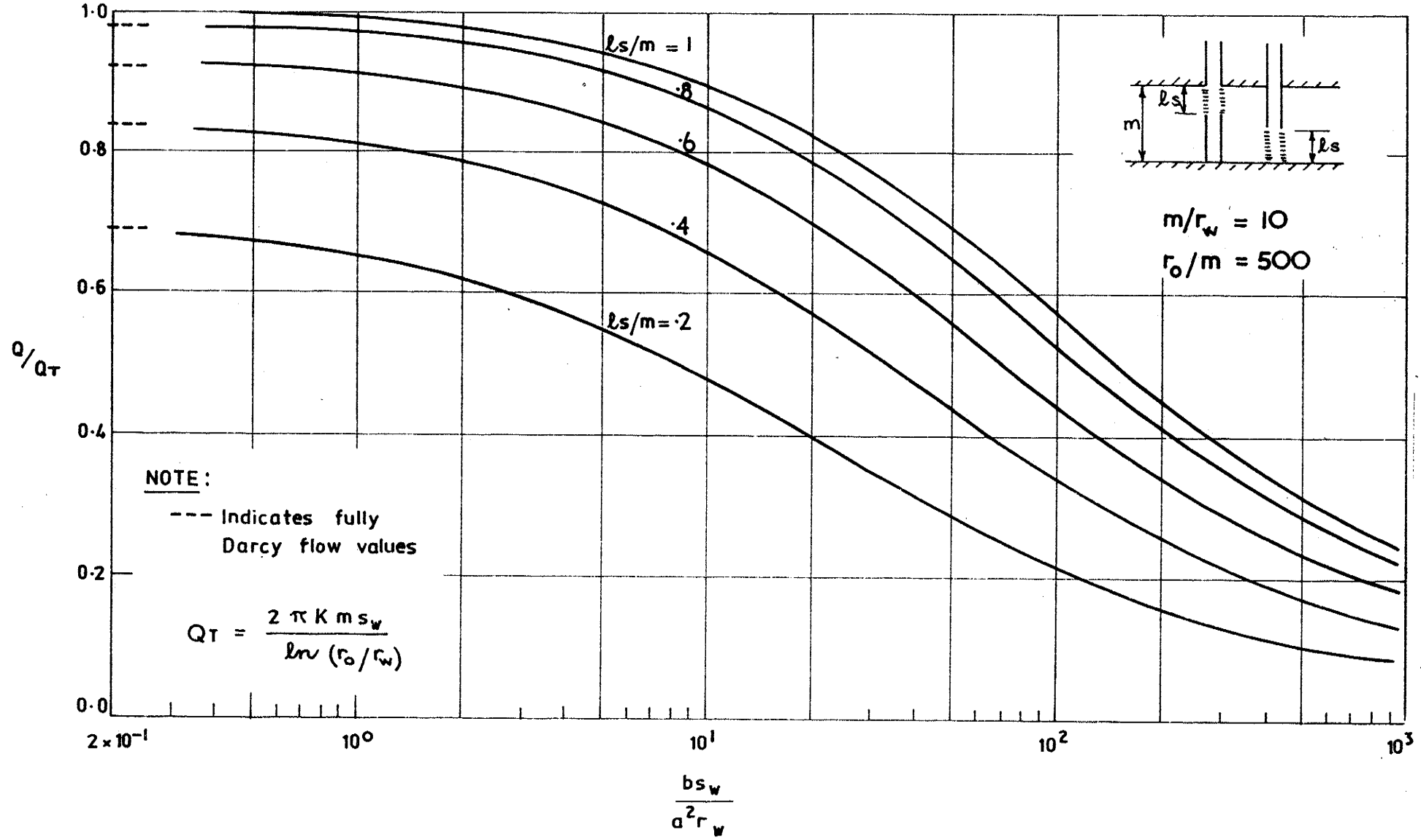

FIGURE A3·6: EFFECT OF NON-LINEAR FLOW ON WELL DRAWDOWN-DISCHARGE RELATIONSHIP. CONFINED AQUIFER

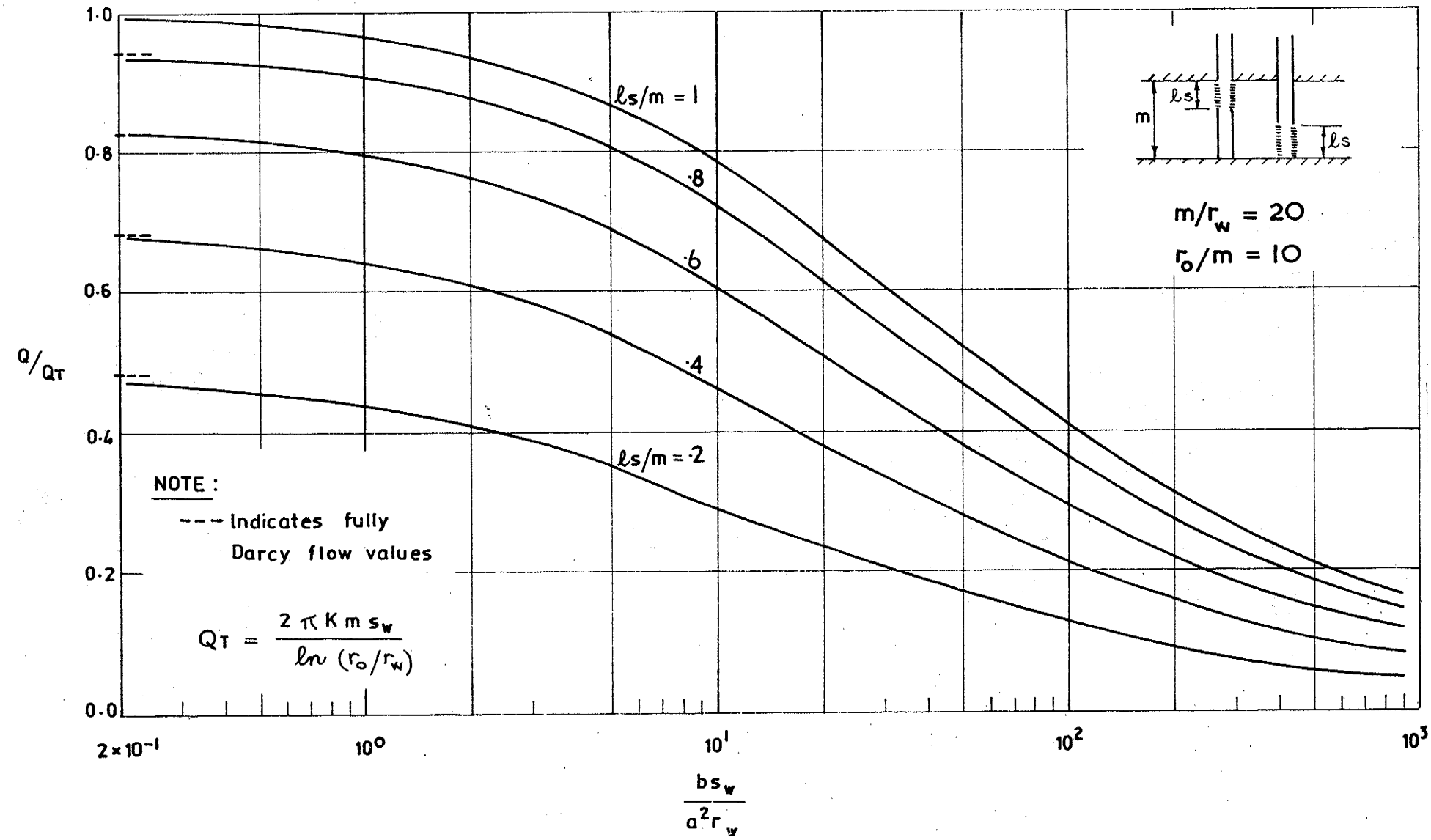

FIGURE A3·7: EFFECT OF NON-LINEAR FLOW ON WELL DRAWDOWN-DISCHARGE RELATIONSHIP. CONFINED AQUIFER

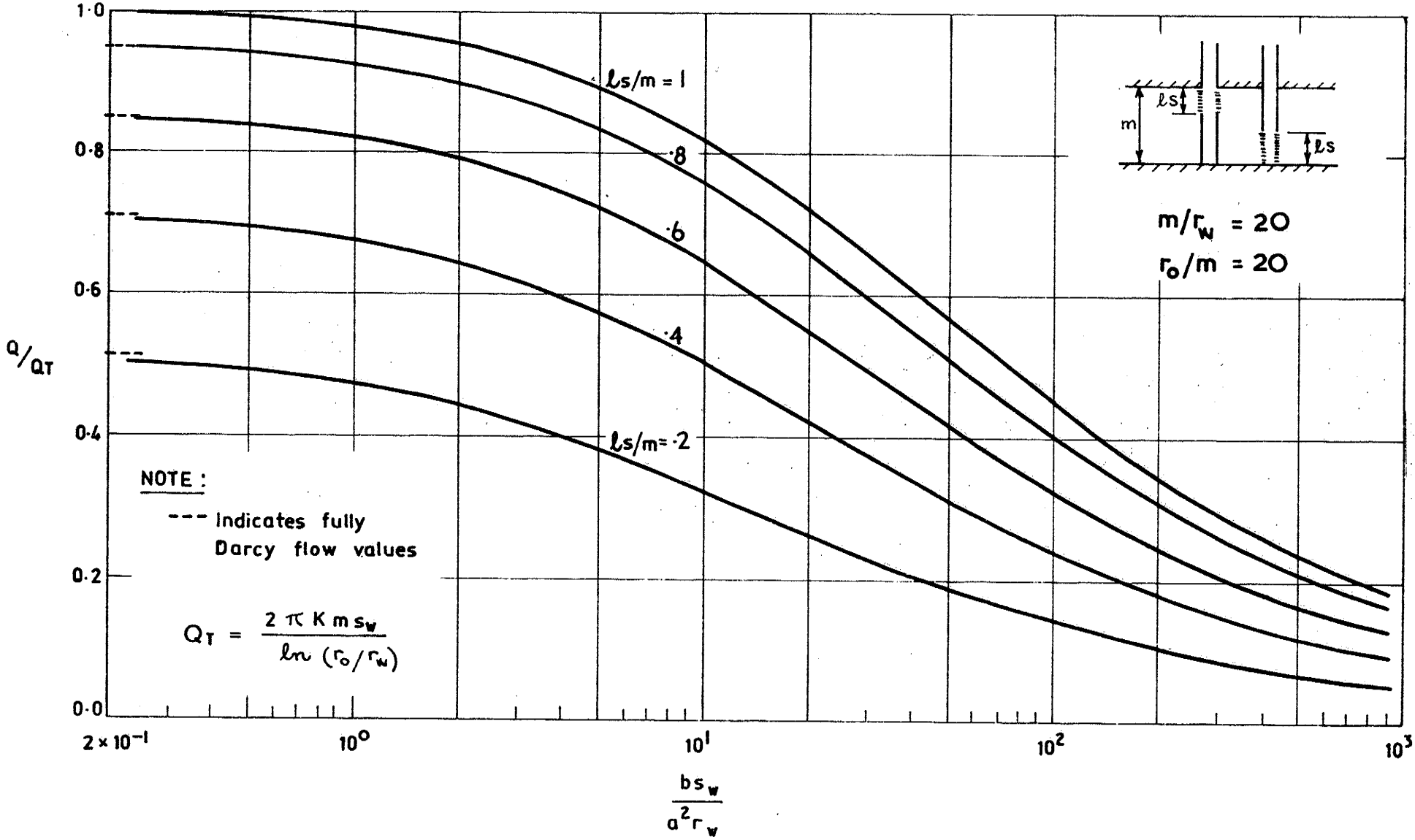

FIGURE A3·8: EFFECT OF NON-LINEAR FLOW ON WELL DRAWDOWN – DISCHARGE RELATIONSHIP. CONFINED AQUIFER

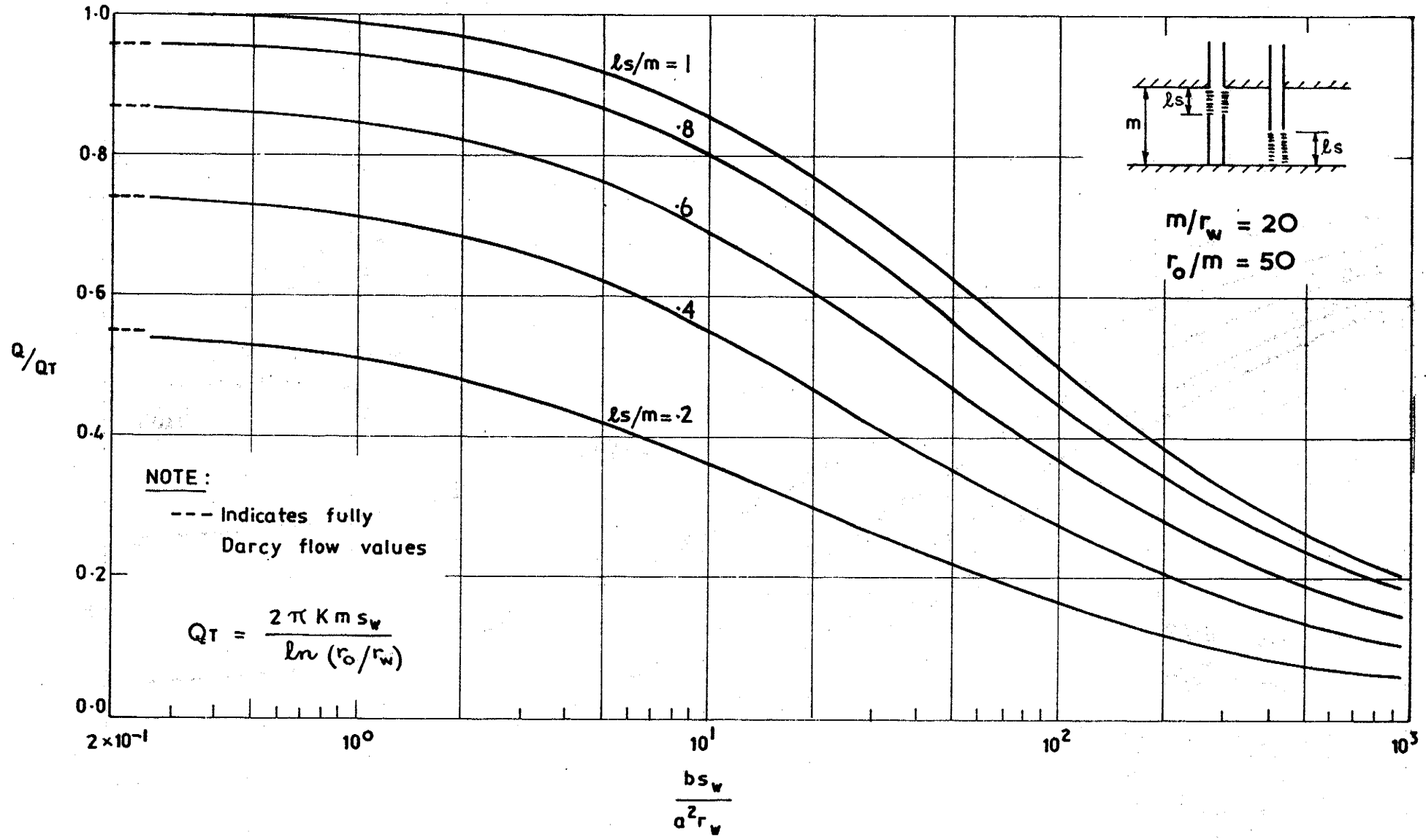

FIGURE A3·9: EFFECT OF NON-LINEAR FLOW ON WELL DRAWDOWN-DISCHARGE RELATIONSHIP. CONFINED AQUIFER

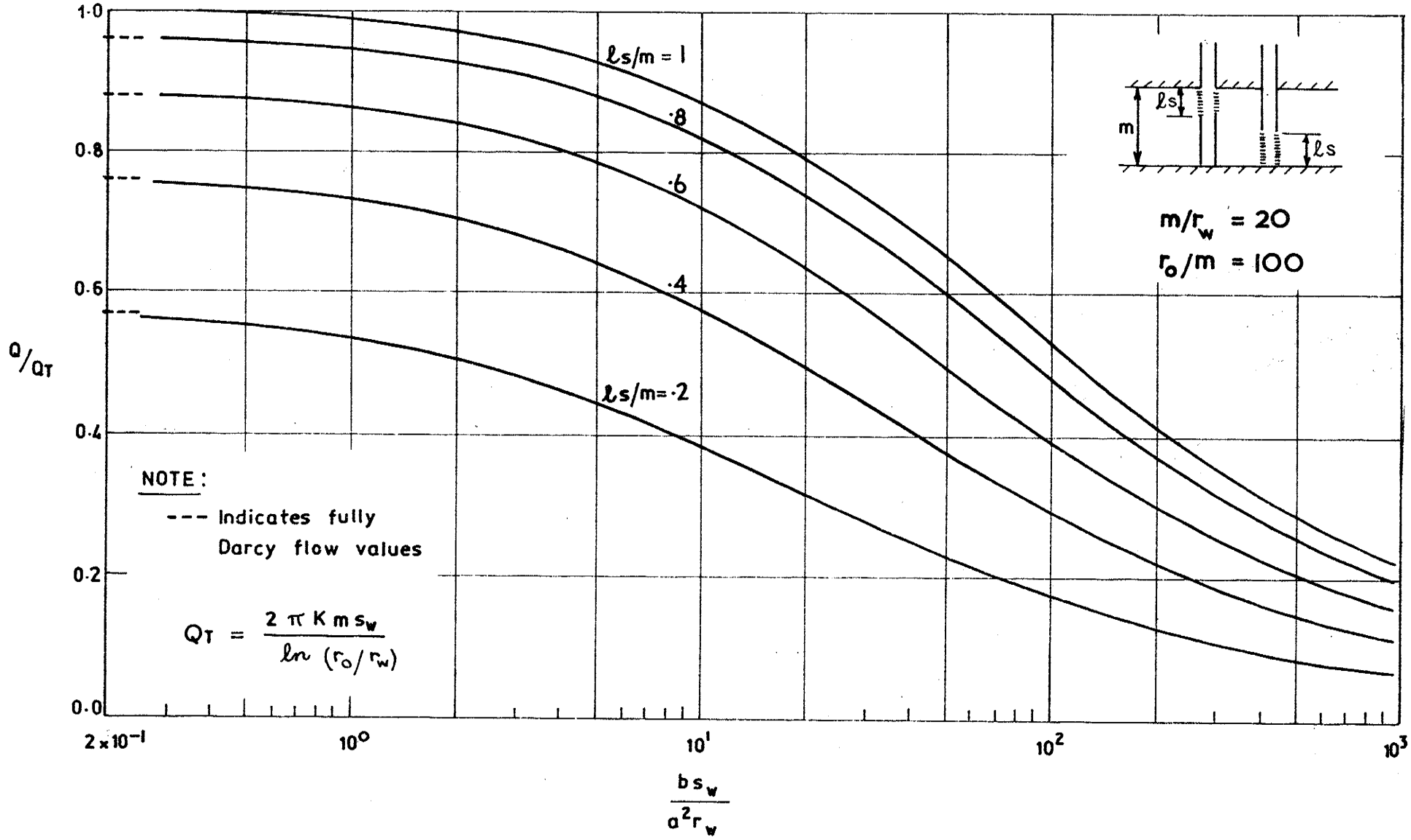

FIGURE A3·10: EFFECT OF NON-LINEAR FLOW ON WELL DRAWDOWN-DISCHARGE RELATIONSHIP. CONFINED AQUIFER

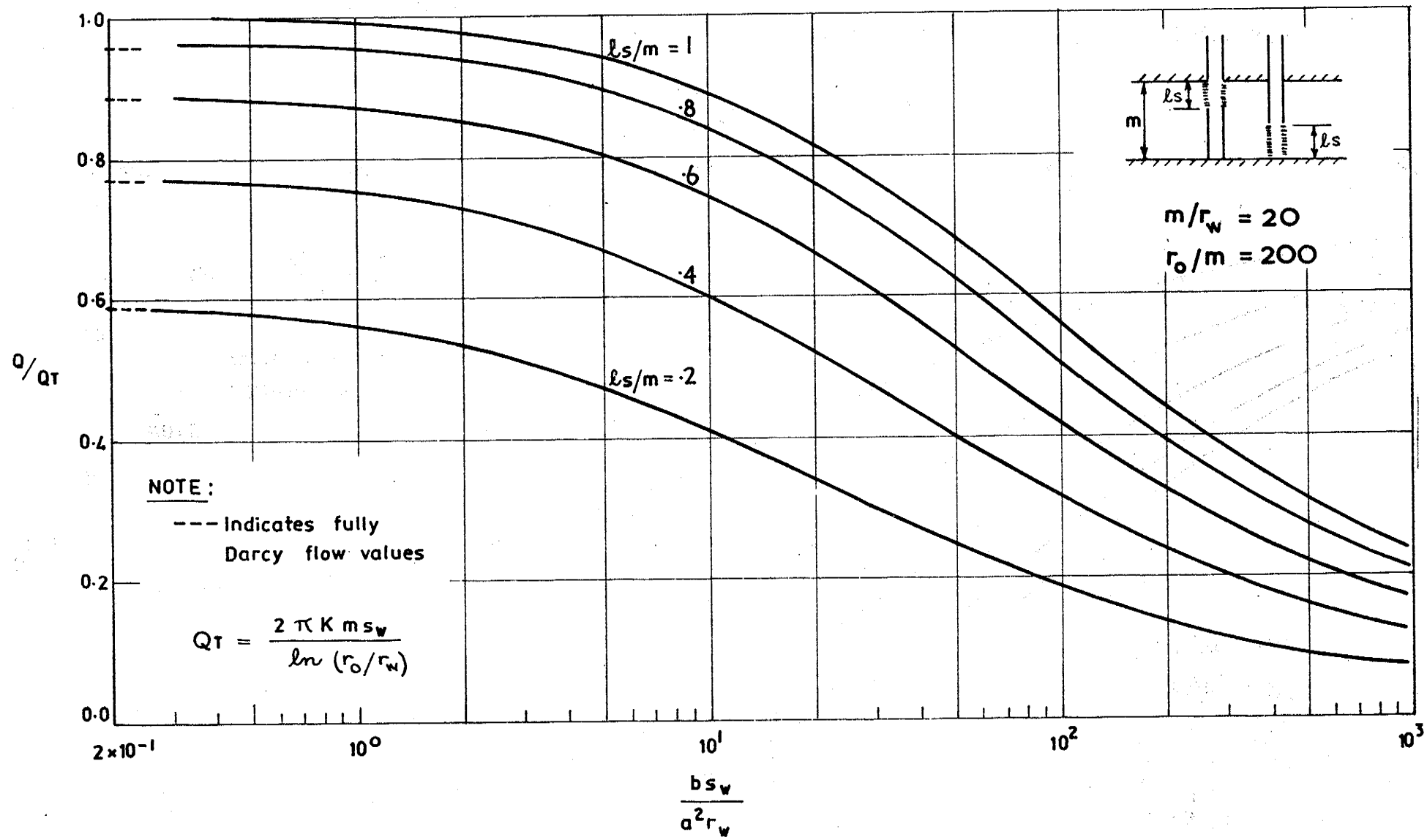

FIGURE A3·11: EFFECT OF NON-LINEAR FLOW ON WELL DRAWDOWN-DISCHARGE RELATIONSHIP. CONFINED AQUIFER

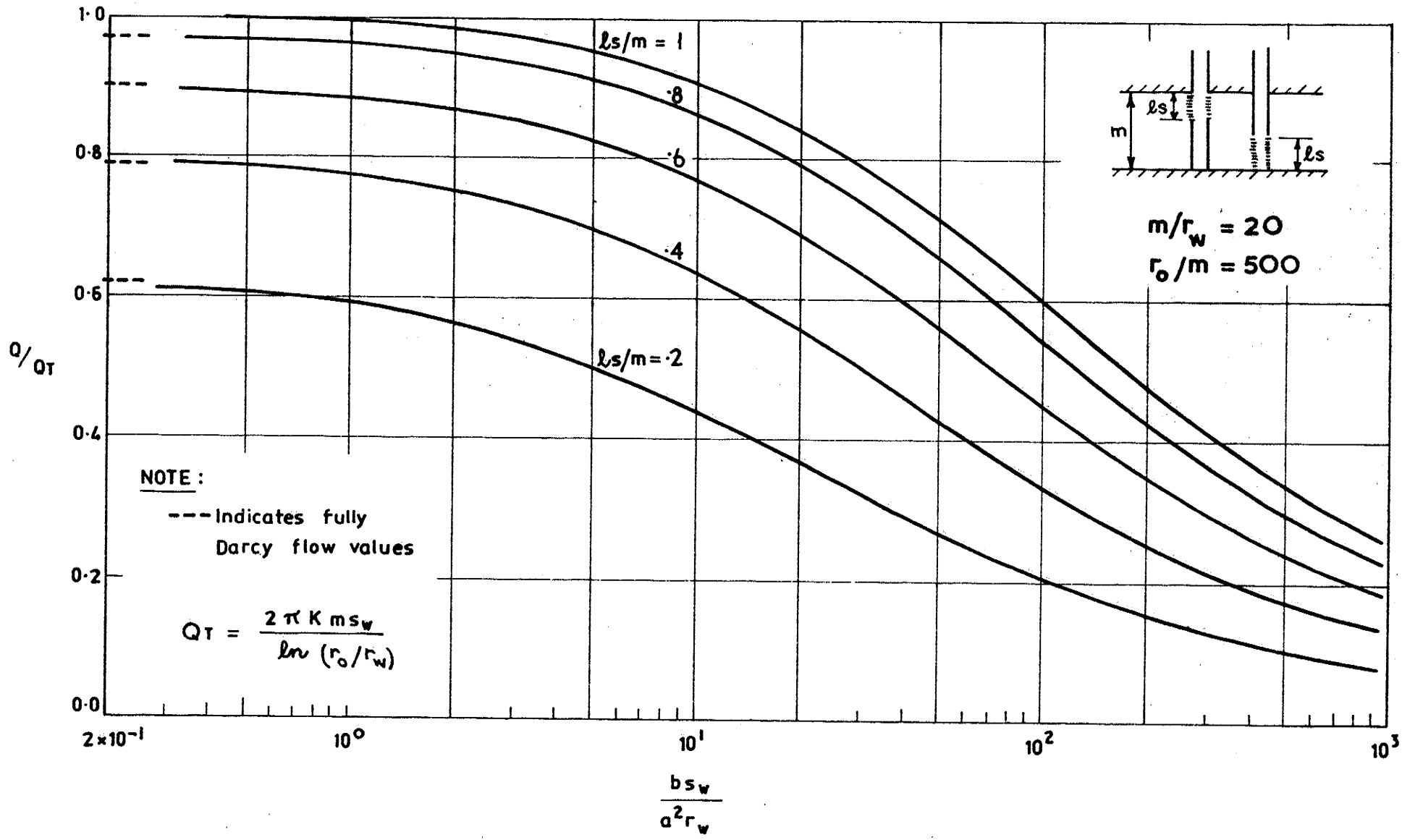

FIGURE A3·12: EFFECT OF NON-LINEAR FLOW ON WELL DRAWDOWN-DISCHARGE RELATIONSHIP. CONFINED AQUIFER

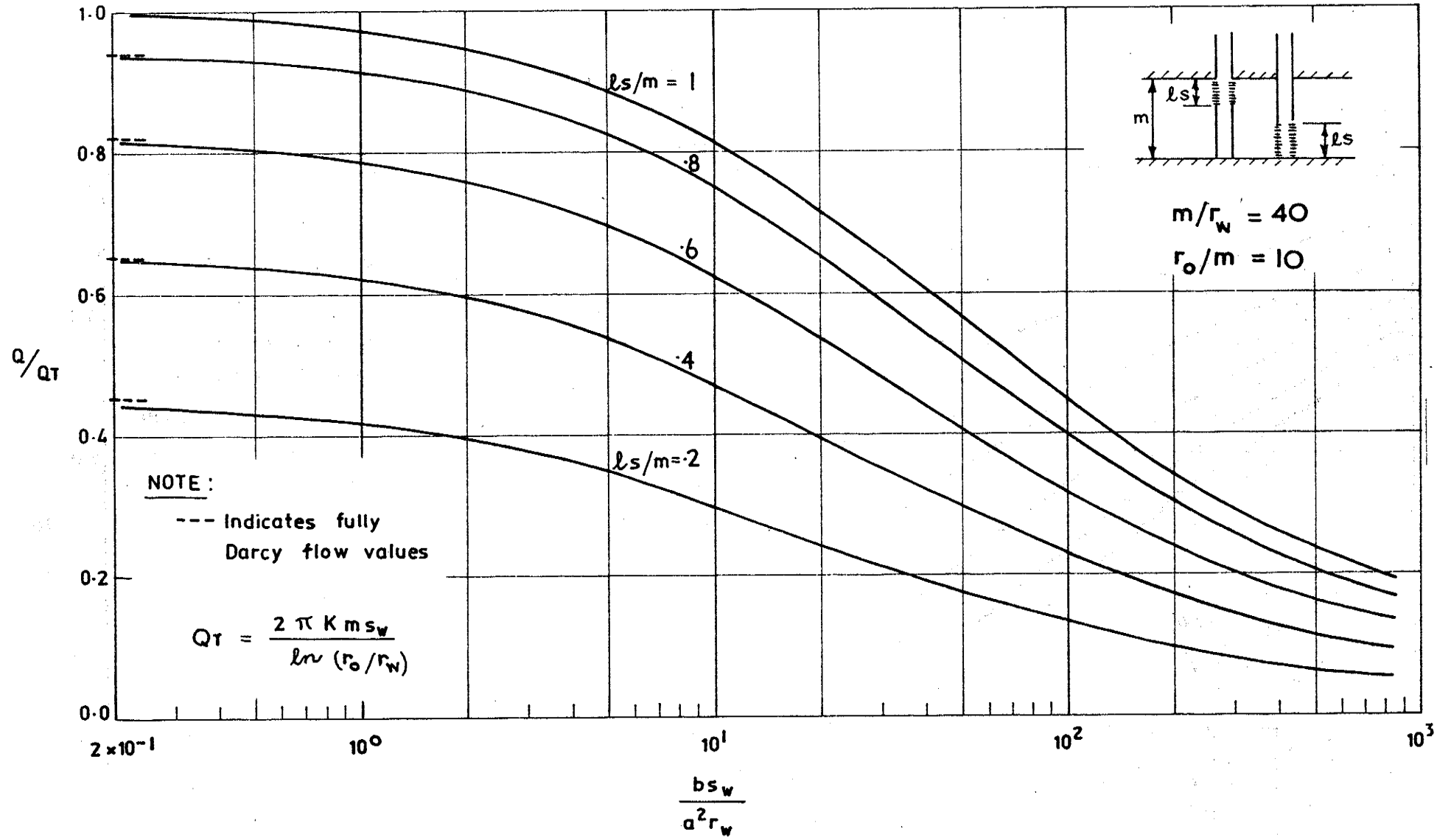

FIGURE A3·13: EFFECT OF NON-LINEAR FLOW ON WELL DRAWDOWN-DISCHARGE RELATIONSHIP. CONFINED AQUIFER

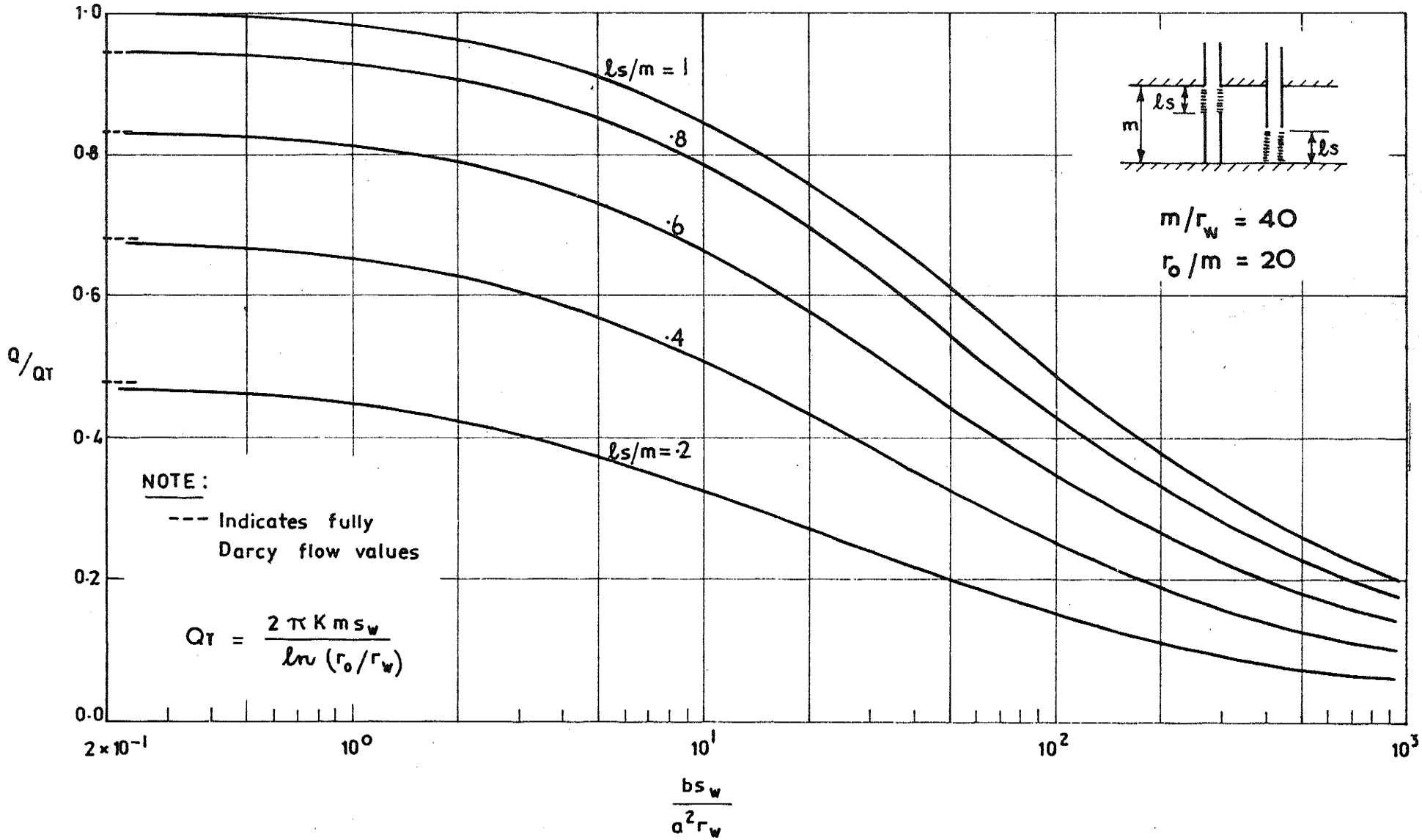

FIGURE A3·14: EFFECT OF NON-LINEAR FLOW ON WELL DRAWDOWN-DISCHARGE RELATIONSHIP. CONFINED AQUIFER

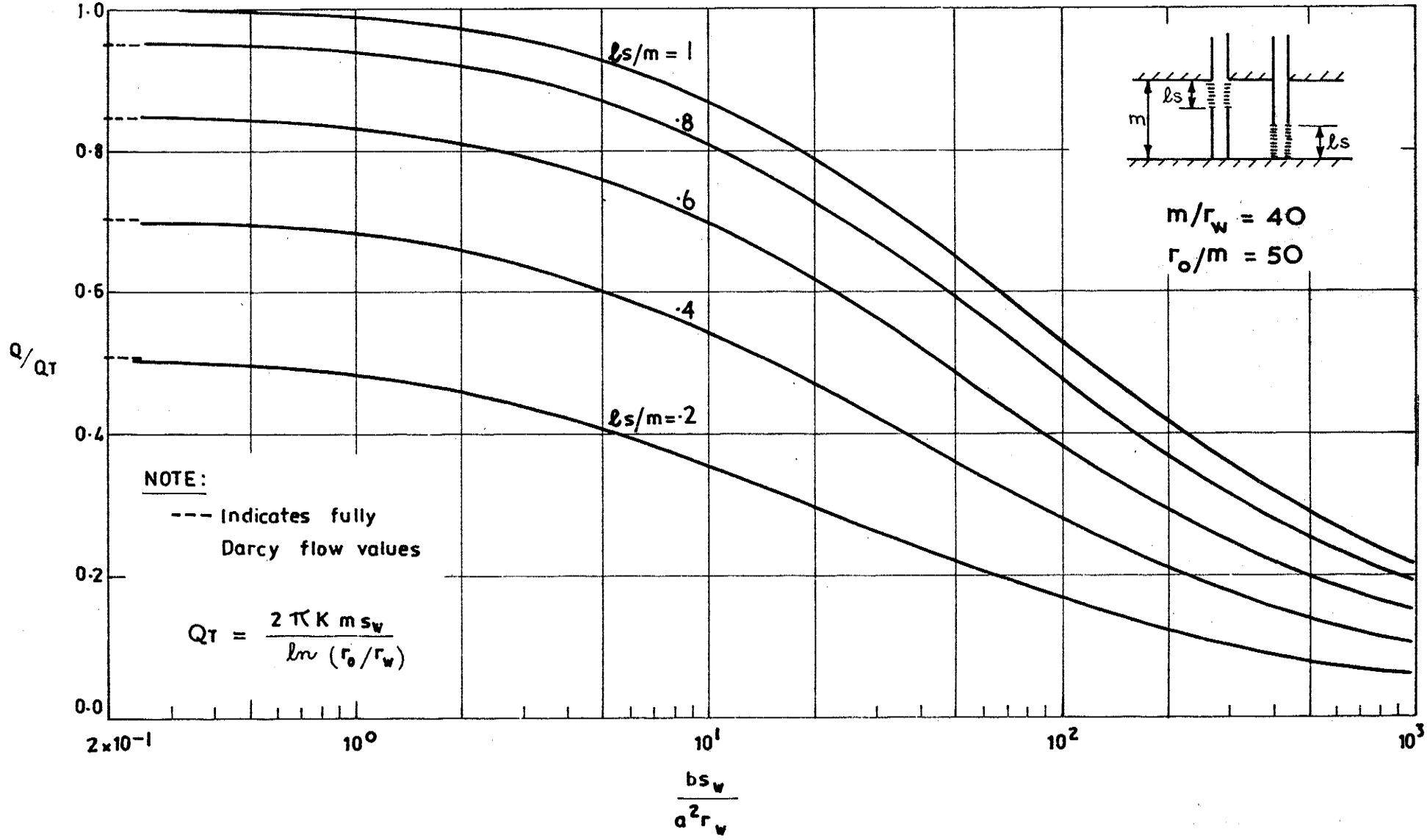

FIGURE A3·15: EFFECT OF NON-LINEAR FLOW ON WELL DRAWDOWN-DISCHARGE RELATIONSHIP. CONFINED AQUIFER

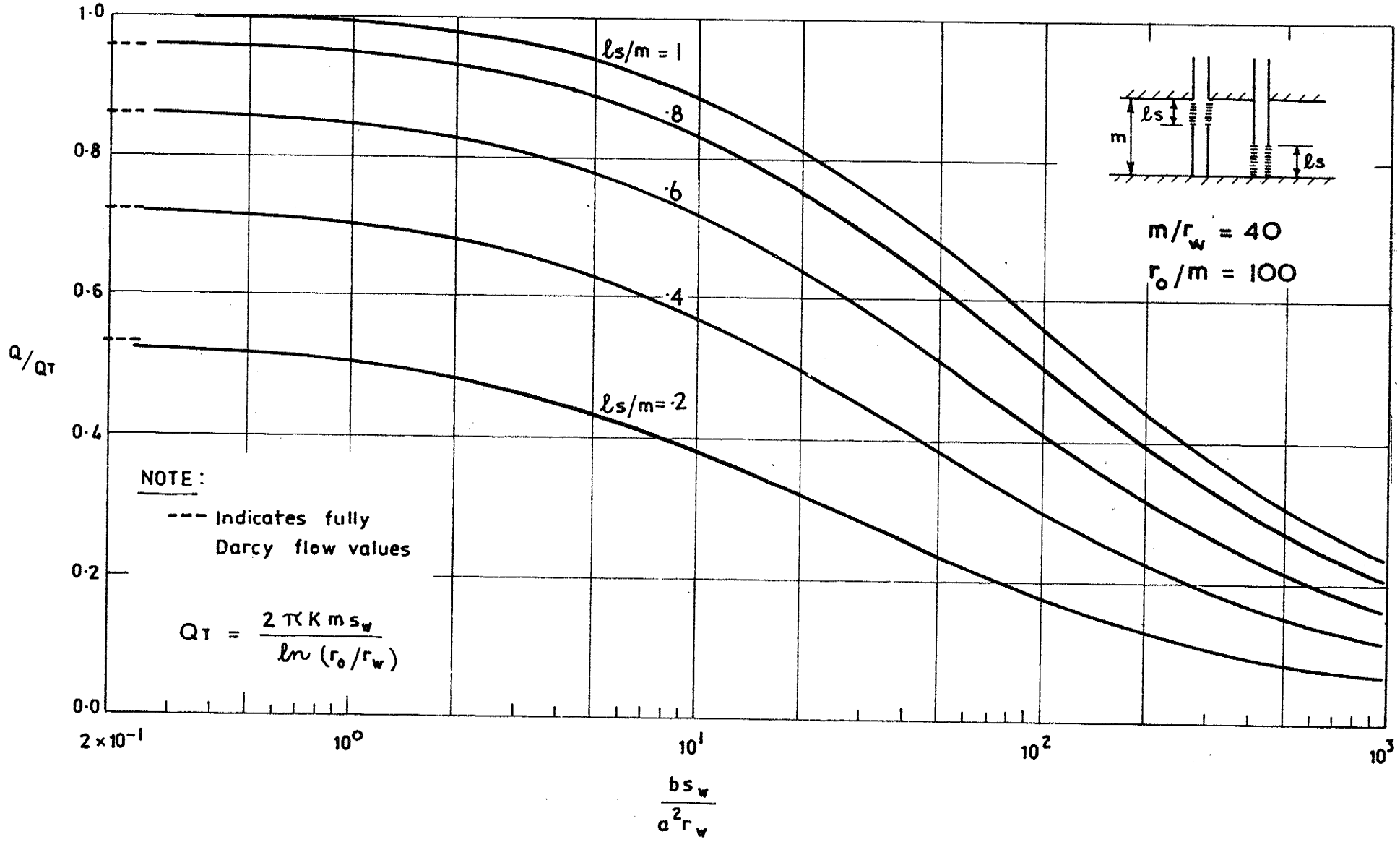

FIGURE A3·16: EFFECT OF NON-LINEAR FLOW ON WELL DRAWDOWN - DISCHARGE RELATIONSHIP. CONFINED AQUIFER

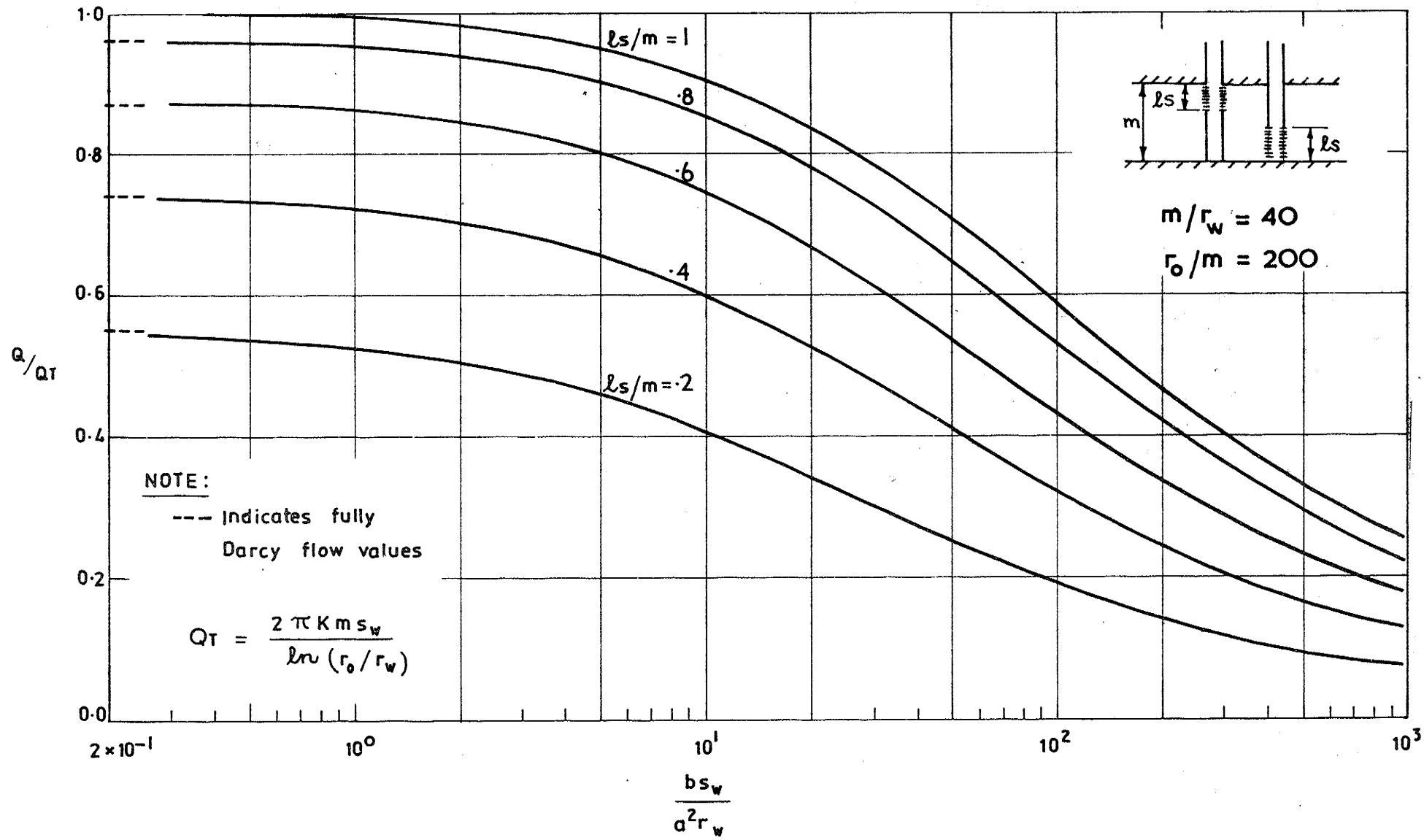

FIGURE A3·17: EFFECT OF NON-LINEAR FLOW ON WELL DRAWDOWN-DISCHARGE RELATIONSHIP. CONFINED AQUIFER

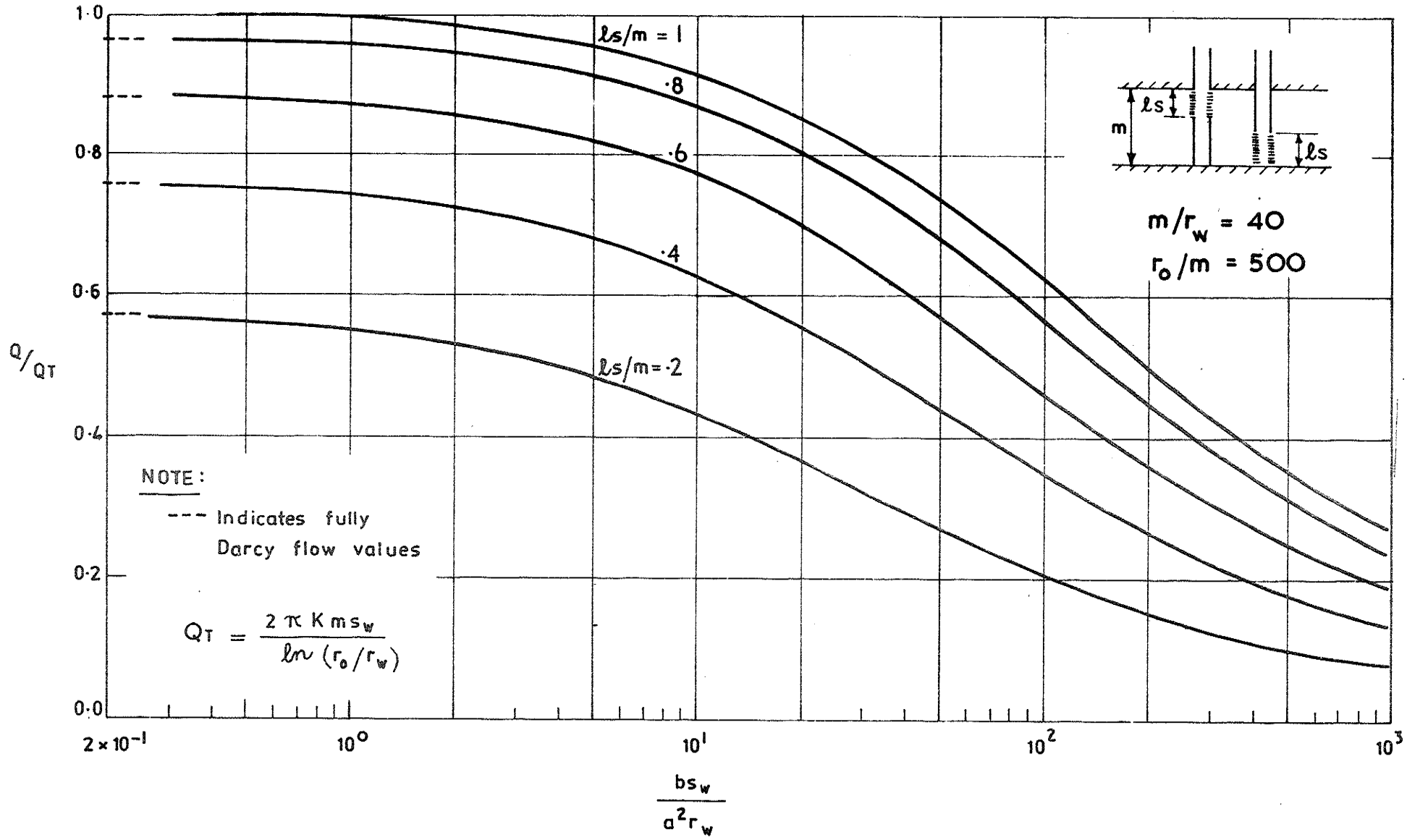

FIGURE A3·18: EFFECT OF NON-LINEAR FLOW ON WELL DRAWDOWN-DISCHARGE RELATIONSHIP. CONFINED AQUIFER

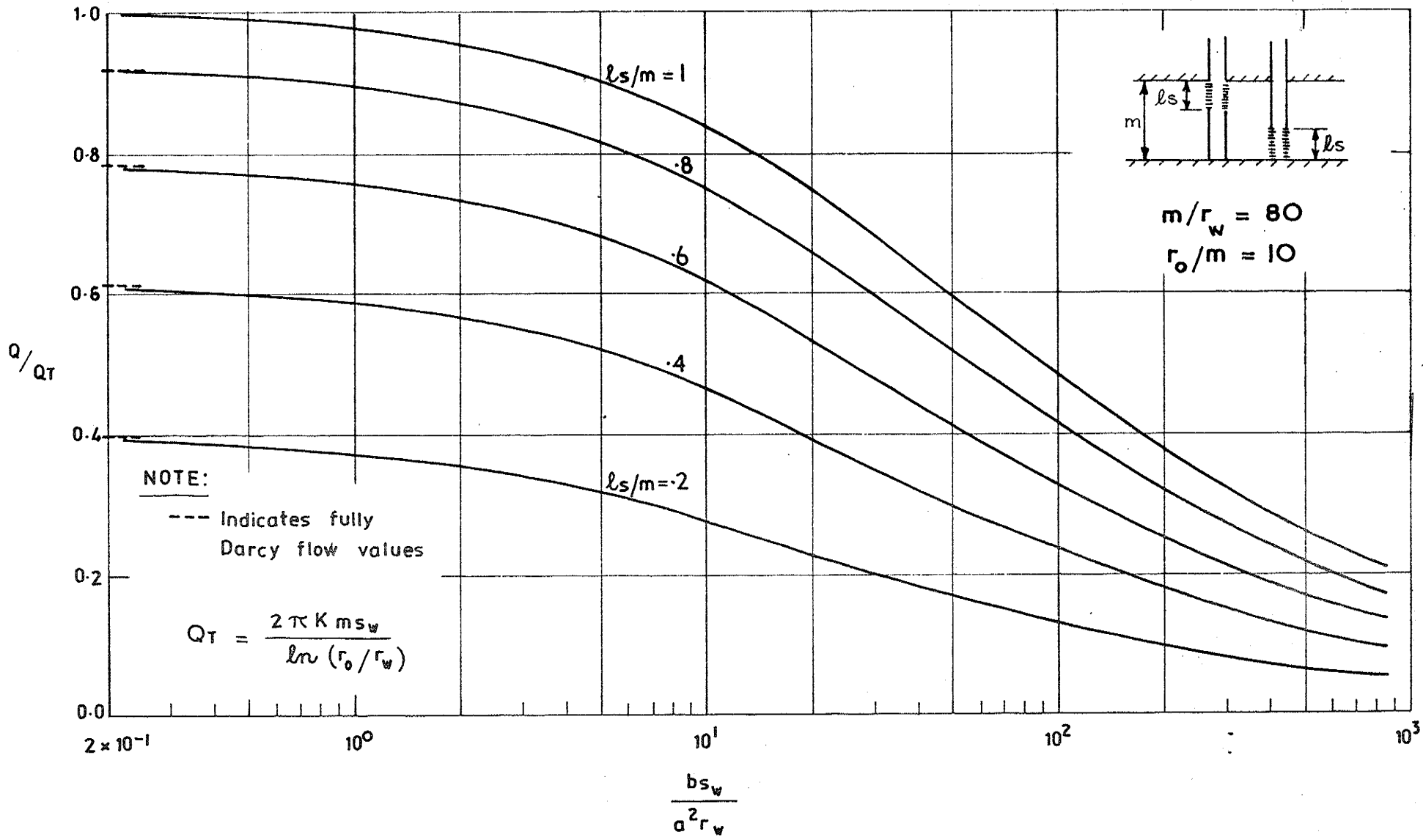

FIGURE A3-19: EFFECT OF NON-LINEAR FLOW ON WELL DRAWDOWN-DISCHARGE RELATIONSHIP. CONFINED AQUIFER

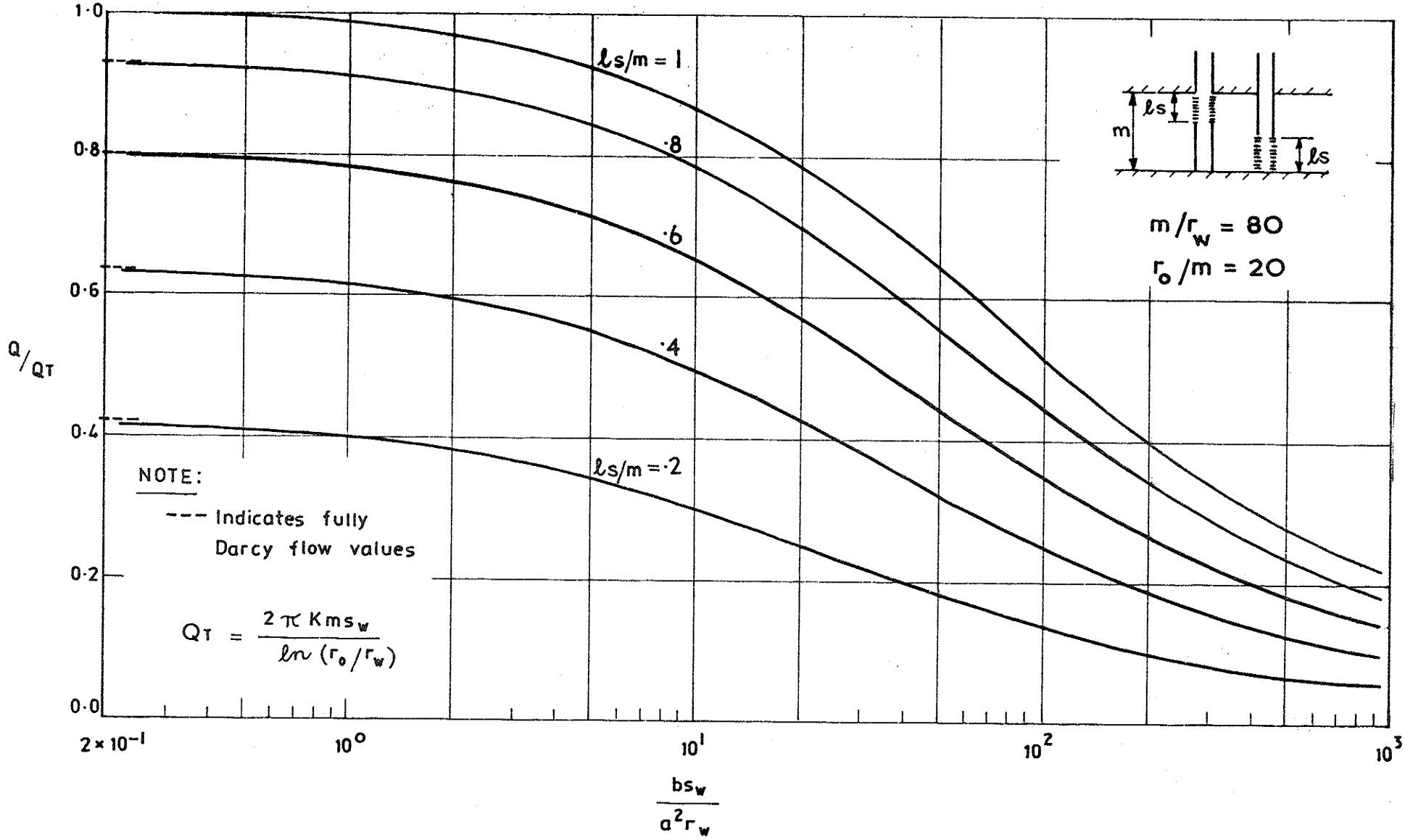

FIGURE A3·20: EFFECT OF NON-LINEAR FLOW ON WELL DRAWDOWN-DISCHARGE RELATIONSHIP. CONFINED AQUIFER

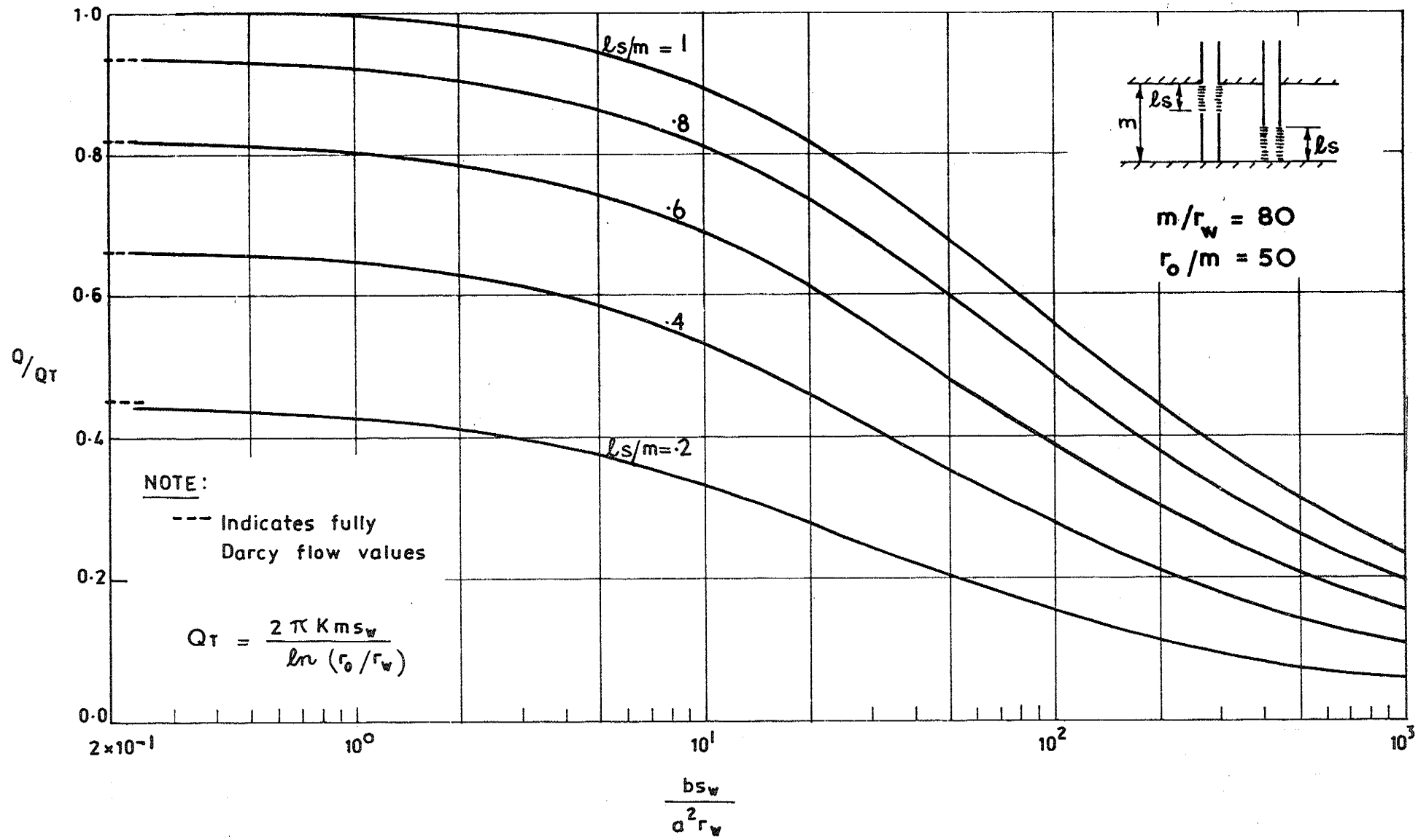

FIGURE A3·21: EFFECT OF NON-LINEAR FLOW ON WELL DRAWDOWN-DISCHARGE RELATIONSHIP. CONFINED AQUIFER

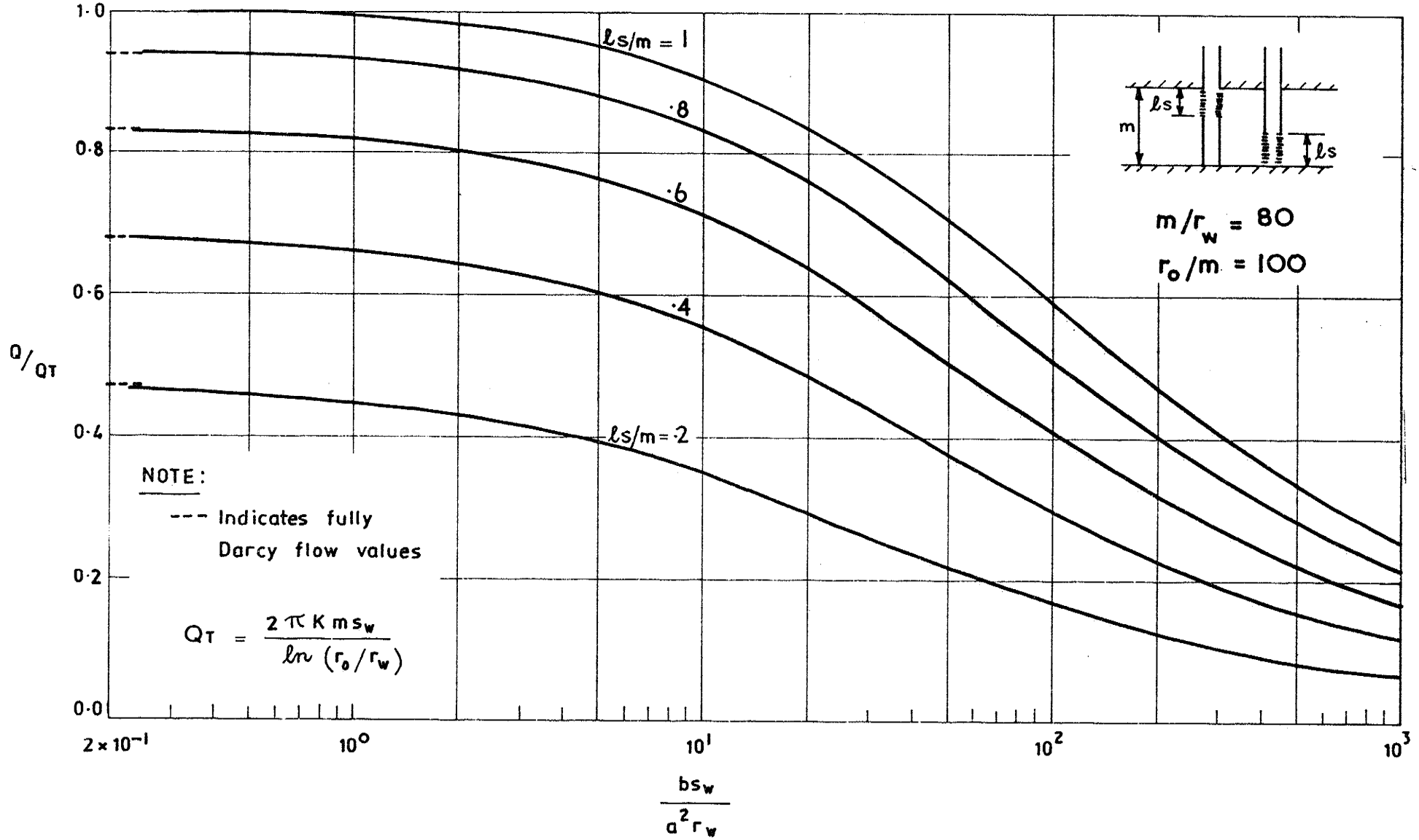

FIGURE A3·22: EFFECT OF NON-LINEAR FLOW ON WELL DRAWDOWN-DISCHARGE RELATIONSHIP. CONFINED AQUIFER

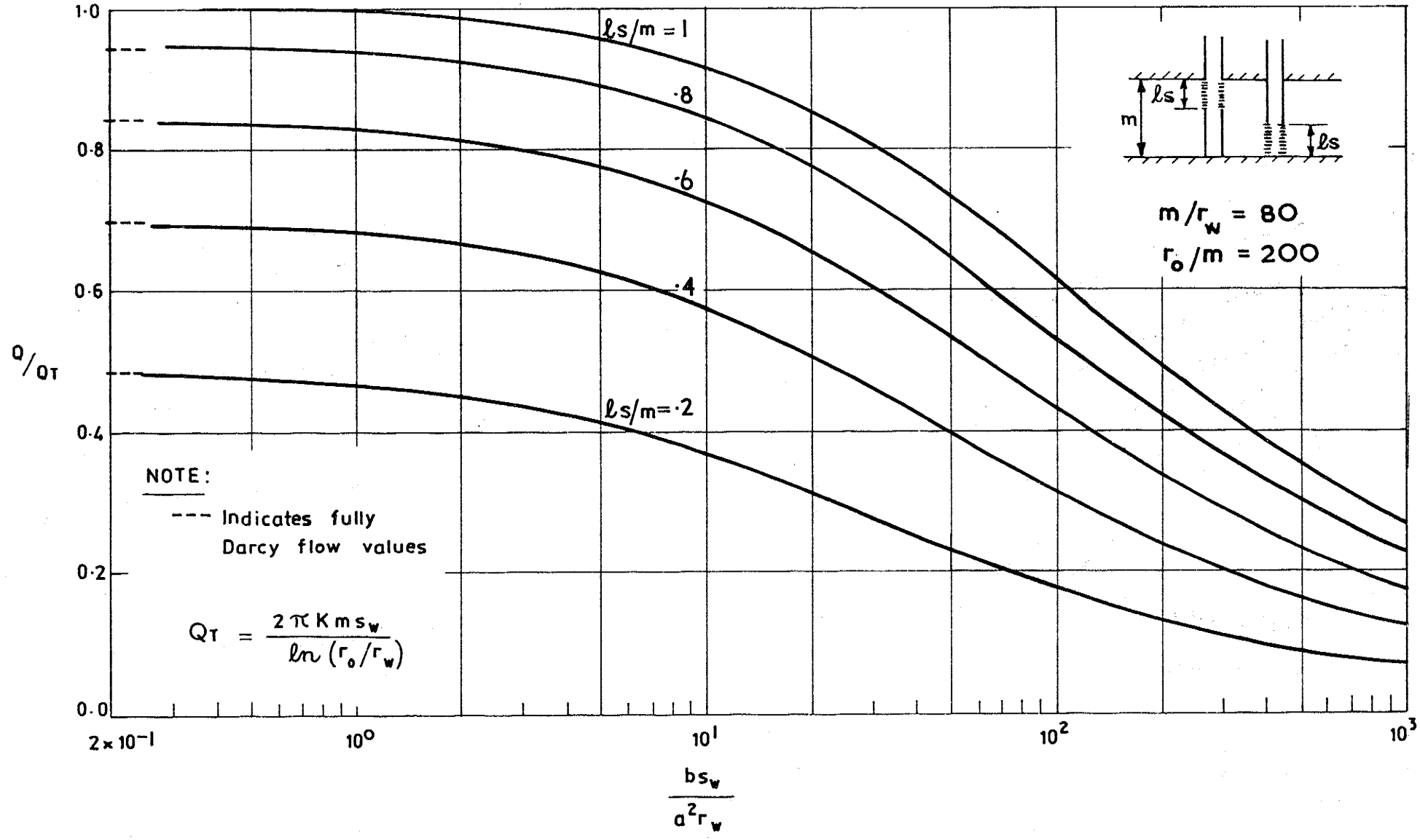

FIGURE A3·23: EFFECT OF NON-LINEAR FLOW ON WELL DRAWDOWN-DISCHARGE RELATIONSHIP. CONFINED AQUIFER

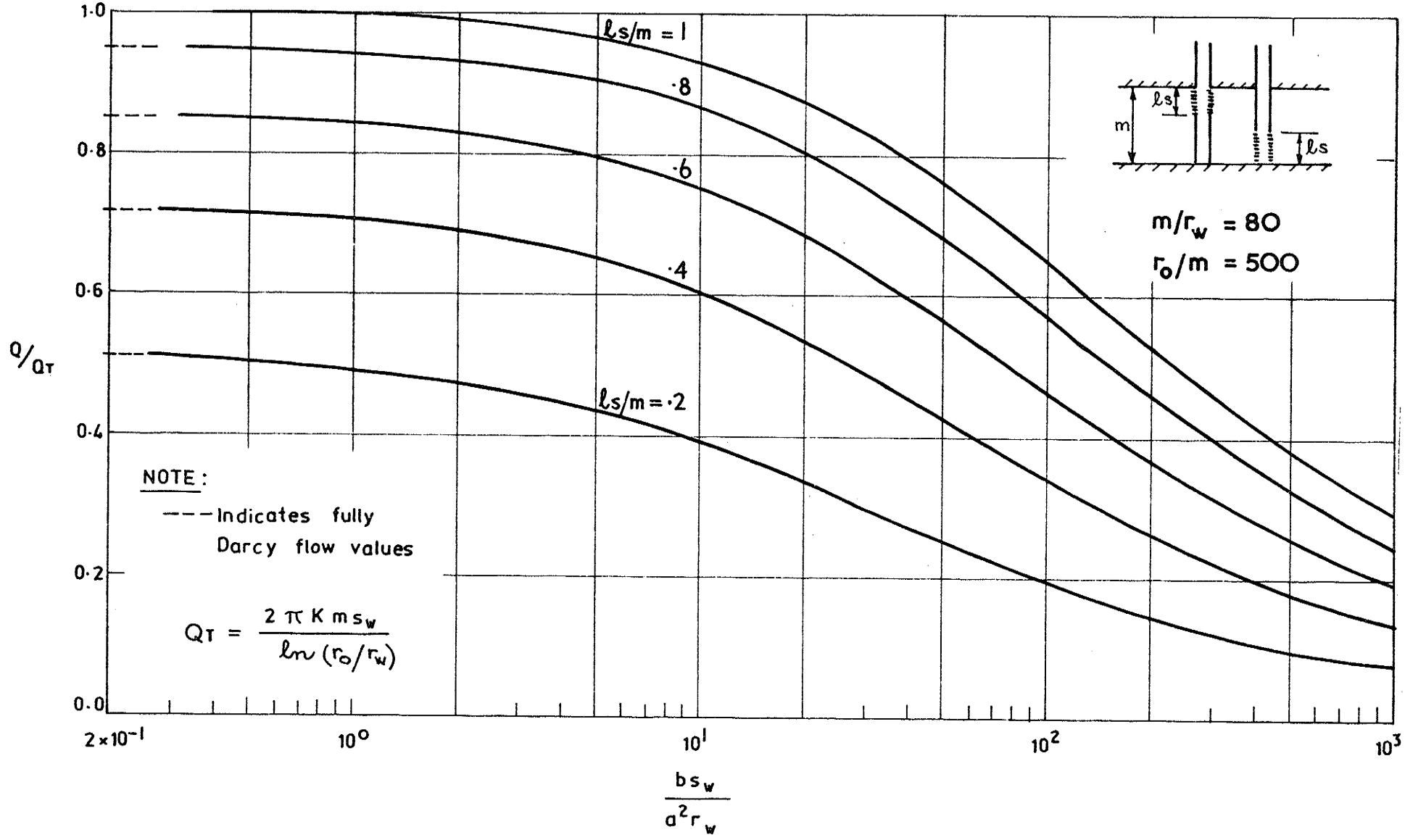

FIGURE A3·24: EFFECT OF NON-LINEAR FLOW ON WELL DRAWDOWN-DISCHARGE RELATIONSHIP. CONFINED AQUIFER

APPENDIX I

FINITE ELEMENT MATRICES

A1.1 Triangular Ring Element

Consider the typical triangular ring element shown in Figure A1.1.

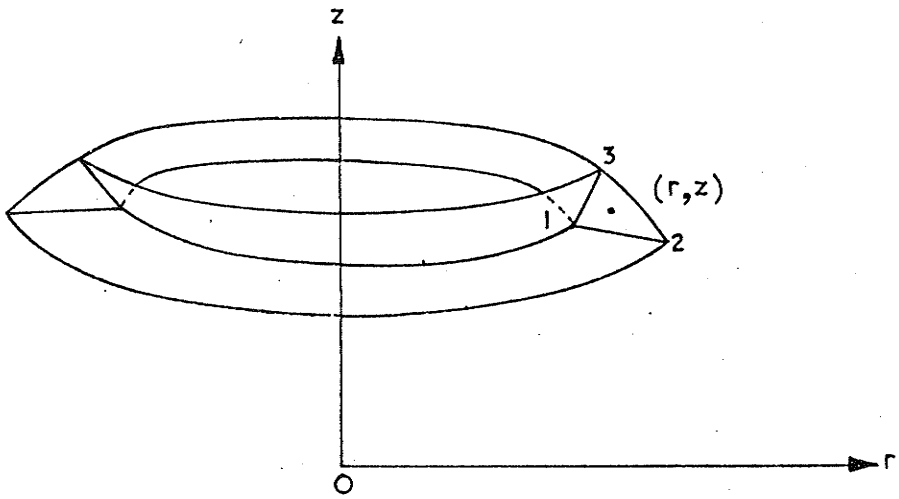

FIGURE A1·1: A TRIANGULAR RING ELEMENT

If the hydraulic head distribution at point (r, z) in the element is represented by a linear function of r and z in terms of the nodal values, then it can be shown (Zienkiewicz and Cheung (1967)) that the shape functions may be expressed as

$$N_I = a_I + b_I r + c_I z \qquad \text{(A1.1)}$$

where a_1, b_1 and c_1 are given by

$$a_1 = (r_2 z_3 - r_3 z_2)/2 \qquad \text{(A1.2a)}$$

$$b_1 = (z_2 - z_3)/2 \qquad \text{(A1.2b)}$$

$$c_1 = (r_3 - r_2)/2 \qquad \text{(A1.2c)}$$

and the remaining coefficients are obtained by cyclic permutation of subscripts. Δ is the area of the triangle 1-2-3,

$$\Delta = \frac{1}{2} \begin{vmatrix} 1 & r_1 & z_1 \\ 1 & r_2 & z_2 \\ 1 & r_3 & z_3 \end{vmatrix} \qquad \text{(A1.2d)}$$

From equation (A1.1) it follows that

$$\frac{\partial N_I}{\partial r} = b_I \qquad \text{(A1.3a)}$$

$$\frac{\partial N_I}{\partial z} = c_I \qquad \text{(A1.3b)}$$

Hence the matrix $[S]^T$ from equation (4.26) may be written as

$$[S]^T = \begin{bmatrix} b_1 & b_2 & b_3 \\ c_1 & c_2 & c_3 \end{bmatrix}^T \qquad \text{(A1.4)}$$

For the cylindrical coordinate system, the hydraulic conductivity matrix from equation (4.27) is given by

$$[K] = \begin{bmatrix} K_{rr} & K_{rz} \\ K_{zr} & K_{zz} \end{bmatrix} \qquad \text{(A1.5)}$$

The shape function matrix for triangular elements is

$$[N] = [N_1, N_2, N_3] \qquad \text{(A1.6)}$$

where N_1, N_2, N_3 are given by equation (A1.1).

The expressions for element matrices $[\bar{G}]^e$ and $[G]^e$ from equations (4.25a) and (4.33) can be obtained by direct integration, noting that dR has to be replaced by

$$dR = 2\pi \cdot r \; dr \; dz \qquad \text{(A1.7)}$$

The components of matrices $[\bar{G}]^e$ and $[G]^e$ are given by

$$\bar{G}^e_{IJ} = \int_{R^e} \left[K_{ij} \frac{\partial N_I}{\partial x_i} \frac{\partial N_J}{\partial x_j} \right] 2\pi \, r \, dr dz \qquad \text{(A1.8a)}$$

and $$G_{IJ}^{e} = \int_{R^e} \left[C \quad \frac{\partial N_I}{\partial x_i} \quad \frac{\partial N_J}{\partial x_i} \right] 2\pi \, r \, dr \, dz \qquad \text{(A1.8b)}$$

where the range of subscripts i and j is from 1 to 2 such that $x_1 = r$ and $x_2 = z$. Equations (A1.8) may be approximated by

$$\bar{G}_{IJ}^{e} = 2\pi \bar{r} \Delta (K_{rr} b_I b_J + K_{rz} b_I c_J + K_{zr} c_I b_J + K_{zz} c_I c_J) \qquad \text{(A1.9a)}$$

$$G_{IJ}^{e} = 2\pi \bar{r} \Delta C (b_I b_J + c_I c_J) \qquad \text{(A1.9b)}$$

where $\bar{r}$ is the centroidal radius of the triangular plane section. r and z are not regarded as small letter subscripts in equation (A1.9a).

The integration for the matrix elements of $[D]^e$ and $\{F\}^e$ (equations (4.25b) and (4.25c)) requires more effort. The two matrices have been evaluated by Parekh (1967) for two-dimensional plane triangular elements. They may be simply adapted to triangular ring elements resulting in

$$[D]^e = \frac{2\pi \bar{r} S_s \Delta}{3} \begin{bmatrix} \frac{1}{2} & \frac{1}{4} & \frac{1}{4} \\ \frac{1}{4} & \frac{1}{2} & \frac{1}{4} \\ \frac{1}{4} & \frac{1}{4} & \frac{1}{2} \end{bmatrix} \qquad \text{(A1.10)}$$

$$\{F\}^e = 2\pi \bar{r} \bar{q} L \begin{bmatrix} \frac{1}{2} \\ \frac{1}{2} \\ 0 \end{bmatrix} \qquad \text{(A1.11)}$$

where it is assumed that side 1-2 of triangle 1-2-3 corresponds to the exterior boundary portion on which the flux is prescribed and that $\bar{q}$ is constant on side 1-2 of the triangle. The length of this side is denoted by L.

A1.2 Curved, Isoparametric, Quadrilateral Elements

In solving two-dimensional flow problems "quadrilateral" elements may be used to improve the accuracy of the numerical solution. This

type of element provides higher forms of approximation to the hydraulic head function than a simple triangular element. Generally the use of higher order elements allows an appreciable reduction in the total number of nodes required in the flow region for a given degree of accuracy.

Consider the general elements shown in Figure A1.2 where the position within an element can be defined by the local curvilinear coordinates (ξ , η) such that ξ and η take values of $\pm$ 1 on the sides of the elements.

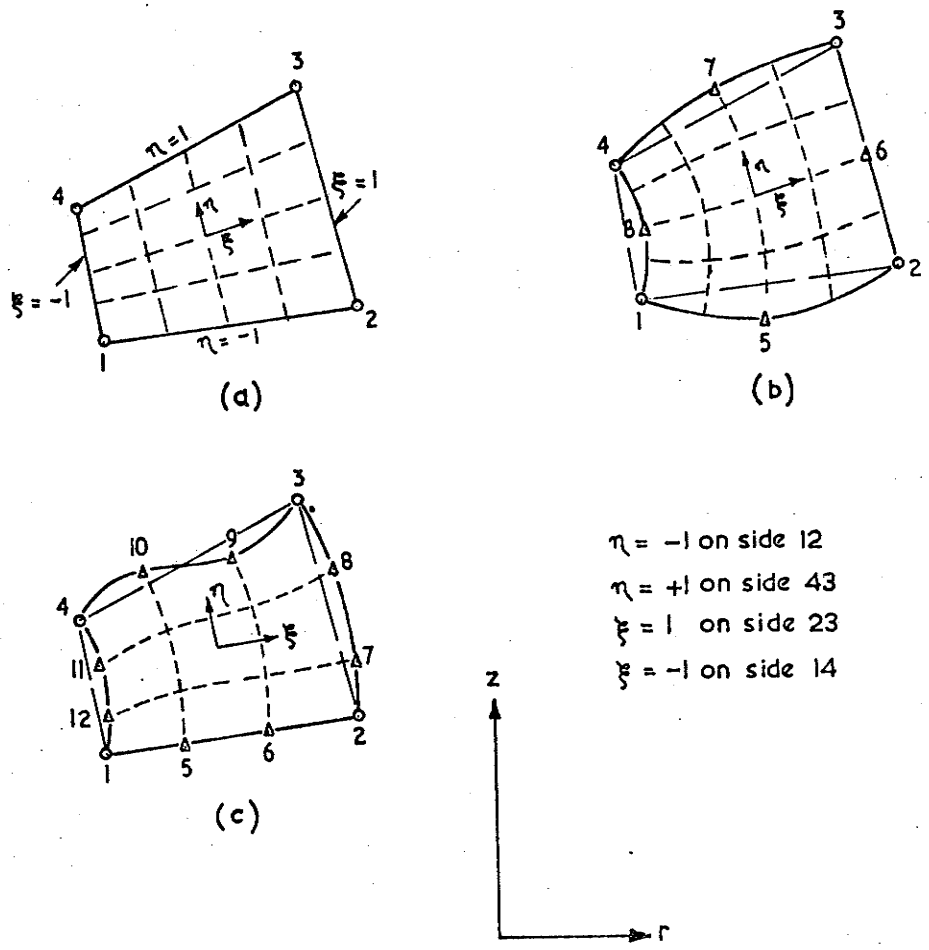

FIGURE A1·2: ISOPARAMETRIC QUADRILATERAL ELEMENTS

A quadrilateral ring element for use in axisymmetric well flow problems can be generated by revolving an element of Figure A1.2 about the z axis.

The relationships between the global (r, z) coordinates and the local (ξ, η) coordinates are given by

$$r = N_I \ (\xi, \eta) \ r_I \qquad \text{(A1.12a)}$$

$$z = N_I \ (\xi, \eta) \ z_I \qquad \text{(A1.12b)}$$

where I ranges from 1 to m the number of nodes in the element.

The expressions for the shape functions N_I have been developed by Ergatoudis et al (1968) and may be written in terms of the variables $\xi_o = \xi \xi_I$ and $\eta_o = \eta \eta_I$ as follows:-

(a) Linear Element - Figure A1.2(a)

$$N_I = \tfrac{1}{4} (1 + \xi_o) (1 + \eta_o) \qquad \text{(A1.13)}$$

(b) Parabolic Element - Figure A1.2(b)

Corner Nodes $N_I = \tfrac{1}{4} (1 + \xi_o)(1 + \eta_o) (\xi_o + \eta_o - 1)$ (A1.14)

Mid-Side Nodes $\xi_I = 0$; $N_I = \tfrac{1}{2} (1 - \xi^2) (1 + \eta_o)$

$\eta_I = 0$; $N_I = \tfrac{1}{2} (1 - \eta^2) (1 + \xi_o)$

(c) Cubic elements - Figure A1.2(c)

Corner Nodes $N_I = \dfrac{1}{32} (1 + \xi_o)(1 + \eta_o) \left[-10 + 9(\xi^2 + \eta^2) \right]$ (A1.15)

$\xi_I = \pm 1$ and $\eta_I = \pm 1/3$, $N_I = \dfrac{9}{32} (1 + \xi_o)(1 - \eta^2)(1 + 9 \eta_o)$

$\eta_I = \pm 1$ and $\xi_I = \pm 1/3$, $N_I = \dfrac{9}{32} (1 + \eta_o)(1 - \xi^2)(1 + 9 \xi_o)$

The differential operators with respect to r and z and those with respect to ξ and η are related by

$$\begin{bmatrix} \dfrac{\partial}{\partial r} \\ \dfrac{\partial}{\partial z} \end{bmatrix} = [J]^{-1} \begin{bmatrix} \dfrac{\partial}{\partial \xi} \\ \dfrac{\partial}{\partial \eta} \end{bmatrix} \qquad \text{(A1.16)}$$

where $[J]$ is the Jacobian transformation matrix which is given by

$$[J] = \begin{bmatrix} \frac{\partial r}{\partial \xi} & \frac{\partial z}{\partial \xi} \\ \frac{\partial r}{\partial \eta} & \frac{\partial z}{\partial \eta} \end{bmatrix} \qquad \text{(A1.17a)}$$

$$[J] = \begin{bmatrix} \frac{\partial N_1}{\partial \xi} & \frac{\partial N_2}{\partial \xi} & \cdots\cdots & \frac{\partial N_m}{\partial \xi} \\ \frac{\partial N_1}{\partial \eta} & \frac{\partial N_2}{\partial \eta} & \cdots\cdots & \frac{\partial N_m}{\partial \eta} \end{bmatrix} \begin{bmatrix} r_1 & z_1 \\ r_2 & z_2 \\ \vdots & \vdots \\ r_m & z_m \end{bmatrix} \qquad \text{(A1.17b)}$$

Now $dR = 2\pi r\, dr dz$ (A1.18a)

and $dr dz = |J|\, d\xi\, d\eta$ (A1.18b)

where $|J|$ is the determinant of the Jacobian matrix.

The slope matrix [S] (equation (4.26)) may now be expressed as

$$[S] = [J]^{-1} \begin{bmatrix} \frac{\partial N_1}{\partial \xi} & \frac{\partial N_2}{\partial \xi} & \cdots\cdots & \frac{\partial N_m}{\partial \xi} \\ \frac{\partial N_1}{\partial \eta} & \frac{\partial N_2}{\partial \eta} & \cdots\cdots & \frac{\partial N_m}{\partial \eta} \end{bmatrix} \qquad \text{(A1.19)}$$

Hence the element matrices $[\bar{G}]^e$, $[G]^e$ and $[D]^e$ (equations (4.25a), (4.33) and (4.25b)) are now obtained as

$$[\bar{G}]^e = 2\pi \int_{-1}^{1} \int_{-1}^{1} [S]^T [K][S]\, N_I\, r_I\, |J|\, d\xi\, d\eta \qquad \text{(A1.20a)}$$

$$[G]^e = 2\pi \int_{-1}^{1} \int_{-1}^{1} C\, [S]^T [S]\, N_I\, r_I\, |J|\, d\xi\, d\eta \qquad \text{(A1.20b)}$$

$$[D]^e = 2\pi \int_{-1}^{1} \int_{-1}^{1} S_s\, [N]^T [N]\, N_I\, r_I\, |J|\, d\xi\, d\eta \qquad \text{(A1.20c)}$$

Exact integration of these expressions for the matrices of general distorted quadrilateral elements is not feasible and numerical integration is essential. Zienkiewicz and Cheung (1967) have described the procedure for numerically evaluating the definite integrals of equations (A1.20) by employing the Gaussian quadrature formula.

The elements shown in Figure A1.2 have equal order response along all four sides. "Mixed" type elements are possible as shown in Figure A1.3 where a quadrilateral has cubic, linear and parabolic response along sides 3-4, 1-2 and the other two sides respectively.

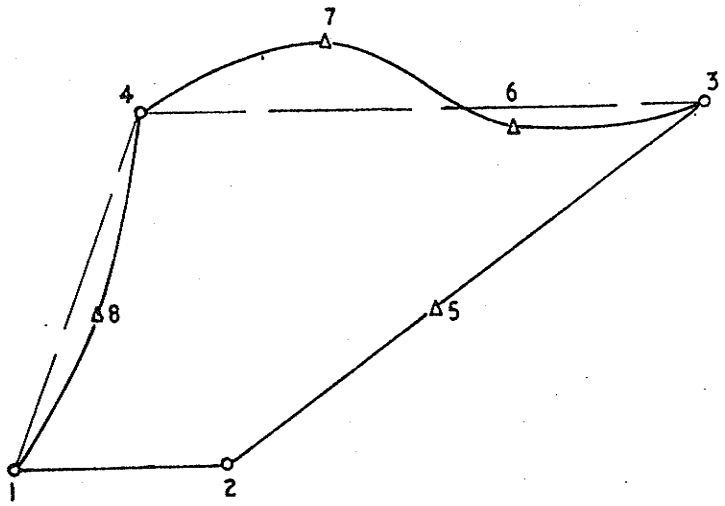

FIGURE A1.3: POSSIBLE "MIXED" TYPE QUADRILATERAL ELEMENT

In the majority of flow problems, necessary finite element mesh refinement will result in the use of several "mixed" type elements. Once the shape functions for such elements are evaluated the element matrix formulations follow the general procedures outlined for elements of Figure A1.2. Several "mixed" type elements were formulated for use in well flow problems to be investigated by the author.

A1.3 Rectangular Ring Elements

A special case arises when the general quadrilateral shaped elements described in the previous section become rectangular. In this case, by employing the technique described in this section for a linear rectangle element, element matrices may be easily generated with a considerable saving in computational time.

Consider a typical linear rectangular element shown in Figure A1.4. The four corner nodes are numbered in an anti-clockwise sense and $\bar{r}$ denotes the radial coordinate of the centroid.

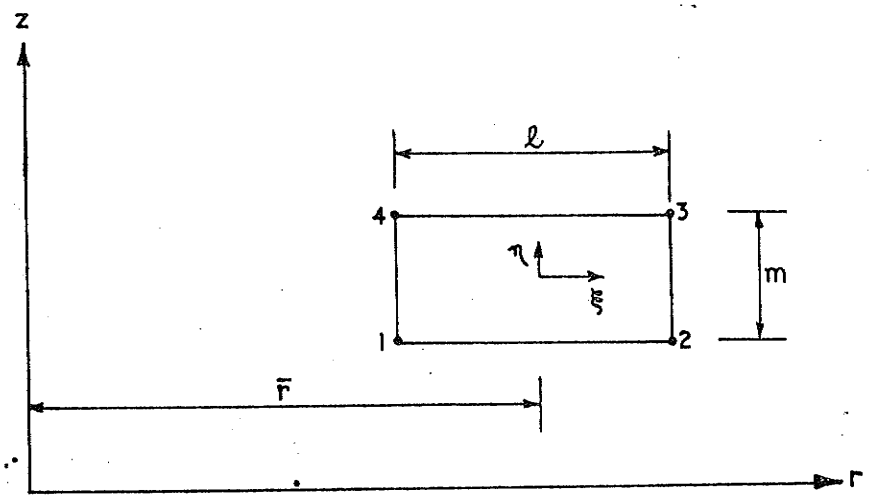

FIGURE A1.4: CROSS-SECTION OF A RECTANGULAR RING ELEMENT

The expression for the element matrix $[G]^e$ from equation (A1.20b) may be approximated by

$$[G]^e = 2\pi \bar{C} \bar{r} \int_{-1}^{1} \int_{-1}^{1} [S]^T [S] |J| \, d\xi \, d\eta \qquad (A1.21)$$

where $\bar{C}$ is the coefficient of non-linear effective hydraulic conductivity at the centroid.

For linear rectangular elements it can be shown that $|J|$ and $[S]$ are given by

$$|J| = \frac{lm}{4} \tag{A1.22a}$$

$$[S] = \begin{bmatrix} \frac{2}{l} & 0 \\ 0 & \frac{2}{m} \end{bmatrix} \begin{bmatrix} \frac{\partial N_1}{\partial \xi} & \frac{\partial N_2}{\partial \xi} & \frac{\partial N_3}{\partial \xi} & \frac{\partial N_4}{\partial \xi} \\ \frac{\partial N_1}{\partial \eta} & \frac{\partial N_2}{\partial \eta} & \frac{\partial N_3}{\partial \eta} & \frac{\partial N_4}{\partial \eta} \end{bmatrix} \tag{A1.22b}$$

where l and m are the width and height of the rectangle respectively.

Substitution of equations (A1.22) into (A1.21) leads to

$$[G]^e = 2\pi \bar{C} \bar{r} \left(\frac{m}{l} [A]^e + \frac{l}{m} [B]^e \right) \tag{A1.23a}$$

where $[A]^e$ and $[B]^e$ are the influence coefficient matrices whose components are given by

$$A^e_{IJ} = \int_{-1}^{1} \int_{-1}^{1} \frac{\partial N_I}{\partial \xi} \frac{\partial N_J}{\partial \xi} \, d\xi \, d\eta \tag{A1.23b}$$

and

$$B^e_{IJ} = \int_{-1}^{1} \int_{-1}^{1} \frac{\partial N_I}{\partial \eta} \frac{\partial N_J}{\partial \eta} \, d\xi \, d\eta \tag{A1.23c}$$

On applying the 9-point Gaussian quadrature formula (Zienkiewicz (1971) pp. 147-149), the integrals in equations (A1.23b) and (A1.23c) may be evaluated. The matrices $[A]^e$ and $[B]^e$ are obtained as

$$[A]^e = \begin{bmatrix} \frac{1}{3} & \frac{-1}{3} & \frac{-1}{6} & \frac{1}{6} \\ -\frac{1}{3} & \frac{1}{3} & \frac{1}{6} & \frac{-1}{6} \\ -\frac{1}{6} & \frac{1}{6} & \frac{1}{3} & \frac{-1}{3} \\ \frac{1}{6} & \frac{-1}{6} & \frac{-1}{3} & \frac{1}{3} \end{bmatrix} \tag{A1.24a}$$

$$|B|^e = \begin{bmatrix} \frac{1}{3} & \frac{1}{6} & \frac{-1}{6} & \frac{-1}{3} \\ \frac{1}{6} & \frac{1}{3} & \frac{-1}{3} & \frac{-1}{6} \\ \frac{-1}{6} & \frac{-1}{3} & \frac{1}{3} & \frac{1}{6} \\ \frac{-1}{3} & \frac{-1}{6} & \frac{1}{6} & \frac{1}{3} \end{bmatrix} \qquad \text{(A1.24b)}$$

Substitution of equations (A1.24a) and (A1.24b) in equation (A1.23a) leads to the required matrix $[G]^e$ in terms of l and m.

Similarly from equation (A1.20c) the expression for matrix $[D]^e$ may be approximated by

$$[D]^e = 2\pi S_s \bar{r} \frac{lm}{4} \int_{-1}^{1}\int_{-1}^{1} [N]^T [N] \, d\xi \, d\eta \qquad \text{(A1.25)}$$

On applying the 9-point Gaussian quadrature formula, the integral in equation (A1.25) can be evaluated. The expression for matrix $[D]^e$ is obtained as

$$[D]^e = \frac{1}{2} \pi \bar{r} \, lm \, S_s \begin{bmatrix} \frac{4}{9} & \frac{2}{9} & \frac{1}{9} & \frac{2}{9} \\ \frac{2}{9} & \frac{4}{9} & \frac{2}{9} & \frac{1}{9} \\ \frac{1}{9} & \frac{2}{9} & \frac{4}{9} & \frac{2}{9} \\ \frac{2}{9} & \frac{1}{9} & \frac{2}{9} & \frac{4}{9} \end{bmatrix} \qquad \text{(A1.26)}$$

A1.4 One-Dimensional Elements

The problem of one-dimensional radial flow towards a pumped well may be solved by using one-dimensional isoparametric ring elements.

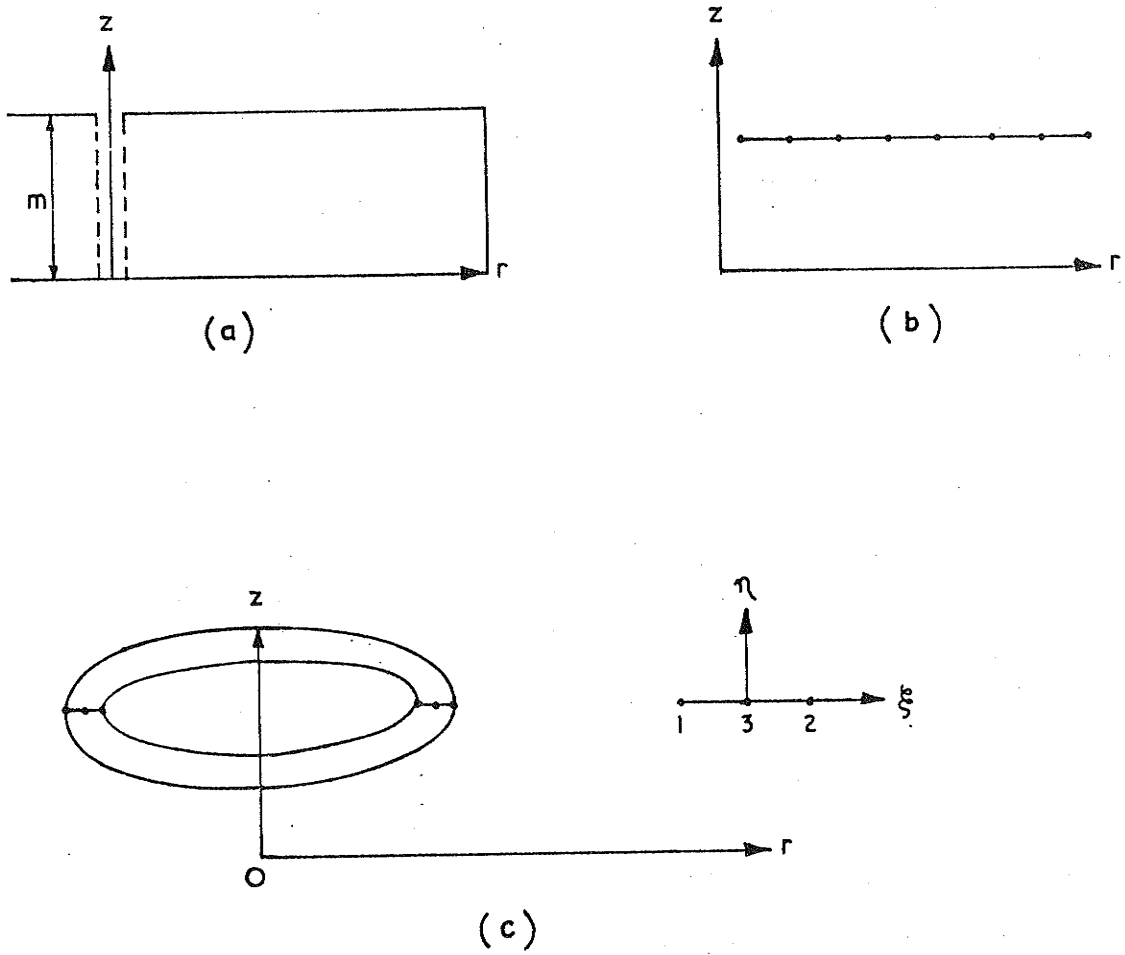

FIGURE A1·5: IDEALISED ONE-DIMENSIONAL REGION AND ONE-DIMENSIONAL ISOPARAMETRIC ELEMENTS

In the typical well aquifer system shown in Figure A1.5 it is sufficient to solve the hydraulic head distribution along any radial line. Accordingly the two-dimensional region in the r-z plane shown in Figure A1.5a may be reduced to a radial line shown in Figure A1.5b. This line is discretized into a network of line elements. A typical 3-node element is shown in Figure A1.5c. The planar ring section is readily generated by revolving the line element about the z-axis.

Let ξ be the local co-ordinate associated with each line element such that ξ = 0, 1 and -1 at nodes 3, 2 and 1 respectively. The re-

lationship between r and ξ is given by,

$$r = \alpha_1 + \alpha_2 \xi + \alpha_3 \xi^2 \qquad \text{(A1.27)}$$

The expressions for the shape functions of the 3-node line element were obtained by applying the general techniques described by Ergatoudis et al (1968) for isoparametric elements. They are,

$$[N_1, N_2, N_3] = \left[-\frac{1}{2}(\xi - \xi^2), \frac{1}{2}(\xi + \xi^2), (1 - \xi^2)\right] \qquad \text{(A1.28)}$$

The differentials are related by

$$dr = \frac{dr}{d\xi} \, d\xi \qquad \text{(A1.29)}$$

from which it follows that

$$dr = \left(\frac{dN_I}{d\xi} \, r_I\right) d\xi = |J| \, d\xi \qquad \text{(A1.30)}$$

where subscript I ranges from 1 to 3, and $|J|$ is the determinant of the Jacobian transformation matrix given by,

$$|J| = \frac{1}{2}(-1 + 2\xi) r_1 + \tfrac{1}{2}(1 + 2\xi) r_2 - 2\xi r_3 \qquad \text{(A1.31)}$$

Also $$\frac{dN_I}{dr} = \frac{dN_I}{d\xi} \frac{d\xi}{dr} = \frac{1}{|J|} \frac{dN_I}{d\xi} \qquad \text{(A1.32)}$$

Hence the slope matrix $[S]$ for the 3-node line element takes the form

$$[S] = \left[\frac{dN1}{dr}, \frac{dN2}{dr}, \frac{dN3}{dr}\right] \qquad \text{(A1.33a)}$$

$$= \frac{1}{|J|}\left[\tfrac{1}{2}(-1+2\xi), \tfrac{1}{2}(1+2\xi), -2\xi\right] \qquad \text{(A1.33b)}$$

From equation (4.33) it follows that

$$[G]^e = \int_{Re} C \, [S]^T \, [S] \, dR \qquad \text{(A1.34a)}$$

where $$dR = 2\pi r \, dr \qquad \text{(A1.34b)}$$

Substituting equations (A1.34b) and (A1.30) into equation (A1.34a) results in

$$[G]^e = 2\pi \int_{-1}^{1} C \; [S]^T [S] \; N_I \; r_I \; |J| \; d\xi \qquad (A1.35)$$

The 3-point Gaussian quadrature formula (Zienkiewicz (1971) pp. 147-149) was applied to the integral of equation (A1.35) and after matrix multiplication the following expression was found

$$[G]^e = 2\pi \sum_{i=1}^{3} \frac{C(\xi_i)}{J(\xi_i)} N_I(\xi_i) \; r_I \; W(\xi_i)$$

$$\times \frac{1}{4} \begin{bmatrix} (-1+2\xi_i)^2 & (4\xi_i^2 - 1) & -4\xi_i(-1+2\xi_i) \\ (4\xi_i^2 - 1) & (1+2\xi_i)^2 & -4\xi_i(1+2\xi_i) \\ -4\xi_i(-1+2\xi_i) & -4\xi_i(1+2\xi_i) & 16\xi_i^2 \end{bmatrix} \qquad (A1.36)$$

where $C(\xi_i)$, $N_I(\xi_i)$ and $J(\xi_i)$ are functions of the ξ coordinate to be evaluated at the Gaussian points (ξ_i) and $W(\xi_i)$ are the values of the weighting coefficient at the Gaussian points.

Similarly expressions for matrices $[\bar{G}]^e$ and $[D]^e$ can be obtained from the following equations:

$$[\bar{G}]^e = 2\pi \int_{-1}^{1} [S]^T [K] [S] \; N_I \; r_I \; |J| \; d\xi \qquad (A1.37)$$

$$D^e = 2\pi \int_{-1}^{1} S_S \; [N]^T [N] \; N_I \; r_I \; |J| \; d\xi \qquad (A1.38)$$

APPENDIX 2: ANALOGUE MODEL - ELECTROLYTIC TANK

A2.1 General

In this appendix an electrolytic tank analogue model for solving two dimensional axisymmetric well flow problems is described. Solutions obtained from this analogue model were used in Chapter 5 to verify the finite element analysis of problems for which no exact mathematical treatment can be found.

The utilisation of electrolytic tank models for the solution of steady state field problems governed by Laplace's equation has been extensive since the concept was introduced by Adams (1875). A wide range of porous media flow problems has been solved using electrolytic tank modelling techniques (see list of references in Todd (1959), De Wiest (1965) and Bear (1972)). Detailed treatment of the use of electrolytic tanks is given in the specialised texts on analogue modelling by Karplus (1958) and Karplus and Soroka (1959) to which the reader is specifically referred.

In presenting the essential features of the model used by the author, it has been assumed that the reader is conversant with the general techniques of electrolytic tank modelling as described in the above references.

A2.2 Electrolytic Tank Model Description

A schematic diagram of the electrolytic tank model is given in Figure A2.1. The electrical circuit shown in the figure is a simplified version of that actually employed. The model may be thought of in terms of three basic components; the electrical circuitry; the probe and positional location unit; and the tank itself. Each of these components will now be discussed.

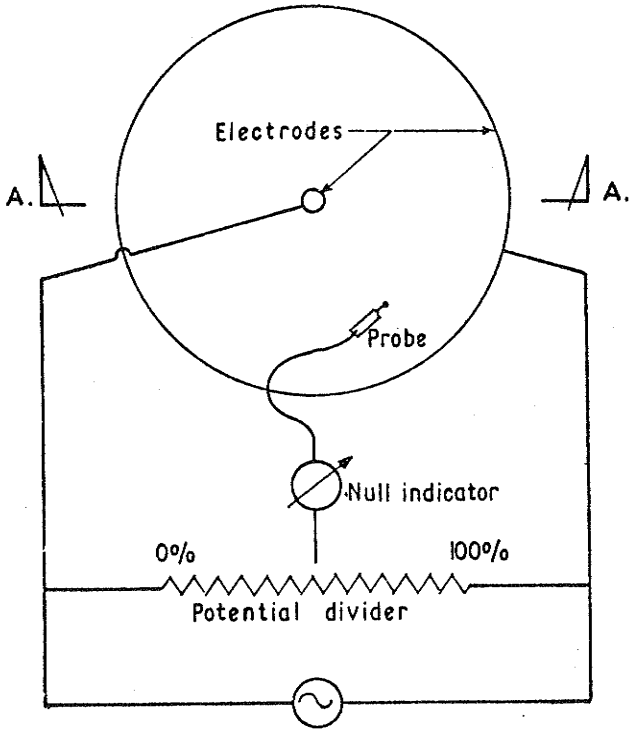

r_w = 12·7 mm

r_o = 254 mm

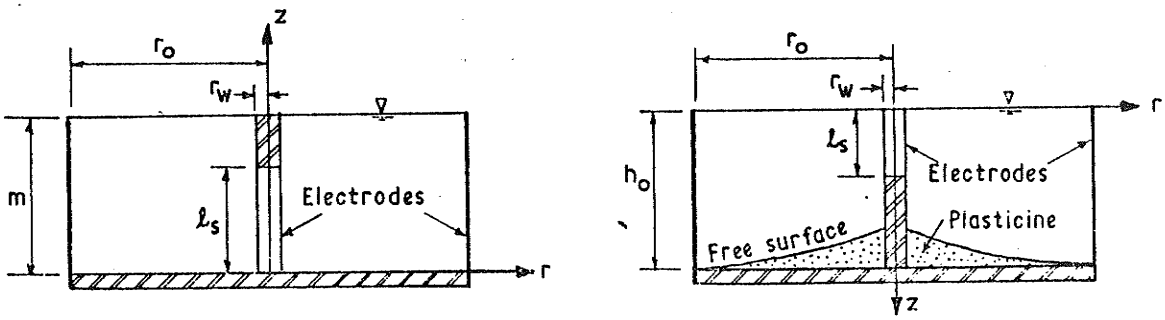

Insulating material-perspex

FIGURE A2·1: ELECTROLYTIC TANK FOR AXISYMMETRIC WELL FLOW PROBLEMS.

A2.2.1 Electrical Circuitry

If d-c voltage supplies are used in an electrolytic tank, polarization-type electrochemical phenomena will occur almost immediately at the electrodes. Therefore a-c supplies are preferred and used almost exclusively. The selection of the a-c voltage supply frequency involves a compromise. As frequency is increased, polarization effects decrease but stray capacitance effects become more pronounced. Frequencies in the vicinity of 1500 cps appear to be the most satisfactory. The author used a 5 volt a-c voltage supply at a frequency of 1564 cps.

Standard earthing techniques were used to eliminate 50 cps interference.

In the case of a-c electrical systems (as used here) a true null can be obtained only if both the amplitude and the phase of the signal at the probe tip are identical to those at the sliding arm of the potentiometer. Capacative reactances associated with the polarization of the electrolyte act to shift the phase of the probe signal. To obtain a sharp null, this quadrature component of the probe signal was compensated by adjustment of a decade capacitance box connected across one arm of the potentiometer. The effects upon both amplitude and phase of stray capacitances were minimised by careful shielding of the probe and by employing a Wagner ground (Terman and Pettit (1952)).

A cathode ray oscilloscope proved to be an extremely satisfactory null indicator.

A2.2.2 Probe and Position Location Unit

Softky and Jungerman (1952) described a probe suitable for measuring equipotential lines within a three dimensional electrolytic tank. Based on such a design, a probe was made from 0.8 mm diameter stainless steel hypodermic needle insulated by an 0.1 mm layer of heat shrink P.V.C. based sleeving, except for the 1 mm tip which was silver plated.

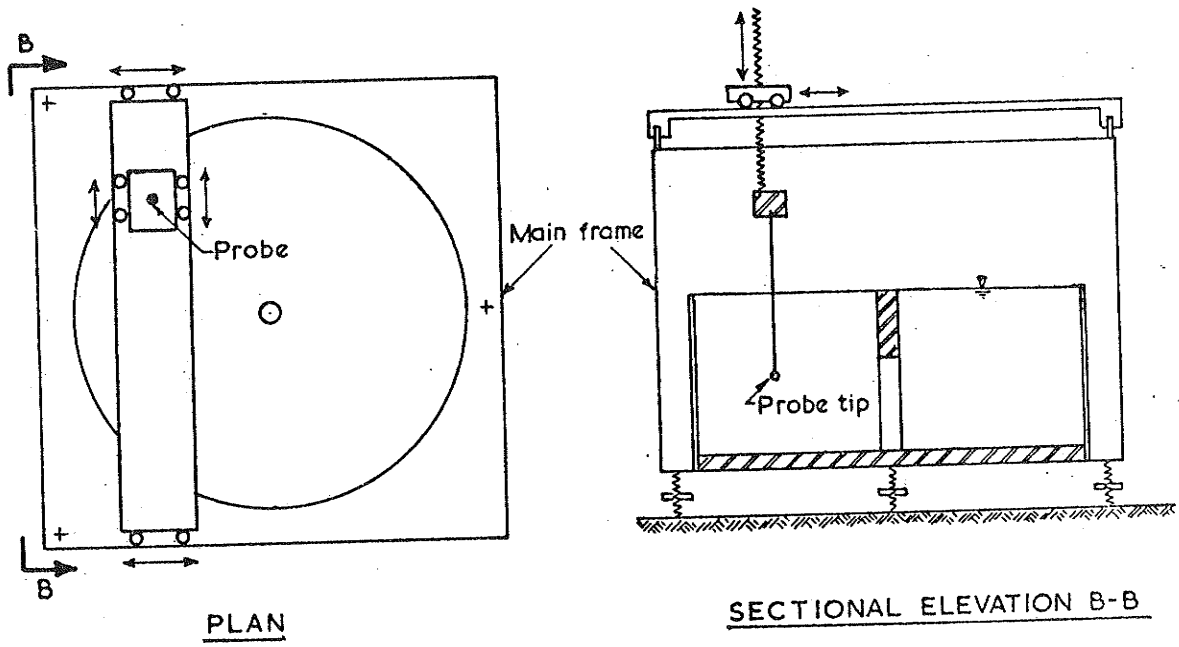

FIGURE A2·2: PROBE LOCATION - SCHEMATIC DIAGRAM

The mechanism for locating the probe within the electrolytic tank is shown schematically in Figure A2.2. The tank was seated in a main frame which was provided with three levelling screws and mounted on a solid foundation to avoid vibrations. The probe was

attached to an insulated probe block whose height was adjustable. Movement of the probe within the horizontal plane was achieved by the twin carriage arrangement running above the main frame as shown. Vernier scale adjustment in all three directions of probe movement permitted accurate location within 0.2mm.

A2.2.3 Electrolytic Tank

The arrangement of the electrolytic tank for modelling partially screened wells in both confined and unconfined aquifers is shown in Figure A2.1.

The equipotential boundary at the radius of influence of the well aquifer system was modelled in the tank by a polished brass cylindrical electrode having an internal diameter 508 mm. The well boundary was formed by a 25.4 mm diameter composite bar. Polished brass rod was used for the electrode to correspond to the equipotential boundary along the screened portion of the well and perspex bar was used as an insulator for the equivalent impermeable cased portion of the well.

Singly distilled water was used for the electrolyte. The aquifer thickness being modelled was controlled by the depth of electrolyte within the tank since the air-electrolyte interface behaves as a flow boundary.

In confined aquifer modelling the impermeable base of the aquifer was represented by the perspex insulating bottom of the tank.

The electrolytic tank modelling of a partially screened well in an unconfined aquifer, being complicated by the free surface, was carried out upside down. The air-electrolyte interface acted as the base of the aquifer whilst plasticine within the bottom of the tank was adjusted to

represent the a priori unknown free surface. Accurate sculpting of the plasticine to a required axisymmetric surface was achieved by rotating a radial metal sheet form about the central well boundary. A trial free surface was prepared, potentials along the surface were measured, and the shape of the plasticine adjusted until the free surface condition h = z was satisfied at all points of the surface. The convergence was rapid. Once the free surface had been established, equipotentials within the flow domain were located.

A2.3 Accuracy of Electrolytic Tank Model

In discussing the accuracy of the electrolytic tank model it is convenient to define the percentage error $\epsilon\%$ as

$$\epsilon\% = \frac{100\ E_{true} - E_{measured}}{\Delta E_{max}} \qquad (A2.1)$$

where ΔE_{max} is the largest voltage potential difference appearing in the system, that is the potential difference of 5 volts between the electrodes.

Liebmann (1953) reported that an accuracy of 5% is easily obtained and accuracies of 0.1% to 0.2% have been achieved.

The principal sources of errors in electrolytic tanks are mechanical errors, polarization, surface tension, probe effects and non-uniformity of the electrolyte.

Mechanical errors include inaccuracies in the shapes of electrodes and boundaries and errors in the positioning and measuring of the probe location within the electrolyte. Electrode surfaces were machined within tolerances of $\pm$ 0.05 mm. By careful levelling of the model and accurate measurement, the electrolyte depth was estim-

ated to within 0.2 mm. The free surface location in unconfined aquifer modelling was determined within $\pm$ 0.5 mm. While it is difficult to assess the over-all error introduced by the above mechanical inaccuracies, the voltage error due to false positioning of the probe can be estimated by multiplying the probe position error by the maximum voltage gradient in the electrolyte. For example, for a fully screened well in a confined aquifer (r_w = 12.7, r_o = 254) modelled by the electrolytic tank, the maximum voltage gradient, the probe-position error and the resulting voltage error were respectively 0.13 volts/mm, 0.2mm and 0.52%.

Einstein (1951) investigated the polarization effect to determine the combination of electrolyte and electrode giving the least inaccuracy, the criterion used being a figure of merit, F, defined as -

$$F = \frac{\text{resistance of 1 cm}^3 \text{ of electrolyte}}{\text{surface impedance of 1 cm}^2 \text{ of electrode}}$$

His experiments were conducted with an a-c voltage supply of 1500 cps and in all cases the current density was 4.2 mA r.m.s/cm^2. The results indicated that F decreased with increasing concentration and increased with the temperature of the electrolyte. Typical values of F are given in Table A2.1. The combination of polished brass electrodes and singly distilled water electrolyte used by the author could be expected to yield a figure of merit of the order of 200 cm^{-1}. Such a value of F guaranteed that polarization errors would be small compared to mechanical errors. Further possible inaccuracies due to the phase shift caused by polarization were eliminated by the modified electrical circuit discussed in Section A2.2.1.

Table A2.1: Figure of Merit of Various Electrode-Electrolyte Combinations. (After Einstein (1951))

Electrode	Electrolyte	F(cm^{-1})
Copper (polished)	M/2 Cu SO_4 solution	12.4
Brass (polished)	Tap water	105
Brass (etched)	Tap water	111
Brass (etched and graphited)	Tap water	232
Brass (etched and graphited)	M/30 Cu SO_4 solution	41.8
Brass (etched and graphited)	Singly distilled water	480
Brass (platinized)	Singly distilled water	940

Surface tension effects were all but eliminated by having the electrolyte surface coincident with the plane of the top of the inner and outer cylindrical boundaries.

The distortion of the flow field caused by the presence of the probe shank within the electrolyte was negligible since the probe diameter was small compared to the dimensions of the electrolyte system.

Errors due to nonuniformity in the electrolyte were minimised by ensuring thermal equilibrium in the system. The tank was operated at room temperature in a thermally insulated room. At other than room temperature, serious errors due to thermal convection currents within the electrolyte are extremely difficult to avoid.

Figure A2.3 illustrates the results of accuracy tests for the electrolytic tank model used by the author; the accuracy assessment was carried out for fully radial flow between two concentric cylindrical electrodes (r_w = 12.7, r_o = 254) simulating a fully screened well in a confined aquifer (l_s = m = 127 mm).

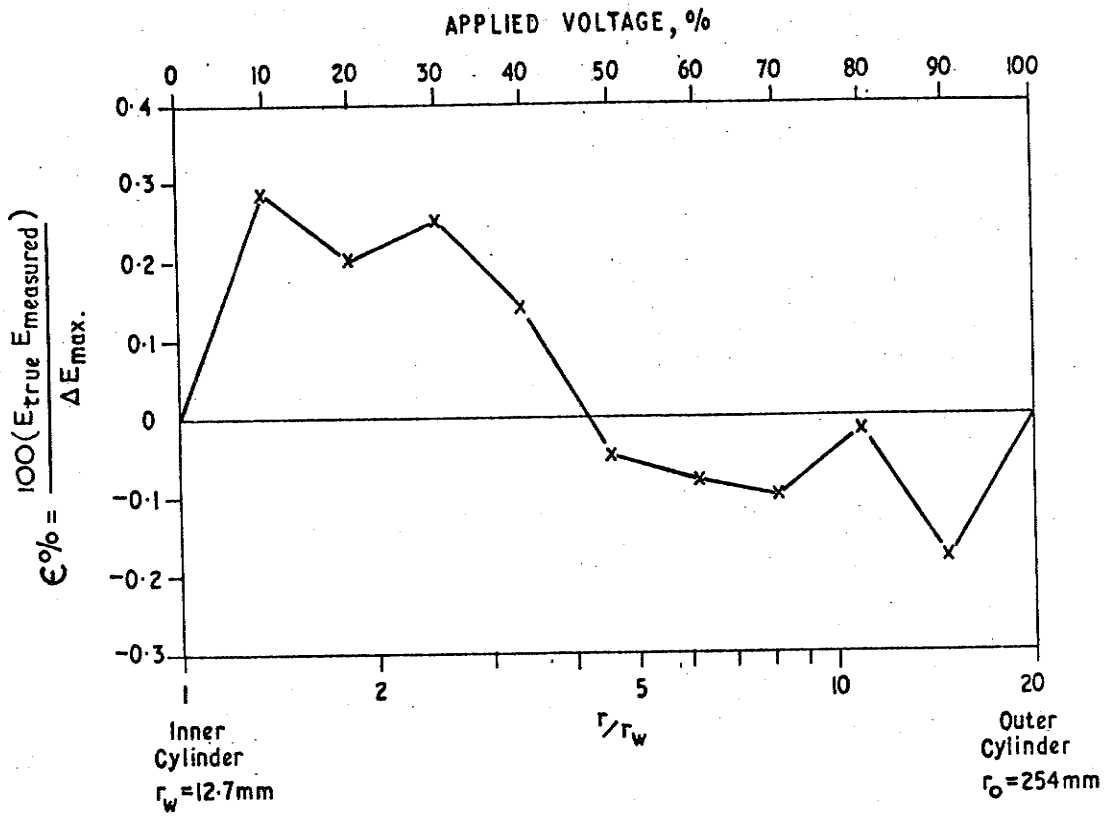

FIGURE A2·3: ACCURACY OF ELECTROLYTIC TANK

The accuracy obtained, $\epsilon\% < 0.3\%$, was very good and fully justified the care taken in preparing the model.